

**Studies on Photoinduced Electron Transfer
and Charge Transfer Processes Involving
Organic Donor-Acceptor Systems,
Lanthanide Complexes and Uranyl Ions**

by

Poonam Verma

(CHEM 01200804011)

Bhabha Atomic Research Centre, India

A thesis submitted to the

Board of Studies in Chemical Sciences

In partial fulfillment of requirements

for the Degree of

DOCTOR OF PHILOSOPHY

OF

HOMI BHABHA NATIONAL INSTITUTE

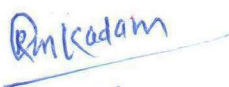


July 2015

Homi Bhabha National Institute

Recommendations of the Viva Voce Committee

As members of the Viva Voce Committee, we certify that we have read the dissertation prepared by Kum. Poonam Verma (CHEM 01200804011), entitled "*Studies on photoinduced electron transfer and charge transfer processes involving organic donor-acceptor systems, lanthanide complexes and uranyl ions*" and recommend that it may be accepted as fulfilling the thesis requirement for the award of Degree of Doctor of Philosophy.

Chairman -	Dr. K. L. Ramakumar		Date: 15/11/2015
External Examiner -	Prof. A. K. Mishra		Date: 13/11/2015
Guide / Convener -	Dr. H. Pal		Date: 13/11/2015
Co-Guide -	Dr. R. M. Sawant		Date: 16/11/2015
Member 1 -	Dr. D. K. Palit		Date: 13/11/2015
Member 2 -	Dr. R. M. Kadam		Date: 13/11/2015

Final approval and acceptance of this thesis is contingent upon the candidate's submission of the final copies of the thesis to HBNI.

* I/We hereby certify that I/we have read this thesis prepared under my/our direction and recommend that it may be accepted as fulfilling the thesis requirement.

Date: 13-11-2015

Place: BARC, Mumbai


(Dr. R. M. Sawant)

(Co-Guide)


(Dr. H. Pal)

(Guide)

STATEMENT BY AUTHOR

This dissertation has been submitted in partial fulfillment of requirements for an advanced degree at Homi Bhabha National Institute (HBNI) and is deposited in the Library to be made available to borrowers under rules of the HBNI.

Brief quotations from this dissertation are allowable without special permission, provided that accurate acknowledgement of source is made. Requests for permission for extended quotation from or reproduction of this manuscript in whole or in part may be granted by the Competent Authority of HBNI when in his or her judgment the proposed use of the material is in the interests of scholarship. In all other instances, however, permission must be obtained from the author.



Poonam Verma

DECLARATION

I, hereby declare that the investigation presented in the thesis has been carried out by me. The work is original and has not been submitted earlier as a whole or in part for a degree / diploma at this or any other Institution / University.



Poonam Verma

List of Publications

Journal Publications

1. Effect of block size of pluronic polymers on the water structure in corona region and its effect on the electron transfer reactions.
Poonam Verma, Sukhendu Nath, Prabhat K. Singh, Manoj Kumbhakar, and Haridas Pal
J. Phys. Chem. B, 2008, 112 (20), 6363-6372
2. Intriguing H-aggregate and H-dimer formation of coumarin-481 dye in aqueous solution as evidenced from photophysical studies.
Poonam Verma and Haridas Pal
J. Phys. Chem. A 2012, 116, 4473–4484
3. Unusual H-Type Aggregation of Coumarin-481 Dye in Polar Organic Solvents.
Poonam Verma and Haridas Pal
J. Phys. Chem. A 2013, 117, 12409–12418
4. Aggregation studies of dipolar Coumarin-153 dye in polar solvents: A Photophysical Study.
Poonam Verma and Haridas Pal
J. Phys. Chem. A 2014, 118, 6950-6964
5. Tuning Electron Transfer Reaction through Modulating Solute Locations in Composite Supramolecular Assembly of Pluronic Copolymers and Cationic Surfactant
Poonam Verma and Haridas Pal
Phys. Chem. Chem. Phys., 2015, 17, 15400-15411
6. Intriguing multichannel photoinduced electron transfer in lanthanide (III) - diphenylamine systems.
Poonam Verma, R. M. Sawant and Haridas Pal
Phys. Chem. Chem. Phys., 2015,17, 23214-23222

Symposia Publications

1. ET Reactions in Pluronic 88 Tri-block Co-polymer micelle.
P. Verma, S. Nath, M. Kumbhakar and H. Pal
National Symposium on Radiation and Photochemistry (NSRP-2007), National Centre. for Ultrafast Processes, University of Madras, Chennai, Jan 29-31, 2007, PC-64

2. Unusual Photophysical behavior of coumarin dye in water.
Poonam Verma, Haridas Pal and Sukhendu Nath
National Symposium on Radiation and Photochemistry, Kumaun University, Nainital,
March 12-14, 2009, PC-64
3. Fluorescence Quenching of Diphenylamine by Lanthanide and Uranyl Ions through
Electron Transfer Mechanism.
Poonam Verma, R. M. Sawant and H. Pal
NUCAR-2011, Feb. 22-26, 2011, Gitam University, Vishakapatnam, 414-415
4. H-aggregates of coumarin-481 dye in aqueous solution: A photophysical study.
Poonam Verma and Haridas Pal
TSRP-2012, Jan. 4-7, 2012, BARC, Mumbai, PC-119, 421-422
5. Intriguing H-Type Aggregation of Coumarin-481 dye in Polar Organic Solvents as
Evidenced from Photophysical Studies.
Poonam Verma and Haridas Pal
TSRP-2014, Jan. 6-9, 2014, BARC, Mumbai, PC-85, 221-222
6. Tuning Electron Transfer Rate in Composite Supramolecular Assembly of Pluronic
Copolymers and Cationic Surfactant by Modulating Solute Locations.
Poonam Verma and Haridas Pal
TSRP-2014, Jan. 6-9, 2014, BARC, Mumbai, PC-91, 229-230



Poonam Verma

Dedicated to....

My Parents

ACKNOWLEDGEMENTS

In my long journey towards Ph.D., first and foremost, I would like to express my deepest heartfelt thanks to my advisor, Prof. H. Pal for guiding me through the rough/exciting road to finish this thesis. His immense patience, encouragement and knowledge were key motivations throughout my Ph.D. I am truly thankful for his steadfast integrity and selfless dedication towards my academic development and imbining me with the scientific aptitude.

I express my sincere thanks to Dr. R. M. Sawant, my co-guide for having faith in me and giving me the freedom to carry out the research work. I am extremely grateful to my doctoral committee members, Dr. K. L. Ramakumar (chairman), Dr. D. K. Palit, Dr. S. V. Godbole and Dr. R. M. Kadam for their valuable criticisms, suggestions and recommendations.

Words are short to express my deep sense of gratitude for Dr. S. Nath, with whom I initiated my Ph.D. work that was totally different from my departmental work. His kind gesture and thoughtful behavior built up my confidence to work in an entirely new field.

I gratefully acknowledge Dr. S. D. Choudhury, Dr. J. Mohanty and Dr. A. C. Bhasikuttan for their help in the Laser Flash Photolysis experiments. It's my pleasure to express gratitude to Dr. V. Sudarsan for SEM measurements and time-resolved fluorescence experiments involving lanthanide emissions. My special thanks to Shri A. K. Mora for fluorescence up-conversion measurements, Dr. R. Ganguly for DLS measurements, Dr. C. B. Basak for SEM measurements and Dr. A. K. Satpati for cyclic voltametry measurements.

I would like to extend my gratitude to Dr. S. D. Choudhary, Dr. P. K. Singh, Dr. S. Nath, Dr. J. Mohanty, Dr. M. Kumbhakar, Dr. N. Barouha, Dr. A. C. Bhasikuttan, Dr. M. Sayed, Shri A. K. Mora and other laboratory members of Molecular Photochemistry Section for their precious help and cooperation during my thesis work. I convey my heartfelt gratitude to all the members of Radioanalytical Chemistry Division, my friends in RLG and well wishers for their support, motivation and good wishes. I am thankful to Dr. B. S. Tomar, Dr. K. L. Ramakumar and Dr. B. N. Jagatap for their constant support and encouragement.

I am highly obliged to BARC for granting me the permission for Ph.D. registration with HBNI and using its infrastructure for the research work. I am also thankful to HBNI to approve my registration. I am extremely grateful to Dr. S. K. Ghosh, who was the Dean of Academics, Chemical Sciences, HBNI during the time of my Ph.D. topic approval. This thesis is able to see the light due to his interventions to resolve many difficulties.

I express my warmest appreciation to my lovely friend Smt. Abha N. Kumar for her motivational speeches, refreshing ideas and for sharing light moments in canteen and home.

This Ph.D. would not have been possible without my dear friend, Ms. P. Mathi who stood like a rock and was the main driving force behind the completion of my thesis. In addition to being my 3 A.M. friend, she was the sink of all my tantrums.

I owe my sincere gratitude to all the teachers and mentors in my life for inducing within me the spirit of free thinking and the quest for knowledge.

Above and beyond all, my parents (nothing can define their love and support) and my family for just being there for me.

This Ph.D. would have remained a dream for not Dr. K. L. Ramakumar, to whom I owe a great debt of gratitude for granting me the permission to fulfill my scientific endeavors' outside his regime.

Finally, I would like to thank, the Almighty, for His blessings which helped me in fulfilling this ambition of my life.

*BARC, Mumbai
July, 2015*



(Poonam Verma)

CONTENTS

	Page No.
Distribution of Chapters, Sections & Sub-sections	i
Synopsis	v
List of Figures	xiii
List of Tables	xvii
List of Charts and Schemes	xix
Glossary	xxi

CHAPTER 1

General Introduction: Basic Aspects of Photophysical Processes and Electron Transfer Reactions

Abstract	1
1.1 Photoinduced Processes	2
1.2 Electron Transfer Reaction: Theoretical Background	3
1.2.1 <i>Marcus Classical Electron Transfer Theory</i>	4
1.2.2 <i>Quantum Mechanical Refinement of Marcus ET Theory</i>	7
1.2.3 <i>Effect of High Frequency Vibrational Modes on ET Rates</i>	9
1.2.4 <i>Sumi-Marcus Two-dimensional ET (2DET) Theory: ET under Non-equilibrium Solvent Relaxation</i>	10
1.2.5 <i>Hybrid Model for 2DET: Incorporation of the High Frequency Vibrational Modes</i>	12
1.3 Energetics of Photoinduced Electron Transfer Reactions	14
1.4 Photoinduced Electron Transfer under Diffusive Condition	14
1.5 Solvation Dynamics	16
1.6 Fluorescence Quenching Studies: Stern-Volmer Equation	18
1.7 Tri-Block Copolymers and their Solution Behavior	21
1.8 Kashas Exciton Theory for Dye-Aggregation	23
1.9 Motivation and Objective of the Present Work	24

CHAPTER 2

Instruments and Methods

2.1 Introduction	29
2.2 Ground State Absorption Measurement	30

2.3	Steady-State Fluorescence Measurements	31
2.4	Fluorescence Lifetime Measurements	32
	2.4.1 TCSPC Technique: Basic Principles and the Instrument Used	33
	2.4.2 Analysis of Fluorescence Decays from TCSPC Measurements	35
2.5	Fluorescence Anisotropy Measurements	37
2.6	Fluorescence up-conversion Measurements	39
2.7	Time Resolved Transient Absorption Measurements	41
2.8	Redox Potential Measurements	42
2.9	Dynamic Light Scattering	43

CHAPTER 3

Photoinduced Electron Transfer reactions in Pluronic Micellar Media: Observation of Marcus Inversion

	Abstract	45
3.1	Introduction	46
3.2	Experiments Methods and Materials	48
3.3	Results and Discussion	48
	3.3.1 Characterization of Microenvironment in F88 Micelle	48
	3.3.1.1 Determination of critical micellar temperature (CMT) and size of F88 micelles	48
	3.3.1.2 Characterization of probe location and micropolarity around it	49
	3.3.1.3 Solvation dynamics studies	
	3.3.1.4 Anisotropy studies	51
	3.3.1.5 Number of water molecules associated with each EO unit in pluronic micelle	52
	3.3.2 PET reactions in F88 micellar media	54
	3.3.2.1 Quenching studies using SS fluorescence measurements	54
	3.3.2.2 Quenching studies using TR fluorescence measurements	55
	3.3.2.3 Correlation of the quenching rates with the free energy changes of the ET reactions	58
3.4	Conclusions	61

CHAPTER 4

Photoinduced Electron Transfer Reactions in Pluronic-Surfactant Supramolecular Assemblies: Tuning of Electron Transfer Rates

	Abstract	63
--	----------	----

4.1	Introduction	64
4.2	Experiments Methods and Materials	65
4.3	Results and Discussion	67
4.3.1	<i>Absorption and fluorescence characteristics of C343 dye</i>	67
4.3.2	<i>Absorption and fluorescence studies on the interaction of C343 dye with DMAN quencher</i>	70
4.3.3	<i>TR fluorescence studies on the interaction of C343 dye with DMAN quencher</i>	72
4.3.4	<i>Modulations of the ET rates for C343-DMAN system in the CTAC-pluronic mixed micellar media</i>	75
4.4	Conclusions	81

CHAPTER 5

Photoinduced Electron Transfer and Charge Transfer interactions of lanthanide and Uranyl Ion with Fluorogenic Diphenyl Amine Donor

	Abstract	83
5.1	Introduction	84
5.2	Experiments Methods and Materials	86
5.3	Results and Discussion	87
	Part 5.3.A	87
	Photophysical behavior of C481 dye in polar organic solvents	
5.3.A.1	<i>Ground-state absorption and SS fluorescence measurements.</i>	87
5.3.A.2	<i>TR fluorescence measurements</i>	89
5.3.A.3	<i>TRES and TRANES analysis for C481 dye in EtOH and ACN solutions</i>	95
	Part 5.3.B	97
	Photophysical behavior of C481 dye in aqueous solution	
5.3.B.1	<i>Ground-state absorption and SS fluorescence measurements</i>	97
5.3.B.2	<i>TR fluorescence measurements</i>	99
5.3.B.3	<i>Construction and analysis of TRES and TRANES for C481 dye</i>	102
5.3.B.4	<i>Temperature-dependent TR fluorescence study</i>	104
5.3.B.5	<i>Fluorescence up-conversion measurements</i>	105
5.3.B.6	<i>Dynamic light scattering measurements</i>	107
5.3.B.7	<i>Measurements with supersaturated aqueous solution of C481 dye</i>	108
	Part 5.3.C	109
	Photophysical behavior of C153 dye in polar organic solvents	
5.3.C.1	<i>Ground-state absorption and SS fluorescence measurements.</i>	109
5.3.C.2	<i>TR fluorescence measurements</i>	110
5.3.C.3	<i>TRES and TRANES analysis for C153 dye</i>	113

5.3.C.4	<i>Temperature effect on TR fluorescence of C153 in EtOH solution</i>	114
5.3.C.5	<i>TR fluorescence anisotropy studies</i>	115
5.3.C.6	<i>Femtosecond fluorescence up-conversion measurements</i>	116
5.3.C.7	<i>DLS and SEM measurements</i>	118
5.3.C.8	<i>TR fluorescence studies in strongly protic trifluoroethanol solvent</i>	119
Part 5.3.D		119
	Photophysical behavior of C153 dye in aqueous solution	
5.3.D.1	<i>Ground-state absorption and SS fluorescence measurements</i>	119
5.3.D.2	<i>TR fluorescence measurements</i>	120
5.4	Conclusions	121

CHAPTER 6

Photoinduced Electron Transfer and Charge Transfer interactions of Lanthanide and Uranyl Ion with Fluorogenic Diphenyl Amine Donor

	Abstract	123
6.1	Introduction	124
6.2	Experiments Methods and Materials	127
6.3	Results and Discussion	127
6.3.1	Investigations in aqueous solution.	127
6.3.1.1	<i>Ground state interaction of DPA with lanthanide ions: Formation of charge transfer complexes</i>	128
6.3.1.2	<i>SS and TR fluorescence studies following DPA excitation and monitoring DPA emission</i>	130
6.3.1.3	<i>Studies following lanthanide excitation and monitoring lanthanide emission</i>	132
6.3.1.4	<i>Laser flash photolysis studies following DPA excitation</i>	134
6.3.1.5	<i>Correlation of bimolecular quenching constants with free energy changes of the ET reactions</i>	135
6.3.1.6	<i>Studies on the possibility of energy transfer from excited DPA to lanthanide ions</i>	136
6.3.1.7	<i>Visualization of multiple PET channels for DPA-Ln³⁺ systems</i>	138
6.3.2	Investigations in acetonitrile solution	140
6.4	Conclusions	141

CHAPTER 7

	<i>Concluding Summary and Future Scope</i>	143
--	---------------------------------------------------	-----

	REFERENCES	149
--	-------------------	-----

SYNOPSIS

Electron transfer (ET) and charge transfer (CT) are the most fundamental processes in chemistry, biology and geology.¹ Knowledge of the various parameters that govern and modulate the ET and CT reactions plays an utmost role in designing a reaction as per desire. ET is the key step in many biological processes that have enormous relevance to life, for example, photosynthesis and respiration.¹⁻⁷ It is also a fundamental step in countless processes of vast technological applications related to information storage, energy conversion, etc.¹⁻¹⁴ Photoinduced electron transfer (PET) reactions in homogeneous and heterogeneous solutions have been investigated quite extensively to understand different aspects of ET dynamics and mechanism.¹⁻¹⁶

One of the most interesting aspects of ET studies is the realization and understanding of the inversion behavior in the ET rates at the higher exergonicity region, a unique behavior that is theoretically predicted by Prof. R. A. Marcus and is universally known as Marcus Inversion (MI).¹⁻⁷ Though MI is quite common for intramolecular ET reactions, such behavior could hardly be realized for bimolecular ET reactions. The lack of MI behavior in bimolecular ET reactions in homogeneous solution is mainly due to the influence of reactant diffusion that limits the maximum observable reaction rate. In organized assemblies like micelles, as the diffusion of the reactants is largely restricted, the bimolecular ET effectively occurs between spatially distributed reactants that are already within reaction spheres and hence can be envisaged as equivalent to intramolecular ET among the spatially distributed reactant pairs. Further, in micelles, taking the advantage of slow solvent relaxation, the difficulty of finding suitable donor–acceptor series to achieve very high reaction exergonicity can be circumvented to a large extent by bringing down the effective reorganization energy for the ET reaction quite significantly in comparison to that in homogeneous solution.

With the viewpoint discussed above, in a part of the present study, photoinduced ET (PET) reactions have been investigated in pluronic micellar media using coumarin acceptors and amine donors to explore if Marcus inversion can be observed easily for bimolecular ET reaction. The aim of the present study is also to understand the effect of such organized media on the energetics and dynamics of PET reactions under non-diffusive conditions. Subsequent to getting experience of the various parameters governing the ET dynamics and energetics, these parameters can be desirably modulated by suitably using the reactants and reaction media, especially in the mixed micelles, where the reactant location and hence, the local environment of the reactant can be significantly modulated by changing the co-surfactant compositions. A series of desired modulations can thus be effectively achieved in a single reaction media by using a novel method of employing the charged

reactant and oppositely charged mixed micellar media and thereby harnessing the columbic interaction for our benefit. Thus, PET studies have been carried out in pluronic-ionic surfactant mixed micellar systems to realize a controlled modulation of bimolecular ET rates. Present study on PET reaction has direct relevance to solar energy conversion, biology, medicinal chemistry, host-guest chemistry, catalysis and many other applied areas of interest.¹⁻¹⁶

As a continuation of PET studies, interaction of trivalent lanthanide ions and uranyl ion with well known electron donor, diphenylamine has also been carried out in homogeneous solution under diffusive conditions. The aim of this study is to understand the possible ET/CT reactions, considering the relevance of such studies in the control of lanthanide/uranyl ions mitigation in the geological environment.

It is apparent that the photophysics of chromophoric/ fluorogenic dyes used as the reactants to investigate PET reactions need to be characterized thoroughly to ensure that no unusual behaviour of these dyes does have any influence on the observed PET results. Therefore, photophysical behaviour of some selective coumarin dyes used as electron acceptors have been independently investigated in aqueous and organic media, even though reports on coumarin photophysics is quite rich in the literature. Results of the present study reveal the interesting new aspect of H-type aggregation of the studied dyes not reported so far in the literature, even though dye monomers invariably dominate in the studied medium. It is, however, realized from the observed results that the dye aggregation as such does not affect the of PET results as the observed fluorescence changes due to H-type dye aggregation mainly occur at the extreme blue edge of the emission spectra while the PET process is investigated following the changes in the fluorescence and absorption of the dye at their respective peak positions.

The results of the different studies carried out under my Ph. D. program are presented and discussed in the thesis to be submitted to HBNI in due course. Based on the theme of the work, different aspects of the present work are discussed in a systematic manner in six different chapters of the thesis. Brief accounts of the contents arranged in different chapters of the thesis are summarized below.

Chapter 1: This is the introductory chapter of the thesis and describes the fundamental aspects of ET and CT reactions, giving a brief theoretical background of the process. Since most of the investigations involve photoinduced reactions, general photophysical and photochemical aspects of the excited molecules are discussed in this chapter. A brief account of the aspects of solvation dynamics, a process that is directly coupled to ET reaction in solution phase, has also been included in this chapter. Since a significant part of the present study deals with the PET reactions in microheterogeneous media, this chapter also describes the general aspects of micellar and mixed

micellar aggregates, used as the reaction media in present study. As the photophysical characterization of the fluorogenic reactant molecules investigated in the present study encounters aggregation, basic aggregation behavior of chromophoric organic dyes has also been discussed in brief. At the end of the chapter, the objective and motivation of the present research work is briefly discussed.

Chapter 2: Chapter 2 presents the required details of the experimental techniques and data analysis methods employed in this research work. Time-correlated single photon counting (TCSPC) spectrometer, used for fluorescence lifetime measurements, is the main work-horse for our PET and other photophysical and photochemical studies. Hence, the TCSPC technique has been discussed quite extensively in this chapter.¹⁷ Basic principles of other instrumental facilities used in the present study, e.g. absorption spectrophotometry, steady-state spectrofluorimetry, cyclic voltammetry, femtosecond up-conversion and laser flash photolysis have also been described briefly. The data analysis methods namely fitting of observed fluorescence decays, construction of time-resolved emission spectra (TRES) and conversion of TRES time-resolved area normalised emission spectra (TRANES) are also described briefly in this chapter.

Chapter 3: This chapter deals with the PET studies carried out in pluronic micellar media involving organic donor-acceptor systems.^{1-5,14-16} In the present study, the aromatic amine, N,N-dimethylaniline (DMAN) is used as the electron donor and coumarin dyes, namely coumarin 151 (C151), coumarin 152 (C15), coumarin 153 (C153), coumarin 481 (C481) and coumarin 522 (C522) are used as the electron acceptors.

Present study involving PET reaction was carried out with two main objectives, (i) to explore if Marcus inversion (MI) can be realized for bimolecular ET reactions in the micellar media which is known to be elusive in homogeneous media and (ii) to understand the effect of different micellar microenvironments on the energetics and dynamics of the ET reactions. In this study aqueous micelles of the pluronic F88 (EO₁₀₃-PO₃₉-EO₁₀₃) has been used as the reaction media and observed results have been compared with those reported earlier in pluronic P123 (EO₂₀-PO₇₀-EO₂₀) micelle where, (EO)_n and (PO)_n denote the poly(ethylene oxide) and poly(propylene oxide) blocks of the pluronics, also called the tri-block copolymers. Fluorescence-quenching experiments for a series of coumarin dyes by DMAN quencher were carried out and the quenching constant (k_q^{TR}) obtained from time-resolved (TR) measurements were correlated with the free energy changes (ΔG^0) of the ET reactions. The correlation interestingly displayed a clear MI behavior and onset of MI is observed at $-\Delta G^0 \sim 0.77$ eV, which is much lower than the solvent reorganization energy ($\lambda_s \sim 1$ eV) in the present micellar medium. It is realized that in the restricted reaction environment of F88 micelles, MI is

observed easily because of the suppression of the reactants diffusion (due to high viscosity and reactant entanglement) and the partial contribution of the solvent reorganization energy (due to slow solvent relaxation).

The results of solvation dynamics studies showed that corona of pluronic F88 is relatively more hydrated than that of P123 and this is due to the presence of more labile water molecules in the former case as a consequence of its higher EO/PO ratio. Time-resolved rotational relaxation study also showed that increase in the EO/PO ratio of F88 results in a decrease in the microviscosity of the corona region compared to that of P123. In accordance with these results, the ET kinetics in the F88 micelles is found to be relatively faster as compared to that in P123 micelles. The observation that the onset of MI appears at $-\Delta G^0 \sim 0.77$ eV in F88 micelles in comparison to $-\Delta G^0 \sim 0.68$ eV in P123 micelle is also in accordance with the faster solvation dynamics and rotational relaxation dynamics in the former micelle than in the latter. From the present study, it is evident that by changing the EO/PO ratio of the pluronics it is possible to tune the kinetics and dynamics of the PET reactions quite effectively to enhance the PET efficiency for better utilization.

Chapter 4: In this chapter we present the results of PET studies carried out in composite supramolecular assemblies (mixed micelles) comprising of a pluronic copolymer (P123 or F88) and a cationic surfactant (CTAC: cetyltrimethylammonium chloride),¹⁸ involving an anionic acceptor (A), coumarin-343 (C343), and a neutral donor (D), (DMAN); following fluorescence quenching measurements. The aim of the present study is to see if ET rates can be modulated by changing the composition of the mixed micelles. Observed results in fact indicate a systematic increase in the ET mediated quenching rates for the studied D-A system with an increase in the CTAC to pluronic molar ratio in the composite assemblies, demonstrating a large modulation in the ET rates. Present mixed micellar systems are formed such that the hydrocarbon chains of CTAC get embedded into the poly-PO core of the pluronic micelles while the cationic surfactant head groups are placed at the periphery of the micellar core, protruded into the hydrated poly-EO corona region, leading to the formation of a positively charged layer deep inside these mixed micelles. Thus, the anionic C343 dye, initially dissolved at the micelle-water interface, experiences a gradually increasing electrostatic attraction and thereby systematically dragged deeper inside the micellar corona, as the CTAC composition is increased in the mixed micellar systems.¹⁸ As DMAN donor is a neutral and relatively hydrophobic molecule, it is preferentially solubilized at the deeper region of the micellar corona than at the micelle-water interface. Accordingly, while the C343 acceptor is dragged deeper into the micellar corona, it encounters an increased concentration of DMAN and hence undergoes an enhanced ET kinetics. Therefore, a large modulation in the ET rates can be achieved just by changing

the surfactant to pluronic ratio in the mixed micellar system, a strategy very easy to be implemented and can be extremely useful to enhance the desired effect following PET reaction.

Chapter 5: In the present work, PET studies were carried out using chromophoric molecules, namely coumarin dyes, as one of the reactants, for which a complete photophysical characterization is important to ascertain that observed PET results are not influenced by any unusual photophysics of the dyes. Among the 7-N,N-dialkylaminocoumarin dyes used in the PET studies discussed in chapter 3 and 4, the dye C481 is known to display an efficient intramolecular charge transfer (ICT) state to twisted intramolecular charge transfer (TICT) state conversion process, exhibiting very low fluorescence quantum yield (Φ_f) and fluorescence lifetime (τ_f) values in polar solvents.¹⁴ Evidently such low Φ_f and τ_f values makes the C481 dye quite susceptible towards PET results if any unusual solution behavior has any influence on the PET reaction. For some coumarin derivatives unusual aggregation has been reported in the literature in polar solvent environments.¹⁹ Anticipating a similar aggregation for the coumarin dyes used in the PET investigations, we thus carried out detailed photophysical properties of two selective dyes, one having TICT characteristics, namely C481, and the other devoid of TICT process, namely coumarin 153 (C153), in polar organic and aqueous solutions.

For C481 dye in polar organic solvents, namely protic ethanol (EtOH) and aprotic acetonitrile (ACN), Concentration, temperature and wavelength dependent fluorescence decays and TRES and TRANES analysis clearly suggest the coexistence of dye monomers and small extent of dye aggregates in the studied solutions. Due to efficient ICT to TICT conversion, the dye monomers show significantly shorter fluorescence lifetime (~ 0.64 - 0.68 ns) in both the solvents. The fluorescence lifetimes of the aggregates show longer lifetimes than the monomers as the ICT to TICT conversion is sterically hindered in the aggregated state. It is observed that there is a systematic increase in the lifetime of the aggregated species on the dilution of the dye solution, arises due to the conversion of the higher aggregates (~ 1.2 ns) mainly to dye dimers. TRES and TRANES show that the emission spectra of the aggregates are substantially blue shifted, suggesting the H-type aggregation of the dye in the solution. Important aspect of the present study is that unlike the most other dyes, the H-aggregates of the present dye are fluorescent in nature, which is quite an unusual observation.^{14,19}

Following the aggregation of C481 dye in polar organic solvents, the studies were further extended in aqueous solution. Concentration, temperature and wavelength dependent fluorescence decays and TRES and TRANES analysis supports the coexistence of dye monomers, dimers and some higher dye aggregates (mostly trimers) in the aqueous solution. Like in polar organic solvents, the dye monomers show very short fluorescence lifetime, ~ 0.2 ns, due to efficient ICT to TICT conversion. Fluorescence lifetimes of dimers (~ 4.1 ns) and higher aggregates (~ 1.4 ns) are relatively

longer as expected due to steric constrain towards ICT to TICT conversion. In the present case also the aggregates are of H-type, as evidenced from the blue shift in the TRES and TRANES.

With intriguing findings of C481, studies were then carried out with C153 dye in two polar organic solvents, ACN and EtOH. Unlike C481, no unusual behavior was observed for C153 in aprotic ACN, suggesting the presence of only monomeric C153 in ACN solution. Unlike ACN solution, multiple emitting species were observed for C153 dye in protic EtOH solvent. The nature of the concentration, temperature and wavelength dependent fluorescence decays and the TRES and TRANES analysis demonstrated the coexistence of smaller and larger H-type of dye aggregates in EtOH solution along with the dye monomers. Lifetimes of the aggregates ($\tau_1 \sim 0.04$ ns for larger aggregates and $\tau_2 \sim 1.4$ ns for smaller aggregates) are much smaller for the present dye than its monomer lifetime ($\tau_3 \sim 4.8$ ns). This is because even in the monomeric form the dye is devoid of TICT formation and hence is having a longer lifetime and in the aggregated state the nonradiative internal conversion process becomes faster with the degree of aggregation.

It is understood from the present study that the highly dipolar character of coumarin dyes (dipole moment ~ 6 D) drives the aggregation process through strong electrostatic dipole-dipole interaction and hence is favored in polar solvents. The emissive nature of the H-aggregates for the studied dyes is also ascribed to the same dipole-dipole interaction which helps to overcome the restriction on the electronic transitions in H-aggregates arising from Kasha's exciton theory.¹⁹ Protic nature of the solvents, e.g. EtOH and water, evidently assists the aggregation via hydrogen bonding,¹⁴ which is supported by scanning electron microscopy results.

Chapter 6: This last chapter of the thesis describes the studies on PET and CT interactions of $\text{Ln}^{3+}/\text{UO}_2^{2+}$ ions as electron acceptors with diphenylamine (DPA) dye as the electron donor. The studies have been carried out in aqueous solution under diffusive condition using both steady-state (SS) and time-resolved (TR) fluorescence quenching measurements.¹⁴ Formation of ground state CT complexes in the present systems is very evident from the ground state absorption studies. SS fluorescence measurements indicate that there is no emissive exciplex formation in the present systems. SS fluorescence quenching results, however, indicate quite strong static quenching, attributed to ground state CT complex formation. TR fluorescence quenching studies indicate quite efficient dynamic quenching as well for the present systems. Hence, k_q^{TR} were estimated from TR fluorescence measurements. Two mechanisms can be anticipated for the observed dynamic fluorescence quenching, namely, energy transfer from excited DPA to $\text{Ln}^{3+}/\text{UO}_2^{2+}$ ions or PET from DPA to $\text{Ln}^{3+}/\text{UO}_2^{2+}$ ions. Auxiliary SS and TR fluorescence measurements in relation to the possible energy transfer from excited DPA to lanthanides negate the possibility. Excluding energy transfer, the other probable quenching mechanism anticipated is the PET from DPA to $\text{Ln}^{3+}/\text{UO}_2^{2+}$ ions. The

direct evidence for this PET mechanism has been obtained from laser flash photolysis measurements in the present study. Thus, the transient absorption band observed around 670 nm for the DPA-lanthanide systems clearly establishes the DPA cation formation,²⁰ ascertaining the PET mechanism in the studied systems. Time constant for the growth of DPA cation also confirms that the PET occurs from the excited single state (S_1) of DPA to Ln^{3+} ions, which is thus responsible for the fluorescence quenching observed in the studied systems.

REFERENCES

1. G. J. Kavarnos, *Fundamentals of Photoinduced Electron Transfer*, VCH Publishers, New York, **1993**.
2. *Electron Transfer in Chemistry*, V. Balzani (Ed.), Wiley-VCH Publishers Inc., New York, **2001**, Vol. I to V.
3. *Electron Transfer from Isolated Molecules to Biomolecules*, J. Jortner, M. Bixon (Eds.), *Advances in Chem. Phys.* Wiley, New York, **1999**, Parts 1 & 2, Vols. 106 and 107.
4. *Electron Transfer in Inorganic, Organic and Biological Systems*, J. R. Bolton, N. Mataga, G. L. McLendon (Eds.), American Chemical Society, Washington, DC, **1991**.
5. M. Gratzel, *Heterogeneous Photochemical Electron Transfer*, CRC Press, Boca Raton, FL, **1989**.
6. L. Stryer, *Biochemistry*, 3rd Edn., Freeman, San Francisco, **1995**.
7. S. J. Formosinho, L. G. Arnaut, R. Fausto, *Prog. Reac. Kin.*, **1998**, *23*, 1.
8. R. D. J. Miller, G. L. McLendon, A. J. Nozik, W. Schmickler, F. Willig, *Surface Electron Transfer Processes*, VCH Publishers, Inc., New York, **1995**.
9. M. Gratzel, *Coord. Chem. Rev.*, **1991**, *111*, 167.
10. N. Serpone, E. Pelizzetti, *Photocatalysis: Fundamentals and Applications*, Wiley, New York, **1989**.
11. P. V. Kamat, D. Meisel, *Semiconductor Nanoclusters: Physical, Chemical and Catalytic Aspects*, Elsevier, Amsterdam, **1997**.
12. H. Weller, A. Eychmuller, *Semiconductor Nanoclusters-Studies in Surface Science and Catalysis*, P. V. Kamat, D. Meisel (Eds.), Elsevier Science, **1996**, *103*, 5.
13. R. A. Marcus, N. Sutin, *Biochim. Biophys. Acta*, **1985**, *811*, 265.
14. J. R. Lakowicz, *Principle of Fluorescence Spectroscopy*, 3rd ed.; Spinger: New York, 2006.
15. K. Kalyansundaram, *Photochemistry in Microheterogeneous Systems*, Academic Press, Orlando, **1987**.
16. H. Sumi, R. A. Marcus, *J. Chem. Phys.*, **1986**, *84*, 4894.
17. O'Connor, D. V.; Philips, D., *Time correlated single photon counting*; Academic press: New York, **1984**
18. P. K Singh, M. Kumbhakar, H. Pal, S. Nath, *J. Phys. Chem. B* **2009**, *113*, 1353-1359
19. M. Cigan, J. Donovalova, V. Szocs, J. Gaspar, K. Jakusova, A. Gaplovsky, *J. Phys. Chem. A*. **2013**, *117*, 4870-4883.
20. T. Shida, *Electronic Absorption Spectra of Radical Ions*, Elsevier, Amsterdam, 1988 (in physical science data)

LIST OF FIGURES

Figure No.	Figure Caption	Page No.
Figure 1.1	Schematics of dark and photoinduced electron transfer (PET) reactions	2
Figure 1.2	Jablonski diagram for an electronically excited molecule	3
Figure 1.3	Schematic free energy diagram for electron transfer (ET) reactions	4
Figure 1.4	Changes of ET rates vs free energy change by Marcus ET theory	6
Figure 1.5	Schematics of electronic coupling for an ET reaction	8
Figure 1.6	Involvement of multichannel free energy surfaces for ET reaction	9
Figure 1.7	Asymmetric Marcus correlation plot for ET reactions	9
Figure 1.8	Schematic free energy diagram for two-dimensional ET (2DET) reactions	11
Figure 1.9	Conceptual drawing of the hybrid ET reaction.	13
Figure 1.10	Schematics of dynamic fluorescence Stokes shifts by solvent relaxation	16
Figure 1.11	Schematics of formation of block copolymer-surfactant mixed micelles	22
Figure 1.12	Schematic diagram for dye aggregation and Kasha's exciton theory	23
Figure 2.1	Schematics of a double beam UV-vis spectrophotometer	30
Figure 2.2	Schematics of a steady-state fluorescence spectrometer	31
Figure 2.3	Schematics of a time correlated single photon counting spectrometer	34
Figure 2.4	Conceptual presentation of creation of anisotropy by polarized excitation	38
Figure 2.5	Schematic diagram for the measurement of fluorescence anisotropy	38
Figure 2.6	Schematics of a femtosecond fluorescence	40
Figure 2.7	Conceptual presentation of sum-frequency regeneration & detection	41
Figure 2.8	Block diagram of a nanosecond laser kinetic spectrometric setup	42
Figure 3.1	Fluorimetric and DLS measurements of the CMT of F88 micelle	49
Figure 3.2	Fluorescence spectral changes of C153 dye in different solvent media	50
Figure 3.3	Wavelength dependent fluorescence kinetic traces and constructed time-resolved emission spectra (TRES) for C153 dye in F88 solution	52
Figure 3.4	Fluorescence anisotropy decay for C153 dye in F88 solution	53
Figure 3.5	Steady-state (SS) fluorescence quenching and Stern-Volmer plots for coumarin-DMAN systems in F88 micellar solution	55
Figure 3.6	Time-resolved (TR) fluorescence quenching and Stern-Volmer plots for coumarin-DMAN systems in F88 micellar solution	56
Figure 3.7	The $\ln(k_q)$ vs ΔG^0 plot for the coumarin-amine systems in F88 solution	59
Figure 4.1	Absorption and fluorescence spectra of C343 dye in different solvents	68

Figure 4.2	SS and TR fluorescence of C343 in CTAC-P123 mixed micelles	69
Figure 4.3	Fluorescence decays, absorption spectra and fluorescence spectra of C343 in EtOH-water solvent mixtures	70
Figure 4.4	SS fluorescence quenching and Stern-Volmer plots for C343-DMAN system in P123 micellar solution	71
Figure 4.5	TR fluorescence quenching for C343-DMAN system in pure P123 and CTAC-P123 mixed micellar systems	73
Figure 4.6	TR fluorescence quenching for C343-DMAN system in pure F88 and CTAC-F88 mixed micellar systems	73
Figure 4.7	TR fluorescence quenching for C343-DMAN system in CTAC-P123 and CTAC-F88 mixed micelles with changing CTAC to pluronic molar ratios	74
Figure 4.8	Changes in the fluorescence lifetime of C343 with DMAN concentrations and CTAC to pluronic ratios in CTAC-P123 and CTAC-F88 micelles	75
Figure 4.9	Stern-Volmer plots at different CTAC to pluronic molar ratios in CTAC-P123 and CTAC-F88 mixed micelles	76
Figure 4.10	K_{SV} vs CTAC to pluronic molar ratio plots in CTAC-pluronic micelles	77
Figure 5.1	Concentration dependent absorption spectra of C481 dye in ethanol (EtOH) and acetonitrile (ACN) solutions	88
Figure 5.2	Concentration dependent fluorescence spectra of C481 dye in EtOH and ACN solutions	88
Figure 5.3	Peak normalized fluorescence spectra of C481 dye for different excitation wavelengths in EtOH and ACN solutions	89
Figure 5.4	Peak normalized excitation spectra of C481 dye for different emission wavelengths in EtOH and ACN solutions	89
Figure 5.5	Concentration dependent fluorescence decays of C481 dye in EtOH solutions at blue edge and at emission peak of the dye	90
Figure 5.6	Concentration dependent fluorescence decays of C481 dye in ACN solutions at blue edge and at emission peak of the dye	90
Figure 5.7	Wavelength dependent fluorescence decays of C481 dye in ETOH and ACN solutions	96
Figure 5.8	TRES and TRANES for C481 dye in EtOH solution	96
Figure 5.9	TRES and TRANES for C481 dye in ACN solution	96
Figure 5.10	Concentration dependent absorption & fluorescence spectra of C481 dye in aqueous solution	98
Figure 5.11	Concentration dependent changes in the absorbance and fluorescence intensity for C481 dye in aqueous solution.	99
Figure 5.12	Peak normalized excitation and emission spectra of C481 dye in aqueous solution for different emission and excitation wavelengths, respectively.	99
Figure 5.13	Concentration dependent fluorescence decays of C481 dye at 460 nm	100
Figure 5.14	Wavelengths dependent fluorescence decays of C481 in aqueous solution	103
Figure 5.15	TRES and TRANES for C481 dye in aqueous solution	103

Figure 5.16	Temperature-dependent decays of C481 dye in aqueous solution	105
Figure 5.17	Ultrafast fluorescence kinetic traces for C481 dye in water and water-ACN mixed solvent from up-conversion measurements	106
Figure 5.18	Absorption and fluorescence spectra for supersaturated solution of C481 dye in water	108
Figure 5.19	SS fluorescence spectra and peak normalized excitation spectra of C153 dye in EtOH	110
Figure 5.20	Wavelength dependent fluorescence decays of C153 dye in ACN and EtOH solutions	111
Figure 5.21	Concentration dependent fluorescence decays of C153 dye in ACN and EtOH solutions	111
Figure 5.22	TRES and TRANES for C153 dye in EtOH solution	114
Figure 5.23	Temperature dependent fluorescence decays of C153 in EtOH solution	115
Figure 5.24	Fluorescence anisotropy decays of C153 dye in ACN and EtOH solutions	116
Figure 5.25	Ultrafast fluorescence kinetic traces for C153 dye in ACN and EtOH solutions	117
Figure 5.26	SEM images of the microfilms from C153 in ACN and EtOH solutions	118
Figure 5.27	Comparison of fluorescence decays of C153 dye in TFE and EtOH solutions and wavelength dependent decays in TFE solution	119
Figure 5.28	Concentration dependent absorption and fluorescence spectra of C153 dye in aqueous solution	120
Figure 5.29	Peak normalized excitation and emission spectra of C153 dye in aqueous solution for different emission and excitation wavelengths respectively	120
Figure 5.30	TRES and TRANES for C153 dye in aqueous solution	121
Figure 6.1	Changes in the absorption characteristics of DPA with Eu^{3+} concentration in aqueous solution	128
Figure 6.2	SS and TR fluorescence quenching of DPA by Eu^{3+} in aqueous solution	131
Figure 6.3	Stern-Volmer plots from TR quenching for DPA- $\text{Ln}_3^+/\text{UO}_2^{2+}$ systems	131
Figure 6.4	SS emission spectra of Ln^{3+} ions with DPA addition and Ln^{3+} excitation	133
Figure 6.5	Transient absorption spectra for DPA/ Eu^{3+} system following LFP	134
Figure 6.6	Decay and growth kinetic traces for DPA cation in DPA/ Ln^{3+} systems	135
Figure 6.7	Conceptual single and multi-channel ET reactions in DPA/ Ln^{3+} systems	136
Figure 6.8	SS fluorescence results in DPA- Ln^{3+} systems for sensitized Ln^{3+} emissions	137
Figure 6.9	DPA concentration dependent TRES for Ln^{3+} emissions in DPA- Ln^{3+} systems following DPA excitation	138
Figure 6.10	Potential energy diagram of Ln^{3+} ions suggesting multichannel ET	139
Figure 6.11	Changes in the absorption spectra of DPA by Eu^{3+} in ACN solution	140
Figure 6.12	SS and TR fluorescence quenching of DPA by Eu^{3+} in ACN solution	141

LIST OF TABLES

Table No.	Table Caption	Page No.
Table 3.1	Solvation and rotational parameters for C153 in F88 and P123 solutions	52
Table 3.2	Quenching constants and ET parameters for coumarin-DMAN systems	58
Table 4.1	Parameters related to the estimation of the $[DMAN]_{eff}^{av}$ values	66
Table 4.2	Absorption and fluorescence parameters of C343 dye in different solutions	69
Table 5.1	Fluorescence decay parameters for C481 dye in EtOH and ACN solutions	94
Table 5.2	Fluorescence decay parameters for C481 dye in aqueous solution	100
Table 5.3	Temperature-dependent decay parameters for C481 in aqueous solution	105
Table 5.4	Ultrafast fluorescence decay analysis results for C481 dye	107
Table 5.5	Fluorescence decay parameters for C153 dye in EtOH solution	112
Table 5.6	Temperature-dependent decay parameters for C153 dye in EtOH solution	115
Table 6.1	Electron configurations of lanthanides and redox potentials of Ln^{3+} ions	125
Table 6.2	Formation constants for DPA- Ln^{3+} CT complexes in aqueous medium	130
Table 6.3	Quenching constants of DPA- Ln^{3+}/UO_2^{2+} systems in aqueous solution	132
Table 6.4	Quenching constants for the DPA- Ln^{3+} systems in acetonitrile solution	141

LIST OF CHARTS & SCHEMES

Sr. No.	Description of the Charts & Schemes	Page No.
Chart 3.1	Structures of coumarin acceptors and DMAN donor used in the study	47
Scheme 4.1	Molecular structures of the acceptor, donor, pluronics & surfactant used	67
Scheme 4.2	Pictorial presentation of the cationic layer formation and its assistance to drag the probe dye in the CTAC-pluronic mixed micellar systems	74
Scheme 5.1	Conceptual presentation of the stacking of two dye molecules in H-aggregate formation with antiparallel orientation of permanent dipoles	92

GLOSSARY

ET	Electron transfer	Σ	Electron-vibrational coupling strength
ID	Ion dissociation	EtOH	Ethanol
T	Absolute temperature	EO	Ethyleneoxide
A	Acceptor	E_{00}	Excitation energy of the photoinduced reactant
ACN	Acetonitrile	G_P	Free energy of the Product
ΔG^*	Activation free energy	G_R	Free energy of the reactant
κ_{ad}	Adiabaticity parameter	ν_n	Frequency of nuclear motion along the transition state
N_{agg}	Aggregation number	ν_h	Frequency of the concerned high-frequency vibrational mode
ADC	Analog-to-Digital converter	FWHM	Full-width half-maximum
PD	Avalanche photodiode	IC	Internal conversion
BET	Back electron transfer	ISC	Intersystem crossing
BBO	Beta barium borate	λ_i	Intramolecular reorganization energy
k_B	Boltzmann's constant	ICT	Intramolecular charge transfer
CTAC	Cetyl triethylammonium chloride	IVR	Intramolecular vibrational relaxation
Δq	Change in the equilibrium nuclear coordinate	LFP	Laser flash photolysis technique
CR	Charge recombination	LED	Light-emitting diode
CT	Charge transfer	V_{el}	Magnitude of the electronic-coupling strength between the reactant and the product states
RX	Chemical reaction	MCP-PMT	Micro-channel plate PMT
CFD	Constant fraction discriminator	MCA	Multichannel analyzer
C151	Coumarin 151	DMAN	N,N-dimethylaniline
C152	Coumarin 152	k_{nr}	Nonradiative decay rate constants
C153	Coumarin 153	κ_N	Nuclear reorganization factor
C343	Coumarin 343	OD	Optical density
C481	Coumarin 481	n	Optical dielectric constant
C522	Coumarin 522	PET	Photoinduced electron transfer
CMC	Critical micelle concentration	PMT	Photomultiplier tube
CMT	Critical micelle temperature	PPO	Polypropylene oxide polymer
CV	Cyclic voltametry		
D	Donor		
(D-A) pairs	Donor-acceptor pairs		
DLS	Dynamic light scattering		

κ_{cl}	Probability of crossing of the reactant state to the product state at TS configuration	K_{SV}	Stern-Volmer constant
P	Product	τ_s	Time constant for solvent relaxation dynamics
PO	Propyleneoxide	TR	Time resolved
Φ_f	Quantum yield of fluorescence	TAC	Time to Amplitude Converter
Q	Quencher	TCSPC	Time-correlated single photon counting spectrometer
k_r	Radiative decay rate constant	TRANES	Time-resolved area normalized emission spectra
r_A	Radius of the acceptor	TRES	Time-resolved emission spectra
r_D	Radius of the donor	λ	Total reorganization energy
k_{et}	Rate constant of the ET reaction	TS	Transition state
R	Reactant	TFE	2,2,2-trifluoroethanol
SEM	Scanning electron microscope	TX100	Triton-X-100
SDS	Sodium dodecyl sulphate	TICT	Twisted intramolecular charge transfer
λ_s	Solvent reorganization energy	2DET	Two-dimensional ET
ΔG^0	Standard free energy change	VR	Vibrational relaxation
ϵ	Static dielectric constant		
SS	Steady state		
SV	Stern-volmer		

Chapter 1

General Introduction: Basic Aspects of Photophysical Processes and Electron Transfer Reactions

Abstract

Electron transfer (ET) and charge transfer (CT) reactions are the most fundamental processes in chemistry, biology and geology. Knowledge of the various parameters that govern and modulate the ET and CT reactions play the utmost roles in designing such reactions for the desired applications. Photoinduced electron transfer (PET) reaction is the most useful experimental scheme to investigate the dynamics and mechanism of ET reactions. In the present study, PET and CT reactions have been investigated in both homogeneous and heterogeneous media, aiming towards the understanding of the kinetic and mechanistic insight of the studied reactions and also to find methodologies in modulating these reactions, especially in heterogeneous media. This introductory chapter of the thesis describes the fundamental aspects of ET reactions, giving a brief theoretical background of the energetic and kinetic correlations of these processes. The photophysical characteristics of the chromophoric systems that are directly related to the PET processes investigated in the present work are also discussed in short. A brief account of the aspects of solvation relaxation process is also discussed in this chapter, as the ET reactions in condensed phase are directly coupled to the energetics and dynamics of the solvation process. Since a significant part of the present study deals with the PET reactions in microheterogeneous media, this chapter also describes the general aspects of micellar and mixed micellar assemblies, used as the reaction media in present work. As the possibility of aggregation of the chromophoric acceptor dyes used in our PET studies has also been investigated extensively, basic aspects of dye aggregation with respect to their absorption and fluorescence characteristics are also briefly discussed in this chapter. The objective and motivation of the present research work is presented in short at the end of this chapter.

1.1. Photoinduced Processes

Photochemistry is concerned with reactions which are initiated by electronically excited molecules produced by the absorption of suitable radiation in the visible and near ultraviolet region of the electromagnetic spectrum.¹⁻⁴ Absorption of photon makes some of the reactions to be feasible that do not take place in dark. This happens because the energy acquired in the photoexcitation process favorably adds to the overall energy changes of the reaction.⁵⁻¹¹ The situation is schematically shown in Figure 1.1. In this Figure, case (a) represents a kinetically slow dark reaction because of low exergonicity ($-\Delta G^\circ$) but unusually fast photoinduced reaction because of large exergonicity. Case (b) in Figure 1.1 corresponds to a reaction that cannot take place in dark because of positive ΔG° but light absorption makes the reaction thermodynamically feasible, with negative ΔG° value.⁵⁻¹¹

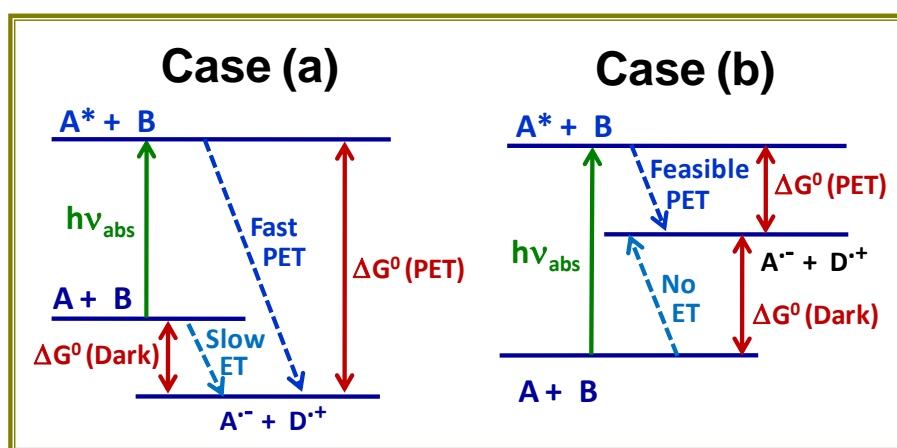


Figure 1.1: Schematic representation of the two possible energetic situations for electron transfer reactions in dark and under photoexcitation conditions.

Absorption of UV and visible light results in the excitation of molecules to the higher electronic state. Different relaxation processes that these excited molecules can undergo include internal conversion (IC), intersystem crossing (ISC), intramolecular vibrational relaxation (IVR), vibrational relaxation (VR) through thermal bath, radiative decay (fluorescence and phosphorescence), solvent reorganization, bond reorganization, bond breaking, bond formation, proton/electron/energy transfer, etc. The schematic representations of the important photophysical relaxation pathways for excited molecules are shown in Figure 1.2, which is commonly known as the Jablonski diagram. Different relaxation processes for excited molecules take place in a wide range of time scales, few femtoseconds to milliseconds. These time scales are dictated by the rapidity of the nuclear or electronic rearrangements that are associated with these processes. To understand the details of these

elementary processes it is necessary to monitor the species in real time that are formed through photoexcitation and are short lived. With the advent of various time-resolved (TR) spectroscopic techniques it is now possible to study the dynamics of the elementary processes even with a sub-picosecond time resolution¹⁻⁴

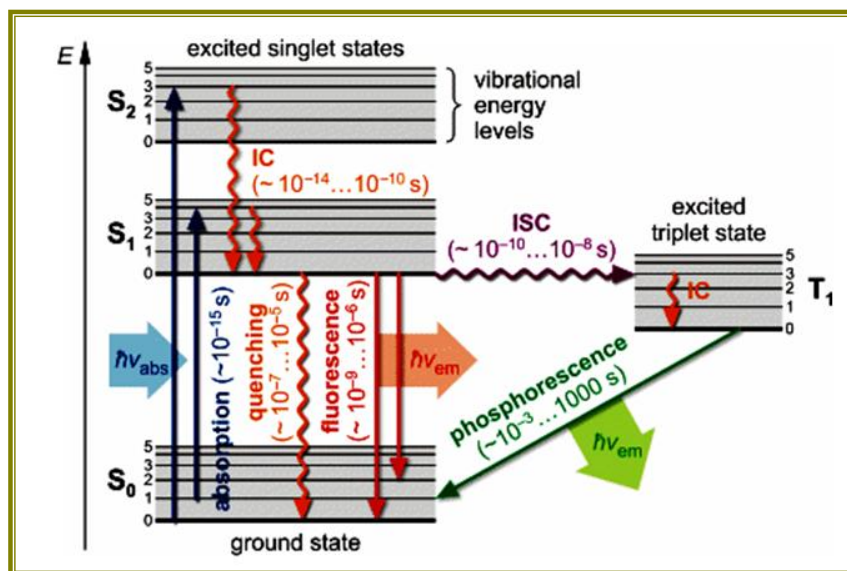


Figure 1.2: Jablonski diagram, showing different photophysical processes for an electronically excited molecule along with their timescales. Straight arrows and wavy arrows represent the radiative and nonradiative processes, respectively; IC: Internal Conversion; ISC: Intersystem Crossing.

In the present research our major focus is to understand the kinetic and energetic correlations of an important photoinduced reaction, namely, the bimolecular photoinduced Electron Transfer (PET) reaction, following the most commonly used photophysical technique of fluorescence quenching, both in micellar media and in homogeneous solutions. The reactant dye molecules used in the PET studies are also photophysically characterized to understand any unusuality in their solution behavior, especially their aggregation in solution. In the following we briefly describe of the important photoinduced processes that are the essential parts of the research work reported in this thesis.

1.2. Electron Transfer Reaction: Theoretical Background

Understanding various factors that govern and control the rates of chemical reactions is an important and thrust area of research in chemistry and more specifically in chemical physics. Among diverse chemical reactions, electron transfer (ET) is undoubtedly the most simplest and fundamental reaction. ET is the key step in many biological processes that have enormous relevance to life, for example, photosynthesis and respiration.⁵⁻¹³ It is also a

fundamental step in countless processes of vast technological applications related to information storage, solar energy conversion, photovoltaic, biotechnology, solid state electronics, molecular electronics, sensing, catalysis, and many others.⁵⁻²¹ ET is in fact ubiquitous in chemistry and biology. In 1992, Prof. R. A. Marcus was awarded with the Nobel Prize for his outstanding contribution in theoretically relating ET rates with the free energy changes of the reactions.²¹⁻²⁶ In order to understand the efficiency and dynamics of ET processes, one needs to know the following important aspects, (i) electronic coupling between the ET partners, (ii) energetics for the condition of electronic resonance, and (iii) the barrier crossing dynamics. These three aspects are essential for both homogeneous and heterogeneous ET reactions.

1.2.1. Marcus Classical ET Theory. For ET reactions, a simple but an unusually important theoretical formalism has been developed by Prof. Marcus in 1956, which describes ET rates in terms of a small number of experimentally accessible parameters.^{5-10,21-24} Marcus classical ET theory is based on two important concepts, namely, the Franck-Condon principle and the law of conservation of energy. According to this theory, ET takes place only at the transition state (TS; *cf.* Figure 1.3), where the nuclei of the reactant and product states do not undergo any displacement during ET and accordingly energy of the system remains conserved.^{5-10,21-31}

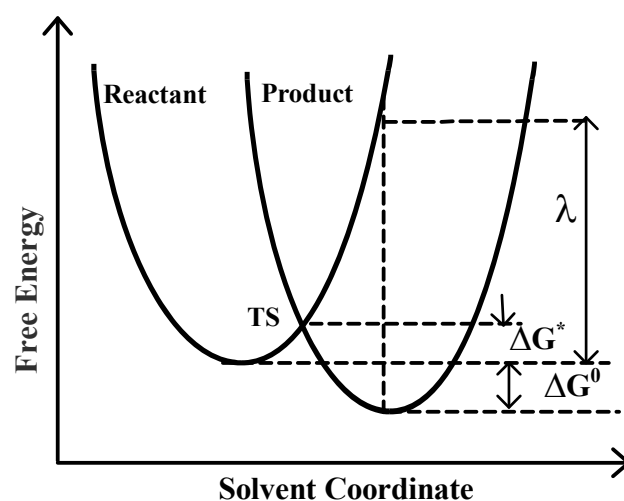


Figure 1.3: Free energies of the reactant and product states involved in the ET reaction. ΔG^0 is the free energy change, ΔG^* is the free energy of activation and λ is the total reorganization energy. T.S. represent the transition state.

Marcus considered that the free energies of the reactant and product states, G_R and G_P , respectively, for the ET reaction, are the quadratic functions of a generalized reaction

coordinate, which in principle is synonymous to the solvent polarization coordinate. Thus, G_R and G_P , and their crossing at the transition state (T.S.) can pictorially be shown as in Figure 1.3, where ΔG^* is the activation free energy, ΔG^0 is the standard free energy change and λ is the total reorganization energy composed of both solvent (λ_s) and intramolecular (λ_i) reorganization energies. To be mentioned here that the reactant and product states in the present context are consisting of the reacting species along with their solvent surroundings, which in effect are the supramolecular systems.^{5-10,21-31}

Thermal fluctuations in the nuclear and solvent coordinates effectively lead the reactant to reach the T.S. state. Thus, ET basically is a free energy surface crossing process, equivalent to other chemical reactions. In classical theory, it is assumed that during ET the distribution of both the reactant and the product states maintain a thermal equilibrium along the reaction coordinate.^{5-10,21-31} This means that relaxations along nuclear and solvent coordinates are much faster than ET rates. In this theory, it is further assumed that the reacting system once reaches the T.S., it just slides to the product state with unit probability. In other words, the reactive trajectories cross the energy barrier only once on the free energy surface. Once the reactant state crosses the TS region, the product state is necessarily formed with excess energy. However, the latter quickly dissipates its excess energy to the surrounding solvent bath⁵⁻¹⁰ and thus attains the equilibrium product state very quickly.

According to classical ET theory, the rate constant of the ET reaction (k_{et}) is given by the product of three governing factors; (i) the frequency (ν_n) of nuclear motion along the TS, (ii) the probability (κ_{el}) of crossing of the reactant state to the product state at TS configuration, and (iii) the nuclear reorganization factor (κ_N).^{5-10,21-31}

$$k_{et} = \nu_n \kappa_{el} \kappa_N \quad (1.1)$$

The parameter ν_n is usually very high, of the order of about 10^{13} s^{-1} . The factor κ_{el} depends on the electronic coupling of the reacting species. In the classical theory, this factor is considered to be unity for simplicity. The nuclear reorganization factor κ_N is determined by the activation free energy (ΔG^*) for the ET reaction, and is expressed as,^{5-10,21-31}

$$\kappa_N = \exp\left(\frac{-\Delta G^*}{k_B T}\right) \quad (1.2)$$

where k_B is the Boltzmann's constant and T is the absolute temperature. In classical Marcus theory, not only the G_R and G_P surfaces are considered to be quadratic but also their force constants are considered to be the same (equal curvatures). With this assumption, ΔG^* can be expressed in terms of the ΔG^0 and λ parameters of the ET reaction as,^{5-10,21-31}

$$\Delta G^* = \frac{(\Delta G^0 + \lambda)^2}{4\lambda} \quad (1.3)$$

where, $\lambda = \lambda_i + \lambda_s$ (1.4)

Physically, λ_i is the measure of the reorganization in the intramolecular vibrational modes for going from the reactant to the product states via ET reaction, and is given by,^{5-10,21-31}

$$\lambda_i = \frac{1}{2} \sum_j f_j (\Delta q_{eq,j})^2 \quad (1.5)$$

where f_j is the force constant and $\Delta q_{eq,j}$ is the change in the equilibrium nuclear coordinate for the j^{th} vibrational mode. These parameters can be obtained from vibrational spectroscopy and/or X-ray structures. The solvent reorganization energy, λ_s , is a measure of the rearrangement of the polar solvent around the reacting system following the ET reaction. A reasonable estimate for λ_s can be obtained by considering the reacting species (donors and acceptors) as the effective spheres and the solvent as the dielectric continuum. Thus, λ_s can be expressed as,^{5-10,21-31}

$$\lambda_s = \frac{e^2}{2} \left(\frac{1}{r_D} + \frac{1}{r_A} - \frac{1}{r} \right) \left(\frac{1}{n^2} - \frac{1}{\epsilon} \right) \quad (1.6)$$

where r_D , r_A , are the donor and acceptor radii, respectively, r is the distance between donor and acceptor, n is the refractive index and ϵ is the static dielectric constant of the solvent.

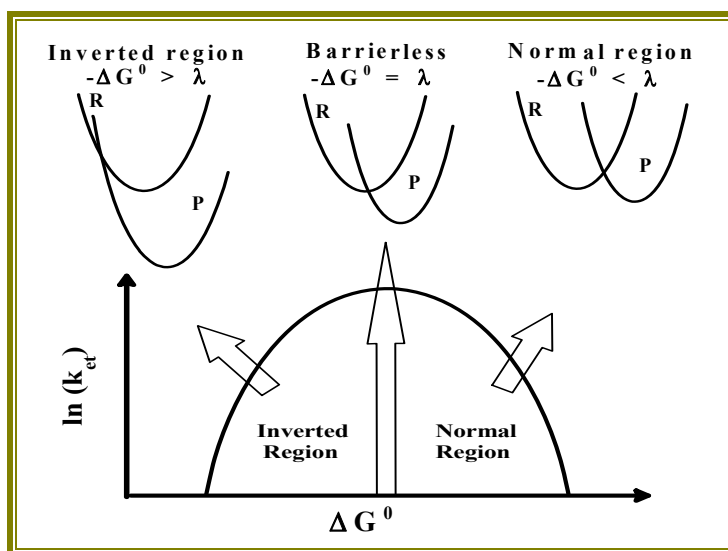


Figure 1.4: $\ln(k_{et})$ vs ΔG^0 plot, showing inversion in the ET rates as predicted by Marcus ET theory.

The most important prediction from Marcus ET theory is the inversion of the ET rates at the higher exergonicity region.⁵⁻¹¹ Figure 1.4 shows qualitatively the nature of dependence

of the ET rate constants on the free energy changes (ΔG^0) of the ET reactions. As shown in this figure, the ΔG^0 dependence of the ET rate constants can be classed into three regions: (i) $-\Delta G^0 < \lambda_s$ region, where reaction rate increases with an increase in the exergonicity ($-\Delta G^0$) and the region is termed as the normal Marcus region, (ii) $-\Delta G^0 = \lambda_s$ situation, where ET rate is the fastest (maximum) and the situation is called the Marcus barrierless condition (no activation barrier), (iii) $-\Delta G^0 > \lambda_s$ region, where reaction rate decreases with an increase in the exergonicity and the region is called the Marcus inverted region. Following Marcus ET theory, therefore, the ET rate constants should show a bell-shaped curve on plotting against ΔG^0 , as quantitatively shown in Figure 1.4. Although this bell-shaped curve was predicted by Marcus long back in mid fifties,²¹⁻²⁴ it took more than 25 years to obtain the first experimental evidence for this unique inversion behavior for the ET rates. It was Closs and Miller, who first demonstrated Marcus inversion behavior for the ET rates experimentally in 1984, using covalently linked donor-acceptor molecules as the reacting systems.³²⁻³⁵

1.2.2. Quantum Mechanical Refinement of Marcus ET Theory: Adiabatic and Non-adiabatic ET Reactions. Conceptually, quantum mechanical refinement of the Marcus ET theory stems from the basic rate equation as given by Eq. 1.1.^{5-11,25-31,36-48} Following quantum mechanical treatment, however, the transmission probability κ_{el} for the crossing of reactant state to product state at the TS configuration can have any value between 0 to 1, depending on the magnitude of the electronic-coupling strength (V_{el}) between the reactant and the product states, than just being equal to unity, as considered in the classical ET theory. The physical significance of the electronic-coupling strength V_{el} is shown in Figure 1.5, and it arises from the mixing of the reactant and product states at the crossing point, due to the quantum mechanical concept of avoid crossing of the potential energy surfaces. In quantum mechanical approach, the reactant (R) and product (P) states are considered as the supermolecules that include the reactants and products with their surrounding solvent shells as the whole which undergo changes during ET reaction. Moreover, in this treatment, the ET process is effectively considered as equivalent to the radiationless transition between the energy states of R and P. Depending on the magnitude of V_{el} , the concerned ET process can fall anywhere between a strongly nonadiabatic ET (i.e., $V_{el} \cong 0$) to a strongly adiabatic ET (roughly $V_{el} \geq 0.5$ kcal mol⁻¹), as are briefly described below.

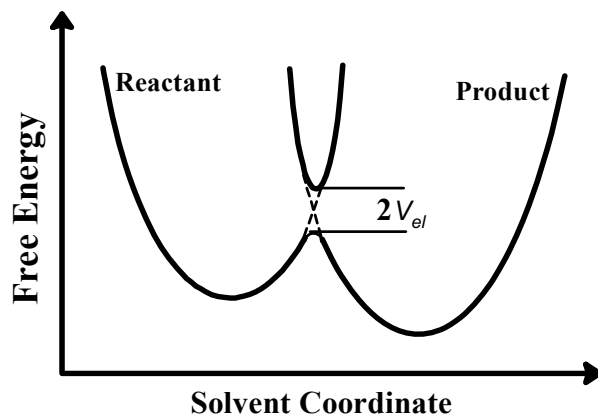


Figure 1.5: Pictorial representation of the electronic coupling matrix element V_{el} for an ET reaction.

Following quantum mechanical treatment, the rate constant for ET reaction can be expressed by the following generalized equation.^{5-11,25-31,36-48}

$$k_{et} = \frac{1}{1 + \kappa_{ad}} \left\{ \frac{2\pi}{h} \frac{V_{el}^2}{\sqrt{4\pi\lambda_s k_B T}} \exp\left(\frac{-\Delta G^*}{k_B T}\right) \right\} \quad (1.7)$$

where κ_{ad} is the adiabaticity parameter, a function of V_{el} , λ_s and solvation time (τ_s) as,³⁶⁻³⁸

$$\kappa_{ad} = \frac{4\pi V_{el}^2}{\hbar\lambda_s} \tau_s \quad (1.8)$$

Under the situation where V_{el} is very small, it implies that $\kappa_{ad} \ll 1$, and the rate constant for the corresponding nonadiabatic ET is given as,²⁵⁻⁴⁸

$$k_{NA} = \frac{2\pi}{h} \frac{V_{el}^2}{\sqrt{4\pi\lambda_s k_B T}} \exp\left(\frac{-\Delta G^*}{k_B T}\right) \quad (1.9)$$

The characteristic feature of nonadiabatic ET is that the rate constant is proportional to V_{el}^2 . It is indicated from Eq. 1.9 that the nonadiabatic ET rate depends only on the static parameters of the solvent (λ_s), but the dynamics of solvent relaxation (τ_s) does not affect the nonadiabatic ET rate. On the contrary, other extreme of the ET reaction is the situation where V_{el} is very large which implies that $\kappa_{ad} \gg 1$ and the rate constant for the corresponding adiabatic ET is given as,^{27-31,36-43}

$$k_A = \frac{1}{\tau_s} \sqrt{\frac{\lambda_s}{16\pi k_B T}} \exp\left(\frac{-\Delta G^*}{k_B T}\right) \quad (1.10)$$

In this case, ET rate is strongly dependent on the solvent relaxation dynamics (τ_s). At room temperature the value of $16k_B T$ is about 1.3 eV. Since in common solvents the value of λ_s is

normally close to or less than this value, Eq. 1.10 indicates that the maximum ET rate constant (for barrierless ET reaction) can approximately be of the order of $1/\tau_s$.

1.2.3. Effect of high frequency vibrational modes on ET rates. In the discussion so far, contributions of the intramolecular vibrational degrees of freedom in the ET rates have not been considered to maintain simplicity. Logically, however, vibrational modes can play a significant role in determining the ET dynamics. Intramolecular vibrational modes include both high-frequency ($h\nu \gg k_B T$) and low frequency ($h\nu \ll k_B T$) modes. As the vibrational energy levels associated to the low-frequency modes can be easily accessed by thermal energy ($k_B T$), reorganisation for these modes can simply be treated classically, as is done for solvent reorganisation (*cf.* Section 1.2.1). On the other hand, the vibrational energy levels associated to the high frequency modes cannot be accessed by thermal energy and thus their contributions are to be treated quantum mechanically. The high frequency modes in effect introduces multiple reaction channels, and their effect can be incorporated by generalizing the expression for the ET (*e.g.* non-adiabatic) rate as,^{5-11,25-31,36-48}

$$k_{NA} = \sum_n k_{NA,n} \quad (1.11)$$

where $k_{NA,n}$ is the rate constant involving the ground vibrational level ($n = 0$) of the reactant and the n^{th} vibrational level of the product. The basis of this consideration is that under normal circumstances all the reactants are in the $n = 0$ state and during ET an n^{th} vibrational level of the product state can be easily produced as schematically shown in Figure 1.6.

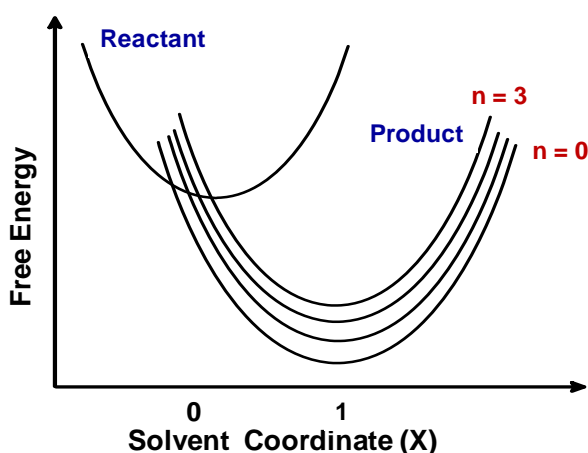


Figure 1.6: Multichannel free energy surface crossings due to the involvement of the high-frequency vibrational modes of the product state.

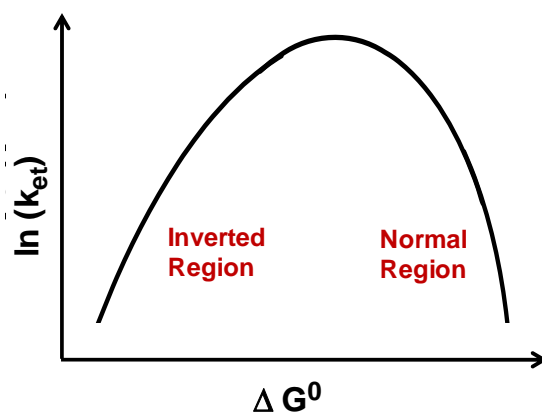


Figure 1.7: $\ln(k_{et})$ vs ΔG^0 plot showing the asymmetric nature of the Marcus correlation curve.

Following Figure 1.6, free energy change associated to $k_{NA,n}$ is given as,^{5-11,25-31,36-48}

$$\Delta G^{0,n} = \Delta G^0 + nh\nu_h \quad (1.12)$$

In this case, since $k_{NA,n}$ involves both electronic and vibrational energy levels, one can express $V_{el,n}$ in terms of the electronic-coupling for the ground vibrational levels $V_{el,0}$ and the Franck-Condon overlap factor $\langle 0|n \rangle$ as,^{5-11,25-31,36-48}

$$V_{el,n}^2 = V_{el,0}^2 |\langle 0|n \rangle|^2 \quad (1.13)$$

The factor $\langle 0|n \rangle$ can be further expanded by using the following relation,^{5-11,25-31,36-48}

$$|\langle 0|n \rangle|^2 = (S^n/n!) \exp(-S) \quad (1.14)$$

where S is the electron-vibrational coupling strength and is given by $S = \lambda_h/h\nu_h$, where λ_h is the reorganization energy and ν_h is the frequency of the concerned high-frequency vibrational mode. Following above discussions, the effective ET rate constant involving zero vibrational level of the reactant state and n^{th} vibrational level of the product state is expressed as,

$$k_{NA,n} = \frac{2\pi}{\hbar} \frac{(V_{el,n})^2}{\sqrt{4\pi\lambda_s k_B T}} \exp\left\{ \frac{-(\Delta G^{0,n} + \lambda_s)^2}{4\lambda_s k_B T} \right\} \quad (1.15)$$

The point to be noted here is that the contribution of high frequency vibrational mode is quite insignificant in the normal Marcus region but is very significant in the inverted region. In fact, the asymmetric nature of the Marcus correlation curve as often found experimentally (*cf.* Figure 1.7) than the symmetric bell-shaped behavior predicted from Marcus classical ET theory (*cf.* Figure 1.4) is understood to arise mainly due to the participation of the high frequency vibrational modes in the inverted region of the reactions causing the observed ET rates higher than otherwise expected. Accordingly, the correlation curve in the inverted region becomes less stiff than in the normal region, as quantitatively shown in Figure 1.7, in comparison to the symmetric bell-shaped curve quantitatively shown in Figure 1.4.⁵⁻¹¹

1.2.4. Sumi-Marcus Two-dimensional ET (2DET) Theory: ET under Non-equilibrium Solvent Relaxation. In a reaction medium, where solvent relaxation is extremely fast, ET process can suitably be described considering solvent polarization as the effective reaction coordinate, as it is being used in the conventional ET theory. In a slow relaxing reaction medium, however, solvent relaxation can lag behind the ET reaction such that the ET effectively occurs along the intramolecular coordinate q keeping the solvent relaxation at

non-equilibrium conditions along solvation coordinate X. The ET reaction under this situation is referred as the two-dimensional ET (2DET), which has been theoretically modeled and analyzed initially by Sumi and Marcus²⁵ and later extended by Nadler and Marcus.²⁶ The conceptual picture of 2DET model is shown in Figure 1.8 where coordinate q represents the low frequency intramolecular vibrational modes of the reacting system that assist the ET process. In this figure, for simplicity, both X and q coordinates are considered in their normalized forms, which means that the (X,q) coordinates for the equilibrium reactant and product states are represented as (0,0) and (1,1), respectively.

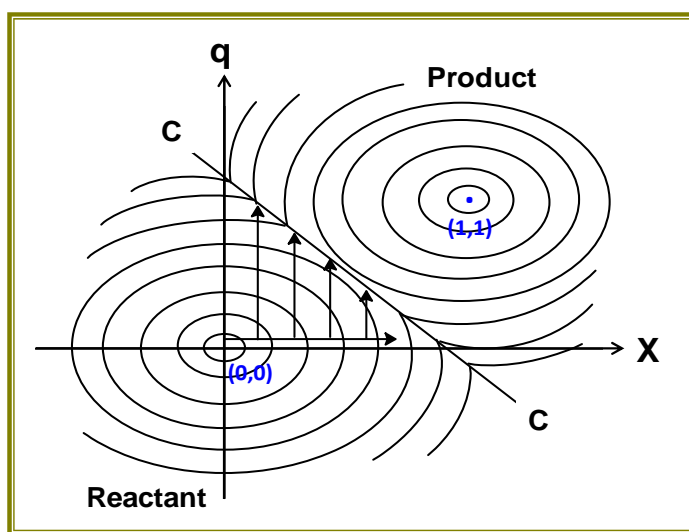


Figure 1.8: Conceptual presentation of the free energy contours for the reactant and product states, spanned by the solvent coordinate X and nuclear coordinate q (2DET model). Curve CC indicates the transition state.

In 2DET model, it is assumed that the free energies of both reactant and product states are the quadratic functions of both q and X coordinates and accordingly are expressed as,²⁵⁻²⁸

$$G_r(X,q) = \lambda_s X^2 + \lambda_i q^2 \quad (1.16)$$

$$G_p(X,q) = \lambda_s (X-1)^2 + \lambda_i (q-1)^2 + \Delta G^0 \quad (1.17)$$

where λ_i and λ_s are the intramolecular and solvent reorganization energy, respectively. In Sumi-Marcus 2DET model, relaxation along q coordinate is considered to occur much faster than that along X coordinate. Thus, reactant and product states always maintain a thermal equilibrium along q coordinate, while both the states are at nonequilibrium along X coordinate during ET process. This otherwise means that depending on the X value, ET along q occurs with different rates with X-dependent rate constants given as,²⁵⁻²⁸

$$k_{et}(X) = \frac{2\pi}{\hbar} \frac{V_{el}^2}{\sqrt{4\pi \lambda_s k_B T}} \exp\left\{-\frac{\Delta G^*(X)}{k_B T}\right\} \quad (1.18)$$

Point to note here is that the activation free energy $\Delta G^*(X)$ in 2DET is also a function of X , which is, however, not the case in conventional ET theory. Using expressions 1.16 and 1.17 for the free energies of the reactant and product states, and assuming no participation of high frequency vibrational modes, the explicit expression for $\Delta G^*(X)$ can be obtained as,

$$\Delta G^*(X) = \frac{[\lambda_s(1-2X) + \Delta G^0 + \lambda_i]^2}{4\lambda_i} \quad (1.19)$$

To be noted from Eq. 1.19 that following 2DET, the λ_s contributes only partially towards the free energy of activation and this effective solvent reorganization energy is expressed as,

$$\lambda_{s,eff} = \lambda_s(1-2X) \quad (1.20)$$

Following the above discussion, if solvent motion is considered to be completely frozen (no solvent relaxation), the time-dependent population $P(t)$ of the reactant state can be given as,

$$P(t) = \int p(X, 0) \exp\{-k(X)t\} dX \quad (1.21)$$

where $p(X,0)$ is the distribution of the reactant state along X at time zero. Obviously, due to the X -dependent changes in the reaction rates the distribution of the reactant state will temporarily evolve during the progress of the ET reaction causing the function $P(t)$ and hence the 2DET kinetics to be non-exponential in nature. For most ET systems, however, solvent reorganization may not be completely frozen. Under this situation, one needs to define and solve a time-dependent distribution function of the reactant state to understand the ET kinetics. In the present context, we avoid these details as such analyses are not pertinent to our PET studies described in this thesis.

1.2.5. Hybrid Model for 2DET: Incorporation of the High Frequency Vibrational Modes.

The Sumi-Marcus' 2DET model treats both the solvent and intramolecular modes classically, where frequency of all the modes are considered to be much lower than the thermal energy ($h\nu \ll k_B T$).²⁵⁻²⁸ In a real system, however, not only the classical low frequency modes, but also a few high-frequency modes ($h\nu \gg k_B T$) can also participate in the ET process, which have to be treated quantum mechanically. Jortner and Bixon developed a theoretical model to incorporate the effect of high frequency modes on the ET rates.³⁶⁻⁴³ In this model, crossing of reactant and product energy surfaces corresponding to different high frequency vibrational levels are considered separately and ET rate is expressed as the sum of all these possible ET

channels. At room temperature, since the reactants will be at the zero vibrational level of the high frequency modes, to describe ET reactions thus, the high frequency vibrational levels of the product state are only needed to be considered,³⁶⁻⁴³ as schematically shown in Figure 1.9. It is evident that the effect of these high frequency modes will be important only in the inverted region, where energy released from ET reaction is large enough to vibrationally excite the product state.³⁶⁻⁴³ Due to this reason, the ET rates are enhanced in the inverted region, causing the asymmetry in the bell-shaped Marcus correlation plots as often observed experimentally (*cf.* Section 1.2.3 and Figure 1.7).

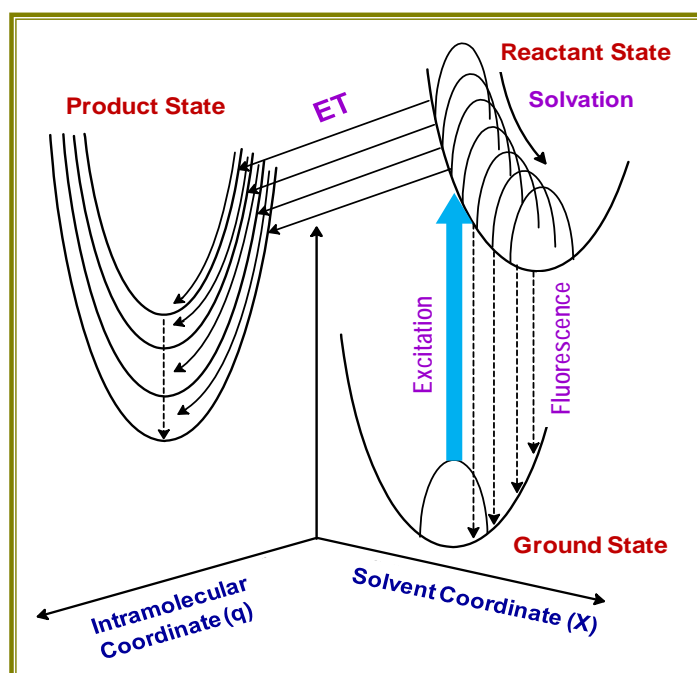


Figure 1.9: Conceptual drawing of the free-energy surfaces in hybrid 2DET model. The solvation process occurs along the solvent coordinate (X), while ET occurs along intramolecular coordinate (q ; consisting of classical low frequency vibrational modes of the reactants) involving high frequency vibrational levels of the product states that are treated quantum mechanically.

Nuclear tunneling presents another route by which ET products can also be formed in situation where classical ET reaction, i.e. free energy crossing at the transition state seems impossible. In the tunneling mechanism the products are formed by the finite tunneling probability across the activation barrier as given by quantum mechanics. At room temperature, contribution of this tunneling mechanism to the observed ET rate is negligible, especially in the normal region. In the inverted region, a reasonable enhancement in the ET rates may arise due to tunneling effect,^{5-11,21-31} causing an additional contribution towards the asymmetry of the Marcus correlation plots especially at lower temperatures.

1.3. Energetics of PET Reactions

On photoexcitation, the electron donating as well as the electron accepting power of a molecule increases in comparison to that in the ground state.^{5-11,29-31} Thus, many electron donor-acceptor pairs, which do not give ET reaction in their ground states, undergo efficient ET reaction when either of them is photoexcited to the higher electronic state. ET reactions involving the excited donor or acceptor molecules are commonly known as the PET reaction and most of the dynamic aspects on ET reactions are investigated following such PET reactions, to understand the details of the ET mechanism and dynamics and also to correlate the experimental finding with the theoretical predictions.

The feasibility of ET reaction in a donor-acceptor system is determined by the overall free energy change (ΔG^0), which can be estimated from the redox potentials of D and A. The ion-pair (IP) formed by the ET reaction also encounter a electrostatic work term that depends on the dielectric properties of the medium used. In the case of PET, one also needs to account the excitation energy supplied to the reactant in the estimation of the ΔG^0 value. Thus, ΔG^0 for a PET process is given by the well known Rehm-Weller equation as,^{5-11,29-31,49}

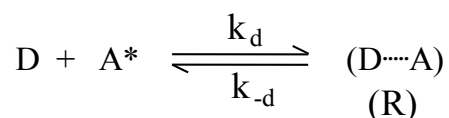
$$\Delta G^0 = E_{D/D^+} - E_{A/A^-} - \frac{e^2}{\epsilon_s r} - E_{00} \quad (1.22)$$

where E_{D/D^+} and E_{A/A^-} are the redox potentials of D and A, respectively, E_{00} is the excitation energy of the photoinduced reactant, $e^2/\epsilon_s r$ is the Coulombic interaction term for the ion-pair formed by the ET reaction, ϵ_s is the static dielectric constant of the medium and r is the separation between the two radical-ions in the ion-pair state.

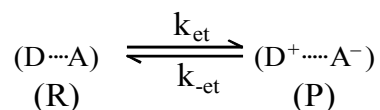
1.4. PET under Diffusive Condition

PET reaction between an excited acceptor (A^*) and a ground state donor (D) in a low viscous solvent medium can be visualized in terms of the following reaction steps:⁵⁻¹¹

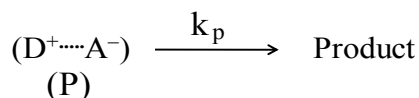
1) The reactants first undergo diffusion to come within interaction distance to form the encounter (or precursor) complex, which in true sense is the reactant state (R) for the ET reaction.



2) The ET takes place in the encounter complex to form the ion-pair state (also called the successor complex), which is actually the product state (P) in relation to the ET reaction.



3) The ion-pair state formed by the ET reaction would disappear by the reactions, like (i) back ET to produce the reactant state R back, (ii) charge recombination (CR) reaction to produce the ground state reactants, D and A, (iii) ion dissociation (ID) to produce the solvent separated ions, D^+ and A^- and (iv) any chemical reaction (RX) that leads to some permanent product. Considering all these channels together, the decay of an ion-pair state is,



where $k_p = k_{CR} + k_{ID} + k_{RX}$. Needless to say that the PET reaction between an excited donor (D^*) and a ground state acceptor (A) will be presented by similar steps as shown above considering the excited acceptor A^* .

Following these mechanistic steps and applying a steady-state condition, it is easy to show that the effective quenching rate constant k_q for A^* by D can be expressed as,⁵⁻¹¹

$$k_q = \frac{k_d}{1 + \left(\frac{k_{-d}}{k_{et}}\right) \left(1 + \frac{k_{-et}}{k_p}\right)} \quad (1.23)$$

Eq. 1.23 can be further simplified by assuming that $k_p \gg k_{-et}$, which is quite expected because back ET (k_{-et}) is a uphill process while CR is a downhill process. Moreover, in polar solvents, ion-dissociation process (k_{ID}) also contributes substantially towards the decay of the ion-pair state. Thus, considering that $k_p \gg k_{-et}$ situation prevails, Eq. 1.23 is modified as,

$$k_q = \frac{k_d}{1 + \frac{k_d}{Kk_{et}}} \quad (1.24)$$

where $K = (k_d / k_{-d}) =$ equilibrium constant for the formation of the encounter complex via diffusional process, which on approximation can be expressed as,⁵⁻¹¹

$$K = \frac{4\pi N r_{DA}^2 \delta r}{1000} \exp\left(\frac{-w_c}{RT}\right) \quad (1.25)$$

where, N is Avogadro's number, r_{DA} is the contact distance between D and A^* , δr is the distance beyond r_{DA} over which ET can take place and w_c is work required to bring D and A^* at a distance of r_{DA} . For neutral reactants like the systems investigated in the present work, w_c can be considered to be close to zero. For ET reactions, δr is usually considered to be of the

order of about 2 \AA^5 .⁵⁻¹¹ Thus, from Eq. 1.25, K is approximately estimated as $1 \text{ mol}^{-1} \text{ dm}^3$. In fact, for all practical purposes K is considered to be $1 \text{ mol}^{-1} \text{ dm}^3$, for all the bimolecular ET reactions involving neutral donor and/or acceptor molecules in solution.

1.5. Solvation Dynamics

Chemical reactions in solution are often strongly influenced by the relaxation dynamics of solvents surrounding the reacting species. Studies on solvent relaxation dynamics are thus very important for the detailed understanding of the reaction dynamics in solution, especially for processes like ET, CT, proton transfer, etc. Dynamic fluorescence Stokes shifts have been extensively used to understand the solvent relaxation dynamics in large number of solvent media employing suitable fluorescence probes.⁵⁰⁻⁵⁹ On photoexcitation, the dipole moment of the probe molecule increases instantaneously. The polarisation of the surrounding solvent molecules responds to this change and undergoes a time-dependent reorganization. Therefore, the energy of the whole system relaxes, causing a time-dependent shift in the fluorescence spectra of the probe towards longer wavelengths. Accordingly, measurement of the dynamic Stokes' shift of the probe describes the dynamics of the solvent relaxation process. The idea of solvation dynamics has been conceptually illustrated in Figure 1.10.

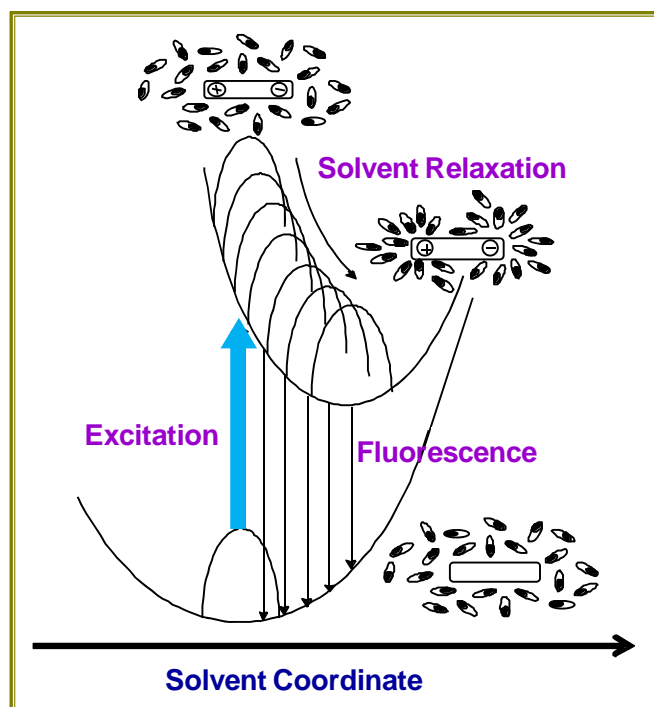


Figure 1.10: Dynamic fluorescence Stokes shift caused by the solvation process following photoexcitation of the fluorescent probe.

Experimentally, fluorescence decays of the probe dye are first measured at regular wavelength intervals covering the whole emission spectra of the dye. Observed decays are then uniformly analyzed following a suitable function, usually a tri-exponential function. The decay parameters thus obtained are used to construct the TR emission spectra (TRES) following the standard procedure as given by Fleming and coworkers.⁵⁰⁻⁵³ Briefly, in this procedure, the intensity normalized decays $D_N(\lambda, t)$ at each of the measuring wavelengths are first calculated using the fitted parameters of experimental decays at the respective wavelengths, following Eq. 1.26.

$$D_N(\lambda, t) = \frac{D(\lambda, t)}{\int_0^{\infty} D(\lambda, t) dt} \quad (1.26)$$

where $D(\lambda, t) = \sum_{i=1}^3 \{B_i(\lambda)\} \exp[-t/\{\tau_i(\lambda)\}]$ and the parameters $\{B_i(\lambda)\}$ and $\{\tau_i(\lambda)\}$ are the pre-exponential factor and the decay time, respectively, for the i^{th} decay component at wavelength λ . The normalized decays are then used in combination with the SS emission spectrum $I_{SS}(\lambda)$ of the dye to calculate the time-dependent changes in the fluorescence intensity at different wavelengths $I(\lambda, t)$, by using the following relation.

$$I(\lambda, t) = D_N(\lambda, t) \times I_{SS}(\lambda) \quad (1.27)$$

The TRES thus are in the wavelength scale and these spectra are finally converted to the wave-number scale (energy scale, $\bar{\nu}$) by using the following relation.

$$I(\bar{\nu}, t) = \lambda^2 I(\lambda, t) \quad (1.28)$$

Since the number of data points in the TRES thus constructed is limited due to the limited number of wavelengths for which fluorescence decays are actually measured experimentally, the TRES data obtained from the above procedure is further fitted using a log-normal line shape function, defined by Eq. 1.29, to obtain the smooth TRES for the system studied.⁵⁰⁻⁵³

$$I(\bar{\nu}) = a \exp \left\{ -\ln(2) \left(\frac{\ln[1 + 2b(\bar{\nu} - \bar{\nu}_p) / w]}{b} \right)^2 \right\}, \text{ when } \{2b(\bar{\nu} - \bar{\nu}_p) / w\} > 1$$

$$= 0, \text{ when } \{2b(\bar{\nu} - \bar{\nu}_p) / w\} \leq 1 \quad (1.29)$$

where the amplitude a , the peak wave-number $\bar{\nu}_p$, the width parameter w , and the asymmetry parameter b , are used as the adjustable parameters.

In solvation dynamics studies, time-dependent shifts in the emission maxima $\bar{\nu}_{\max}(t)$ are analyzed using a suitable functional form to extract the parameters for solvent relaxation dynamics. Thus, in many cases $\bar{\nu}_{\max}(t)$ is directly analyzed as a sum of exponentials as,

$$\bar{\nu}_{\max}(t) = \sum_{i=1}^n a_{s_i} \exp(-t/\tau_{s_i}) + \bar{\nu}(\infty) \quad (1.30)$$

In most solvation dynamic studies, however, a spectral shift correlation function $C(t)$ is first constructed as defined by the following equation,

$$C(t) = \frac{\bar{\nu}(t) - \bar{\nu}(\infty)}{\bar{\nu}(0) - \bar{\nu}(\infty)} \quad (1.31)$$

The $C(t)$ function is then analyzed following a suitable exponential function (eg. Eq. 1.32) to extract the parameters for the solvent relaxation dynamics.

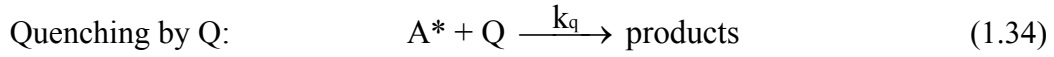
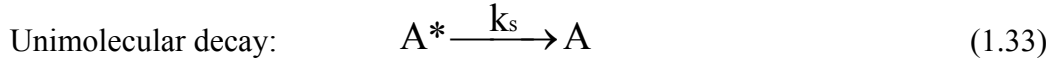
$$C(t) = \sum_{i=1}^n A_{s_i} \exp(-t/\tau_{s_i}) \quad (1.32)$$

The TRES constructed by the above procedure are also often used to understand the presence as well as to resolve the spectral characteristics of multiple emissive species that contribute in the observed emission spectra. Often, the TRES are further converted to the TR area normalized emission spectra (TRANES), as the TRANES reports the features of the multiple emissive species in a system better than the TRES. The TRANES are constructed by normalizing the integrated area under each of the TRES concerned. As will be seen in Chapter 5, both TRES and TRANES have been used very extensively to understand the intricate solution behavior of the chromophoric dyes that are used as the electron acceptors in our studies on the PET reactions.

1.6. Fluorescence Quenching Studies: Stern-Volmer Equation

Fluorescence quenching refers to any process that causes a reduction in the fluorescence intensity of the fluorophore. A variety of processes that can lead to fluorescence quenching include excited state reactions like energy transfer, ET, ground and/or excited state complex formation, collisional quenching, etc.¹⁻⁴ The quenching that results from collisional encounters between the fluorophore and quencher, is called the dynamic quenching, which is a time dependent process, and is very important phenomenon in photochemical investigations. Quenching that occurs as a result of non-fluorescent ground state complex formation is also an important aspect in the photochemical studies and this phenomenon is often called as the static quenching which is a time-independent process.

The dynamic quenching of an excited molecule (A^*) by a quencher, Q , is always in competition with the inherent unimolecular decay process of the excited molecule. Therefore, one can write,



Thus, following steady-state (SS) condition, the concentration of A^* is given as

$$[A^*] = \frac{I_a}{k_s + k_q[Q]} \quad (1.35)$$

Fluorescence yield in the absence (Φ_0) and in presence (Φ_q) of the quencher are given as,

$$\Phi_0 = \frac{k_f}{k_s} \quad \text{and} \quad \Phi_q = \frac{k_f}{k_s + k_q[Q]} \quad (1.36)$$

The ratio of the two quantum yields thus results,¹⁻⁴

$$\frac{\Phi_0}{\Phi} = \frac{I_0}{I} = \frac{k_f + k_f[Q]}{k_s} = 1 + \frac{k_q}{k_s}[Q] = 1 + k_q\tau_0[Q] = 1 + K_{SV}[Q] \quad (1.37)$$

Expression 1.37 is known as the Stern-Volmer equation and K_{SV} ($= k_q\tau_0$) is called the Stern-Volmer constant, where τ_0 is the fluorescence lifetime of the probe in the absence of Q . Thus, following Stern-Volmer plots, the K_{sv} and k_q values can be easily obtained following SS quenching measurements. Similar to Eq. 1.37, Stern-Volmer equation for TR quenching studies can be written in terms of the fluorescence lifetime of the molecules as,¹⁻⁴

$$\frac{\tau_0}{\tau} = 1 + K_{SV}[Q] = 1 + k_q\tau_0[Q] \quad (1.38)$$

where τ_0 and τ are the lifetimes in the absence and in presence of Q .

Deviations from expected linearity in Stern-Volmer plots are often encountered in many quenching processes especially in SS fluorescence quenching, and arise mainly due to static quenching, via the formation of ground-state complexes,



where K_f is the association or formation constant. Thus, in the presence of both static and dynamic quenching, the Stern-Volmer relation is modified as,¹⁻⁴

$$\frac{\Phi_0}{\Phi} = (1 + K_{SV}[Q])(1 + K_f[Q]) \quad (1.40)$$

This modified Stern-Volmer relation is second order in [Q], which accounts for the upward curvature of the Stern-Volmer plots often observed in SS fluorescence quenching studies.

SS fluorescence quenching study alone is often not sufficient to unambiguously distinguish between static and dynamic quenching, if both are present together. The lifetime measurements or temperature and viscosity dependence studies are useful in distinguishing the static and dynamic aspects of the quenching process. Static quenching, which is a time independent process, cannot have any effect on the observed fluorescence decays. For the dynamic quenching, however, the fluorescence lifetime gradually reduces with [Q], following Eq. 1.38. Thus, Stern-Volmer linearity are in general expected in the τ_0/τ vs [Q] plots, even when the I_0/I vs [Q] plots show positive deviation from Stern-Volmer linearity due to static quenching. As the dynamic quenching depends on the diffusion of the molecules in the solvent medium, an increase in the temperature and a decrease in the solvent viscosity increase the rate of the dynamic quenching process.

In solution two reactants surrounded by solvent molecules come closer by diffusion. It is generally assumed that the reaction take place instantaneously when the two reactants come at their close contact, i.e., the distance of separation $r_{AB} = (r_A + r_B)$, where r_A and r_B are the radii of the two reactants A and B. To be more specific, all the diffusional encounters will lead to the quenching process, provided the activation energy for the concerned reaction is very low or negligible. Such reactions are known as the “diffusion controlled bimolecular reactions”. The rate constant (k_d) for such a reaction has been derived by Debye from Smoluchowski equation based on Fick’s law of diffusion and is expressed as,¹⁻⁴

$$k_d = 4 \pi \rho r_{AB} N(D_A + D_B) 10^{-3} \text{ dm}^3 \text{ mol}^{-1} \text{ s}^{-1} \quad (1.41)$$

where, D_A and D_B are the diffusion coefficients for the two reacting partners, r_{AB} as already defined, ρ is a probability factor per encounter and N is the Avogadro number. The diffusion coefficients are given by the Stokes-Einstein equation as,¹⁻⁴

$$D = \frac{k_B T}{6 \pi \eta r} \quad (1.42)$$

where, k_B is the Boltzmann constant, r is the radius of the diffusing molecule and η is the solvent viscosity in poise.

If $r_A = r_B = r$ so that $r_{AB} = 2r$ and $\rho = 1$, the reaction is called a diffusion controlled reaction for which the rate constant can be obtained by the simplification of Eq. 1.41 as,¹⁻⁴

$$k_d = \frac{8RT}{3000 \eta} \text{ dm}^3 \text{ mol}^{-1} \text{ s}^{-1} \quad (1.43)$$

Thus, the diffusion controlled bimolecular rate constant would depend mainly on the viscosity and the temperature of the solution. For typical organic solvents at 25°C, k_d is in the order of 10^9 to $10^{10} \text{ dm}^3 \text{ mol}^{-1} \text{ s}^{-1}$.¹⁻⁴ The maximum values for the quenching constant k_q are also normally found to be in this range in most conventional solvents.

1.7. Tri-Block Copolymers and their Solution Behavior

Pluronics are the triblock copolymers made up of poly ethyleneoxide (EO)_n and poly propyleneoxide (PO)_n blocks with general molecular formula as (EO)_n-(PO)_m-(EO)_n. These water soluble non-ionic surfactants have attracted considerable attention in the last two decades partly because of their complex behavior in solution⁶⁰⁻⁶⁴ and partly because of their wide range of industrial applications, as detergent, lubricant, emulsifier, etc.⁶⁵⁻⁷⁰ The low toxicity have also made these polymers very useful in many pharmaceutical formulations.⁶⁶⁻⁷⁰ These materials have also been extensively used as templates for the synthesis of various nano-structured materials.^{71,72}

Although pluronic molecules lack the polar head groups, as are present in conventional surfactants, yet they form micelles in aqueous solution.⁶⁶ In pluronics, the solubility of both EO and PO blocks in water decreases at elevated temperatures, but the effect is less pronounced for relatively hydrophilic EO block compared to the relatively hydrophobic PO block. Due to this disparity in the solubilities of the two blocks, the triblock copolymers form micellar aggregates in water above a temperature called the critical micelle temperature (*cmt*) and also above a concentration called the critical micelle concentration (*cmc*), whereby the core of the micelle is formed predominantly by the PO blocks and the corona by the hydrated EO blocks. Thus, the self-assembly of block copolymers in solution can be initiated either by increasing the concentration above *cmc* at a particular temperature or by changing the temperature above *cmt* at a particular concentration. For block copolymers, often a small increase in temperature causes a dramatic reduction in the *cmc* value, a feature rather quite unique for the pluronic surfactants, in contrast to the conventional non-ionic surfactants. For triblock copolymers, both *cmc* and *cmt* values are lower when their PO block size is larger. Moreover, the aggregation number (N_{agg}) of these micelles in general increases on increasing the PO block size and on decreasing the EO block size. The N_{agg} also increases on increasing temperature.⁶⁰⁻⁷⁰ Importantly, an increase in N_{agg} with increasing temperature does not change the hydrodynamic radius significantly. This has been observed for a number of block copolymers and the effect is understood as because of the fact that the

dehydration of EO block becomes increasingly important at elevated temperatures, that results in the reduction of the coronal volume of the micelle.⁶⁰⁻⁷⁴

Micellization process as well as structure of pluronic micelles have been studied extensively using techniques like neutron scattering,^{63,75} X-ray scattering,⁷⁶ light scattering,^{74,77} absorption⁷⁸ and fluorescence measurements.^{61,79} Though extensive studies have been carried out on the structural aspects of these micellar systems, studies on the dynamical processes in these micelles are very limited. Rotational dynamics of solubilized probes in different phases of pluronic micelles have been investigated extensively using fluorescence anisotropy measurements to explore the local environments of different regions of the copolymer micelles.⁸⁰⁻⁸³ Relaxation of the water molecules in different regions of pluronic micelles have also been reported in the literature.⁸⁴⁻⁸⁶ All these studies indicate that the dynamical processes in pluronic micelles largely depend on the EO to PO ratios of the copolymers concerned.

In several industrial applications, pluronics are often used in combination with low molecular weight ionic surfactants.^{87,88} This feature has prompted experimental studies on the solution behavior of these mixed surfactant systems.⁸⁹ Interaction of pluronics with low molecular weight ionic surfactants like sodium dodecyl sulphate (SDS), cetyl triethylammonium chloride (CTAC), etc. have been studied quite extensively by using light scattering,⁷⁵⁻⁷⁷ neutron scattering,⁷⁵ and calorimetric methods.^{77,90} These studies have shown that at low ionic co-surfactant concentrations, unique supramolecular assemblies are formed by the pluronics where hydrocarbon chains of the small ionic surfactants are embedded into the PO core of the pluronic micelles with their head groups placed at the periphery of the core, protruding into the hydrated corona region,⁷⁵ as schematically shown in Figure 1.11. In the present study these mixed micellar systems have been used as the reaction media to modulate the rate of PET reactions as are described in Chapter 4.

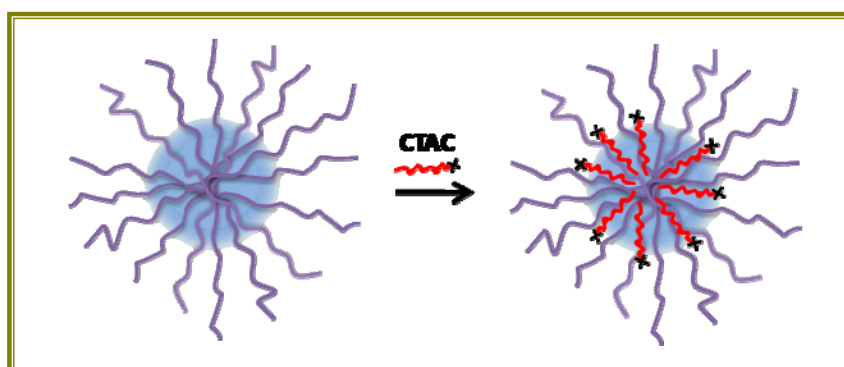


Figure 1.11: Schematic presentation of the formation of block copolymer-surfactant mixed micelle.

1.8. Kasha's Exciton Theory for Dye-Aggregation

The electronic transitions in the aggregates of chromophoric dyes are best explained by Kasha's exciton theory given on the basis of the interactions of the transition dipoles of the monomeric units present in the aggregates.^{91,92} Due to this interaction the excited state energy level of the chromophore undergoes a splitting, generating a higher and a lower energy state relative to the monomeric excited state, as shown in Figure 1.12. As suggested in this theory, the nature of this splitting depends on the angle θ between the direction of the transition dipoles of the dye molecules and the axis of the dye aggregates (i.e. the line passing through the centers of the dye molecules in the aggregate; *cf.* Figure 1.12). Thus, when $\theta = 90^\circ$, as it happens in the case of H-type of aggregate formation where molecular planes of the dyes are stacked one above other (i.e. sandwich-type face-to-face stacking of the dyes), the electronic transition between the ground state and the higher excitonic state is the allowed transition while that involving the ground and the lower excitonic state is the forbidden transition. Accordingly, absorption band for the H-type aggregates is seen to be hypsochromically shifted relative to that of the dye monomer. On the contrary, if $\theta = 0^\circ$ (i.e. head-to-tail stacking of the dyes; *cf.* Figure 1.12), the transition between the ground and the lower excitonic state is the allowed transition and accordingly there is a bathochromic shift for the absorption band of the J-type of aggregates relative to that of the dye monomer.

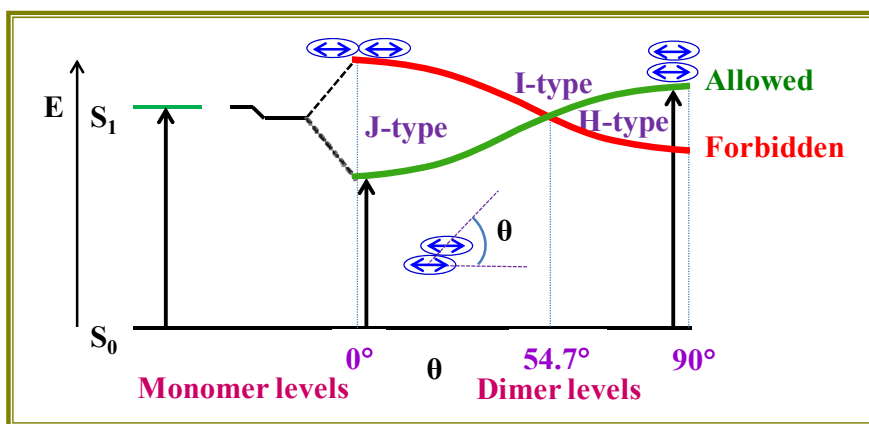


Figure 1.12: Schematic energy diagram for aggregated dimers with coplanar inclined transition dipoles. The geometry and angle θ are illustrated above. Arrows indicate allowed transitions.

As Kasha's theory suggests and one can anticipate from Figure 1.12, for aggregates having $\theta > 54.7^\circ$, the electronic transition from the ground state to the excitonic state would lead to a hypsochromic shift. Similarly, for aggregates with $\theta < 54.7^\circ$, the electronic transition from the ground state to the excitonic state would lead to a bathochromic shift.

Interestingly, for the aggregates with $\theta = 54.7^\circ$ (magic angle), there will be no spectral shift for the absorption band of the dye and such unique aggregates are characteristically designated as the I-type (intermediate type) aggregates.

1.9. Motivation and Objective of the Present Work

Understanding the correlation between the bimolecular PET dynamics and the associated energetics in heterogeneous media has been the inspiration for the work presented in this thesis. The importance of such studies can be perceived by the example of photosynthesis, where the primary step after the absorption of light is the ET reaction to effectively produce the energy rich products.⁵⁻¹¹ Logically the efficiency of charge separation following ET can approach 100%. However, in real systems, the net charge transfer efficiency is only few percent due to loss factors that acts in opposite to the charge separation process. If one looks into the details of the primary steps of photosynthetic systems, one finds that the ET reaction occurs close to the “barrierless” condition, where as the back ET (BET) reaction (loss process) occurs at the inverted regime (*cf.* Figure 1.4). Such a situation is essential to suppress the energy wasting back ET process. Thus, a clear understanding of dynamics and energetics of ET reactions is very essential in designing artificial photosystems with enhanced efficiency for better utilization of the ET reaction.

The study of PET reactions in restricted heterogeneous media, like in micelles, has attracted considerable attention in the last two decades. The main interest in such studies arises due to the fact that in many practical applications of ET reactions, e.g., solar energy conversion or its storage, the reaction is needed to be carried out in heterogeneous media. The heterogeneous media provide an opportunity to separate the primary products of the ET reactions, through increasing their lifetimes and thus preventing the energy wasting BET process.⁵⁻¹¹ Among the heterogeneous media, reactions in micellar solutions have attracted the attention of many researchers in order to understand the effect of the topology of the media on chemical reactions and further to understand if such a medium can provide a protocol to control the kinetics of the reaction by modulating the microscopic environment of the systems. In fact, micellar media have been used extensively to modulate ET reactions between various donor-acceptor systems. It is understood that by appropriate selection of the micelle the ET reaction can either be enhanced or inhibited as compared to that in bulk solvent.⁹³⁻⁹⁵ The importance of the ET reactions in micellar systems is also due to the structural resembles of the micelles with biological membranes.^{96,97} Though lot of efforts

have been made to understand ET processes in normal solvents, literature reports on ET dynamics in heterogeneous media are not very extensive.

The most remarkable prediction of Marcus ET theory is the inversion behavior of the ET rates with the exergonicity ($-\Delta G^0$) of the reaction as discussed in Section 1.2.^{5-11,21-30} The theoretical prediction of this inversion had generated a lot of controversy for long time, due to the lack of its experimental verification. At present, however, several experimental evidences for the presence of the inversion behavior have been demonstrated. The point to be noted is that in most of the cases where Marcus inverted region has been observed experimentally, the donor and acceptor are either chemically bonded (intramolecular ET)^{32-35,98-101} or in close contact.¹⁰²⁻¹⁰⁴ In all these cases, the distance between the reactants is effectively fixed, or otherwise to say, there is no effective diffusion of the donors and acceptors during the interaction. Experimental evidence of Marcus inversion for bimolecular ET reactions under diffusive conditions is however, very rare.¹⁰⁵⁻¹⁰⁹ In most of these reactions, the variation in the ET rates with the exergonicity of the reactions is seen to follow the Rehm-Weller type of behavior,⁴⁹ where ET rate initially increases with the exergonicity ($-\Delta G^0$) of the reaction but ultimately reaches a saturation limit at the higher exergonicity region. The diffusion of reactants, which is the rate determining step for the bimolecular ET reactions at higher exergonicities, limits the maximum reaction rate to be observed and thus causes the saturation of the ET rates to the diffusion-controlled rate, k_d , at the higher exergonicity of the reactions.⁵⁻¹⁰ Tachiya et. al. have made a judicial distinction between the Marcus and the Rehm-Weller type of ET kinetics.¹¹⁰ Marcus theory deals with the first order rate constant for a donor-acceptor pair separated by a fixed distance, where as the Rehm-Weller model deals with the bimolecular reactions involving the diffusion of the donors and acceptors. Thus, Tachiya et al. has calculated the second order diffusion mediated ET rate constants incorporating the distance dependence in the first order ET rate constants. They have shown that the Marcus inverted region can also be observed for the bimolecular ET reactions, provided the exergonicity of the reactions are made extremely high, greater than about 2 eV.¹¹⁰ These authors argued that it would have been possible to see Marcus inverted region in the experimental results of Rehm and Weller in their historic article if the exergonicity of the reaction had been increased further than they had actually encountered.

There are two main difficulties in observing Marcus inverted region in bimolecular ET reactions, namely, (i) the limiting effect of reactants diffusion on the observed rate and (ii) the lack of availability of suitable donor-acceptor series to achieve very high reaction

exergonicity. Micelles are supposed to provide an inductive reaction environment to observe Marcus inverted region for bimolecular ET reactions.^{5-10,49,110} Because of the rigid structures of the micelles, reactants will be entangled by the surfactant chains and thus their movements will be highly restricted.¹¹¹⁻¹¹⁶ In other words, the high viscosity of the micellar media will prevent the diffusion of the reactants, and if the ET reactions are relatively faster than diffusion, then the bimolecular reactions in micellar solutions can be envisaged as equivalent to the intramolecular reactions. Thus, the bimolecular reaction dynamics in micellar media is expected to differ largely as compared to that in homogeneous media. Another factor for not observing Marcus inverted region in the bimolecular ET reactions in homogeneous solutions is the limitation in attaining very high reaction exergonicity, substantially higher than the total reorganization energy for the ET reaction. This can possibly be also overcome in micellar media. Thus, instead of increasing the exergonicity of the ET reactions to an unreasonably high value, a decrease in the overall reorganization energy, as may be possible in micellar media, can also help to attain the Marcus inverted region easily. The total reorganization energy for most outer-sphere ET reactions is mainly due to the solvent reorganization energy, λ_s . Thus, a reduction in contribution of λ_s can shift the Marcus inversion towards lower exergonicity and hence can be easier to be observed as compared to that in homogeneous solution. It is well known that the reorganization of the solvent molecules in the restricted media, e.g. in micelles, is retarded by several order of magnitudes compared to that in homogeneous solvents.⁵⁴⁻⁵⁷ Thus, solvent reorganization energy may not contribute completely within the time scale of the ET reactions in micellar solutions (*cf.* Section 1.2.4). Under such circumstances, the contribution of λ_s towards the effective reorganization energy can be much less compared to that in homogeneous solution and consequently the Marcus inverted region can be shifted to a much lower exergonicity in comparison to that in homogeneous solution. Thus, micellar media seems to be a promising reaction environment to observe Marcus inversion behavior for bimolecular ET reactions.

Present thesis elaborates various important phenomena that have been investigated to get a better understanding of the ET reactions between different donor-acceptor pairs in pluronic micelles. One of the objectives of the present work has been to see if Marcus inverted region can be observed under the conditions where ET reactions occur under restricted conditions. The aim of this study is also to investigate the effect of changing EO and PO block sizes of triblock copolymers (pluronic) on the kinetics and energetics of the PET process. As solvent relaxation dynamics often play a significant role in the ET reactions,

wherever required, solvation dynamics have also been investigated in the context of the ET reactions in micellar media. With the aim to find a possible modulation of the PET kinetics, mixed micelles composed of pluronic polymers and ionic surfactant have also been used in part of the PET studies in the present work. It is reported that in these mixed micelles the hydrophobic chains of the ionic surfactants are dissolved in the core of the pluronic micelles and the charged head groups of the ionic surfactants are in the peripheral region of the core projecting into the hydrated corona region of the micelles (*cf.* Section 1.7).⁷⁵ Because of this unique structure of these assemblies, a charged layer is formed inside these mixed micelles. Accordingly, any solute having a charge opposite to that of the charged layer inside these supramolecular assemblies, can experience an electrostatic attraction and hence can move deeper into the micelles on changing the ionic surfactant to pluronic ratio of the mixed micelles. Such a change in the position of the reactant in the micelles can thus help in modulating the ET reaction, as has been investigated in a part of the present work using ionic surfactant-pluronic mixed micellar systems. In the present work, as these PET studies have been carried out using coumarin dyes as the fluorescence probes and electron acceptors, we felt it to be very important to understand if these dyes show any unusual solution behaviour which might affect the PET results. Thus, detailed photophysical characterization has been carried out for two selected coumarin dyes in polar organic solvents and in aqueous solution with special emphasis on their possible aggregation behaviour in the solution. With the experience gained from the PET studies in micellar media, the studies have been extended to understand the PET and Charge Transfer (CT) interaction of lanthanide/uranyl ions with organic donors under diffusive conditions considering the possible presence of these species in geoenvironments from industrial wastes and accidental leakages from nuclear plants.

The results of the different parts of the present study have been systematically presented and discussed in Chapters 3 to 6 of the present thesis. The necessary details of the experimental methods and data analysis procedures are separately presented in Chapter 2 of the thesis for the completeness of the presentation.

Chapter 2

Instruments and Methods

2.1. Introduction

This chapter describes the necessary details of various experimental techniques that are used in the present research work. Steady-state (SS) and time-resolved (TR) spectroscopic techniques have been exhaustively used to investigate electron transfer (ET) and charge transfer (CT) processes as well as the solution behavior of chromophoric dyes in the present study. Thus, the basic principles of the techniques like UV-vis spectrophotometer, SS spectrofluorimeter, time-correlated single photon counting (TCSPC) spectrometer, femtosecond fluorescence up-conversion instrument and laser flash photolysis measurements are systematically presented in this chapter. Auxiliary techniques like cyclic voltametry (CV) and dynamic light scattering (DLS), as used in the present study, are also briefly presented in this chapter. As far as possible, both instrumentation and data analysis procedures are briefly discussed for the above techniques in the present chapter.

2.2. Ground State Absorption Measurement

Knowing absorption characteristics is a primary requirement for most photochemical studies. UV-vis absorption spectroscopy is thus widely used in photochemical studies to obtain ground-state absorption characteristics of the chemical systems studied, namely their absorption spectra, molar extinction coefficients, etc. Changes in the solvent polarity, polarizability and hydrogen bonding characteristics often induce significant changes in the absorption spectra of the absorbing species.¹⁻⁴ Ground state complex formation also induces changes in the absorption spectra.¹⁻⁴ Hence, UV-vis spectroscopic measurements can give wealth of information for all these processes, often encountered in photochemical studies.

The absorbance (A; also called optical density, OD) of a solution is directly proportional to the concentration (C) of the absorbing species and its molar extinction coefficient (ϵ_λ), as given by,¹⁻⁴

$$A = OD = \log (I_0/I) = \epsilon_\lambda C l \quad (2.1)$$

where I_0 and I are the intensities of the incident and transmitted light, respectively, and l is the optical path length in the sample. In absorption studies with dilute solutions, the sample is usually taken in a quartz cuvette of 1 cm path length. For concentrated solutions, however, thinner cells are usually used with typical path length of either 0.1 or 0.2 cm. In the present study absorption measurements were carried out using either Shimadzu 160A (Kyoto, Japan) or Jasco V530 (Kyoto, Japan) double beam UV-vis spectrophotometers, both works in the spectral range of 200-1100 nm, with wavelength resolution of 0.2 nm and lowest measurable absorbance of 0.005. Both the spectrophotometers use D₂-lamp for the 200-350 nm region and W-lamp for the 350-1100 nm region as the light source and Si-photodiodes as the light detectors. The schematic diagram of these spectrophotometers are shown in Figure 2.1.

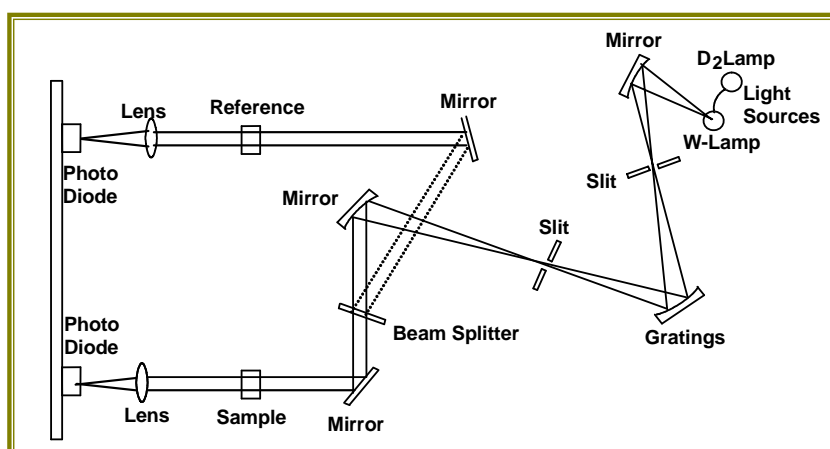


Figure 2.1: Schematic diagram of the UV-vis absorption spectrophotometers used in this study.

2.3. Steady-State Fluorescence Measurements

Fluorescence spectroscopy is a very important technique in various photochemical studies. The fluorescence intensity, peak position (emission maximum), as well as the spectral shape are very sensitive to environmental effects and the nature of interaction with the quenchers.¹⁻⁴ In the present study SS fluorescence measurements were carried out using either Hitachi F-4500 or Hitachi F-4010 (Tokyo, Japan) spectrofluorimeters, both works in the spectral range of 220-800 nm, with wavelength resolution of 0.2 nm and dynamic range of 0 to 9999 for fluorescence counts. Both the spectrofluorimeters use 150 watt continuous powered high pressure Xe-lamp as the excitation source and R-928F PMT (Hamamatsu) as the photodetector. Sample was usually taken in a 1 cm x 1 cm quartz cuvette and fluorescence was detected in perpendicular direction with respect to the excitation beam. The schematic diagram of these spectrofluorimeters is shown in Figure 2.2.

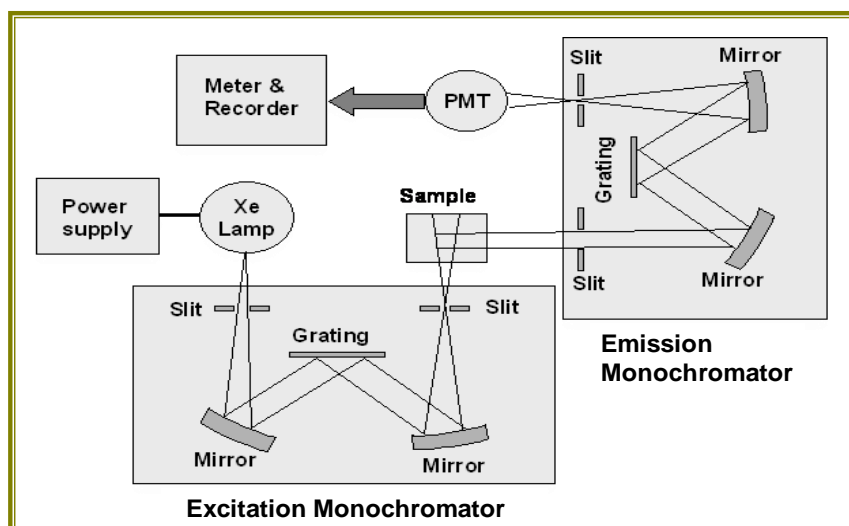


Figure 2.2: Schematic diagram of the steady-state spectrofluorimeters used in this study.

2.3.1. Correction of Emission Spectra. Emission spectra are distorted quite significantly due to the wavelength dependent responses of different components used in the spectrofluorimeter, namely, light source, monochromator, PMT, etc. Therefore it is necessary to know the overall wavelength-dependent responses of the spectrofluorimeter to obtain the corrected emission spectra of the studied sample. In the present work, spectrum of standard quinine sulfate solution were recorded and compared with its reported spectrum (given in the unit of photon/nm),¹¹⁷ to get the wavelength-dependent correction factors for the instrument used. All the measured spectra were multiplied by this correction factors to get the corrected emission spectra of the samples. The measured spectra, $I(\lambda)$, were in the wavelength domain.

Whenever required, the measured spectra in the wavelength domain $I(\lambda)$ were converted to that in the frequency domain $I(\nu)$, by using the following equation.¹¹⁷

$$I(\nu) = \lambda^2 I(\lambda) \quad (2.2)$$

2.3.2. Fluorescence Quantum Yield Measurement. Quantum yield of fluorescence (Φ_f) is defined as the ratio of the number of fluorescence photons emitted from the sample to the number of light quanta absorbed by the sample. Since the absolute number of light quanta absorbed and fluorescence emitted by the sample is very difficult to be estimated, the Φ_f of the studied sample was determined following a comparative method,¹⁻⁴ where the integrated emission intensity of the sample (F_{sample}) is compared with that (F_{ref}) of an optically matched (very close absorbance at the excitation wavelength) reference sample, whose quantum yield, Φ_{ref} is already known, keeping their excitation wavelength same, whereby Φ_f is related to Φ_{ref} by the following equation,¹⁻⁴

$$\Phi_f = \frac{A_{\text{ref}}}{F_{\text{ref}}} \times \frac{F_{\text{sample}}}{A_{\text{sample}}} \times \frac{n_{\text{sample}}^2}{n_{\text{ref}}^2} \times \Phi_{\text{ref}} \quad (2.3)$$

where A_{ref} and A_{sample} are the absorbances of the reference and sample at the excitation wavelength and n_{ref} and n_{sample} are the refractive indices for the reference and the sample solutions, respectively.

2.4. Fluorescence Lifetime Measurements

TR fluorescence measurements are very essential to obtain information regarding the kinetics and dynamics of various photoinduced processes. Excitation of a sample with an ultra-short light pulse results in the generation of initial excited state population (n_0) for the fluorophores. With time, these excited molecules undergo spontaneously decay, following either radiative or nonradiative processes. Since deexcitation of an excited molecule is a random process, the time-dependent decay of the excited state population n_t should be expressed as,^{1-4,118-120}

$$\frac{dn_t}{dt} = -\{k_r + k_{nr}\} n(t) \quad (2.4)$$

where k_r is the radiative decay rate constant and k_{nr} is the sum of all the nonradiative decay rate constants for the excited fluorophores. Solving this differential equation we get,

$$n_t = n_0 \exp\{-(k_r + k_{nr}) t\} = n_0 \exp\{-t/\tau\} \quad (2.5)$$

where $\tau = (k_r + k_{nr})^{-1}$ is defined as the excited state lifetime time of the chromophoric molecules and it is the measure of the average survival time for an ensemble of excited molecules in a given sample. In an actual experiment it is often difficult to measure the exact number of the excited molecules present in the sample. However, considering that the fluorescence intensity at any time would be directly proportional to the number of excited molecules present at that time in the sample, Eq. 2.5 can be expressed in terms of the time-dependent fluorescence intensity I_t and the integration of the resulting equation gives us the expression for the fluorescence decay $I(t)$ as,

$$I_t = I_0 \exp(-t/\tau_f) \quad (2.6)$$

where I_0 is the intensity at time zero and $\tau_f = (k_r + k_{nr})^{-1}$ and is conventionally defined as the fluorescence lifetime, as it is estimated from fluorescence measurement, though τ_f is actually synonymous to τ , as defined in Eq. 2.5. Following Eq. 2.6 it is evident that the main aim of TR fluorescence measurement is to record the fluorescence decays I_t of the sample, which can subsequently be analyzed following a suitable procedure to estimate the τ_f value. Among different techniques the Time-Correlated Single Photon Counting (TCSPC) technique is the most widely used method to record fluorescence decays of the samples that span over nanosecond to picosecond time scales. In the present study a TCSPC spectrometer from Horiba Jobin Yvon IBH, UK (model Data Station Hub) was extensively used to record the fluorescence decays of the studied samples. Important aspects of the TCSPC method of fluorescence decay measurements and their analysis are described in the following sections.

2.4.1. TCSPC Technique: Basic Principles and the Instrument Used. The principle of TCSPC measurement relies on the fact that the time-dependent fluorescence intensity of the sample following a δ -pulse excitation is equivalent to the time-dependent probability of the photon emission from a single excited molecule.¹¹⁸⁻¹²⁰ In a TCSPC spectrometer, thus, each single photon emitted by the sample following its excitation by a short light pulse is detected effectively as a function of time spend.¹¹⁸⁻¹²⁰ The schematic diagram of a typical TCSPC set up is shown in Figure 2.3.

According to Figure 2.3, the light beam from a pulsed excitation source is split into two, one beam is used to excite the sample and the other is directed to a start PMT to generate an electrical START pulse which is routed through a Constant Fraction Discriminator (CFD) to the START input of the Time to Amplitude Converter (TAC). On receiving this start pulse, the TAC initiates the charging of its capacitor linearly with time. In the mean time the excited

sample produces its emission photons which are then detected by the stop PMT (at the right angle to the direction of excitation pulse) to generate electrical STOP pulses corresponding to each individual photon received. These STOP pulses are routed through a CFD and a variable delay line to the STOP input of the TAC which on receiving the first STOP pulse terminates its charging operation and subsequently generates a TAC-output pulse having its amplitude proportional to the time difference (Δt) between the START and the STOP pulses received by the TAC unit. The TAC output pulse is then fed into the Multichannel Analyzer (MCA) through an Analog-to-Digital Converter (ADC) which converts the voltage signal into a numerical value proportional to the height of the TAC pulse and consequently a measure of the Δt . The numerical value thus generated by the ADC selects the corresponding memory channel in the MCA where a count is added to complete the cycle.

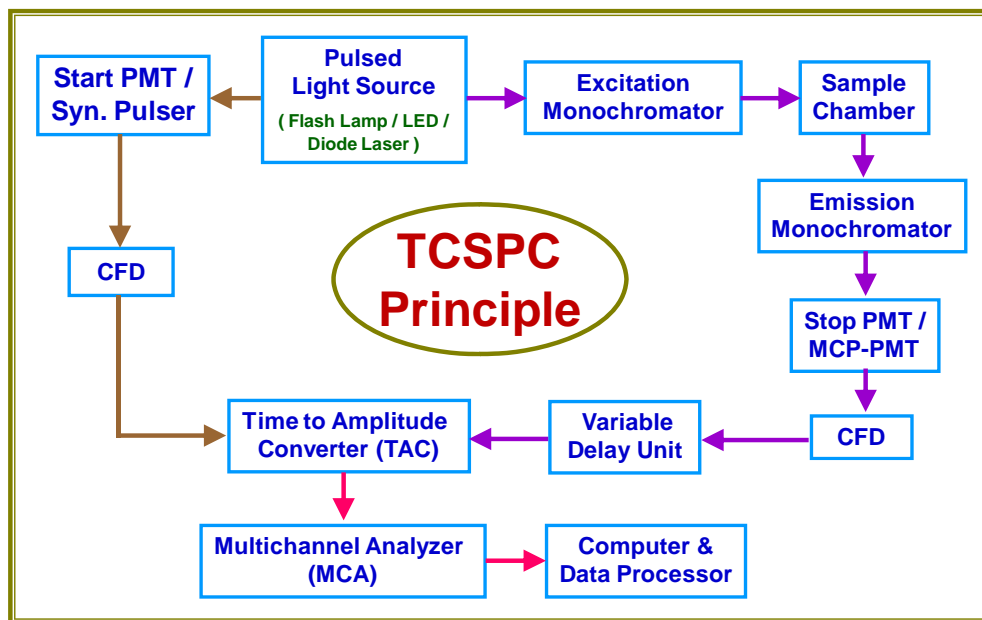


Figure 2.3: Schematic diagram of time-correlated single photon counting spectrometer.

In the TCSPC measurement, the cycle described above (i.e. from triggering of the excitation light source to adding of count in the MCA channel) is repeated for a very large number of times and thereby a histogram of counts is collected in the MCA channels. The distribution of the counts against the channel number in the MCA thus represents the fluorescence decay of the sample, provided the collection rate of the emission photons by the stop PMT is kept very low, only about 2% or less of the pulsing rate of the excitation source.¹¹⁸⁻¹²⁰ This experimental condition effectively means that following an excitation pulse at the most one emission photon is only detected by the stop PMT. Thus, in the TCSPC

measurement, for about 98% cases of the excitation pulses, there is effectively no emission photon emitted from the sample in the direction of the stop PMT. For only about 2% cases of the excitation pulses a photon is emitted in the direction of the stop PMT and hence counted in the MCA channel. Such a low count rate is essential to maintain the time-dependent probability distribution of the photon emission from a single excited molecule following its excitation process. Using the fluorescence decay thus measured, the fluorescence lifetime of the sample is estimated following a suitable analysis method.¹¹⁸⁻¹²⁰

In the present study, a TCSPC spectrometer from Horiba Yobin Yvon IBH, UK, has been extensively used for TR fluorescence measurements. The design of this instrument is qualitatively very similar to that discussed above and schematically shown in Figure 2.3. In the present setup, however, an electrical pulse synchronized with the pulsed light source (diode laser or LED) is used as the start pulse for the TAC than using a start PMT and a MCP-PMT or a fast PMT is used for fluorescence detection (acts as STOP PMT) depending on the availability. Moreover, unlike the first generation TCSPC instruments, the IBH instrument uses a PC card to integrate all the TCSPC components, namely, CFD, TAC, ADC and MCA in a single unit. In the present study, depending on the chromophoric systems involved, different excitation sources, namely, 408 nm diode laser (1 MHz, 100 ps), 374 nm diode laser (1 MHz, 100 ps) and 292 nm LED (1 MHz, 800 ps) were used suitably. In all the cases, the fluorescence decays were measured with magic angle configuration with respect to the vertically polarized excitation beam, to avoid the effect of rotational relaxation of probes on their fluorescence decays. IRF of the experimental setup, $P(t)$, was measured in each case by replacing the sample cell with a dilute scatterer solution (TiO_2 suspension in water) and found to be ~ 230 ps for 408 laser (with fast PMT), ~ 110 ps for 374 laser (with MCP-PMT) and ~ 800 ps for 292 LED (with MCP-PMT).

2.4.1.2. Analysis of fluorescence decays from TCSPC measurements. As the light pulses used in the TCSPC measurements are having a finite time width and also there is a finite response of the components used in the TCSPC instrument, the experimentally measured fluorescence decay, $I(t)$, is effectively a convolution of the true fluorescence decay, $G(t)$, and the actual time profile of the excitation pulse, $P(t)$. Imagining that the excitation pulse profile $P(t)$ is composed of a large number of δ -pulses, the observed decay, $I(t)$, can be expressed in the form of convolution integral of $G(t)$ and $P(t)$ as,¹¹⁸⁻¹²⁰

$$I(t) = \int_0^t P(t') G(t-t') dt' \quad (2.7)$$

Experimentally one can obtain both $I(t)$ and $P(t)$. For the analysis of $I(t)$, a decay function $G(t)$ is first assumed for the sample and this function is convoluted with the observed $P(t)$ following the integral 2.7 to obtain the calculated curve $Y(t)$, which is then compared with the experimentally observed decay $I(t)$.¹¹⁸⁻¹²⁰ In the analysis procedure, the variables in the function $G(t)$ is iteratively varied until a best fit is obtained between $Y(t)$ and $I(t)$. In most cases, for best fit the function $G(t)$ is found to be the sum of exponentials, such that,

$$G(t) = \sum_i a_i \exp -t/\tau_i \quad (2.8)$$

where a_i is the pre-exponential factor for the i^{th} component and τ_i is the corresponding fluorescence lifetime. The success of an analysis and accordingly the acceptance of a fit to the observed decay curve is determined from the judgement of some statistical parameters, the most important ones are given below,

(a) Reduced Chi-square (χ_r^2) values: The reduced chi-square (χ_r^2) for a fit of a fluorescence decay is defined as,¹¹⁸⁻¹²¹

$$\chi_r^2 = \frac{\sum_i W_i \{Y(i) - I(i)\}^2}{(n - p)} \quad (2.9)$$

where $Y(i)$ is the count at the i^{th} channel of the fitted curve, $I(i)$ is the count at the i^{th} channel of the experimentally measured decay curve, $W_i [=1/I(i)]$, is the weighting factor of the counts in the i^{th} channel, n is the number of channels used for the decay to be analysed and p is the number of degrees of freedom (variables) in the $G(t)$ function considered in the analysis. For a good fit, the χ_r^2 value should be very close to unity. Normally a χ_r^2 value between 1.00 to 1.20 is considered to represent a very good fit for the observed decay.

(b) Distribution of weighted residuals: To judge the quality of the fit of a decay curve from TCSPC measurement, the nature of distribution of the weighted residuals among the data channels is considered to be an important criterion. For a data set, the weighted residual for the i^{th} channel, r_i , is defined as,¹¹⁸⁻¹²¹

$$r_i = \sqrt{W_i} \{Y(i) - I(i)\} \quad (2.10)$$

where W_i , $Y(i)$ and $I(i)$ are as defined earlier. For a good fit, the r_i should be randomly distributed about the zero line for the whole range of the data channels used in the analysis.

2.5. Fluorescence Anisotropy Measurements

In a homogeneous solution, the ground-state fluorophores are all randomly oriented. When such an isotropic ensemble of chromophores is irradiated with a polarized light beam there will be selective excitation of the suitably oriented chromophoric molecules only, and hence an anisotropic distribution will be generated in the excited state (also in the ground-state, which is not considered here). Thus, observation and measurement of fluorescence anisotropy is based on the photoselective excitation of fluorophores, which can be better understood in the following manner. Each fluorophore has within its molecular framework the definite orientations of its absorption and emission transition dipoles, inclined to each other by a fixed angle β . A fluorophore preferentially absorbs the excitation photons if its absorption transition dipole is parallel to the electric field vector of the polarized excitation light. The probability of absorption for a molecule whose absorption dipole is oriented at an angle θ with respect to the electric field vector of the polarized light is proportional to $\cos^2 \theta$. Therefore absorption is maximum when $\theta = 0^\circ$ and becomes negligible when θ approaches 90° .^{1-4,118-120} Thus, the ensemble of excited state molecules produced following excitation by a polarized excitation pulse are not randomly oriented any more but are anisotropic with respect to their orientation of absorption dipoles, as is schematically shown in Figure 2.4. Similarly, an excited molecule emits a photon preferentially with its electric field vector parallel to the emission transition dipole of the molecule. At any other angle θ , the probability of emission is again proportional to $\cos^2 \theta$, where θ is the angle between the electric field vector of the emitted light and the emission transition dipole of the molecule. Thus, due to the selective excitation and emission, the fluorescence obtained following excitation of sample with a polarized light is highly anisotropic in nature.

In dilute solution, where depolarization of the excited molecules via intermolecular energy transfer among chromophoric molecules is very insignificant, the excited-state anisotropy of the system decays mainly due to the rotational relaxation of the excited species. Therefore, fluorescence anisotropy measurements can reveal the extent of angular displacement that the fluorophores undergo between the absorption and emission process. The time dependent angular displacement is dependent upon the rate of rotational diffusion of the excited fluorophore, which in turn depends upon the size and shape of the molecule and also on the viscosity and/or rigidity of its local microenvironments. Thus, studies on the fluorescence anisotropy have been utilized extensively to explore the local environment of

the chromophoric dyes as well as to investigate their interactions with various host molecules or supramolecular assemblies.

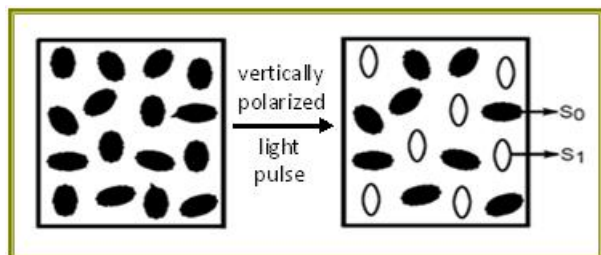


Figure 2.4: Creation of ground-state and excited state anisotropies from an isotropic distribution of molecules.

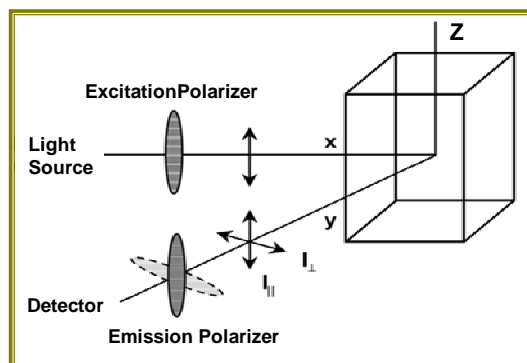


Figure 2.5: Schematic describing measurement of fluorescence anisotropy

Fluorescence anisotropy can be measured using both SS and TR fluorescence spectrometers. In SS measurement, the sample is illuminated with a continuous beam of plane polarized light, and the intensities of the fluorescence emission are recorded for both parallel and perpendicular polarizations of the emitted light with respect to the vertically polarized excitation light. In TR anisotropy measurement, the sample is excited with a vertically polarized excitation pulse and the fluorescence decays are collected for both parallel and perpendicular polarizations of the emitted light with respect to the excitation polarization. The schematic of the fluorescence anisotropy measurement (both SS and TR) is illustrated in Figure 2.5, where sample is excited with a vertically polarized light, (i.e. electric vector oriented along z-axis) and emission is measured through a polarizer oriented either parallel (\parallel) or perpendicular (\perp) to the excitation polarization. With emission polarizer parallel to the excitation polarization, the observed fluorescence intensity is labeled as I_{\parallel} . Similarly, when emission polarizer is perpendicular to the excitation polarization, the observed intensity is designated as I_{\perp} . Since the responses of the detection components are not the same for both parallel and perpendicularly polarized light, the measured perpendicular component I_{\perp} is corrected by an appropriate correction factor, known as G-factor, to rectify the polarization bias of the detection setup. Thus, from the measured I_{\parallel} and I_{\perp} values the SS anisotropy ($\langle r \rangle$) is calculated as,^{1-4,118-120}

$$\langle r \rangle = \frac{I_{\parallel} - GI_{\perp}}{I_{\parallel} + 2GI_{\perp}} \quad (2.11)$$

In the measurement, G factor is independently determined by keeping the excitation polarization horizontal i.e. along Y- axis and measuring the fluorescence intensities with the emission polarizer oriented vertical (I_{HV}), and horizontal (I_{HH}), respectively, where the intensity ratio I_{HV}/I_{HH} gives the measure of the G factor for the detection setup at the measuring emission wavelength.

Similar to SS anisotropy, the TR fluorescence anisotropy can also be expressed by the following equation,¹⁻⁴

$$r(t) = \frac{I_{\parallel}(t) - GI_{\perp}(t)}{I_{\parallel}(t) + 2GI_{\perp}(t)} \quad (2.12)$$

where $I_{\parallel}(t)$ and $I_{\perp}(t)$ are the two polarized fluorescence decays with emission polarizations parallel and perpendicular to the vertically polarized excitation light. To be mentioned that in the present work we mainly measured the TR fluorescence anisotropy to characterize the micellar systems used for the PET studies. The $r(t)$ function thus obtained is subsequently analyzed, generally considering it as a sum of exponentials as,^{1-4,118-120}

$$r(t) = \sum_{i=1}^n r_{0,i} \exp(-t/\tau_{r,i}) \quad (2.13)$$

where $r_{0,i}$ is the initial anisotropy immediately after the δ -excitation pulse and $\tau_{r,i}$ is the rotational correlation time or simply the reorientation time for the i^{th} rotational component.

2.7. Fluorescence up-conversion Measurements

In TR fluorescence measurements, using the state of art TCSPC technique in conjunction with a fast PMT or a MCP-PMT it is possible to achieve time-resolution at the best of about few tens of picoseconds only.¹¹⁸⁻¹²⁰ To obtain time-resolution in the sub-picosecond to femtosecond domain, it is required to have a technique that uses nonlinearity induced in the system by high energy laser pulses as the timing gate for emission measurement.¹²²⁻¹²⁴ Such a nonlinear method is known as the fluorescence up-conversion technique, first introduced by Mahr and Hirsch,¹²³ utilizing the frequency mixing principle in a non-linear crystal to achieve an ultrafast time-resolution in fluorescence measurement. In this technique, the emission from the sample is mixed with an ultra-short laser pulse (gate pulse) in a nonlinear crystal to generate the sum frequency light. Since the mixing process takes place only for a small time window for which there is a temporal overlap between the gate pulse and the fluorescence emission, this technique can provide time-resolution effectively comparable to the width of the gate pulse used for the frequency mixing process. The fluorescence up-conversion

method is undoubtedly the most widely used technique for ultra-fast fluorescence studies not achievable by any other TR fluorescence techniques.

Figure 2.6 shows the schematics of the femtosecond fluorescence up-conversion setup used in the present study. A mode-locked Ti: sapphire oscillator (from CDP Inc. Russia) that is optically pumped by a diode pumped solid state laser from Coherent (Verdi, 5W at 532 nm) produces ultra short laser pulses of ~50 fs duration at around 800 nm with a repetition rate of 82 MHz. The second harmonic (~400 nm) of this laser pulse is generated using nonlinear barium borate (BBO) crystal (thickness 1 mm).

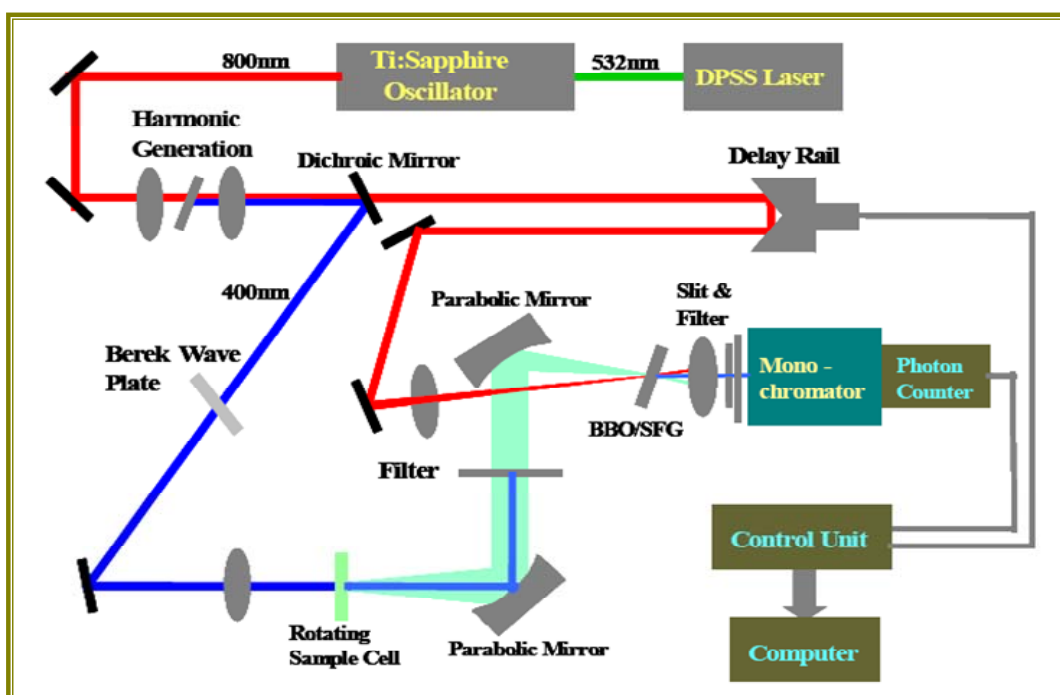


Figure 2.6: Schematic diagram of femtosecond fluorescence up-conversion setup

A dichroic mirror is used to separate the 400 nm, second harmonic light from 800 nm fundamental light. While the 400 nm light is used to excite the sample the residual 800 nm light is used as the gate pulse to up-convert the fluorescence from the sample in a suitable BBO crystal (thickness 0.5 mm). In the experimental arrangement, to minimize photo-degradation, the sample solution is kept in a rotating quartz cell of 1 mm thickness that helps to avoid the localized heating and hence to reduce the photo-decomposition of the sample. To avoid the residual excitation light and/or Raman light to reach the up-conversion crystal, a cut off filter is used just after the sample cell. The short-lived fluorescence originating from the samples is collected by using two elliptical mirrors focused onto the up-conversion crystal. The 800 nm gate pulse is first passed through an optical delay line and subsequently

focused onto the up-conversion crystal to mix with the fluorescence from the sample, resulting the sum-frequency signal given as,¹²²⁻¹²⁶

$$I_{\text{sum}}(\tau) = \int_0^{\infty} I_{\text{fl}}(\tau) I_{\text{gate}}(t - \tau) dt \quad (2.14)$$

where τ is the optical delay between the excitation (400 nm) and the gate (800 nm) pulses, I_{sum} , I_{fl} and I_{gate} are the intensities of the sum frequency, fluorescence and gate pulse, respectively, at the concerned times. Eq. 2.14 clearly suggest that recording $I_{\text{sum}}(\tau)$ versus τ will reproduce the fluorescence decay of the sample as schematically shown in Figure 2.7. Since the gate pulse is much shorter than the time dependent fluorescence, it acts as an optical gate for the up-conversion signal. The time resolution of the measurement directly depends on the temporal width of the gate pulse.

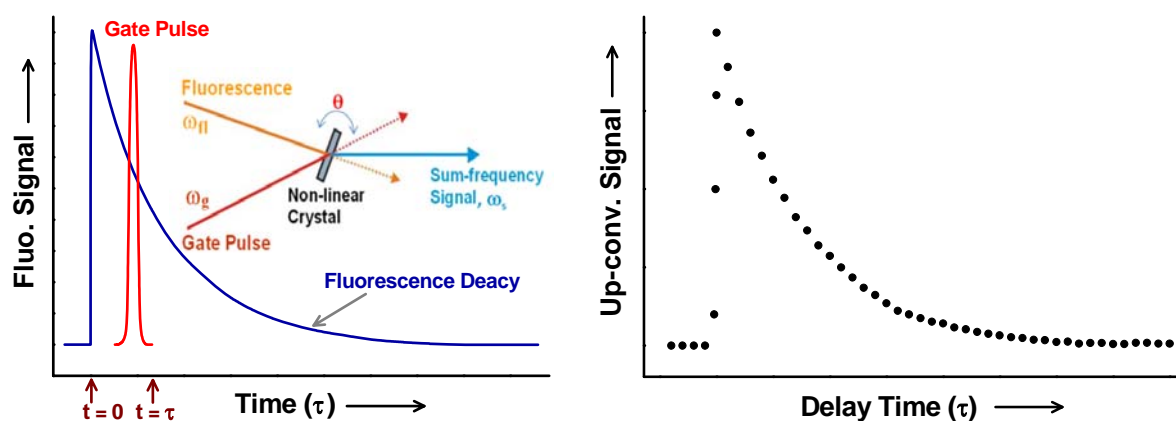


Figure 2.7: Schematics of mixing of fluorescence and gate pulses and the collection of a kinetic trace using up-conversion technique.

2.8. Time Resolved Transient Absorption Measurements

In 1949 Norrish and Porter showed that the photochemically induced transient species e.g. electronically excited molecules, radical intermediates, etc. can be generated in sufficiently high concentrations using very intensity and short duration light pulses.^{127,128} Since the transients are produced in times shorter than their lifetimes, the temporal evolution of these species can be monitored using a suitable method, the widely used one being the transient absorption technique and the overall technique is commonly known as “Flash Photolysis Technique”. A similar procedure of transient studies, where a short duration laser pulse is used instead of the conventional light flash, the technique is termed as the “Laser Flash Photolysis Technique (LFP)”, a very important technique used for transient detection.

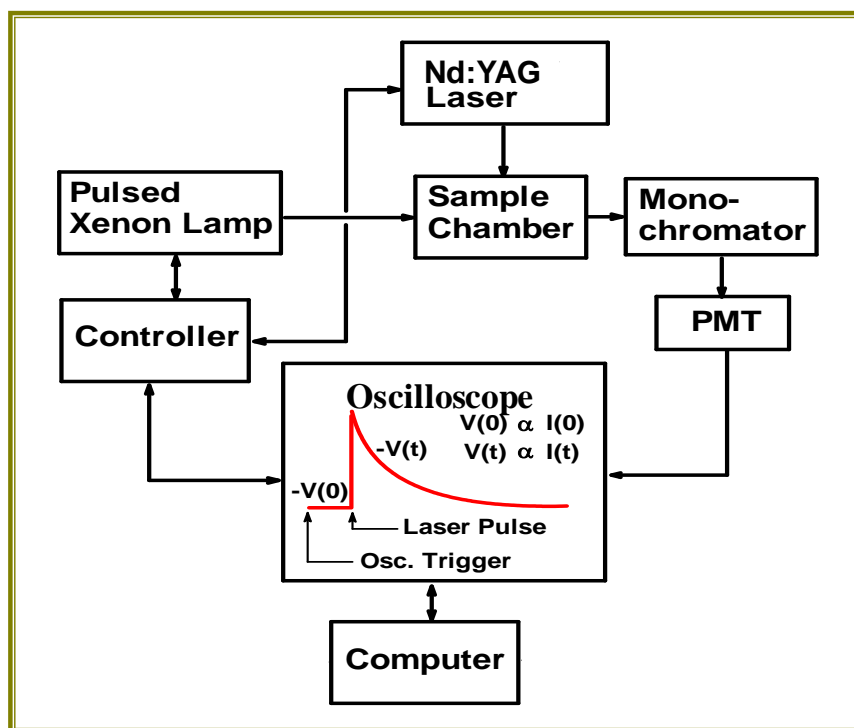


Figure 2.8: Block diagram of nanosecond laser flash photolysis setup used in the present study.

In our nanosecond LFP setup, sample was irradiated with the fourth harmonic of a picosecond Nd:YAG laser (Model PL 2251c, Ekspla, Lithuania) and transient kinetic traces at different wavelengths were recorded using a pulsed xenon lamp-based nanosecond kinetic spectrometer (Model LP 920, Edinburg Instruments, UK). The block diagram of the present LFP setup is shown in Figure 2.8. In this setup full experiment is carried out under computer controlled condition, obtaining the transient kinetic traces which can be further processed to extract the kinetic information as well as to construct the TR transient absorption spectra.

2.9. Redox Potential Measurements

The reduction potentials of the coumarin dyes and the oxidation potential of N,N-dimethyl amine donor in micellar solutions were measured by cyclic voltammetric (CV)¹²⁹ method using a Eco-Chemie Potentiostat/Galvanostat-100, with a GPES 4.9 software. Sample solutions containing 0.1 mol dm⁻³ potassium chloride as the supporting electrolyte were first de-aerated by purging high purity N₂ gas for about 30 minutes. CV measurements were then carried out using dropping mercury as the working electrode, carbon black rod as counter electrode and saturated calomel (SCE) as the reference electrode.

2.10. Dynamic Light Scattering

Dynamic light scattering (DLS) is one of the most commonly used techniques for particle size determination.¹³⁰ In the present work, DLS studies were carried out using Malvern 4800 autosizer coupled with a 7132 digital correlator and PCS0078 software for the determination of the sizes of the studied micelles and dye aggregates. The minimum particle size measurable with the present instrument is about 5 nm.

An Argon ion laser with 514.5 nm emission was used as the light source. The light scattered from the sample was collected at right angle using an avalanche photodiode (APD) detector. Diffusion coefficients of the scattering particles were calculated from the autocorrelation function, $C(t)$, according to the following equation.

$$C(t) = 1 + e^{-2Dq^2t} \quad (2.15)$$

where D is the diffusion coefficient of the scattering particles and q is the scattering vector defined by the following equation.

$$q = \frac{4\pi n}{\lambda} \sin(\theta/2) \quad (2.16)$$

where n is the refractive index of the medium, λ is the wavelength of the laser light and θ is the scattering angle, 90° in the present case. The hydrodynamic radius, R_h of the scattering particles was calculated using the Stokes-Einstein equation.

$$R_h = \frac{k_B T}{6\pi\eta D} \quad (2.17)$$

where k_B is the Boltzmann constant, T is the absolute temperature and η is the viscosity of the medium.

2.11. Scanning electron microscopy (SEM)

Scanning electron microscopy (SEM) is a type of electron microscope. It is a very powerful tool to understand high resolution and high magnification topography and morphology of surfaces, chemical compositions, crystalline structure of materials, orientations of grains, size and shape of nano/micro-particles, and many others. In SEM technique a beam of high-energy incident electrons is generated in an electron column above the sample chamber. This electron beam is focused at the surface of the solid specimen to be investigated. The incident electrons cause the sample of investigation to emit secondary electrons due to elastic and inelastic scattering of the surface and near-surface materials sample. To create an SEM image, the incident electron beam is scanned across the surface of sample and the emitted

secondary electrons are detected for each position in the scanned area by an electron detector. The intensity of the emitted electron signal is displayed as brightness on a display monitor and/or in a digital image file. By synchronizing the position in the image scan with the position of the scanning incident electron beam, the display recorded represents the topography and morphology of the scanned sample surface. Magnification of the image is the ratio of the image display size to the sample area scanned by the electron beam.

In the present study, SEM measurements were carried out using a Zeiss Auriga SEM instrument, having resolution of <2.5 nm and magnification range of 300x - 500 kx. Microfilms for the SEM studies were prepared by putting a drop of the sample solution of interest on a highly polished copper stub and allowing the solvent to evaporate at ambient condition to obtain the microfilms for SEM measurements. Images of the microfilms were then recorded in the SEM instrument under high vacuum with different magnifications ranging from 8 kx to 50 kx, to obtain the necessary details of the studied samples.

Chapter 3

Photoinduced Electron Transfer reactions in Pluronic Micellar Media: Observation of Marcus Inversion

Abstract

Photoinduced electron transfer (PET) reaction involving N,N-dimethylaniline (DMAN) as electron donor and 7-aminocoumarin dyes (C151, C152, C153, C481 and C522) as electron acceptors has been investigated in pluronic micellar media of 5% w/v F88 (EO₁₀₃-PO₃₉-EO₁₀₃; where EO: ethylene oxide and PO: propylene oxide) at 38 °C, following fluorescence quenching studies. In addition to PET studies, F88 micelles have also been characterized in regard to the critical micellar temperature (CMT), micellar dimension, micropolarity, microviscosity, hydration characteristics, etc. The results of the present study in F88 micelle are compared with those in P123 (EO₂₀-PO₇₀-EO₂₀) micelle, reported in the literature. Due to its higher EO to PO ratio, the water molecules in the corona of F88 micelle are found to be more labile than that in P123 micelle. The higher hydration in F88 micelles results in the observed ET rates to be much higher than those in P123 micelles. Interestingly, Marcus inversion is observed and its onset for the ET reactions in F88 micelles appears at an exergonicity ($-\Delta G^0$) of about 0.77 eV, which is significantly lower than what otherwise expected in conventional solvents. This is attributed to the suppressed reactant diffusion and significantly slow solvent relaxation in micellar media. Onset of Marcus inversion in F88 micelle, however, appears at a comparatively higher exergonicity (0.77 eV) in comparison to that reported in P123 micelle (0.68 eV). This is understandably due to the higher EO to PO ratio and the consequent higher hydration of F88 micelle than that of P123 micelle. Present results demonstrate that by tuning the EO to PO ratio of the pluronic polymers it is possible to modulate the ET rates quite substantially and finds application in areas where bimolecular ET is an integral step of the reaction sequences.

3.1. Introduction

Theoretical background of ET reactions has been discussed with necessary details in Chapter 1. In the literature ET reactions have been investigated extensively in microheterogeneous media as these reactions have direct relevance to many practical applications like solar energy conversion, photovoltaic, biotechnology, information storage, solid state electronics, molecular electronics, sensing, catalysis, and many others.⁵⁻²¹ In this chapter we present the results of our study on PET reactions in pluronic F88 (EO₁₀₃-PO₃₉-EO₁₀₃; where EO: ethylene oxide and PO: propylene oxide) micellar solution to understand if these micellar media can be useful in modulation of the kinetics and energetics of the ET reactions, especially in relation to Marcus inversion behavior.

Realization and understanding of Marcus inversion, that is the reduction in the ET rates at higher exergonicity ($-\Delta G^0$), is the most intriguing aspect of ET studies.^{5-11,21-31,131-133} As discussed in Section 1.2, following Marcus ET theory,⁵⁻¹⁰ the changes in the ET rate constant k_{et} with reaction exergonicity ($-\Delta G^0$) should follow a bell-shaped curve with the rate increasing in the normal region ($-\Delta G^0 < \lambda$) and decreasing in the inversion region ($-\Delta G^0 > \lambda$), giving the onset of Marcus inversion at $-\Delta G^0 = \lambda$ where ET rate is the maximum. The exergonicity corresponding to the onset of Marcus inversion is a very important consideration for an efficient PET process, as the energy wasting back ET process producing the ground state reactants is always associated with the forward PET. Since, the back ET invariably occurs with higher exergonicity than the forward PET,⁵⁻¹⁰ to have an efficient PET system, the forward PET should occur around the onset of Marcus inversion, causing the associated back ET to be pushed deep into the inversion region such that the forward ET occurs with much faster rate than the back ET. In fact, this important criterion is efficiently being utilized by nature in photosynthetic systems to maximize the desired yield of the ET process.⁵⁻¹⁰ It is thus very important to know the Marcus correlation curve for the ET reactions to design an efficient PET system for useful application.

In the literature, most of the experimental evidences of Marcus inversion are reported for intramolecular ET reactions, where donor and acceptor are covalently linked.^{32-35,98-101} For bimolecular ET reactions, however, the changes in the ET rates with reaction exergonicity in general follow the typical Rehm–Weller behavior,^{49,110,134,135} as discussed in Section 1.9. The two important difficulties in realizing Marcus inversion: (i) limitation imposed by the diffusion of the reactants and (ii) non-availability of suitable donor–acceptor series to achieve very high reaction exergonicity.^{5-10,49,110} These difficulties are possible to be circumvented by

carrying out PET reactions in organized assemblies like micelles,¹³⁶⁻¹⁴⁵ because in these media the lateral diffusion of the reactants will be largely restricted causing the reactions to occur under non-diffusive condition and hence to resemble like intramolecular reactions. Additionally, due to slow solvation, contribution of solvent reorganization energy (λ_s) towards the activation barrier for ET reaction can be reduced significantly due to non-equilibrium solvent relaxation during the ET process, causing the onset of Marcus inversion to appear at a significantly lower exergonicity.¹³⁶⁻¹⁴¹ Therefore, in a microheterogeneous media the Marcus inversion behavior can be observed easily for bimolecular ET reactions, though it otherwise remains mostly obscured in conventional solvents.^{3,5-10,49,146}

This chapter describes the results of our studies on PET reactions in pluronic F88 micellar solution. Characteristics of pluronics or block copolymers and their micellization behavior have been discussed in Section 1.7.^{60-79,147-149} In this work, PET reactions involving several coumarin dyes as electron acceptors and N,N-dimethylaniline (DMAN) as electron donor (*cf.* Chart 3.1) have been carried out in 5% w/v pluronic F88 micellar solution to understand the correlation between ET rates and reaction exergonicity. Observed PET results have been compared with those reported in P123 micelle¹⁴¹ having largely different EO to PO ratio compared to that of F88, to understand how different microenvironments of the pluronic micelles affect the kinetics and dynamics of the PET reactions. The aim of the present study has also been to explore if Marcus inversion behavior can be observed in the restricted F88 micellar media as observed earlier in P123 micelle.¹⁴¹ In this context, measurements have also been carried out to explore the micellar characteristics of pluronic F88 and the results are compared with those reported for P123 micelle,⁸⁶ to understand the relation between the observed PET rates and the micellar microenvironments of the two pluronic systems and thus to apprehend if there is a possibility to tune Marcus correlation curves by the selection of a suitable pluronic micellar media.

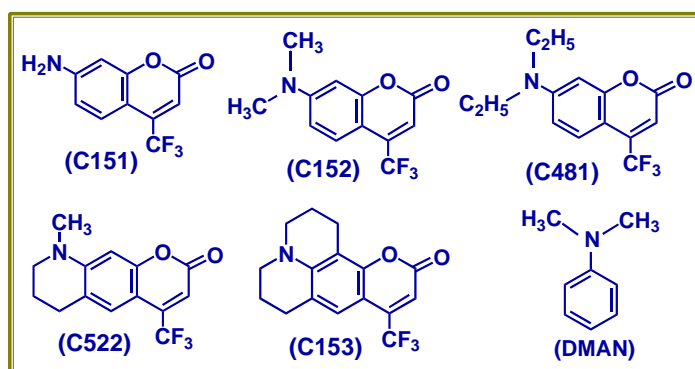


Chart 3.1: Structures of the coumarin acceptors and DMAN donor used in the present study.

3.2. Experimental Methods and Materials

Instrumental facilities used for ground state absorption, SS fluorescence and TR fluorescence measurements are described in Sections 2.2, 2.3 and 2.4, respectively. In the present work, solvation dynamics (*cf.* Section 2.5) and TR fluorescence anisotropy (*cf.* Section 1.5) measurements were also carried out to explore the microenvironments of the the pluronic micelle. In all the TR measurements a 408 nm diode laser (1 MHz and 100 ps) was used as the excitation source. Redox potentials of coumarin acceptors and DMAN donor in the studied micellar solution were estimated using CV measurements (*cf.* Section 2.9). DLS studies (*cf.* Section 2.10) were carried out to estimate the size of the micellar aggregates.

F88 was a gift from BASF corporation, Edison, NJ, USA. Coumarin dyes were from Exciton, USA and used as received. DMAN was from Spectrochem, India and purified by vacuum distillation just before use. F88 solution was prepared by taking 0.05 gm of the pluronic per ml of nanopure water (conductivity 0.1 mS cm⁻¹) from Elix-3/A10 Millipore system. The solution was stirred at room temperature for about 24 hours for the dissolution of the polymer. Coumarin and amine were added directly to F88 solution and stirred for about 4 hours at 38 °C, a temperature where micellization of the pluronic solution is established completely (*vide infra*). All the subsequent studies were also accordingly carried out at 38 °C, maintaining the temperature within ± 1 °C by using a microprocessor based temperature controller from IBH. In the experimental solutions the dye concentrations were always kept very low ($< 5 \mu\text{M}$) to avoid multi-occupancy of the dye molecules in a single micelle.

3.3. Results and Discussion

3.3.1. Characterization of Microenvironment in F88 Micelle

3.3.1.1. Determination of critical micellar temperature (CMT) and size of F88 micelle. The solution behavior of pluronic F88 has been studied extensively to understand its micellization process. Though the CMT values of F88 solution are reported in the literature,^{83,150} in the present study we preferred to measure the CMT independently for 5% w/v F88 solution used in the PET studies because pluronic samples are often quite polydispersed to cause a variation in the estimated CMT values.¹⁵¹

Fluorescence probe that solubilize sparingly in water but preferentially in the micellar phase are commonly used to determine the onset of micelle formation following the changes in the fluorescence characteristics.^{61,152} Polar coumarin dyes are very suitable probes for such

studies as the fluorescence properties of these dyes are quite sensitive to their local microenvironments. In the present study coumarin 153 (C153) dye has been used as the fluorescence probe. Figure 3.1A shows the temperature dependent changes in the emission maxima ($\bar{\nu}_{\max}$) of the dye in 5% w/v F88 solution, indicating a sharp blue shift at around 34 °C, witnessing the onset of micelle formation. Since C153 is a hydrophobic probe, as micelles are formed, the dye preferentially enters the micellar phase where micropolarity is much less than in the bulk water and hence there is a large blue shift in the $\bar{\nu}_{\max}$ value of the dye. From the present result the CMT for 5% w/v F88 solution is $\sim 34^{\circ}\text{C}$, which is in good agreement with the literature report.^{83,150}

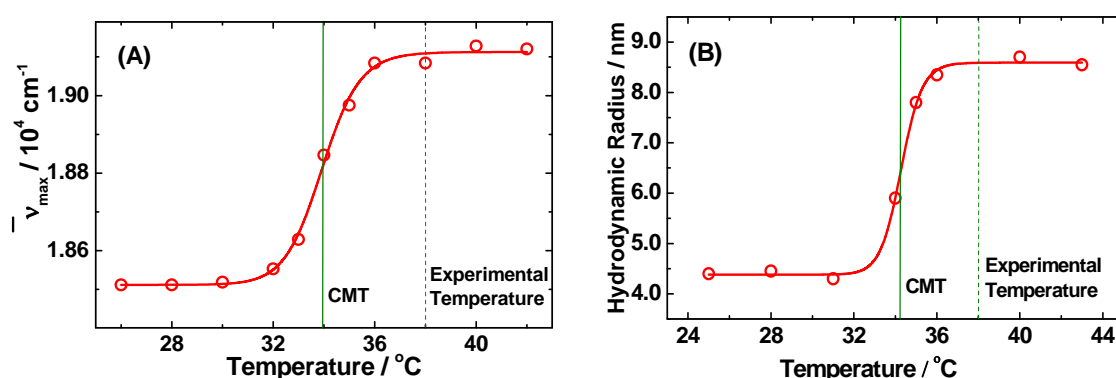


Figure 3.1: (A) Variation of the fluorescence emission maxima of C153 dye and (B) changes in the average radii of the scattering particles measure by DLS studies in aqueous solution of 5% w/v F88. The vertical solid line indicates CMT at 38 °C.

To support the above CMT estimate, the size of the aggregates in 5% w/v F88 solution was also measured as a function of temperature following DLS studies and the results are shown in Figure 3.1B. It is evident from this figure that there is a large sigmoidal change in the particule size at $\sim 34^{\circ}\text{C}$ indicating the onset of micelle formation. Thus, the DLS results are in good agreement with the result obtained from fluorescence measurements establishing the CMT of 5% w/v F88 solution as 34°C . In all our subsequent studies, thus, the solution temperature was maintained at 38°C to ensure complete micellization of F88. From Figure 3.1A and B, it is evident that the plots saturate at $\sim 38^{\circ}\text{C}$, ascertaining the complete micellization process for 5% w/v F88 solution.

3.3.1.2. Characterization of probe location and micropolarity around it. To estimate the micropolarity of the solubilized probe in 5% w/v F88 solution at 38°C , the fluorescence spectrum of C153 was recorded and compared with those of the dye in homogeneous

water-isopropanol solvent mixtures having different solvent polarities. Figure 3.2A shows the SS emission spectra of C153 in water, isopropanol and 5% w/v F88 solution at 38 °C. It is evident from Figure 3.2A that the polarity experiences by C153 dye in the pluronic solution is higher than that in isopropanol but much lower than that in water. Figure 3.2 also shows the spectrum of C153 in neat polypropylene oxide (PPO) polymer for a comparison with that in F88 micellar solution. The emission maximum in neat PPO appears at much shorter wavelength than that in isopropanol and 5% w/v F88 solution. From the present results we infer that the micropolarity around the dye in the present micellar media is much higher than that in neat PPO. Present results thus exclude the possibility of the presence of C153 dye in the nonpolar core of the pluronic micelle studied.

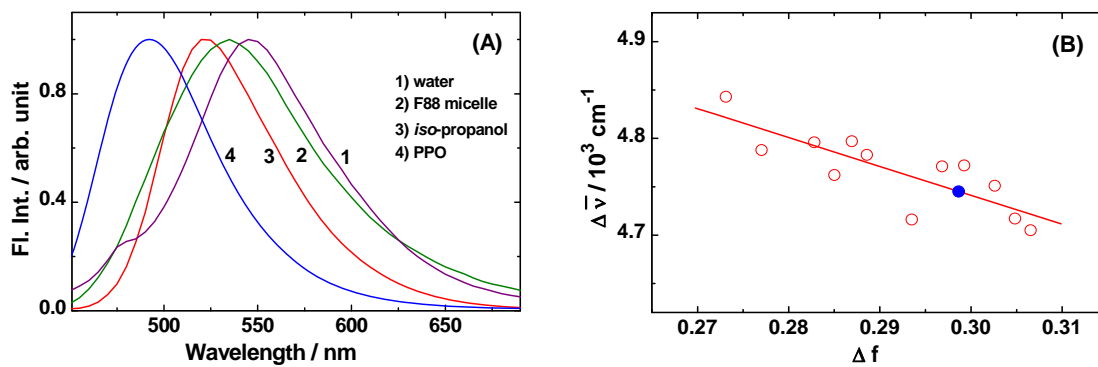


Figure 3.2: (A) SS fluorescence spectra of C153 dye in water (1: purple), 5% w/v of F88 solution at 38°C (2: olive), *i*-propanol (3: red) and liquid PPO (4: blue). (B) Plot of fluorescence maxima ($\bar{\nu}_{fl}$) in different solvent mixtures against the Lippert Mataga solvent polarity function, Δf .

In order to have a quantitative estimate of the micropolarity and hence to characterize the location site of the coumarin dyes in the micellar phase, $\bar{\nu}_{max}$ values of C153 dye were recorded in different isopropanol-water solvent mixtures and correlated with the Lippert Mataga solvent polarity function, Δf , of these solvents (estimated by Eq. 3.1) to obtain a calibration plot, as shown in Figure 3.2B.^{3,153-156}

$$\Delta f = \frac{\epsilon - 1}{2\epsilon + 1} - \frac{n^2 - 1}{2n^2 + 1} \quad (3.1)$$

where ϵ is the static dielectric constant and n is the refractive index of the solvent. For water and *i*-propanol, the ϵ and n values were taken from literature.¹⁵⁶ For solvent mixtures the dielectric constant (ϵ_{mix}) and the refractive index (n_{mix}) were estimated as,¹⁵³⁻¹⁵⁵

$$\epsilon_{mix} = f_A \epsilon_A + f_B \epsilon_B \quad (3.2)$$

$$n_{mix}^2 = f_A n_{mix}^2 + f_B n_{mix}^2 \quad (3.3)$$

where f_A , f_B stand for the volume fractions of the co-solvents A and B. Thus knowing the \bar{v}_{\max} value of the dye in F88 micelle, the ϵ value of the micellar microenvironment at the dye localization site is estimated to be ~ 23 . To be mentioned here that the ϵ value for the dye in P123 micelle (5% w/v) is reported to be ~ 10 .¹⁴¹ From these ϵ values, it is suggested that the polar coumarin dyes preferentially reside in the polar corona region in both the pluronic micelles.^{86,141} It is also very evident from the present result that the effective polarity in the corona region of F88 micelle is significantly higher than that of P123 micelle. Therefore, we infer that the corona region of F88 micelle is more hydrated than that of P123 micelle, certainly due to the higher EO to PO ratio in the former pluronic polymer.

3.3.1.3. Solvation Dynamics studies. The polarity at the micellar corona is largely determined by the water molecules dispersed in this region of the micelle. Solvation dynamics studies were carried out in 5% w/v F88 solution at 38 °C using C153 as the probe and following the procedure given in Section 2.6 to understand the nature of the water molecules. Representative wavelength dependent fluorescence decays of C153 dye and the subsequently constructed TRES in the F88 micelle are shown in Figure 3.3A and B, respectively. Inset of Figure 3.3B shows the time-dependent shift in \bar{v}_{\max} in the TRES, which could be fitted satisfactorily with a bi-exponential function as Eq. 3.4, giving the two time constants τ_{s1} and τ_{s2} and their relative amplitudes a_{s1} and a_{s2} , as are listed in Table 3.1.

$$\bar{v}_{\max}(t) = a_{s1} \exp(-t/\tau_{s1}) + a_{s2} \exp(-t/\tau_{s2}) + \bar{v}_{\infty} \quad (3.4)$$

The solvation parameters for P123 micelle as reported in the literature are also listed in Table 3.1 for comparison. The average solvation time, $\langle \tau_s \rangle$, was also calculated for both F88 and P123 micelles using Eq. 3.5 and the values are also listed in Table 3.1.

$$\langle \tau_s \rangle = (a_{s1} \tau_{s1}^2 + a_{s2} \tau_{s2}^2) / (a_{s1} \tau_{s1} + a_{s2} \tau_{s2}) \quad (3.5)$$

It is evident from this table that the solvation process is much faster in F88 micelle than in P123 micelle, suggesting the corona region of F88 micelle to be much more hydrated than that of P123 micelle. Obviously, solvation in both F88 and P123 micelles are much slower than that in bulk water ($\langle \tau_s \rangle \sim 1$ ps)^{157,158} and this is due to the restricted motion of the water molecules inside the micellar microenvironment.

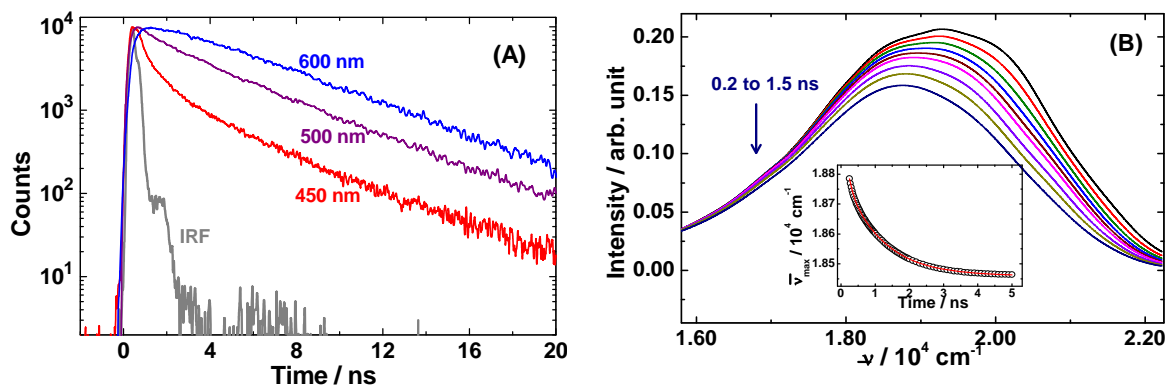


Figure 3.3: (A) Fluorescence kinetic traces for C153 dye in 5% w/v solution of F88 solution at 38 °C measured at different emission wavelengths. (B) TRES for the above system. **Inset:** Time dependent changes in the peak wave number of the TRES for the studied system.

Table 3.1: Parameters for solvation and rotational dynamics for C153 dye in F88 and P123 solutions.^a

Pluronic solution	Parameters for solvation dynamics					Parameters from anisotropy studies				
	a_{s1}	τ_{s1}/ns	a_{s2}	τ_{s2}/ns	$\langle\tau_s\rangle/\text{ns}$	a_{r1}	τ_{r1}/ns	a_{r2}	τ_{r2}/ns	$\langle\tau_r\rangle/\text{ns}$
F88	0.11	0.10	0.89	1.08	0.97	0.45	0.81	0.55	2.66	1.83
P123 ^a	0.46	0.22	0.54	2.23	1.31	0.08	0.42	0.92	3.12	2.89

^aParameters for 10% w/v P123 solution were obtained from ref. 86.

3.3.1.4. Anisotropy Studies. To explore the nature of the micellar corona of F88 further, we carried out time-dependent anisotropy measurements following the procedure given in Section 2.5. Figure 3.4 shows the anisotropy decay measured in the present system using C153 dye as the probe. The anisotropy decay fits with bi-exponential function as,

$$r(t) = a_{r1} \exp(-t/\tau_{r1}) + a_{r2} \exp(-t/\tau_{r2}) \quad (3.6)$$

Estimated rotational time constants τ_{r1} and τ_{r2} and their respective amplitudes a_{r1} and a_{r2} are listed in Table 3.1 along with those of P123 micelle as reported in the literature.⁵⁸ Table 3.1 also lists the average reorientation times, $\langle\tau_r\rangle$, for F88 and P123 micelles by using Eq. 3.7

$$\langle\tau_r\rangle = (a_{r1}\tau_{r1}^2 + a_{r2}\tau_{r2}^2)/(a_{r1}\tau_{r1} + a_{r2}\tau_{r2}) \quad (3.7)$$

The observation that the anisotropy decay in F88 micelle is faster than in P123 micelle is in accordance with the inference that the corona region of the former micelle is much more hydrated than that of the latter micelle.

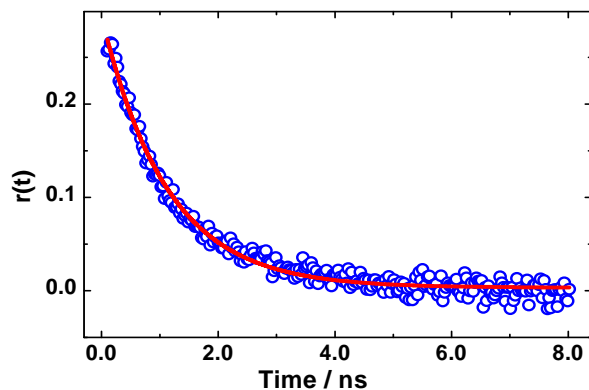


Figure 3.4: Fluorescence anisotropy decay for C153 dye in 5% w/v solution of F88 solution at 38 °C. The solid line is the best fit of the data to the function given in equation 3.6.

The bi-exponential anisotropy decay in the present system can be rationalized on the basis of the well known two-step model used for anisotropy decay in micellar media. According to this model, the anisotropy decay of a probe in a micelle is caused by the contributions of a fast and a slow rotational correlation functions that are separable from each other on the basis of the isotropic and anisotropic nature of the concerned motions.^{84-86,111,159}

$$r(t) = r_{\text{fast}}(t) r_{\text{slow}}(t) \quad (3.8)$$

The $r_{\text{slow}}(t)$ arises due to two slow motions namely the lateral diffusion of the probe along the spherical surface of the micelle and the exceptionally slow motion of the whole micelle rotation in the solution, both of which are isotropic in nature. Hence, the overall $r_{\text{slow}}(t)$ is,

$$r_{\text{slow}}(t) = \exp(-t/\tau_{\text{slow}}) \quad (3.9)$$

where, τ_{slow} is the effective rotational time corresponding to the mutual effect of the lateral diffusion of the probe and the rotation of the whole micelle. The $r_{\text{fast}}(t)$ function arises due to the fast wobbling motion of the probe dye in the micelle at its localization site and accordingly this function is largely dependent on the local structure of the micelle around the dye. From Table 3.1, we can infer that the τ_{r1} and τ_{r2} components are due to the wobbling motion and the lateral diffusion of the dye in the micelle because the rotational motion of the whole micelle occurs with much longer time constants than wobbling and lateral diffusion. In this context, however, we restricted ourselves from the complex analysis of τ_{r1} and τ_{r2} values further as it is beyond the scope of the present PET studies. In any case, from the results in Table 3.1 we conclusively infer that the overall rotational relaxation in F88 micelle is much faster than that in P123 micelle as because the microviscosity in the corona region is much lower (due to more hydration) in the former micelle than latter. These anisotropy results thus corroborate well with the solvation dynamics results discussed in Section 3.3.1.3.

3.3.1.5. Number of water molecules associated with each EO unit in pluornic micelle. The number of water molecules associated with each EO unit in a pluronic micelle can be estimated from the following considerations. The volume of the corona region of a micelle can be expressed as,

$$V_{\text{corona}} = \frac{4\pi}{3}(R_m^3 - R_{\text{core}}^3) \quad (3.10)$$

where, R_m and R_{core} are the micellar radius and the core radius, respectively. For a pluronic micelle, if N is the aggregation number and V_{EO} is the volume of an EO unit, then the average number of water molecules associated with each EO unit can approximately be given as,

$$n_w = \frac{1}{V_{\text{D}_2\text{O}}Nm}(V_{\text{corona}} - NV_{\text{EO}}m) \quad (3.11)$$

where, $V_{\text{D}_2\text{O}}$ is the volume of a D_2O molecule (here D_2O is considered instead of H_2O because in the determination of micellar size following neutron scattering study D_2O is used as the solvent), m is the number of EO units per polymer molecule. The m values are 206 and 40 for F88 and P123 polymers, respectively. The value of V_{EO} and $V_{\text{D}_2\text{O}}$ is calculated to be 64.6 and 30 Å, respectively.^{151,160} The value of N is reported to be 62 and 86 for F88 and P123 micelles, respectively.^{73,147} The micelle and the core radii of F88 micelle are reported to be 84 and 38 Å, respectively,¹⁴⁷ and those for P123 micelle are reported to be 58 and 52 Å, respectively.⁷³ Using these parameters, the n_w values for F88 and P123 micelles are estimated to be 3.7 and 0.6, respectively. The presence of much larger number of water molecules in F88 micelle as compared to P123 suggest that the corona region of the former micelle is much more hydrated than the latter, as are also evident solvation dynamics and anisotropy fluorescence dynamics studies discussed before. The n_w estimates clearly indicate that the larger the EO to PO ratio, more is the hydration of the corona region of the pluronic micelle.

3.3.2. PET reactions in F88 micellar media

3.3.2.1. Quenching studies using SS fluorescence measurements. The absorption and fluorescence spectra of all the coumarin dyes (*cf.* chart 3.1) in F88 micelle were recorded in the absence and in presence of varying concentrations of DMAN. It is observed that the absorption spectra of the dyes do not change even in the presence of the highest DMAN concentrations used in this study, suggesting that there is no ground state complex formation.¹⁻⁴ It is seen that the fluorescence of the dyes in F88 micelle undergo strong quenching by the added DMAN, though there is no change in the shape of the fluorescence

spectra even in the presence of the highest concentration of DMAN used. Typical SS fluorescence quenching results for C151 dye by DMAN quencher are shown in Figure 3.5A. Present results suggest that the excited singlet state (S_1) of the coumarin dyes undergo strong quenching by DMAN, but without involving any excited state complex or exciplex formation. Drawing inferences from the previous studies reported for coumarin-amine systems, the observed fluorescence quenching in the present systems is attributed to the PET process between DMAN donor and excited coumarin dyes.^{136-146,161,162}

SS fluorescence quenching in the present coumarin-DMAN systems were analyzed using Stern-Volmer relationship (*cf.* Eq. 1.37; Section 1.6). Typical Stern-Volmer plots obtained for C481-DMAN and C152-DMAN systems are shown in Figure 3.5B. It is evident from this figure that the Stern-Volmer plots are linear only at lower DMAN concentrations and the plots undergo a clear positive deviation at higher DMAN concentrations. Such deviations in the Stern-Volmer plots from SS quenching results can be rationalized on the basis of the high localized concentration of DMAN in the micellar corona due to its preferred solubilization in this micellar region.¹³⁶⁻¹⁴⁵ Thus, there is significant static quenching (instantaneous quenching) for the coumarin fluorescence due to the presence of the coumarin-DMAN pairs that are within the reaction sphere before photoexcitation.

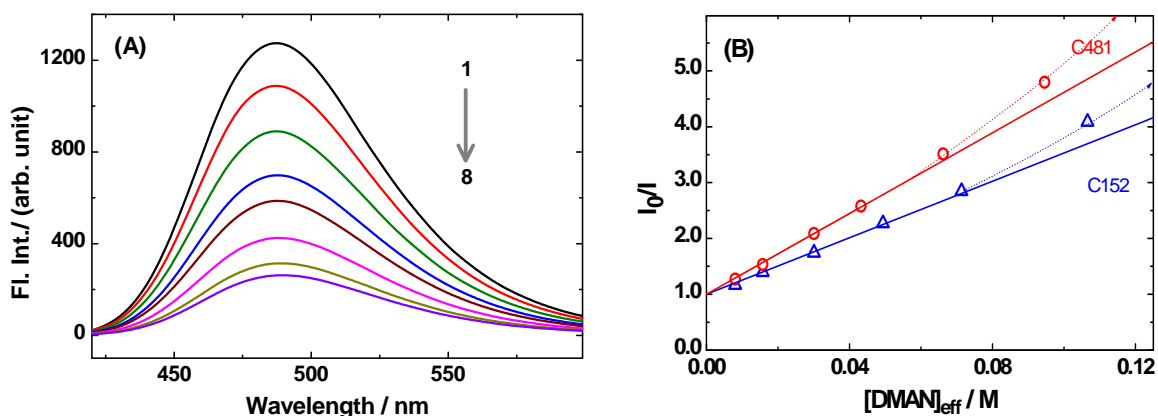


Figure 3.5: (A) SS fluorescence spectra of C152 dye in the presence of different DMAN concentrations in F88 micellar solution. For spectra 1 to 8 the $[DMAN]_t$ are: 0, 0.71, 1.38, 2.64, 3.79, 5.81, 8.30 and 10.89 mM, respectively. (B) Stern-Volmer plots from SS fluorescence quenching: C481-DMAN (O) and C152-DMAN (Δ) systems. $[DMAN]_{eff}$ is as defined in Eq. 3.13.

3.3.2.2. Quenching Studies using TR fluorescence measurements. For the studied coumarin-DMAN systems in F88 micellar media it is found that the average fluorescence lifetime of the dyes decreases significantly with an increase in the DMAN concentration (*cf.* Figure 3.6A). While in the absence of DMAN the fluorescence decays of the dyes show

single exponential nature, the decays display non-exponential behavior in the presence of the quencher, an observation reported earlier for many other micellar media and is attributed to the nondiffusional quenching kinetics in these microheterogeneous environments.¹³⁶⁻¹⁴⁵ In the present systems, the decays in the presence of DMAN could be fitted satisfactorily using a bi-exponential function from which the average lifetime ($\langle\tau\rangle$) values were estimated using the following relation,^{118,119,136-145}

$$\langle\tau\rangle = \frac{1}{100} \times (B_1\tau_1 + B_2\tau_2) \quad (3.12)$$

where τ_1 and τ_2 are the two lifetime components and B_1 and B_2 are their respective percentage contributions in the decays. These $\langle\tau\rangle$ values were subsequently correlated with the DMAN concentrations following the relevant Stern-Volmer relation (*cf.* Eq. 1.38; Section 1.6). Typical Stern-Volmer plots thus obtained for C481-DMAN and C152-DMAN systems are shown in Figure 3.6B. As indicated from this figure, unlike the SS results, the Stern-Volmer plots from TR results are quite linear even upto the highest concentration of the amine used. It is to be noted that the slope of the Stern-Volmer plots from TR data are distinctly lower as compared to that from SS Stern-Volmer plots. These results suggest that there is an interference of static quenching in the Stern-Volmer plots from SS quenching study. To avoid the contribution of the static quenching, thus the quenching constants (k_q) estimated, from TR quenching study have been used as the measure of the ET rates for the present systems.

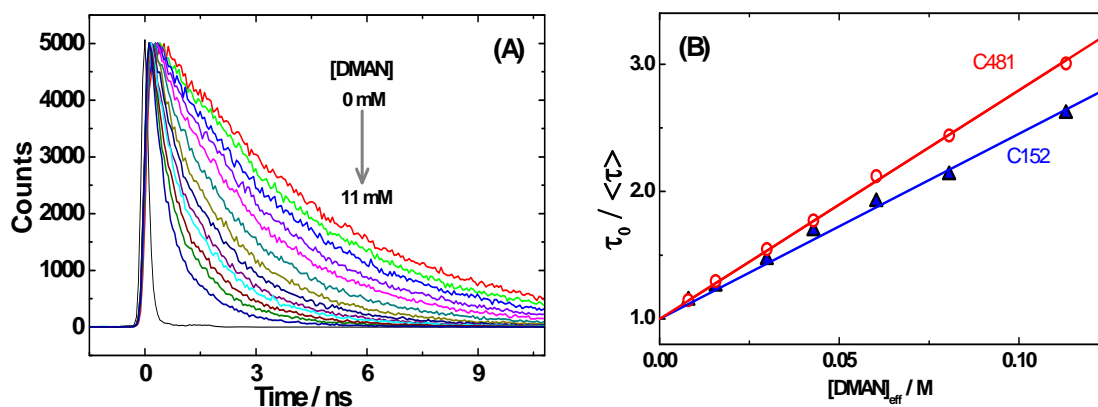


Figure 3.6: (A) Fluorescence decay curves for C152 dye in the presence of different DMAN concentrations in F88 micellar solution. (B) Stern Volmer plots from TR fluorescence quenching for: C481-DMAN (O) and C152-DMAN systems (Δ). $[\text{DMAN}]_{\text{eff}}$ is as defined Eq. 3.13.

To be mentioned here that in the actual estimation of k_q , effective DMAN concentration is used which is estimated using the following relation,

$$[\text{DMAN}]_{\text{eff}} = \frac{N[\text{DMAN}]_t}{V_c N_A \{[\text{Poly}]_t - \text{CMC}\}} = P[\text{DMAN}]_t \quad (3.13)$$

$$\text{and, } P = \frac{N}{V_c N_A \{[\text{Poly}]_t - \text{CMC}\}} = \text{Correction factor} \quad (3.14)$$

where, $[\text{DMAN}]_t$ is the total (or bulk) amine concentration used, N is the aggregation number of the micelle, V_c is the volume of corona region, N_A is the Avogadro number, $[\text{Poly}]_t$ is the total polymer concentration used and CMC is the critical micellar concentration of F88 polymer. The value of P is thus calculated as 11.84 for the present system.

It is noteworthy to mention here that in the cases where diffusion of the reactants is a prerequisite for the reaction, the estimated quenching constant from fluorescence measurement is a function of both ET process and the diffusion of the reactants (*cf.* Section 1.4).^{5-11,49} Such a situation arises mainly in low viscosity homogeneous solvents where reactants are free to move. In the present case we are dealing with micellar media where microviscosity is very high compared to that in the homogeneous solvents. Thus the diffusion of the reactants will be highly restricted in a micellar media. This is in fact reflected from the much longer reorientation time ($\langle\tau_r\rangle$) of a probe molecule in a micelle as compared to that in low viscous homogeneous media. For example $\langle\tau_r\rangle$ values for C153 dye in acetonitrile and in F88 micellar solution have been measured in this study as ~ 30 and 1830 ps, respectively. This indicate that the microviscosity in the present micelle is much higher as compared to that in acetonitrile. The reported bimolecular diffusional rate constant for the amine-coumarin pairs is reported to be in the range of about $1.5 \times 10^{10} \text{ dm}^3 \text{ mol}^{-1} \text{ s}^{-1}$ in acetonitrile solution.^{146,162} Considering this value and comparing the rotational reorientation times in acetonitrile and F88 micelle, the diffusional rate constant in the present micellar solution is expected to be $\sim 2.4 \times 10^8 \text{ dm}^3 \text{ mol}^{-1} \text{ s}^{-1}$. The observed fluorescence quenching constants in the present cases are found to be about two orders of magnitude higher than this estimate of the diffusional rate constant. This clearly indicates that the diffusion of the reactants is not a prerequisite for the ET reaction in the present micellar media. It has been already reported in the earlier studies that the dynamic quenching in the micellar media is due to the quenching contributions of the spatially distributed amine quenchers around the fluorophores without involving diffusion.^{136-146,159,163} In the present TR study, even though we might have missed a small ultrafast ET component, possibly occurring in the ps to sub-ps time scale (due to close contact coumarin-amine pairs), the quenching observed in the ns to sub-ns time domain following TCSPC measurement certainly include those non-diffusive ET reactions between

the coumarin-amine pairs that are at separations other than those in close contact that will give sub-ps quenching kinetics. Thus, we conclude that in the present study, the quenching constants estimated are the direct measures of the average non-diffusive ET rates for the studied systems.

3.3.2.3. Correlation of the quenching rates with the free energy changes of the ET reactions. As already mentioned, k_q values estimated from TR quenching studies are the measure of the ET rates for the concerned coumarin-DMAN pairs in F88 micelle. Accordingly, these k_q values were correlated with the free energy changes, ΔG^0 , of the ET reactions, to understand the relation between the energetics and kinetics for the present ET systems in F88 micellar media. The ΔG^0 values for the present PET systems were calculated according to the Rehm-Weller relation (cf. Eq. 1.22; Section 1.3). In this estimation, the excitation energies of coumarin dyes were calculated from the intersecting wavelength of the normalized emission and excitation spectra. The ϵ value for the corona region of F88 micelle was used as ~ 23 , determined from SS fluorescence measurements (cf. Section 3.3.1.2). The r values for different ET pairs were considered as the sum of radii of the coumarin and DMAN involved, latter being estimated approximately by using Edwards volume addition method.¹⁶⁴ The ΔG^0 values thus calculated for different coumarin-DMAN systems along with other relevant ET parameters are given in Table 3.2.

Table 3.2: Redox potentials of DMAN donor and coumarin acceptors, ΔG^0 values and the quenching constants for the studied coumarin-amine pairs.

Donor	E_{D/D^+} , V vs. SCE	Acceptor	E_{A/A^-} , V vs. SCE	E_{00} , eV	ΔG^0 , eV	$k_q \times 10^{-9}$, $\text{dm}^3 \text{mol}^{-1} \text{s}^{-1}$
DMAN	0.55	C151	-1.56	2.86	-0.84	2.68
		C481	-1.55	2.78	-0.75	8.40
		C152	-1.54	2.77	-0.78	8.30
		C522	-1.57	2.67	-0.64	2.96
		C153	-1.56	2.56	-0.55	2.48

The correlation curve for the observed k_q values with ΔG^0 for different coumarin-amine pairs is shown in Figure 3.7. It is evident from this figure that the correlation follows a bell-shaped behavior as predicted from Marcus ET theory (cf. Section 1.2). Thus, present

coumarin-amine systems in F88 micelle demonstrates the interesting observation of Marcus inversion behavior, though such an inversion always remains obscured for bi-molecular ET reactions in homogeneous solution. To be mentioned here that the Marcus inversion behavior as observed in the present study is qualitatively very similar to that reported in many other micellar media.^{136-146,159,163}

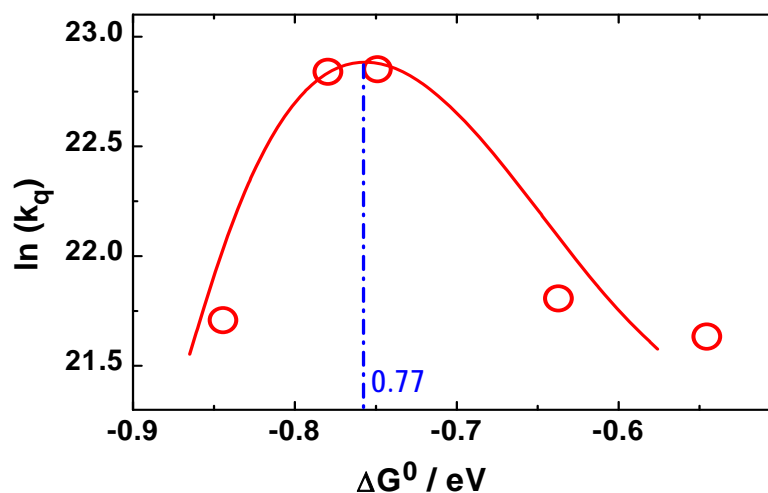


Figure 3.7: The $\ln(k_q)$ vs ΔG plot for the coumarin-amine systems in 5% w/v F88 solution. The solid curve is drawn through the data points just as a visual guide to show the Marcus inversion behavior.

From Figure 3.7 the interesting point to be noted is the onset of inversion that arises at an exergonicity ($-\Delta G^0$) of ~ 0.77 eV. From conventional ET theory, the exergonicity for the onset of inversion should be equal to the total reorganization energy, λ , for the reaction. Total λ for the ET reaction is the sum of intramolecular (λ_i) and solvent (λ_s) reorganization energies. For coumarin-amine systems it is reported earlier that λ_i is quite low and hence the total λ is mainly dominated by λ_s .¹⁴⁶ It is expected from Figure 3.7 that the contribution of λ_s towards ET reaction can at the most be ~ 0.77 eV. Considering the dielectric constant in the corona region of F88 micelle as ~ 23 , the λ_s in the corona region was expected to be ~ 1 eV or more (*cf.* Section 1.2.1).^{5-11,136-141} Thus, it is evident that λ_s does not contribute fully towards the ET reactions in F88 micellar media (*cf.* Section 1.2.4).^{25-28,136-141} That the contribution of λ_s in the present cases is significantly lower than that expected from conventional ET theory, can be explained on the basis of the slow motions of the solvent (water) molecules in the micellar environment in comparison to the fast solvent motions in low viscosity homogeneous media. This is in fact supported by the reasonably long solvation time observed in the present case as compared to that in the bulk water. The lowering in the effective λ_s in

the micellar media suggests that the solvent around the donor-acceptor pairs does not reorganize as quickly as the ET reaction takes place. In other words, micellar media permits only a partial relaxation of the solvent molecules during the course of the ET reaction.

The extent of solvent relaxation during ET reaction would largely depend on the nature of the water molecules present in the micellar media. The k_q vs ΔG^0 correlation for the ET reaction between similar coumarin-amine pairs in P123 micelle was found to display the onset of Marcus inversion at an exergonicity of ~ 0.68 eV.¹⁴¹ This indicates that the contribution of solvent reorganization is still lower in P123 micelle as compared to that in F88 micelle. These results are in agreement with the solvation times measured in P123 and F88 micelles (*cf.* Table 3.1) which suggests that the water molecules in the corona region can reorient relatively faster in F88 micelle than in P123 micelle. Hence the contribution of solvent relaxation towards the ET reaction is expected to be relatively higher in the case of F88 than in P123 micelle, even though a complete reorganization of the solvent molecules is not possible in either of these micelles during the course of the ET reactions (*cf.* Section 1.2.4). Comparing the ET rates in F88 and P123 micelles, it is seen that the rates are also relatively faster in F88 micelle than in P123 micelle. For example the ET rate for C481-DMAN pair in F88 micelle is $\sim 8.40 \times 10^9 \text{ dm}^3 \text{ mol}^{-1} \text{ s}^{-1}$ while that in P123 micelle is $\sim 1.76 \times 10^8 \text{ dm}^3 \text{ mol}^{-1} \text{ s}^{-1}$.¹⁴¹ The substantial increase in the ET rate in F88 micelle compared to that in P123 is certainly related to the increased EO to PO ratio in the former case, and can be explained on the basis of the increased hydration in the corona region of F88 micelle than P123, as indicated earlier from the estimated micropolarity in the two micelles discussed in Section 3.3.1.2. As ET reaction leads to the formation of an ion pair state, the reaction is always more favorable in a medium of higher polarity. Thus the ET reaction is expected to occur with a higher rate in F88 micelle than in P123 micelle. Present results indicate that an increase in the EO to PO ratio in the triblock co-polymer results in a large increase in the rate of the ET reactions occurring in the corona region of the micelles. Thus, by tuning the EO to PO ratio it is possible to tune the ET rates quite significantly in the tri-block copolymer micelles, and this can have important implications in different applied areas that involve PET reactions. Present results are the first report in the literature to show the effect of EO to PO ratio on the nature of the water molecules in the block copolymer micelles and the consequent modulation in the PET reactions for the solutes dissolved in the corona region of such micellar media.

6.4. Conclusion

SS and TR fluorescence measurements have been carried out in F88 triblock copolymer micelles using DMAN as the electron donor and a series of coumarin dyes (C151, C152, C153, C481 and C522) as the electron acceptors. The micellar media of 5% w/v F88 solution are characterized using DLS and photophysical studies like spectral shifts, solvation dynamics, TR anisotropy studies, etc. The results thus obtained have been compared with those reported for the micelle made up of P123 polymer, which has a relatively lower EO to PO ratio. Present results show that an increase in the EO/PO ratio leads to an increase in the hydration of the corona region. As a consequence, the water molecules in the corona region are much loosely bound in F88 micelle than in P123 micelle. This causes a faster solvent relaxation in F88 micelle as compared to that in P123 micelle. TR rotational relaxation study also shows that the increase in the EO to PO ratio in the triblock co-polymer results in a decrease in the microviscosity of the corona region.

The PET studies reveal the existence of Marcus inversion for the bimolecular PET reactions in the F88 micelles. The inversion is observed in the present studies which is mostly elusive in homogeneous media for bimolecular PET reactions and arises due to the restricted diffusion of the reactants and the lowering of the effective solvent reorganization energy towards ET reaction (*cf.* Section 1.2.4) in constrained micellar medium. The inversion appears at a lower exergonicity of about 0.77 eV which is much lower than expected considering the polarity of the corona of F88 micelle. When compared with the reported PET results in P123 micelles, ET rates in F88 micelle are significantly higher due to the higher EO to PO ratio that increases the number of labile water molecules in the corona region. It is also seen that the Marcus inversion appears at a relatively higher exergonicity (0.77 eV) in the case of F88 micelle as compared to P123 micelle (0.68 eV). This is rationalized on the basis of the relatively faster solvent reorganization in F88 micelle as compared to P123 micelle. On the basis of the present results, therefore, it can be concluded that the ET rates and the Marcus inversion can be suitably modulated by selecting the proper EO to PO ratios in the pluronic micellar systems.

Chapter 4

Photoinduced Electron Transfer Reactions in Pluronic-Surfactant Supramolecular Assemblies: Tuning of Electron Transfer Rates

Abstract

Photoinduced electron transfer reaction between an anionic acceptor, coumarin-343 (C343), and a neutral donor, N,N-dimethylaniline (DMAN), has been investigated in composite supramolecular assemblies (mixed micelles) comprising of a pluronic copolymer (P123: EO₂₀-PO₇₀-EO₂₀ or F88: EO₁₀₃-PO₃₉-EO₁₀₃ where EO: ethylene oxide and PO: propylene oxide) and a cationic surfactant (CTAC: cetyltrimethylammonium chloride), following fluorescence quenching studies. Systematic increase in the quenching rates for the studied donor-acceptor system with the increasing CTAC to pluronic molar ratio in the mixed micelles demonstrates a large modulation in the ET rates. The mixed micellar systems in the present cases are formed through the incorporation of the hydrocarbon chains of CTAC into the poly-PO core of the pluronic micelles whereby the cationic head groups of CTAC are placed at the periphery of the micellar core, protruded into the hydrated poly-EO corona region, leading to the formation of a positively charged layer deep inside these mixed micelles. Thus, the anionic C343 dye, initially dissolved at the micelle-water interface, experiences a gradually increasing electrostatic attraction and thereby systematically dragged deeper inside the micellar corona, as the CTAC composition is increased in the mixed micellar systems. Consequently, the ET rate for the C343-DMAN pair undergoes a large enhancement in the studied mixed micellar systems with the increasing CTAC to pluronic molar ratio. Present strategy of modulating ET reactions using such composite supramolecular assemblies can find applications in areas where bimolecular ET is an integral reaction step.

4.1. Introduction

As mentioned in Chapter 1 and 3, ET reactions in microheterogeneous media have relevance to many practical applications.⁵⁻²¹ Thus ET reactions in various self-assembled microheterogeneous systems have been investigated quite extensively with the aim to find a control over the dynamics, energetics and mechanism of the ET processes.^{136-145,165-169} Present chapter discusses the results of our study in a unique surfactant-pluronic composite supramolecular assemblies that can be modulated conveniently in tuning the ET reactions.

In microheterogeneous media, the degree of hydration (i.e. micropolarity) not only determines the rate of the solvent relaxation process but also plays an important role in determining the microviscosity for the reaction environment. While the solvent relaxation rate would directly determine the contribution of solvent reorganization energy towards the free energy of activation for the ET reaction in such media, the microviscosity and the reactant entanglement with surfactant chains in such systems will in effect control the diffusion of the reactants and also the effective separation among the reacting donor-acceptor (D-A) pairs.^{5-11,136-145,165-169} Logically the above effects in relation to the ET reactions can be adjusted to a significant extent by applying suitable strategies that help in modulating the microenvironments of the micellar systems. Two important approaches in this regard can be: (i) addition of an electrolyte in the micellar solution and (ii) changing temperature or pressure of the solution. Addition of an electrolyte invariably increases the degree of hydration of a micelle,^{85,114,152,170,171} which in turn favours the ET reaction. Presence of high concentration of electrolyte, however, can cause a large change in the micellar shape, often leading to the undesired phase separation.^{170,171} Changing temperature can definitely induce significant changes in the micellar microenvironments.¹⁷² However, occurrence of cloud point and large changes in the surfactant solubility with changing temperature often restrict the temperature range suitable for ET studies.^{73,152,174} Though micellar microenvironments can also be modified by changing the solution pressure, this methodology needs very specialized and tedious experimental arrangements.^{174,175}

Another approach, rather simple and quite effective in modulating microenvironment of a micelle is the use of composite micellar systems formed by the combination of pluronic copolymers and conventional surfactants.^{75-77,176-179} Characteristics of pluronic polymers have been discussed with necessary details in Section 1.7. Combination of a pluronic copolymer and a conventional ionic surfactant can form unique mixed micellar systems displaying very distinct characteristics.^{75-77,90,176-184} In these systems, the added surfactants are incorporated

into the basic pluronic micellar structure with hydrophobic chains of the surfactants embedded into the nonpolar core and the charged head groups of the surfactants residing at the peripheral region of the core, protruding into the hydrated corona region.^{75-77,90,176-184} Due to this unique structural arrangement, a charged layer is developed deep inside these mixed micelles and accordingly an ionic solute, having a charge opposite to that of the charged layer and initially localized at the micelle-water interface in the absence of the ionic surfactant, is gradually attracted by the electrostatic effect and hence is dragged deeper into the micelle, a process that can be controlled suitably by changing the surfactant to pluronic molar ratios of the mixed micellar systems.^{176-179,184}

The aim of the present study is to explore the above feature of the ionic surfactant-pluronic copolymer mixed micellar systems for a possible tuning of bimolecular ET reactions. In this study, a cationic surfactant, namely, cetyltrimethylammonium chloride (CTAC), has been used along with two pluronic copolymers, namely, P123 (EO₂₀-PO₇₀-EO₂₀) and F88 (EO₁₀₃-PO₃₉-EO₁₀₃), having largely different sizes of their poly-EO and poly-PO blocks, such that a cationic charge layer is developed inside the mixed micelles. An anionic fluorophore, the deprotonated coumarin-343 (C343) dye, has been used as the electron acceptor (A) in combination with a neutral electron donor (D), DMAN, to study the ET reaction following fluorescence quenching measurements. The versatility of the coumarin-amine systems in carrying out efficient ET reactions and thus to understand the mechanisms and dynamics of these reactions has been well documented in the literature.^{85,136-146,184,185} In the present study, we expect that in these mixed micelles the location of anionic C343 will be gradually changed on changing the surfactant to pluronic ratios and accordingly there will be a modulation in the observed ET rate.

4.2. Experimental Methods and Materials

P123 (Aldrich), CTAC (Aldrich), and C343 dye (Exciton; Laser grade) were used as received. F88 was a gift from the BASF Corporation, Edison, NJ, USA. DMAN (Spectrochem, India) was purified by vacuum distillation just before use. Nanopure water having conductivity $<0.1 \mu\text{S cm}^{-1}$ from a Millipore Elix-3/A10 system was used for solution preparation. Stock solution of P123 (20% w/v) was prepared by dissolving weighed amount of the copolymer in requisite amount of water in a sealed container, keeping the mixture overnight under refrigeration. Similarly, stock solution of F88 (10% w/v) was prepared by dissolving weighed amount of F88 in requisite amount of water, keeping the mixture stirred

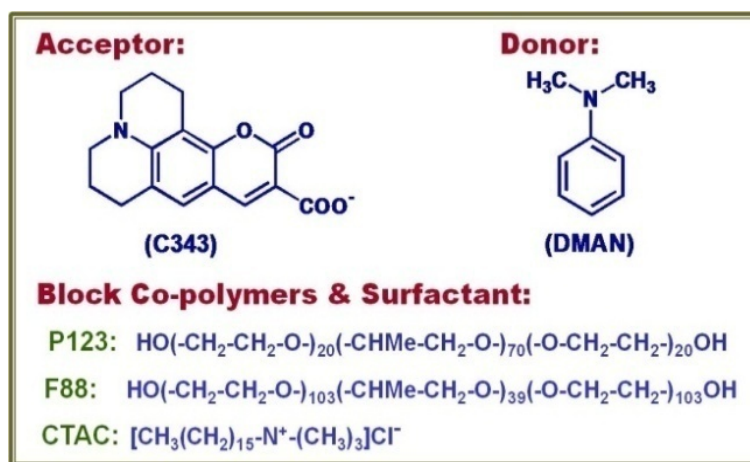
for 24 h at room temperature. A stock CTAC solution was similarly prepared by dissolving required amount of the surfactant in water. P123-CTAC and F88-CTAC composite micellar systems were finally prepared by using the stock CTAC and pluronic solutions, maintaining the pluronic concentrations as 10% w/v for P123 and 5% w/v for F88, while the CTAC concentration was gradually varied as required. C343 was directly added to the micellar solutions and the dye concentration in the experimental solution was adjusted by proper dilution, keeping its concentration quite low ($<5 \mu\text{M}$), to avoid multi-occupancy of the dye in a micelle. For quenching experiments, stock DMAN solution was first prepared by adding a required volume of the neat amine to a known volume of the C343 solution in the concerned micellar system. A corresponding reference solution containing only the dye with the same concentration but without any DMAN was also accordingly made. These two experimental solutions were finally mixed in suitable proportions to carry out the quenching measurements with varying DMAN concentration but keeping the dye concentration as well as the surfactant to pluronic molar ratio constant for each set of the experiments. Since P123 and F88 have largely different CMT values,^{61,74} measurements in the present study were carried out at 25 °C in 10% P123 solution (CMT \sim 13 °C) and at 38 °C in 5% F88 solutions (CMT \sim 31°C), to ascertain complete micelle formation of the pluronics in the studied solutions. For the P123 and F88 systems, the relevant micellar parameters obtained from the literatures^{140,141} are listed in Table 4.1. Fluorescence quantum yield (Φ_f) values for the C343 dye under different solution conditions were estimated following a comparative method¹⁻⁴ using the dye in aqueous solution as reference ($\Phi_f = 0.7$).¹⁸⁶ Molecular structures of C343 acceptor and DMAN donor and also the molecular formulae of CTAC surfactant and P123 and F88 pluronic copolymers, used in the present study, are shown in Scheme 4.1.

Table 4.1: Relevant parameters for the P123 and F88 pluronic systems that required for the estimation of the $[DMAN]_{eff}^{av}$ values.^{140,141}

Pluronic (Avg. MW)	$[P]_t / \text{mM}$ (w/v)	N_{agg}	CMC / mM (w/v)	$r_m / \text{Å}$	$r_c / \text{Å}$
P123 (5750)	17.3 (10%)	86	0.052 (0.03 %)	57.7	52.0
F88 (11400)	4.39 (5%)	62	0.246 (0.28 %)	84	38

The instruments used for ground state absorption, SS fluorescence and TR fluorescence measurements are described in Sections 2.2, 2.3 and 2.4 respectively. In the

present study TR fluorescence was carried out using a 374 nm diode laser (1MHz, ~100 ps) as the excitation source. Typical IRF for the present setup is ~110 ps at full-width half-maximum (FWHM) and the shortest lifetime measurable using re-convolution analysis is about 30 ps.^{118,119} As required in different cases, the decays were fitted either as a single-exponential or a bi-exponential function.



Scheme 4.1: Molecular structures of the acceptor (C343), donor (DMAN), block co-polymers (P123 and F88) and surfactant (CTAC) used in the present study.

4.3. Results and Discussion

4.3.1. Absorption and fluorescence characteristics of C343 dye. The fluorophore, C343, which is also the electron acceptor in the present study, can exist either in the neutral or in the anionic form, depending on the pH of the solution.^{58,150,176-179,184,187,188} To characterize the prototropic form of C343 dye that exists in the experimental solutions, both absorption and fluorescence spectra of the dye were recorded in aqueous solution at different pH conditions and compared with those obtained in P123 and F88 micellar solutions as shown in Figure 4.1. Absorption and fluorescence spectra of the dye in P123 and F88 micellar solutions resemble quite closely with those in aqueous solution at alkaline and neutral pH but differ largely as compared to those in acidic pH condition. These results clearly suggest that C343 mainly exists in its anionic form both in P123 and F88 micellar solutions. Present assignment is also in agreement with the earlier reports showing that in different micellar solutions the dye C343 in fact exists in its anionic form.^{58,150,176-179,184,187,188}

Establishing that C343 exists in its anionic form, the SS emission spectra of the dye were recorded in the mixed micellar solutions with gradually increasing concentration of CTAC but keeping the pluronic concentration constant. Observed results in CTAC-P123

system are shown in Figure 4.2A. Similar results were also obtained in CTAC-F88 system. As indicated from Figure 4.2A, emission spectra of the dye gradually shift toward shorter wavelength as the CTAC content is increased in the pluronic solutions. Observed results clearly suggest that in the mixed micelles there is a gradual decrease in the micropolarity around the probe dye as the CTAC concentration is increased in the solution. As discussed earlier, addition of CTAC to P123 or F88 pluronic solutions results in the formation of unique mixed micelles where a positively charged layer is developed deep inside the micellar phase.^{75-77,90,176-184} Accordingly, the anionic dye C343, which is expectedly localized at the micelle-water interface initially in pure pluronic micelles, experiences an electrostatic attraction due to the formation of mixed micelles in the presence of CTAC and thus, gradually shifts its location deeper inside the micellar corona as the CTAC concentration is increased. Since the extent of hydration would be much lower at the deeper region of the micellar corona than that at the micelle-water interface region, the shifted location of the dye is clearly manifested by the observed blue shift in the emission spectra with the increasing CTAC concentration in the mixed micellar systems.^{75-77,181-184,58,150,187,188} Table 4.2 lists the relevant absorption and fluorescence parameters of C343 dye in aqueous solution at different pH conditions and also in pure pluronic micelles and in typical CTAC-pluronic mixed micellar systems, as investigated in the present study.

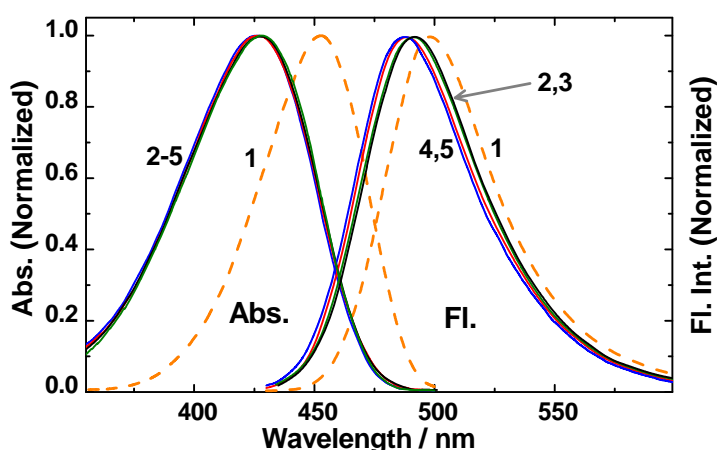


Figure 4.1: Normalized absorption and fluorescence spectra of C343 dye in aqueous solution at different pH conditions; pH 3.2 (1: orange), pH 6.8 (2: black) and pH 9.3 (3: green). Normalized absorption and emission spectra of the dye in 10% w/v P123 solution at 25 °C (4: blue) and 5 % w/v F88 solution at 38 °C (5: red) are also shown in the figure for comparison.

TR fluorescence studies for C343 dye in the two mixed micellar systems were carried out as a function of the changing CTAC concentration, keeping the pluronic concentration

constant. Observed fluorescence decays for C343 dye in CTAC-P123 mixed micelles at different CTAC to pluronic molar ratios are shown in Figure 4.2B. Similar results were also obtained in CTAC-F88 mixed micelles. Observed decays in these cases were seen to fit well with a single exponential function and the fluorescence lifetime (τ_f) values thus obtained are listed in Table 4.2. As indicated from these results, there is no appreciable change in the fluorescence decays of the dye with the changing CTAC concentration in either of the two CTAC-pluronic mixed micellar systems.

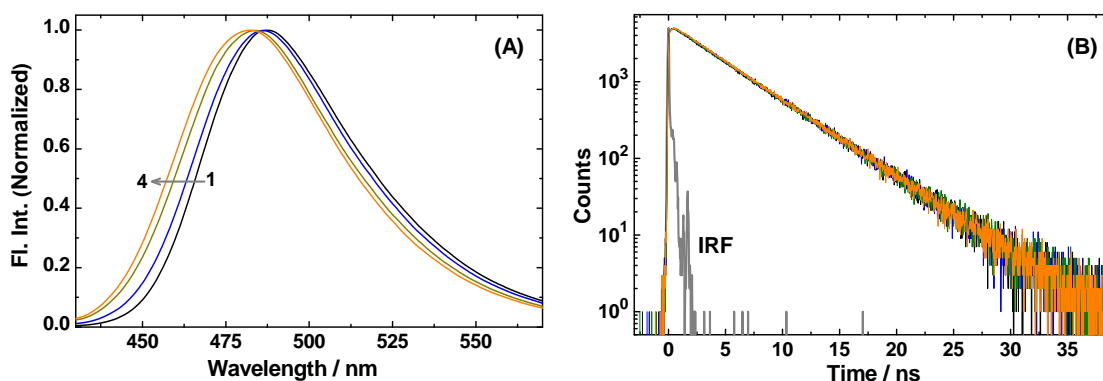


Figure 4.2: (A) SS fluorescence spectra and (B) Fluorescence decays of C343 in P123 solution at CTAC to P123 molar ratios of: 0.0 (1: black), 0.1 2: (blue), 0.3 (3: green) and 0.5 (4: orange).

Table 4.2: List of the absorption and fluorescence parameters of C343 dye in different solution conditions investigated in the present study.

Solution Condition	λ_{abs}^{max} / nm	$\epsilon_{abs}^{max} / M^{-1}cm^{-1}$	λ_{fl}^{max} / nm	Φ_f	τ_f / ns
Aqueous, pH 6.8	428	32,700	492	0.70	4.48
Aqueous, pH 9.3	427	32,800	491	0.71	4.49
Aqueous, pH 3.2	455	45,600	499	0.65	4.25
P123 (10% w/v)	425	32,500	487	0.67	4.33
CTAC-P123 (Mol. ratio 0.5)	425	32,300	482	0.66	4.32
F88 (5% w/v)	426	32,600	489	0.69	4.44
CTAC-F88 (Mol. ratio 0.5)	426	32,400	482	0.68	4.37

The TR fluorescence results (*cf.* Figure 4.2B) observed in the studied mixed micelles are apparently not in accordance with the SS fluorescence results where a reasonable blue shift is observed in the emission spectra indicating a gradual reduction in the micropolarity around the dye in the mixed micelles with an increase in the CTAC concentration. Observed

TR results can, however, be expected if the fluorescence decays of the dye are inherently less sensitive to the polarity of the solvents such that the extent of the micropolarity change resulted from the changing CTAC concentration is not sufficient to cause any observable change in the observed decays. To explore this aspect further, we carried out ground state absorption, SS fluorescence and TR fluorescence measurements for C343 dye in different water-ethanol (EtOH) solvent mixtures, with varying co-solvent compositions. In all these cases, solution was made reasonably alkaline to ascertain the existence of the dye in its anionic form. It is found that while the fluorescence decays show only a nominal change with the changing solvent composition (*cf.* Figure 4.3A), the absorption and fluorescence spectra show quite significant changes, displaying a gradual blue shift in the spectra as the ethanol composition is increased in the solvent mixture (*cf.* Figure 4.3B). From these results it is evident that the fluorescence decays of C343 dye are indeed not that sensitive to the solvent polarity, though the absorption and fluorescence spectra of the dye show quite significant changes on changing the solvent polarity.

4.3.2. Absorption and fluorescence studies on the interaction of C343 dye with DMAN quencher. Ground state absorption measurements indicate that absorption spectra of C343 dye in pure P123 and F88 micelles as well as in CTAC-pluronic mixed micelles remain very similar both in the absence and in presence of the DMAN quencher. Moreover, the spectral feature in all these cases corresponds to that of the anionic form of the dye.^{58,150,176-179,184,187,188} Typical of these results in P123 micellar solution are shown in the inset A of Figure 4.4. Observed results suggest that there is no ground-state complex formation between C343 and DMAN in any of these microheterogeneous systems studied.^{1-4,136-145,166-168}

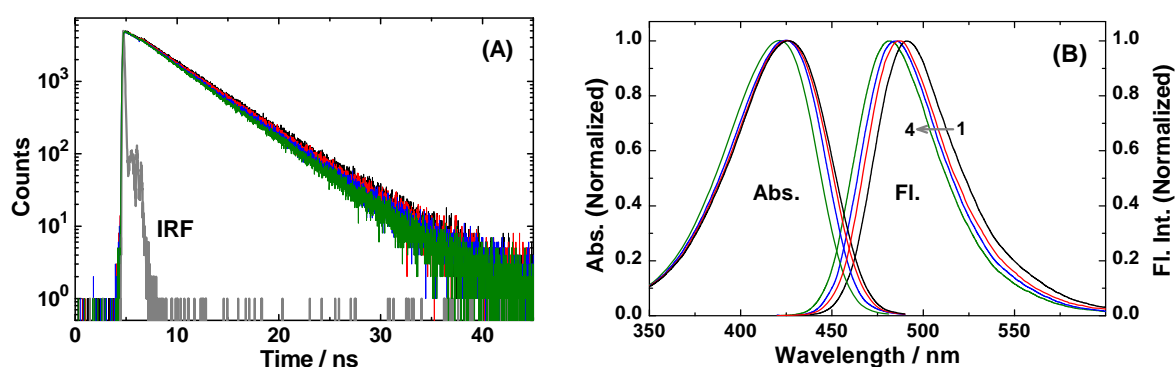


Figure 4.3: (A) Fluorescence decays and (B) absorbance and fluorescence spectra of C343 in EtOH-water solvent mixtures with different co-solvent compositions. Solvent compositions are: 0% EtOH (1: black), 22% EtOH (2: red), 33% EtOH (3: blue), 50% EtOH (4: green).

In the SS fluorescence measurements, even though the spectral characteristics of the dye do not show any observable change in the presence of the DMAN quencher, the fluorescence intensity gradually decreases on increasing the DMAN concentration (*cf.* Figure 4.4). Observed results indicate that there is a strong quenching for the excited C343 dye by DMAN quencher and the quenching in the present systems does not involve any excited state complex or exciplex formation.^{1-4,136-145,166-168} To be mentioned that in the literature there are extensive reports, suggesting and demonstrating experimentally the involvement of PET from ground state amine donors to excited coumarin acceptors as the mechanism for the strong fluorescence quenching observed in the coumarin-amine systems.^{136-146,161,162,166-169,185} Drawing an analogy thus, we attribute the observed fluorescence quenching in the present C343-DMAN system as due to PET process in the micellar media.

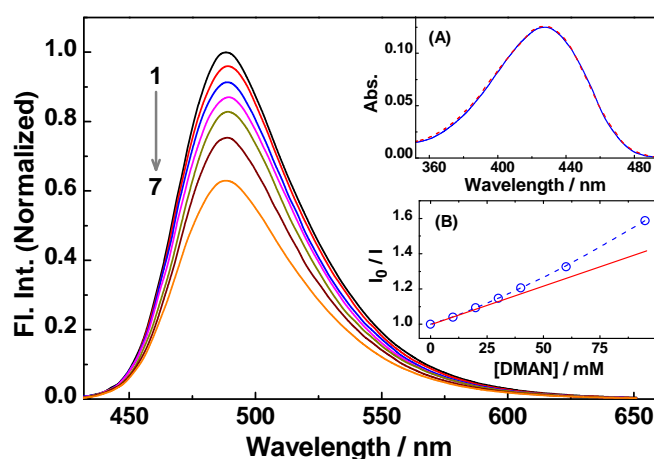


Figure 4.4: SS fluorescence quenching for C343 dye by DMAN quencher measured in P123 solution in the absence of any CTAC. Bulk DMAN concentrations for spectra 1-7 are: 0, 10, 20, 30, 44, 60 and 95 mM. **Inset A:** Absorption spectra in the absence (1: Blue) and in presence (2: red) of 95 mM of DMAN. **Inset B:** Stern-Volmer plot for the SS fluorescence quenching for the above system.

For the present system SS fluorescence quenching was analyzed using Stern-Volmer relationship (*cf.* Eq. 1.37; Section 1.6). Interestingly it is found that in all the micellar media the I_0/I vs $[Q]$ plots always undergo a positive deviation from the expected linearity, as the quencher concentration is increased in the solution (*cf.* Inset B of Figure 4.4). For C343-DMAN system, since there is no ground or excited state complex formation, such positive deviations clearly suggest that in the observed SS results there are significant quenching contributions arising from the ultrafast non-diffusive (static) quenching process.^{1-4,118,119}

In micellar media, the reactant molecules are preferentially solubilized within a very small region of the microheterogeneous systems.^{136-145,166-169} Therefore, even under the conditions where the bulk estimate for the quencher concentration apparently seems quite

low, the actual localized concentration of the quencher can be significantly high such that a good fraction of the fluorophore molecules will already be in close proximity with the quenchers at the moment of their excitation.^{136-145,166-169} As these close proximity fluorophore-quencher pairs can lead to an unusually fast quenching interaction without involving any diffusion of the reactants, the observed SS fluorescence quenching will be much stronger than otherwise expected under normal diffusional quenching kinetics condition.¹⁻¹⁰ Accordingly, the I_0/I vs $[Q]$ plots should show a positive deviation as observed in the present study.¹⁻¹⁰ To be mentioned here that such positive deviations in the SS fluorescence quenching results have invariably been observed in all kind of microheterogeneous media where reactants are confined within a small region of the supramolecular systems.^{136-145,166-169,189,190} Since with such deviations in the I_0/I vs $[Q]$ plots the K_{SV} values cannot be estimated with sufficient accuracy (even on using the initial slopes for the plots), we did not use the observed SS fluorescence quenching results for any quantitative estimation of the quenching kinetics. In the present study, thus, we entirely relied on the TR fluorescence results to estimate the quenching kinetics, as are discussed in the following section.

4.3.3. TR fluorescence studies on the interaction of C343 dye with DMAN quencher. TR fluorescence studies on the interaction of C343 dye with DMAN quencher were carried out in pure pluronic micelles as well as in CTAC-pluronic mixed micellar systems, following quencher concentration dependent changes in the fluorescence decays of the dye. It is observed that the decays gradually become faster as the DMAN concentration is increased in the solution. These results are in accordance with the SS fluorescence quenching results and suggest an efficient ET interaction for the excited C343 dye with the ground state DMAN quencher. Representative decays observed on changing the DMAN concentration in pure P123 micelle and in a selected CTAC-P123 mixed micelle are shown in Figure 4.5A and B, respectively. Similar results in pure F88 micelle and in a typical CTAC-F88 mixed micellar system are shown in Figure 4.6A and B, respectively.

As mentioned in Section 4.3.1, in the absence of the quencher, fluorescence decays of the dye in both pure pluronic and CTAC-pluronic micelles are single exponential in nature. In the presence of the DMAN quencher, however, the decays of the dye in all the micellar systems studied are found to become non-single exponential in nature. Nevertheless, these decays in the presence of the quencher could be fitted reasonably well with a bi-exponential function, at least for the concentration range of the quencher used in the present study.

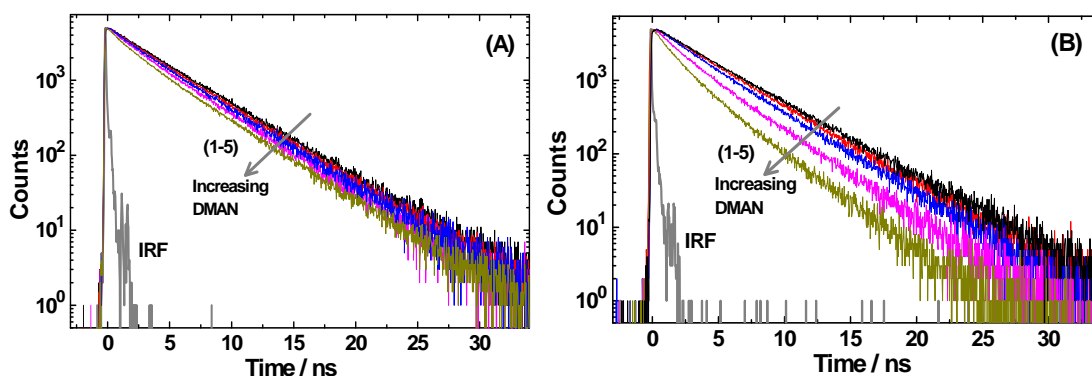


Figure 4.5: Fluorescence decays of C343 dye with changing DMAN concentration; (A) in pure P123 micelle and (B) in CTAC-P123 mixed micelle at CTAC to P123 molar ratio of 0.5. DMAN concentrations for the decays 1-5 were: 0, 10, 20, 44, 95 mM.

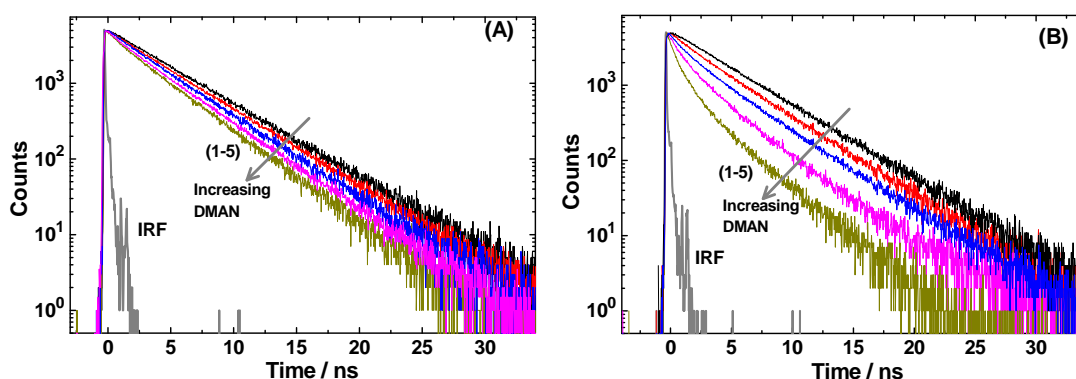


Figure 4.6: (A) Fluorescence decays of C343 dye with changing DMAN concentration; (A) in pure F88 micelle and (B) in CTAC-F88 mixed micelle at CTAC to F88 molar ratio of 0.5. DMAN concentrations for the decays 1-5 were: 0, 4, 12, 20, 40 mM.

An important observation from Figure 4.5 and 4.6 is that the TR fluorescence quenching is always more efficient in the mixed micellar systems than in the corresponding pure pluronic micelles, for a given DMAN concentration. This becomes further evident as we compare the decays as a function of the increasing CTAC to pluronic molar ratios for a given DMAN concentration, as are shown in Figure 4.7A and B, respectively, for CTAC-P123 and CTAC-F88 mixed micellar systems. It is also evident from Figure 4.7 that the effect of the added CTAC in modulating the quenching rate is much more dominant in CTAC-F88 mixed micellar system than in CTAC-P123 mixed micellar system, which corroborates well with the larger poly-EO block size in F88 copolymer than that in P123.^{140,141,176-179,184}

Fluorescence decays in the two mixed micelles at different DMAN concentrations were systematically analyzed following a bi-exponential function. To understand the extent of TR quenching for the dye with the changing DMAN concentration, the average lifetime

($\langle\tau\rangle$) values were estimated as discussed in Chapter 3 (*cf.* Section 3.3.2.2; Eq. 3.12). Figure 4.8A and B shows the changes in the $\langle\tau\rangle$ values as a function of the changing CTAC to pluronic molar ratios at number of fixed DMAN concentrations in the CTAC-P123 and CTAC-F88 mixed micellar systems, respectively. As indicated from Figure 4.8, in both the mixed micelles, the $\langle\tau\rangle$ value of the dye at a given DMAN concentration gradually becomes shorter as the CTAC to pluronic molar ratio is increased. These results clearly suggest that in the studied mixed micelles there is a large modulation in the ET rate for the C343-DMAN pair, achieved simply through a change in the CTAC to pluronic composition. We attribute this effect to the gradual drifting of the anionic C343 dye from its initial solubilization site at the micelle-water interface to deeper into the micellar corona, due to the development of the positively charged layer inside the CTAC-pluronic mixed micelles,^{75-77,90,176-184} which can pictorially be represented by Scheme 4.2 for a simple visualization.

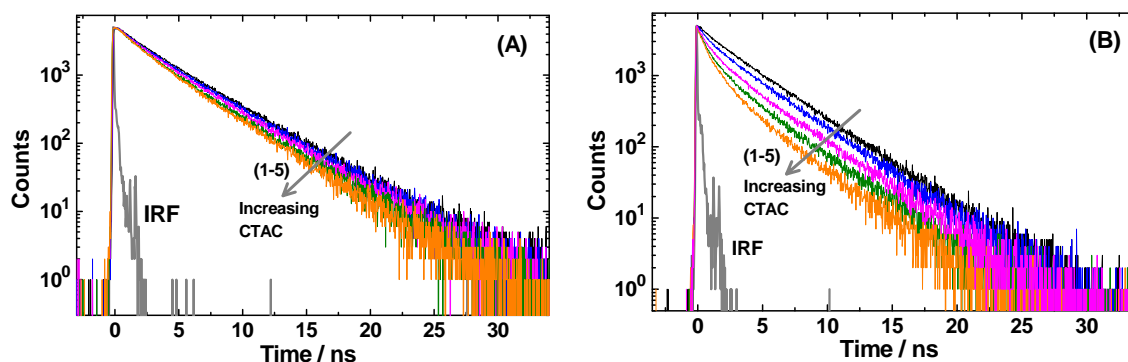
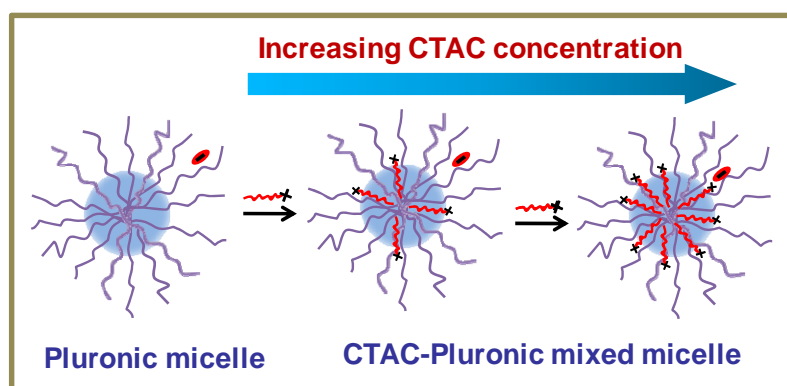


Figure 4.7: Fluorescence decays of C343 in the presence of 40 mM DMAN with changing CTAC concentration in: (A) CTAC-P123 mixed micelle and (B) CTAC-F88 mixed micelle. CTAC to pluronic molar ratios for decays 1-5 in panel A are: 0, 0.024, 0.079, 0.23, 0.5 and in panel B are: 0, 0.073, 0.19, 0.3, 0.5, respectively.



Scheme 4.2: Conceptual presentation of the development of the cationic charged layer in a CTAC-pluronic mixed micelle and the changes in the location of the anionic C343 dye with the increasing CTAC concentration in such a supramolecular system.

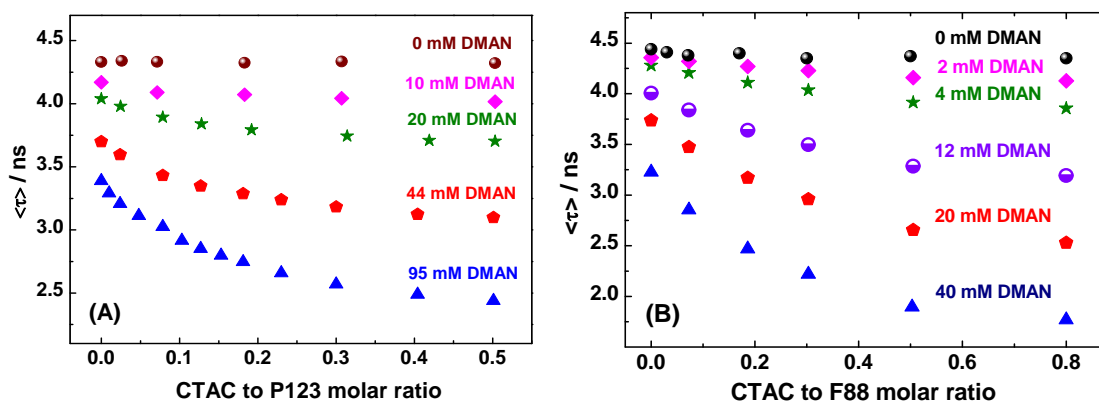


Figure 4.8: Changes in the fluorescence lifetime of C343 at different DMAN concentrations (indicated in the panels), plotted as a function of CTAC to pluronic molar ratios in: (A) CTAC-P123 and (B) CTAC-F88 mixed micelles.

4.3.4. Modulations of the ET rates for C343-DMAN system in the CTAC-pluronic mixed micellar media. With the observations presented and discussed so far, it is evident that the quenching/ET interaction between C343 acceptor and DMAN donor is modulated very largely by changing the CTAC to pluronic molar ratio in the studied mixed micellar systems. To have a quantitative estimate of this effect, the TR fluorescence quenching results were systematically correlated with the changing DMAN concentrations at different CTAC to pluronic molar ratios in the two mixed micellar systems. Since the quenching interaction in the close contact donor-acceptor pairs occurs with an unusually fast rate,^{138,139,136} much faster than the time resolution of the present TCSPC setup (~ 30 ps), unlike in the SS fluorescence quenching, the reductions in the $\langle\tau\rangle$ values observed in the TR studies will not have any significant contribution from the ultrafast (or static) quenching components.^{136-145,166-169} With this assumption, observed changes in the $\langle\tau\rangle$ values as a function of the DMAN concentration in each of the studied micellar media (pure pluronic or CTAC-pluronic micelles) were correlated following the relevant Stern-Volmer relation (*cf.* Eq. 1.38; Section 1.6). Interestingly, in all the micellar systems, unlike the nonlinear I_0/I vs $[Q]$ plots as observed from SS fluorescence quenching, the $\tau_0/\langle\tau\rangle$ vs $[Q]$ plots from TR fluorescence quenching studies are found to be quite linear in nature. Typical of such linear Stern-Volmer plots obtained from TR quenching in CTAC-P123 and CTAC-F88 micellar systems at the CTAC to pluronic molar ratios of 0 and 0.5 are shown in Figure 4.9A and B, respectively. Such linear $\tau_0/\langle\tau\rangle$ vs $[Q]$ plots as obtained in all the micellar systems studied suggest that the dynamic part of the quenching/ET interaction is quite accurately estimated by using the present TCSPC measurements. Accordingly, the K_{SV} values were obtained from these

analyses and are considered as the estimates for the effective quenching/ET rates for the C343-DMAN pair in the different micellar systems studied.

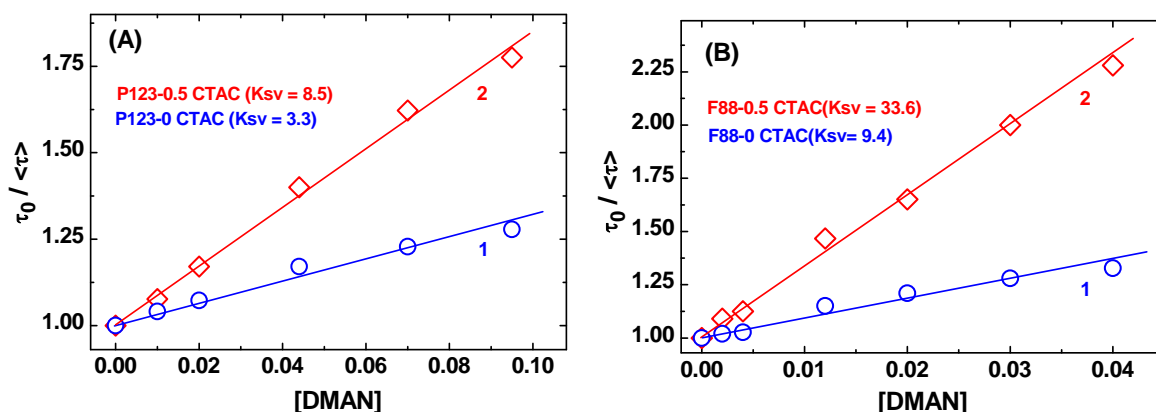


Figure 4.9: Stern-Volmer plots at different CTAC to pluronic molar ratios in: (A) CTAC-P123 and (B) CTAC-F88 mixed micelles. CTAC to pluronic molar ratios are: 0 (1: Blue) and 0.5 (2: Red).

Figure 4.10 shows the changes in the K_{SV} values in the CTAC-pluronic mixed micellar systems as a function of the increasing CTAC to pluronic molar ratios. As indicated from this figure, in both CTAC-P123 and CTAC-F88 mixed micelles, there is a large asymptotic increase in the K_{SV} values (about 2.6 fold in the case of CTAC-P123 and about 3.6 fold in the case of CTAC-F88 systems) with an increase in the CTAC composition and the effect apparently tends towards a saturation limit at a CTAC to pluronic molar ratios of about 0.5 and 0.8, in the two respective mixed micelles. Such a large increase in the K_{SV} values is a very intriguing and important observation and it explicitly suggests that there is a large increase in the overall ET/quenching interaction achieved just by increasing the composition of the cationic CTAC surfactant in the studied surfactant-pluronic mixed micellar systems.

One of the possible reasons for the observed increase in the K_{SV} values for the present ET systems in the studied mixed micelles can be the likely increase in the hydration at the micellar corona due to the incorporation of the more hydrophilic CTAC surfactants into the pluronic micelles.^{75-77,170-173,176-179,180-184} One would expect this because the rate of an ET reaction normally increases with an increase in the solvent polarity.^{5-11,138-142} In one of the earlier study on the ET reactions in surfactant-pluronic mixed micellar systems, albeit on employing the electrically neutral molecules as both the electron acceptor and the donor, it was observed that in the mixed micelles consisting of the neutral surfactant TX100 and the pluronic P123, the ET rate undergoes only a marginal change on changing the surfactant to

pluronic composition.¹⁶⁶ It was thus inferred that the hydration of the mixed micelle does not change much when TX100 is incorporated into the P123 micelle, as both TX100 and poly-EO block of P123 are of comparable hydrophobicity. On the other hand, on using ionic surfactants (e.g. anionic surfactant sodium dodecyl sulfate (SDS) or cationic surfactant CTAC) in combination with P123, it was observed that there is a significant increase in the ET rates, which was logically attributed to the increased hydration of the mixed micelles, as ionic surfactants are more hydrophilic than the poly-EO block of pluronic polymers.¹⁶⁶ In that study, as both the donor and the acceptor molecules are electrically neutral, assignment of the enhanced ET rates to the increased micellar hydration was quite justified because neutral reactants will not suffer any change in their locations in the microheterogeneous systems due to the formation of the charged layers inside the mixed micelles. In the present study, however, assignment of the enhanced quenching rates to the increased micellar hydration seems to be contradicting with the observed blue shifts in the SS fluorescence spectra (*cf.* Figure 4.2A) that suggested the dye to experience a gradually reduced micropolarity with the increasing composition of CTAC in the CTAC-pluronic mixed micellar systems. It is thus expected that in the present systems the enhancement in the ET rates for C343-DMAN pair must be due to some other effect than the increased micellar hydration as normally considered.

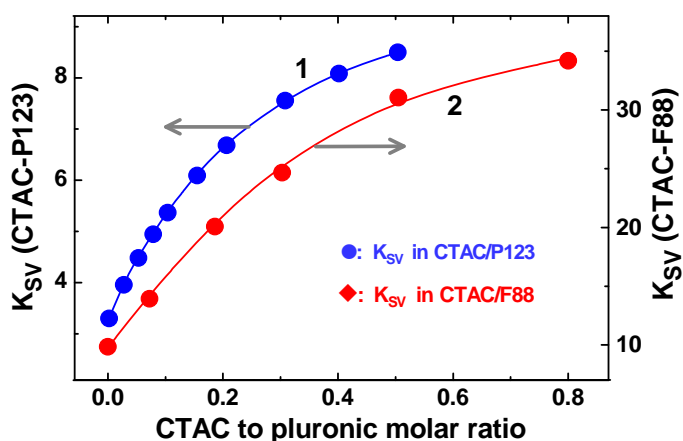


Figure 4.10: Changes in the Stern-Volmer quenching constant (K_{sv}) as a function of CTAC to pluronic molar ratios in the CTAC-P123 (1: Blue) and CTAC-F88 (2: Red) mixed micelles.

In the present study, as the electron acceptor dye C343 is in the anionic form, in the absence of CTAC, the dye is expected to be preferentially localized at the micelle-water interface region of the pure pluronic micelles. With the inclusion of CTAC into these micelles, as a positively charged layer is developed inside the mixed micelles,^{75-77,90,176-184} the

anionic C343 dye is electrostatically attracted by this positively charged layer and consequently the dye is gradually dragged deeper inside the micellar corona (*cf.* Scheme 4.2), causing it to encounter a relatively lower micropolarity with the increasing CTAC composition in the mixed micelle (*cf.* Figure 4.2). With this situation, the enhanced ET/quenching rates for the present donor-acceptor pair must not be related to the increased micellar hydration as suggested in the earlier study,¹⁶⁶ but is certainly associated with the changing location of the dye in the present mixed micellar systems,^{176-179,184} as the CTAC composition is gradually increased.

Considering that the dye gradually moves deeper inside the micellar corona, it is quite expected that its effect on the observed ET/quenching rates will eventually get saturated at a high CTAC concentration, when the dye is already close to the positively charged layer. This is in fact very clearly indicated from the trends of the plots in Figure 4.10. Moreover, based on this consideration and taking into account that the poly-EO block size for pluronic F88 is much larger than that of P123, it is expected that the saturation of the quenching rates would eventually reach at a relatively higher CTAC composition for CTAC-F88 mixed micelle than CTAC-P123 mixed micelle, as indicated from Figure 4.8 and 4.10, because the corona thickness is much larger in the former case than in the latter (*cf.* Table 4.1). These results are thus in direct support of our interpretation that the enhancement in the overall ET/quenching rates in the present mixed micellar systems is mainly due to the changing location of the dye with the changing CTAC composition.

Since the micropolarity around the C343 dye is indicated to decrease with an increase in the CTAC to pluronic molar ratio in the mixed micelles, the enhancement in the ET/quenching rates for the C343-DMAN pair was apparently unexpected under the normal circumstances. We feel that a major contributor to this increase in the quenching rate arises due to the inhomogeneous distribution of DMAN quencher in the micellar corona region. Being neutral and relatively more hydrophobic in nature, it is expected that DMAN quenchers will be more solubilized at the inner region of the micellar corona than at the micelle-water interface. Therefore, as the dye is gradually dragged inside the micellar corona, it consequently encounters a successively higher quencher concentration and hence undergoes a more efficient quenching interaction, which is clearly indicated by the plots in Figure 4.8 and 4.10. Though such a situation of the inhomogeneous solubility seems to be very logical for a neutral and relatively less polar reactant (DMAN in the present case) in a micellar media, to the best of our knowledge no experimental evidence for such a phenomenon has so far been reported in the literature. Results in the present study thus

exemplify this new insight of the fluorescence quenching process in the micellar and other microheterogeneous media where inhomogeneous solubility of the reactants can significantly influence the observed quenching rates. For the studied ET system, one more important point to be mentioned here that there could be an additional contribution towards the observed enhancement in the ET rates with the increasing CTAC to pluronic ratios arising due to the changing redox characteristic of the dye with its changing location in the mixed micellar systems, as reported earlier.¹⁷⁸ In the present study, however, it was not possible to distinguish and quantify the contributions of the above two effects on the observed enhancements in the ET rates with the changing CTAC to pluronic molar ratios.

As indicated from Figure 4.10, for a particular CTAC to pluronic molar ratio, the K_{SV} value is much higher in CTAC-F88 system than in CTAC-P123 system. The higher reaction rate certainly indicates that the microenvironment in the corona region of CTAC-F88 mixed micelle is more conducive for the ET interaction than that of the CTAC-P123 mixed micelle. We attribute this to the greater hydration of F88 micellar corona than that of P123. For F88, the two terminal poly-EO blocks contain 103 EO units each in comparison to only 20 EO units present in each of the two terminal poly-EO blocks in P123. Therefore, due to larger number of EO units, the corona regions of the pure and mixed micelles of F88 pluronic are much larger in thickness and hence much more hydrated compared to those of the micelle and mixed micelles of pluronic P123.^{73,75-77,152,170-173,176-179} Accordingly, the ET reaction in the C343-DMAN pair occurs with much higher propensity in CTAC-F88 mixed micellar systems than in the CTAC-P123 mixed micellar systems.^{5-11,138-142}

It is reported in the literature that for ionic surfactant-pluronic supramolecular assemblies both the hydrodynamic and core radii of the micelles decreases to some extent with an increase in the surfactant to pluronic molar ratio.^{77,140,166,177} In fact, in some of the earlier studies from our group this aspect has been investigated for CTAC-P123 and CTAB-F88 (CTAB: cetyltrimethylammonium bromide) mixed micellar systems using small angle neutron scattering (SANS) measurements and the reduction in the micellar size is found to be about 10-15 % for the surfactant to pluronic molar ratio of about 0.5.^{166,177} For the present CTAC-pluronic mixed micellar systems also we expect quite similar kind of changes in the micellar sizes with an increase in the CTAC to pluronic molar ratios, though we did not go for any explicit measurements for the micellar sizes in the present study. Moreover, as mentioned earlier, the donor DMAN is supposed to have a non-uniform distribution inside the micellar corona, being solubilized more at the deeper region of the corona than at the micelle-water interface. Thus, for the present systems, at any given bulk DMAN

concentration ($[DMAN]_t$), the C343 dye encounters a gradually changing effective DMAN concentration ($[DMAN]_{eff}$) in the course of its changing location in the micellar corona. With this complex situation, the actual $[DMAN]_{eff}$ is difficult to be estimated at each stages of the experimental conditions and hence the Stern-Volmer analysis of the TR fluorescence quenching data using $[DMAN]_{eff}$ is extremely difficult. Hence, for the present systems, the Stern-Volmer analysis of the TR fluorescence quenching data were effectively carried out in terms of the $[DMAN]_t$ as directly used in the experimental solutions. Consequently, the K_{SV} values estimated from these analyses are the apparent Stern-Volmer constants (K_{SV}^{app}) which would be related to true K_{SV} values (K_{SV}^{true}) by the following relation,

$$K_{SV}^{true} = k_q \tau_0 = \left(\frac{[DMAN]_t}{[DMAN]_{eff}} \right) K_{SV}^{app} \quad (4.1)$$

where k_q and τ_0 are having their usual meaning. It is understandable that in the absence of the exact estimates of the $[DMAN]_{eff}$ values, it is not possible to evaluate the true k_q values for the present ET system at different CTAC to pluronic molar ratios of the studied mixed micellar systems. In the present context, however, an approximate range of the k_q values can be adjudged by considering the average values for the effective quencher concentrations ($[DMAN]_{eff}$) in the corona region at different CTAC compositions. Thus, assuming that all the DMAN quenchers are solubilised within the micellar corona and considering that the thickness of the corona remains more or less similar for both the pure pluronic and the CTAC-pluronic micelles, the $[DMAN]_{eff}^{av}$ can be estimated as,^{138-141,166,167}

$$[DMAN]_{eff}^{av} = \frac{N_{agg}[DMAN]_t}{\frac{4}{3}\pi(r_m^3 - r_c^3)N_0\{[P]_t - CMC\}} \quad (4.2)$$

where N_{agg} , r_m , r_c and CMC are the aggregation number, micellar radius, core radius and critical micellar concentration, respectively, for the pluronic used (*cf.* Table 4.1),^{140,141} N_0 is the Avogadro's number and $[P]_t$ is the total pluronic concentration used in the solution.

Following Eq. 4.1 and 4.2 the k_q values in pure P123 and F88 micelles are estimated to be about $2.0 \times 10^7 \text{ M}^{-1}\text{s}^{-1}$ and $1.9 \times 10^8 \text{ M}^{-1}\text{s}^{-1}$, respectively, which are distinctly lower than the expected bimolecular diffusional rate constants (k_d) in P123 ($k_d \sim 1.5 \times 10^8 \text{ M}^{-1}\text{s}^{-1}$) and F88 ($k_d \sim 2.4 \times 10^8 \text{ M}^{-1}\text{s}^{-1}$) micelles as reported earlier.^{140,141} Interestingly, the k_q values estimated for the present ET system are about one order of magnitude lower in comparison to the typical k_q values observed for the ET systems involving different neutral coumarin dyes in combination with DMAN quencher in the same P123 and F88 micellar solutions.^{140,141}

Present results thus clearly indicate that in pure pluronic micelles the ET reaction involving anionic C343 dye is quite less efficient in comparison to that involving neutral coumarin dyes. This we attribute to the preferential solubilization of the anionic C343 dye at the micelle-water interface where population of neutral DMAN quencher is quite low and hence a less proficient ET reaction occurs in this case as compared to that of the neutral coumarin dyes that preferentially reside well within the micellar corona.

In the present mixed micellar systems, the k_q values estimated following Eq. 4.1 and 4.2 also clearly indicate an asymptotic increase, a trend very similar to that shown in Figure 4.10, as the CTAC to pluronic molar ratio is gradually increased. The saturation range for k_q values is thus estimated to be about $5.1 \times 10^7 \text{ M}^{-1}\text{s}^{-1}$ in CTAC-P123 and about $7.2 \times 10^8 \text{ M}^{-1}\text{s}^{-1}$ in CTAC-F88 mixed micellar systems. Interestingly, these values are quite close to the typical k_q values observed earlier in pure P123 and F88 micellar solutions involving different neutral coumarin dyes in combination with DMAN quencher,^{140,141} providing a support to our proposition that the anionic C343 dye is being dragged deeper inside the micellar corona as the CTAC composition is increased in the mixed micellar systems.

As already indicated, both the K_{SV} and k_q values estimated in the present study are actually the apparent values because the true $[\text{DMAN}]_{\text{eff}}$ values could not be estimated in the present study. In spite of this limitation, the observed K_{SV} and k_q values are still informative enough, displaying an intriguing and exceptionally large increase in the quenching rates for the studied ET reaction in the CTAC-pluronic mixed micellar media just by increasing the CTAC to pluronic molar ratios. Present results clearly demonstrate that the kinetics of the ET reactions can be modulated very significantly with proper selection of the electron donor-acceptor systems and the suitable combination of the ionic surfactant and pluronic polymer in the mixed micellar media, simply by changing the composition of the composite microheterogeneous system. Such modulations in the ET rates can have profound implications in the applied areas where bimolecular ET reactions are involved as the elementary steps in the concerned reaction mechanisms.

4.4. Conclusions

Present study demonstrates a large modulation in the rates of the ET reaction involving an anionic electron acceptor (C343) and a neutral electron donor (DMAN), achieved simply by changing the composition of a cationic surfactant (CTAC) to a pluronic polymer (P123 or F88) in the surfactant-pluronic mixed micellar assemblies. It is understood that the location of

the anionic acceptor C343 in the studied mixed micelles is gradually changed as the composition of cationic surfactant CTAC is increased in the mixed micellar systems. Observed results are interpreted on the basis of the reported structural motifs of the mixed micelles where ionic surfactants are embedded with their hydrocarbon chains grafted into the micellar core leaving their ionic head groups projected out of the core protruding into the micellar corona. Accordingly, a positively charged layer is developed deep inside the mixed micelle which attracts the anionic C343, gradually dragging the dye deeper inside the micellar corona, as the CTAC composition is increased in the system. As DMAN donor is a neutral and relatively hydrophobic molecule, it is solubilized more preferentially at the deeper region of the micellar corona than at the micelle-water interface. Accordingly, while the C343 acceptor is dragged into the micellar corona, it gradually encounters an increased concentration of DMAN and hence undergoes an enhanced fluorescence quenching mediated by ET interaction. Observed results in the present study are very interesting and exciting because it demonstrates a large modulation in the ET rates simply by changing the surfactant to pluronic molar ratios in the mixed micellar systems, a strategy very convenient to implement for a desired outcome from an ET reaction. We strongly feel that the present approach of modulating the ET rates will find uses in different applied areas where bimolecular ET reactions are involved as the fundamental reaction steps.

Chapter 5

Photophysical Characterization of Electron Acceptor Dyes: Coumarin 481 and 153

Abstract

This chapter describes the results on photophysical characteristics and solution behavior of two representative coumarin dyes, namely, C481 and C153 (cf. Chart 3.1), used as the electron acceptors in PET studies, investigated to explore any of their unusual behavior, especially their aggregation, in polar organic solvents and aqueous solution. The dye C481 having flexible 7-dialkylamino substituents displays very efficient intramolecular charge transfer (ICT) state to twisted intramolecular charge transfer (TICT) state conversion in polar solvents, exhibiting very low Φ_f and τ_f values, which might cause PET results quite susceptible to errors if there is an aggregation for the dye in solution. The dye C153 has been investigated to understand if the flexibility of the 7-amino substituents of the coumarin dyes have any relevance to their aggregation process. Probing the spectral changes as a function of dye concentration following ground state absorption and SS fluorescence studies do not show any signature of aggregation for both the dyes. However, TR measurements show remarkable changes in the fluorescence decays with changing dye concentration, monitoring emission wavelength and solution temperature, especially at the blue edge of the emission spectra, indicating the presence of dye aggregates in the solutions. Constructed TRES and TRANES confirm the co-existence of blue shifted emissive H-aggregates along with dye monomers both in polar organic solvents and aqueous solutions. It is inferred that the highly dipolar character of the studied dyes (dipole moment ~ 6 D) drives the aggregation process through strong electrostatic interaction and it is accordingly favored in polar solvents, especially in polar protic solvents, as the dye-solvent hydrogen bonding interaction provides extra stability of the dye aggregates. Importantly, the H-type of the aggregates that emit mainly in the blue edge of the SS emission spectra, are realized not to affect our PET results presented in the previous chapters, as all the PET studies have been carried out following fluorescence quenching measurements at the emission maxima of the dyes where dye aggregates do not show any contribution.

5.1. Introduction

In our PET studies as discussed in Chapters 3 and 4, coumarin dyes have been used as the electron acceptors. Photophysical characterization and solution behavior of these dyes are essential to ascertain that observed PET results are not affected by any unusual solution behavior of these dyes. With this perspective, photophysics of two selective coumarin dyes, namely, coumarin 481 (C481) and coumarin 153 (C153) have been investigated to understand their general behavior in polar organic solvents and aqueous solutions.

Coumarin dyes (1,2-benzopyrone derivative) are well known laser dyes in the blue-green region.^{191,192} 7-aminocoumarin dyes (having differently substituted 7-amino groups) show quite remarkable excited state properties, e.g. strong intramolecular charge transfer (ICT) character,^{193,194} large solvatochromism,^{193,194} high fluorescence quantum yields (Φ_f), long fluorescence lifetimes (τ_f),¹⁹³⁻¹⁹⁶ high photostability, etc. These favorable properties have made these dyes as useful fluorescence probes in various chemical and physiochemical studies.^{171,185,197-199} Coumarin dyes have also found useful applications as chemosensors^{200,201} as well in biological and biomedical sciences.²⁰²⁻²⁰⁴ Though photophysical properties of the coumarin dyes are quite extensively reported in the literature, many of their atypical behaviors in different solvents are yet to be explored completely.^{154,193-196,204-208}

An important and well discussed photoinduced process that 7-N,N-dialkylaminocoumarin dyes participate in high polarity solvents is the conversion of their fluorescent planar ICT state to the nonfluorescent twisted intramolecular charge transfer (TICT) state. It is observed that the ICT to TICT conversion occurs only when the solvent polarity exceeds some critical limit, causing a large reduction in the Φ_f and τ_f values of the dyes, as the TICT formation introduces a new nonradiative decay channel for the excited dyes.^{82,194,209-211} Among 7-N,N-dialkylaminocoumarin dyes, the dye C481 (*cf.* Chart 3.1) is known to display most efficient ICT to TICT conversion process.²¹⁰⁻²¹² It is observed that irrespective of the protic or aprotic nature of the polar organic solvents, the reduction in the Φ_f and τ_f values for C481 dye correlate satisfactorily on the consideration of only the ICT to TICT conversion process.²¹⁰⁻²¹² In earlier reports, however, it was unexpectedly observed that when water is used as a polar solvent, the fluorescence decay of C481 dye develops an unusually long decay tail in addition to the usual very fast decay component associated to ICT to TICT conversion process.²¹⁰⁻²¹² This observation suggests that along with ICT to TICT conversion the dye C481 must also be undergoing an additional, hitherto unresolved process in the presence of water. Therefore, in this study the photophysics of C481 dye has

been investigated in both aqueous and polar organic solvents to unravel the reason of the above unusual behavior of the dye. Unlike C481, the dye C153 (*cf.* Chart 3.1) does not undergo the ICT to TICT process due to the presence rigid of its julolidinyl rings at the 7-amino position. Therefore, photophysics of C153 has also been investigated in the present study to understand if the flexibility of the 7-amino substituents has any bearing with the unusual solution behavior of the 7-aminocoumarin dyes. Moreover, as both C481 and C153 dyes are widely used as fluorescence probes in investigating various microenvironments, it is also essential to understand their solution behavior very explicitly.

Since the initial report by Jelley,²¹³ exploring the details of dye aggregation in solution has been the subject of numerous investigations. For many chromophoric dyes, as the concentration increases, the dyes tend to undergo dimer and higher dye aggregate formation in the solution. Various physicochemical and biological processes are significantly influenced by the dye aggregates in the systems. For example, molecular aggregates play a vital role in guiding the energy channels in the solar energy conversion process in biological systems.²¹⁴ Dye aggregates have also found many technological applications in solar cells,^{215,216} electronic devices,^{217,218} light emitting diodes,²¹⁹ optical communication,²²⁰ etc.

Though dye aggregation is advantageous in many applications, there are, however, uses, e.g. in dye lasers, fluorescent sensing/probing, various physiochemical studies, etc. where dye aggregation gives detrimental effects. In such cases, solution behavior of the dyes should be scrutinized thoroughly and strategies should be adopted to minimize/control the aggregation process. In the present context, studies have been carried out to see if 7-aminocoumarin dyes do have any tendency to undergo aggregation in polar solvents of our interest. The inquisitiveness of our present study has also been inspired from the interesting recent reports demonstrating aggregation/self-association for some coumarin derivatives in environments like polar organic solvents,^{221,222} silica/methanol interfaces,²²³ mesoporous molecular sieves,²²⁴ solvent mixtures,^{225,226} Langmuir–Blodgett films,²²⁷ etc..

Reported studies on the photophysics of C481 and C153 dyes have always been discussed exclusively considering the monomeric dyes in the solution.^{196,208-211,228-232} A revisiting of the solution behavior and photophysics of these dyes seemed essential, anticipating their possible aggregation in some solvents. For C481 dye, this is very important, because the dye undergoes efficient ICT to TICT conversion in polar solvents that reduces its Φ_f and τ_f values drastically,^{196,208-211,228-230} rendering the results obtained by employing this dye as a probe quite susceptible to errors, even in the cases of small extent of dye aggregation

in the solution. For C153 dye, it is interesting on the other hand to see if any signature of its aggregation can still be realized, even though its Φ_f and τ_f values are very high, which might expectedly suppress the effect of small extent of dye aggregation in the solution. Therefore, photophysical studies have been carried out for the above two representative 7-aminocoumarin dyes in polar organic solvents and aqueous solutions and the results are systematically discussed in this chapter. For the convenience of presentation, this chapter has been divided into four parts. Thus, Parts A and B describe the results of C481 dye in organic solvents and in aqueous solutions, respectively. Similarly, Parts C and D report the studies on C153 dye in organic solvents and in aqueous solutions, respectively. Chemical structures of C481 and C153 dyes are given in Chart 3.1.

5.2. Experimental Methods and Materials

Laser grade C481 and C153 samples were obtained from Exciton, USA, and used as received. Nanopure water (conductivity $\sim 0.06 \mu\text{S cm}^{-1}$) from an Elix-3/A10 Millipore system was used for preparation of aqueous solutions. While spectroscopic grade acetonitrile (ACN; SD Fine Chemicals, India) was used as received, the spectroscopic grade ethanol (EtOH; Les Alcools de Commerce Inc., Canada) was further purified by distillation before use. Until otherwise stated, measurements were carried out at ambient temperature ($25 \pm 1 \text{ }^\circ\text{C}$).

Since coumarin dyes are only sparingly soluble in water and their dissolution is also very slow, saturated solutions of the studied dyes were prepared by stirring the dye samples overnight in water. The supernatant solutions collected after centrifugation (10,000 rpm, ~ 10 minutes) were kept under stirring again for ~ 4 hours at an elevated temperature ($\sim 70 \text{ }^\circ\text{C}$) to allow equilibration among aggregates, if any. The solutions were then allowed to attend ambient temperature ($\sim 25 \text{ }^\circ\text{C}$) before use. Solutions in EtOH and ACN were prepared by directly dissolving the dyes. The solutions were then centrifuged (10,000 rpm, ~ 10 minutes) and collected supernatant solutions were further sonicated for ~ 10 minutes to avoid any undissolved dyes in the final solution. For studies in water-ACN solvent mixtures, two equal parts of the stock dye solution in ACN were diluted to the same extent by adding water and ACN, respectively. These two solutions were then mixed in required proportions to vary ACN % in the solvent mixtures, keeping the dye concentration constant ($\sim 0.6 \mu\text{M}$).

The instruments used for ground state absorption, SS fluorescence, TR fluorescence, fluorescence up-conversion, DLS and SEM studies are discussed in Chapter 2 with necessary details. In the present study, a 374 diode laser (1 MHz, 100ps) was used in the TCSPC

measurements and the typical IRF for the setup is ~110 ps at FWHM. The lowest lifetime measurable with this setup is ~30 ps. For up-conversion instrument the typical IRF is ~200 fs at FWHM and the lowest lifetime measurable is ~50 fs. The construction methods for the TRES and TRANES of the studied dyes have been given in Section 1.5.

5.3. Results and Discussion

In the present study photophysical characteristics of C481 and C153 dyes have been carried out both in polar organic solvents and aqueous solutions. As mentioned earlier in Section 5.1, the results of these studies are presented in four different parts of this section, namely Part 5.3.A, 5.3.B, 5.3.C and 5.3.D, respectively, describing the studies on the two dyes in polar organic solvents and in aqueous solution separately, as are presented below.

Part 5.3.A

Photophysical behavior of C481 dye in polar organic solvents

Though photophysics of C481 dye in different protic and aprotic solvents of various polarities have been reported earlier,^{196,208-211,228-232} neither of these studies considered the possible aggregation of the dye in the solution. Since a number of recent studies report aggregation of some coumarin derivatives in different solvent environments,²²¹⁻²²⁷ a systematic study has been carried out in the present work on the photophysical properties of C481 dye in two conventional polar organic solvents, namely polar protic solvent ethanol (EtOH) and polar aprotic solvent acetonitrile (ACN), to understand possible aggregation of the dye in the solution.

5.3.A.1. Ground-state absorption and SS fluorescence measurements. Ground state absorption spectra of C481 dye were measured in EtOH and ACN solutions at different dye concentrations and are shown in Figure 5.1A and B, respectively. Dye concentrations were estimated from the peak absorbances ($\lambda_{\text{abs}}^{\text{max}} = 404$ in EtOH and 399 nm and ACN) using molar extinction coefficient values estimated as 1.87×10^4 and $1.85 \times 10^4 \text{ M}^{-1} \text{ cm}^{-1}$, respectively, in EtOH and ACN solutions. As indicated from this figure, there is no obvious

change in the spectral characteristics with the changing dye concentration in both the solvents. Like absorption spectra, the SS fluorescence spectra of C481 also do not show any obvious spectral change with the changing dye concentration, as are shown in Figure 5.2A and B, respectively, in EtOH ($\lambda_{fl}^{max} = 514$ nm) and ACN ($\lambda_{fl}^{max} = 504$ nm) solutions.

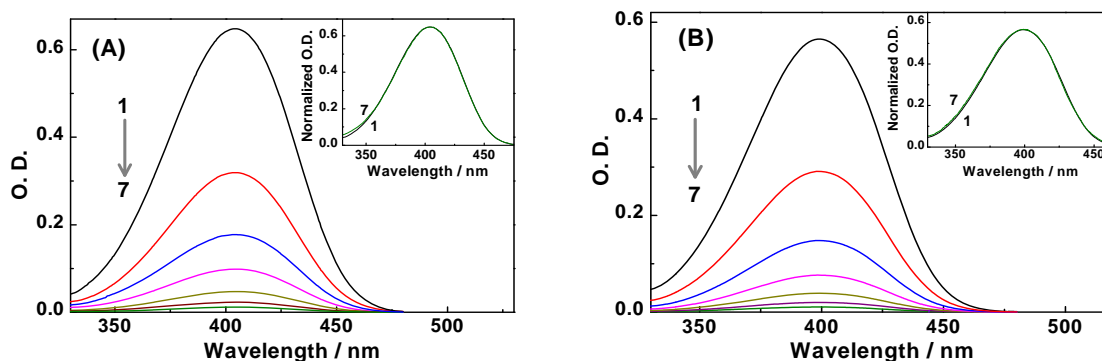


Figure 5.1: Absorption spectra of C481 dye in (A) EtOH and (B) ACN solutions. For spectra 1-7 the dye concentrations in Panel (A) are: 35.0, 17.2, 9.6, 5.3, 2.6, 1.2 and 0.6 μ M, respectively and those in Panel (B) are: 30.2, 15.6, 7.9, 4.1, 2.1, 1.1 and 0.6 μ M, respectively. **Insets:** Peak normalized absorption spectra for the highest and lowest dye concentrations used in the respective solvents.

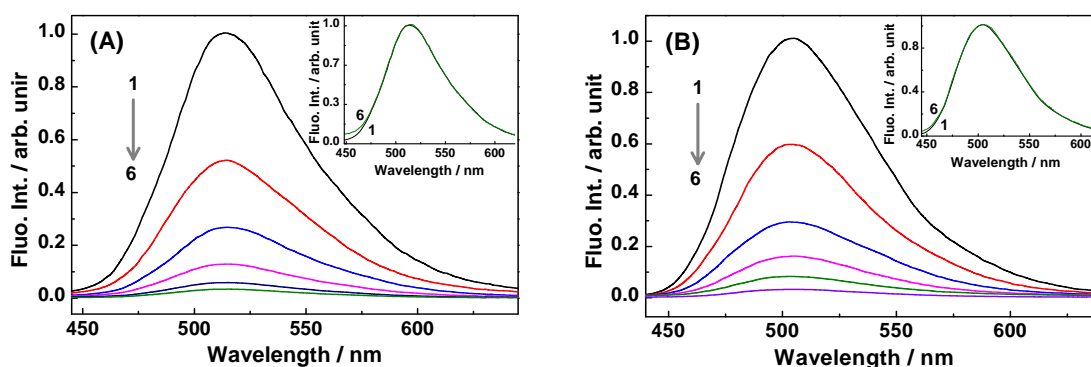


Figure 5.2: Fluorescence spectra of C481 dye in (A) EtOH and (B) ACN solutions. For spectra 1-6 the dye concentrations in Panel (A) are: 9.6, 5.3, 2.6, 1.2, 0.6 and 0.3 μ M, respectively, and in Panel (B) are: 15.6, 7.9, 4.1, 2.1, 1.1 and 0.6 μ M, respectively. **Insets:** Peak normalized fluorescence spectra for the highest and the lowest dye concentrations in the respective solvents. $\lambda_{ex} = 374$ nm.

To investigate the present systems further, SS fluorescence spectra of the dye in both EtOH and ACN solutions were also recorded as a function of the excitation wavelength. The results are shown in Figure 5.3A and B, respectively, indicating that the spectra are effectively independent of the excitation wavelength used. These results thus corroborate well with the absorption and fluorescence results shown above, seemingly indicating the dominance of the monomeric form of dye in both EtOH and ACN solutions. In the present context, we also recorded the excitation spectra of dye in the two solvents keeping emission

wavelengths at extremely blue edge, at peak position and at extremely red edge of the emission spectra, as are shown in Figure 5.4A and B, respectively. These excitation spectra also do not show any significant changes with the changing emission wavelengths. Based on all these results thus it is apparent that the dye C481 seemingly behaves quite normally both in the protic EtOH and aprotic ACN solvents. However, since these SS measurements are not very sensitive, further studies on the dye in these solvents were carried out using the more sensitive TR fluorescence measurements, as are discussed in the next section.

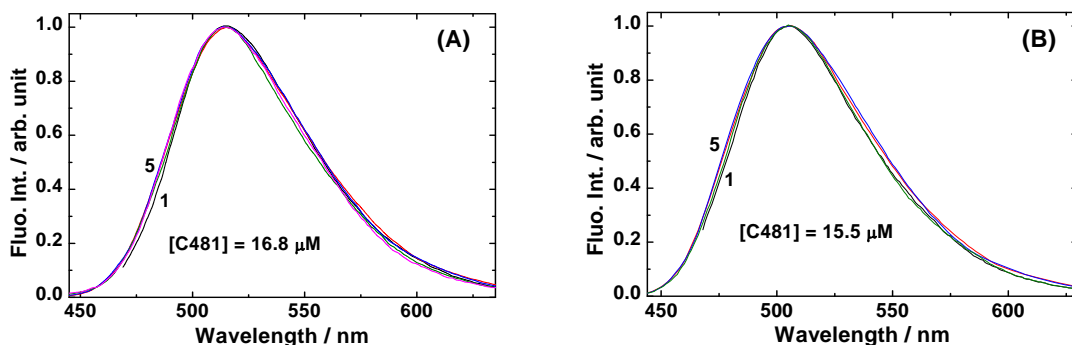


Figure 5.3: Peak normalized fluorescence spectra of C481 dye in (A) EtOH and (B) ACN solutions. For spectra 1 to 5 the excitation wavelengths in Panel (A) are: 450, 404, 374, 350 and 340 nm, respectively, and in Panel (B) are: (1) 450, (2) 399, (3) 374, (4) 350 and (5) 340 nm, respectively.

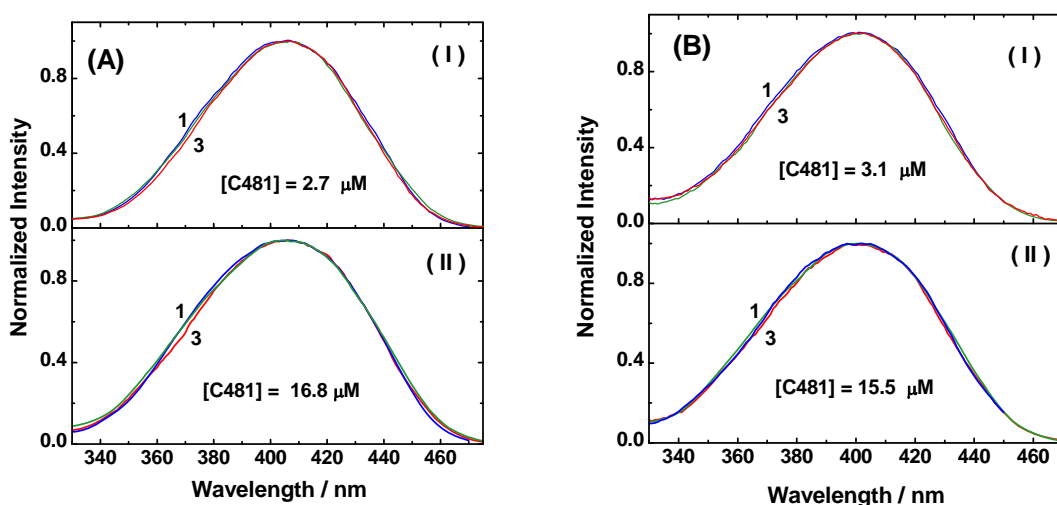


Figure 5.4: Peak normalized excitation spectra of C481 in (A) EtOH and (B) ACN solutions, with a lower (I) and a higher (II) dye concentrations, respectively. For spectra 1-3, the emission wavelengths are: (1) 480 nm (Blue end), (2) 514 nm (Emission peak) and (3) 570 nm (Red end) in EtOH and (1) 450 nm (Blue end), (2) 504 nm (Emission peak) and (3) 570 nm (Red end) in ACN solutions.

5.3.A.2. TR fluorescence measurements. Fluorescence decays of C481 dye were measured in EtOH and ACN solutions at the emission peak ($\lambda_{em}^{max} = 514$ nm in EtOH and 504 nm in ACN) and at a significantly blue shifted emission wavelength ($\lambda_{em} = 480$ in EtOH and 450

nm in ACN), as a function of the dye concentration used. The results are shown in Figures 5.5 and 5.6, respectively. In EtOH solution, though the decays at the emission peak (*cf.* Figure 5.5A) do not show any drastic change, yet the presence of a small extent of decay tail whose contribution changes with the dye concentration is clearly evident. This effect is more pronounced for the decays at the blue edge of the spectra (*cf.* Figure 5.5B). In ACN solution, the characteristics of the decays are more or less similar to those in EtOH solution, though in this case the tailing is less elongated than in EtOH.

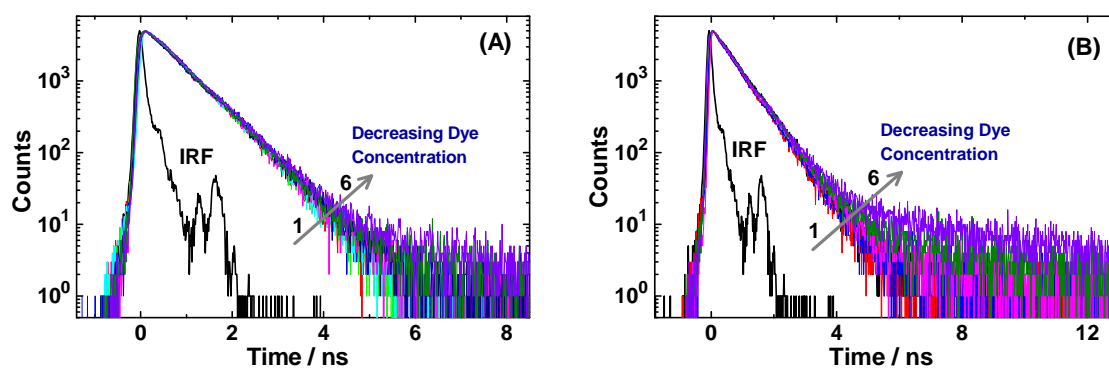


Figure 5.5: Fluorescence decays of C481 dye in EtOH solution, measured at (A) the emission peak (514 nm) and (B) a blue shifted emission wavelength (480 nm). For decays 1 to 6 dye concentrations are: 9.68, 4.84, 2.24, 1.21, 0.61 and 0.30 μM , respectively. $\lambda_{\text{ex}} = 374$ nm.

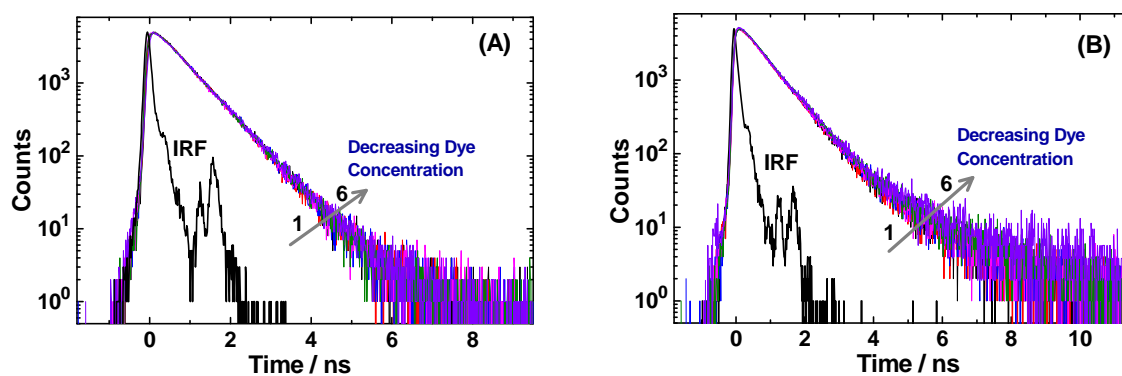


Figure 5.6: (A) Fluorescence decays of C481 dye in ACN solution, measured at (A) the emission peak (504 nm) and (B) a blue shifted emission wavelength (450 nm). For the decays 1 to 6 dye concentrations are: 15.0, 7.8, 3.8, 1.9, 0.94 and 0.47 μM , respectively. $\lambda_{\text{ex}} = 374$ nm.

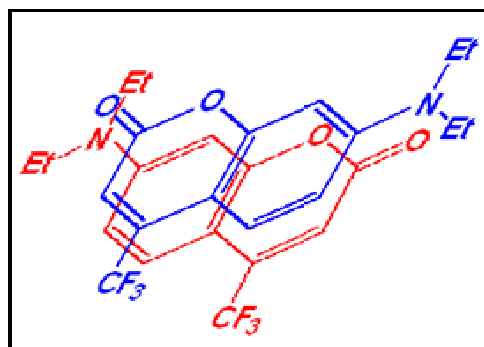
We perceive that the tailing in the decays are due to small extent of dye aggregation, while the faster decaying major components are due to dye monomers. These assignments are in accordance with the efficient ICT to TICT process for monomeric dye in polar solvents.^{208,210,82,228-230} While the ICT to TICT process causes the fluorescence lifetime of the monomeric dye unusually short, the steric constrain of the stacked dyes in the aggregates resists the TICT formation causing their fluorescence decays significantly longer. It is evident

from Figures 5.5 and 5.6 that the decay tails are more prominent at the blue end of the emission spectra than at the emission peak. This observation suggests that the aggregate emissions are largely blue shifted as compared to the monomer emission and accordingly it is suggested that the C481 dye undergoes H-type of aggregation in both EtOH and ACN solutions (*cf.* Kasha's exciton theory; Section 1.8).^{1-4,91,92}

The important point to be noted here is that the H-aggregates of C481 dye are emissive in nature (*albeit with low emission yields, as SS emission measurements cannot distinguish these emissions*), which is evidently an interesting observation. According to Kasha's exciton theory (*cf.* Figure 1.12), the H-aggregates are supposed to be non-fluorescent, because their allowed higher excitonic state undergoes rapid non-radiative relaxation to the lower excitonic state (*due to fast IC*), from where radiative transition is forbidden. Accordingly, a major decay channel for excited H-aggregates would be via triplet state formation (*by the ISC process in lower excitonic state*).^{1-4,91,92} Though non-fluorescent nature of H-aggregates is quite common, yet there are cases where fluorescent H-aggregates are also reported for some of the chromophoric dyes.^{225,233-248} Importantly, however, in most of the cases of H-aggregate emissions they are extremely weak and are also red shifted in comparison to the monomer emission, suggesting that these emissions actually arise from the lower excitonic states. In these cases it is proposed that a non-vanishing electronic transition probability from the lower excitonic state to the ground state arises due to the combined effect of the vibronic coupling and a small extent of rotational twist in the stacking of the dyes than their perfect arrangement with parallel orientation of the transition dipoles.²⁴⁶⁻²⁴⁸

In the literature, there are very few cases where blue shifted H-aggregate emissions have been reported.^{225,233-243} A rapid back conversion from the lower excitonic state to the higher excitonic state through de-phasing of intra-chromophoric transition dipoles caused by solvent perturbations has been suggested as one of the mechanism for such emission.^{240,241} Additionally, it is also likely that for strongly dipolar dyes the IC from higher excitonic state to lower excitonic state of the H-aggregates could be significantly suppressed due to their extra rigidity arising from strong coulombic interaction of the permanent dipoles of the dyes arranged in an anti-parallel configuration (*cf.* Scheme 5.1). It is thus suggested that the weak emissions from H-aggregates of C481 dye in EtOH and ACN solutions are due to the combined effects of the above two effects. To be mentioned here that, even for these cases, the IC from the higher to the lower excitonic states will still be quite efficient (due to small energy gap between the two states) and accordingly the emissions from the higher excitonic state will be weak and short lived.^{242,243} Moreover, it is presumed that with an increase in the

aggregate size there will be a gradual decrease in the lifetime as the increased density of the excitonic states will facilitate the non-radiative deactivation process.^{1-4,91,92,242,243}



Scheme 5.1: Conceptual presentation of the stacking of two C481 dye molecules in H-aggregates with antiparallel permanent dipoles stabilizing the aggregates through Coulombic interaction.

As one can understand from scheme 5.1, aggregation of dipolar dyes is facilitated by electrostatic interaction where Gibbs binding energy would be proportional to the square of the dipole moment of the dyes.²⁴⁹ In H-aggregates, as the permanent dipoles of the dyes are oriented in an anti-parallel configuration, the electron rich and electron-deficient parts of the dyes come on top of each other and hence maximize the electrostatic interactions.^{225,237,249-252} In the present context, it is important to draw attention to the work of Cigan, et al. where the role of the above coulombic interaction between stacked dyes have been invoked to rationalize the formation of H-aggregates in some of their studied coumarin derivatives.^{225,237} In fact, in one of their study, the authors have also employed quantum-chemical calculations showing that the H-dimers are substantially stabilized (*by about 42 kJ mol⁻¹*) when two dye molecules are stacked with their permanent dipoles oriented in an anti-parallel configuration.²³⁷ Thus, these authors have concluded that the H-dimers/aggregates of the dipolar dyes are actually driven by the combined effects of the dipole–dipole and the donor–acceptor π - π interactions between the stacked dyes.²³⁷ It is also suggested by Cigan et. al.^{225,237} that a strong electrostatic interaction actually helps in overcoming the restriction imposed by Kasha’s exciton theory and thus making it possible to observe emission from the higher excitonic states of the H-aggregates. We feel that similar binding interactions are also responsible for the formation of the fluorescent H-aggregates of the highly dipolar C481 dye (dipole moment, $\mu \sim 6.46$ D)¹⁹⁶ investigated in the present study.

From the photophysical studies it is reported that for different ICT dyes the dipolar character is often increased in protic solvents due to dye-solvent intermolecular hydrogen bonding interaction.^{200,238-242} Since C481 is a strong ICT dye, it is suggested that in protic

EtOH solvent the dipolar character of the present dye also increases significantly through dye-solvent hydrogen bonding interaction,^{225,237,249-252} resulting higher aggregation of the dye in EtOH solution than in ACN. Moreover, in EtOH solution, a solvent molecule that is hydrogen bonded to a particular C481 dye (preferably at its C=O group) can additionally participate in the electrostatic interaction with the positive pole of the adjacent dye molecule in the aggregate arranged with an anti-parallel orientation of the dipole, resulting an extra stability to the H-aggregate. In ACN solution, even though there is no dye-solvent hydrogen bonding interaction, the polar nature of the solvent seems quite sufficient to stabilize the dye H-aggregates where highly polar dye molecules are stacked with anti-parallel orientation of the dipoles, resulting in a strong columbic interaction among the constituent partners.

Concentration dependent decays in Figures 5.5 and 5.6 in general required bi-exponential function to obtain acceptable fits. Decay parameters thus obtained with different dye concentrations at two monitoring wavelengths in EtOH and ACN solutions are listed in Table 5.1. To be mentioned that in ACN solution, though the decays at the emission peak could be fitted reasonably well following a single-exponential function, yet to keep a consistency with other decays, a bi-exponential analysis was also carried out in the present cases. As are seen from Table 5.1, in both the solvents the decays are always dominated by shorter decay component, τ_1 , having a lifetime of about 0.64 ns in EtOH and about 0.67 ns in ACN. This component is effectively independent of the dye concentration and the monitoring emission wavelength used. Expecting that the electronically neutral dye C481 would preferentially exist in its monomeric form in an organic solvent and considering that the high polarity of EtOH and ACN would strongly facilitate the ICT to TICT conversion for the excited dye monomer,^{82,208,210,228-230} the shorter τ_1 component is justifiably assigned to the monomeric dyes present in the solution. To be noted that in the literature the fluorescence lifetime of C481 dye in EtOH and ACN solutions are reported to be in the range of about 0.6-0.9 ns and 0.6-0.7 ns, respectively, quite similar to the τ_1 values estimated in the present study. As reported in the literature, unlike in high polarity solvents, the lifetime values for C481 dye in nonpolar to moderately polar solvents are quite long, in the range of about 4-6 ns. Such longer lifetime is due to the absence of ICT to TICT conversion, as the lower solvent polarity cannot stabilize the highly polar TICT state.^{82,208,210,228-230}

In addition to the shorter τ_1 component, the fluorescence decays also show the presence of a relatively longer component τ_2 in both EtOH and ACN solvent which we assign to the dye aggregates present in the solution. As one would observe from Table 5.1, the

Table 5.1: Fluorescence decay parameters for C481 dye in EtOH and ACN solutions as estimated at different dye concentrations and at different emission wavelengths. $\lambda_{\text{ex}} = 374$ nm.

[C481] / μM	a_1 %	τ_1 / ns	a_2 %	τ_2 / ns	χ^2
<i>EtOH solution: $\lambda_{em} = 480$ nm (Blue shifted wavelength)</i>					
35.0	99.2	0.62	0.8	1.22	1.01
17.2	99.1	0.63	0.9	1.30	1.10
9.6	99.0	0.64	1.0	2.30	1.15
5.3	98.9	0.63	1.1	2.63	1.01
2.6	98.9	0.64	1.1	4.09	1.16
1.2	98.2	0.64	1.8	4.39	1.19
0.6	96.3	0.64	3.7	5.12	1.01
<i>EtOH solution: $\lambda_{em} = 514$ nm (emission peak)</i>					
35.0	99.6	0.63	0.36	1.19	1.00
17.2	99.6	0.62	0.39	1.37	1.02
9.6	98.5	0.64	0.54	2.16	1.06
5.3	99.8	0.64	0.21	2.59	1.10
2.6	99.8	0.66	0.22	4.03	0.97
1.2	99.6	0.64	0.44	4.32	0.98
0.6	98.8	0.64	1.22	5.12	1.00
<i>ACN solution: $\lambda_{em} = 450$ nm (Blue shifted wavelength)</i>					
30.2	92.2	0.66	7.8	1.64	1.18
15.6	91.7	0.66	8.3	1.61	1.00
7.9	92.4	0.68	7.6	1.67	1.08
4.1	91.9	0.66	8.1	1.72	0.99
2.1	91.0	0.67	9.0	1.71	1.01
1.1	89.4	0.66	10.6	1.64	1.10
<i>ACN solution: $\lambda_{em} = 504$ nm^s (emission peak)</i>					
30.2	98.5	0.67 (0.67)	1.5	1.66	0.98 (1.08)
15.6	98.7	0.67 (0.69)	1.3	1.66	1.01 (1.13)
7.9	98.9	0.67 (0.68)	1.1	1.65	1.00 (1.10)
4.1	98.8	0.68 (0.68)	1.2	1.66	0.97 (1.06)
2.1	99.0	0.68 (0.67)	1.0	1.65	0.98 (1.10)
1.1	98.7	0.66 (0.68)	1.3	1.65	1.01 (1.18)

^sThe decays at the emission peak of the dye in ACN solution could also be fitted well following single-exponential function and the decay parameters thus obtained are listed in the parentheses.

contribution of τ_2 is higher at the blue edge of the emission spectra than at the emission peak, which is certainly in accordance with the H-type of aggregation of the dye in both the solvents. In EtOH solution, it is seen that the τ_2 value gradually increases on decreasing the dye concentration. Such an observation is indicative of the presence of aggregates of different sizes in the solution. Since in the aggregated dyes the ICT to TICT conversion would be sterically hindered, and also the lifetime of the aggregates would decrease with an increase in the aggregate size, we felt that the increased τ_2 value with the decreasing dye concentration is due to the gradual conversion of the higher dye aggregates to the dye dimers in the solution. Accordingly, the longest lifetime value of ~ 5.12 ns, as estimated for the most diluted dye solution in EtOH is intuitively assigned to the lifetime of dye H-dimer. At higher dye concentrations, however, the estimated τ_2 values are not expected to represent any particular dye aggregate but could be due to the contributions of aggregates of different sizes (dimer, trimer, tetramer, etc.) present in the solution.

Unlike EtOH, in ACN solution the τ_2 value does not show any noticeable change with the changing dye concentration, though the contribution of this component clearly increases as the dye concentration is reduced (*cf.* Table 5.1). Expecting that the dye dimers would not have largely different lifetimes in EtOH and ACN solutions, it is presumed that in ACN solution the decay tails are mostly contributed by the larger dye aggregates than dimers. Thus the results indicate that while the dimers are quite preferred in polar protic EtOH solvent, larger dye aggregates are mostly preferred in polar aprotic solvent ACN. This proposition is also substantiated by the observation that the τ_2 values estimated in ACN solution are quite closer to the τ_2 values in EtOH solution at higher dye concentrations, where larger aggregates would necessarily dominate. Assuming that the above discussed situations prevailed for the dye aggregation in the two solvents, it is imperative to infer that while the higher solvent polarity drives the aggregation of C481 dye, the protic nature of the solvent helps in the stabilization of the dimeric species of the dye. That the protic nature of the solvents provides an additional preference for the formation of C481 dimers is also supported by the results on C481 dye in aqueous solution as will be discussed in part B of this chapter.

5.3.A.3. TRES and TRANES analysis for C481 dye. To understand time-dependent changes in the spectral characteristics of different emitting species for the dye in the solution, the TRES^{52,158} and TRANES^{253,254} were constructed in both EtOH and ACN solutions following procedure given in Section 1.5. Wavelength dependent fluorescence decays of C481 dye thus

measured in both EtOH and ACN solutions are shown in Figures 5.7A and B, respectively. The constructed TRES and TRANES in EtOH solution are shown Figures 5.8A and B and those in ACN solution are shown in Figures 5.9A and B, respectively.

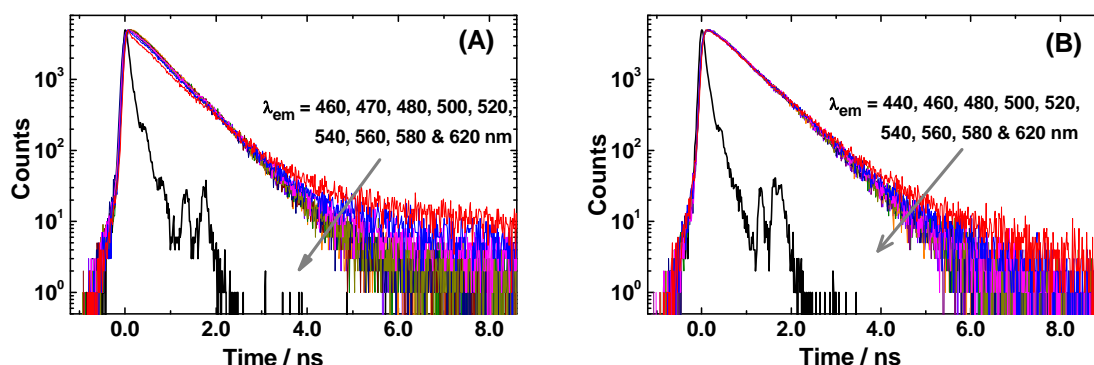


Figure 5.7: Fluorescence decays of C481 dye ($\sim 2.70 \mu\text{M}$) in (A) EtOH and (B) ACN solutions, measured at different emission wavelengths of the dye as indicated in the figure. $\lambda_{\text{ex}} = 374 \text{ nm}$.

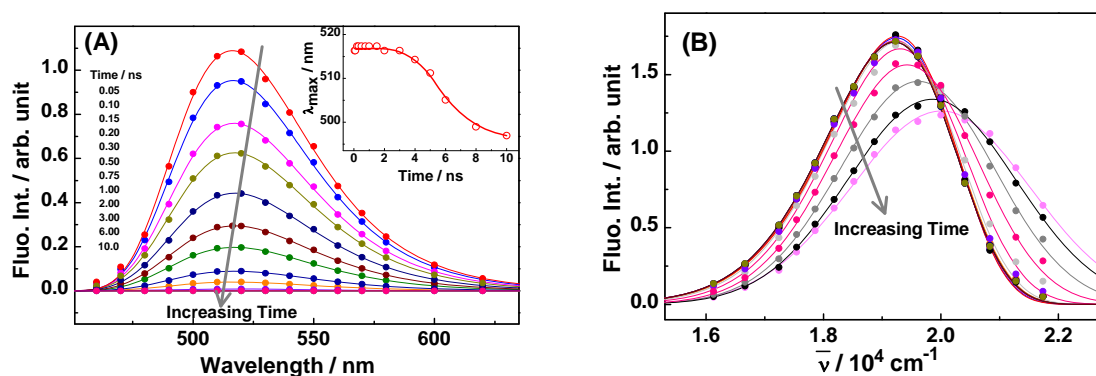


Figure 5.8: (A) TRES and (B) TRANES of C481 dye in EtOH solution. Inset of Figure 5.8A shows the changes in the emission maxima of the TRES and TRANES with time.

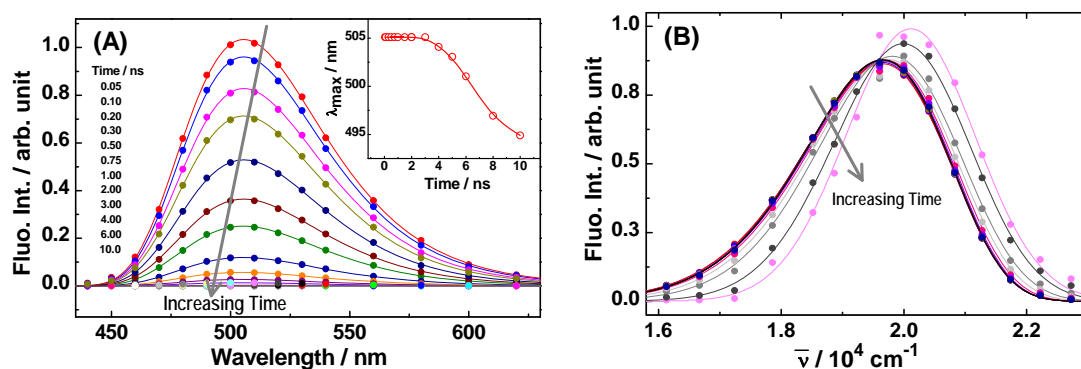


Figure 5.9: (A) TRES and (B) TRANES of C481 dye ($2.67 \mu\text{M}$) in ACN solution. Inset of Figure 9A shows the changes in the emission maxima of the TRES and TRANES with time.

As indicated from Figure 5.8A and 5.9A, fluorescence intensity in the TRES decreases very sharply for the initial time span of about 3 ns. During this time, however, there is hardly any shift in the spectral position, as clearly indicated from the insets in Figure 5.8A

and 5.9A in the two solvents. These observations are in accordance with the inference that the major contribution in the fluorescence decays in the initial time spans is due to excited dye monomers having very short fluorescence lifetime of ~0.6-0.7 ns. At the latter time span, beyond about 3 ns, there is a significant blue shift in the TRES and TRANES, as evident from Figure 5.8B and 5.9B and the inset of these figures. This observation evidently indicates that the major emitting species at the latter time span have largely blue shifted emission spectra in comparison to that of the monomeric emission. Assuming the longer lifetime components in the present cases are due to dye aggregates as discussed earlier, the blue shift in the TRES and TRANES clearly suggests that the dye C481 undergoes H-type of aggregation in the solution, because the alternative J-type of aggregation would have resulted in a largely red shifted emission than the blue shifted emission observed in the present cases.^{91,92,233-236,255-259} In brief, the observations in the TRES and TRANES of C481 dye in both EtOH and ACN solutions are in good agreement with the proposed aggregation of the dye in these polar organic solvents. Present results indicate that even in the sub-micromolar concentration of the dye there is quite reasonable extent of dye aggregation in the studied polar organic solvents.

Part 5.3.B

Photophysical behavior of C481 dye in aqueous solution

Stimulating results of H-type of dimerization/aggregation of C481 dye in protic EtOH solution were very encouraging to explore the phenomenon further in aqueous medium of the dye, as water is the most versatile protic solvent and always a component in various microheterogeneous media where C481 dye has been used as a probe to investigate various chemical and physicochemical processes.¹⁹⁸ Therefore, systematic studies were carried out on the photophysical properties of C481 dye in aqueous solution to understand the possible aggregation of the dye in this medium.

5.3.B.1. Ground-state absorption and SS fluorescence measurements. Absorption and fluorescence spectra measured for saturated aqueous solution of C481 dye are shown in

Figure 5.10, displaying the absorption peak ($\lambda_{\text{abs}}^{\text{max}}$) at 413 nm and emission peak ($\lambda_{\text{fl}}^{\text{max}}$) at 532 nm. The concentration of the dye in the saturated aqueous solution was estimated following its peak absorbance ($\epsilon_{\text{abs}}^{\text{max}} = 16,500 \text{ dm}^3 \text{ mol}^{-1} \text{ cm}^{-1}$) and is found to be about 5.05 μM . As indicated from Figure 5.10, both absorption and fluorescence spectra are very broad and structureless. It is well known that many organic dyes in aqueous solution undergo self association, leading to the formation of dimers or higher dye aggregates.^{233-248,255-259} To investigate the possibility of such aggregation for C481 dye, measurements were carried out following the concentration dependent changes in the absorption and fluorescence spectra of the dye. It is observed that the shape of both absorption and fluorescence spectra effectively remain unchanged even on sufficient dilution of the aqueous dye solution (*cf.* Figure 5.10).

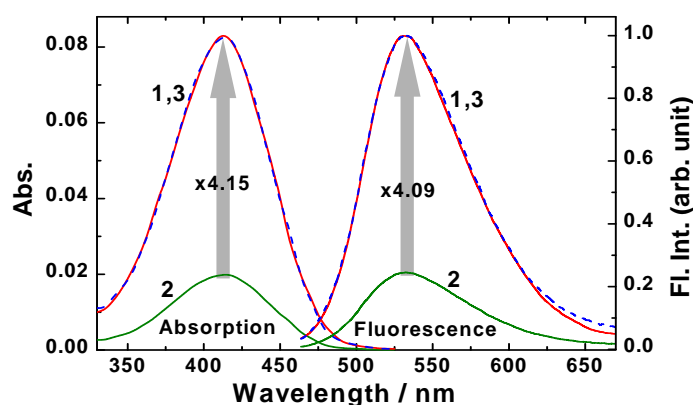


Figure 5.10: Absorption and fluorescence spectra of C481 dye in aqueous solution. Spectra in red (1) and green (2) correspond to the solutions with 5.05 μM and 1.21 μM dye concentrations, respectively. Spectra with dashed blue (3) curve are the normalized spectra for 1.21 μM dye solution, normalized to the peak heights of the respective spectra for 5.05 μM dye concentration in the solution.

To investigate the present system further, the concentration dependent changes in the peak absorbance and the fluorescence intensity were also correlated with the changing C481 dye concentration, as shown in Figure 5.11A and B, respectively. As indicated from Figure 5.11A, for the whole concentration range studied the absorbance effectively changes linearly with the dye concentration. Similarly, as shown in Figure 5.11B, both the normalized (for absorbance at excitation wavelength) fluorescence intensity ($I_{f,N}$) and area under fluorescence spectra ($A_{f,N}$) effectively remain unchanged for the whole dye concentration range studied. These observations apparently do not show any signature for dye aggregation in the solution. Since excitation spectra often provide better information on multiple emissive species,¹⁻⁴ the same were recorded with the saturated solution of the dye for different emission wavelengths as are shown in Figure 5.12. As indicated from this figure, though the differences are not

large, yet the excitation spectrum for the emission at the blue edge is certainly marginally blue shifted in comparison to the other two spectra for emission wavelengths at the peak and at the red edge. Figure 5.12 also shows the emission spectra recorded with different excitation wavelengths. Like excitation spectra, the emission spectra also do not show much of changes for the excitation wavelengths at the absorption peak and red edge. However, the spectrum recorded with blue edge excitation is distinctly blue shifted in comparison to the emission spectra in the other two cases. These results clearly suggest that more than one emitting species are present in the aqueous solution of the dye¹⁻⁴ which we anticipate is due to the formation of small extent of emissive dye aggregates in the solution.^{233-248,255-259}

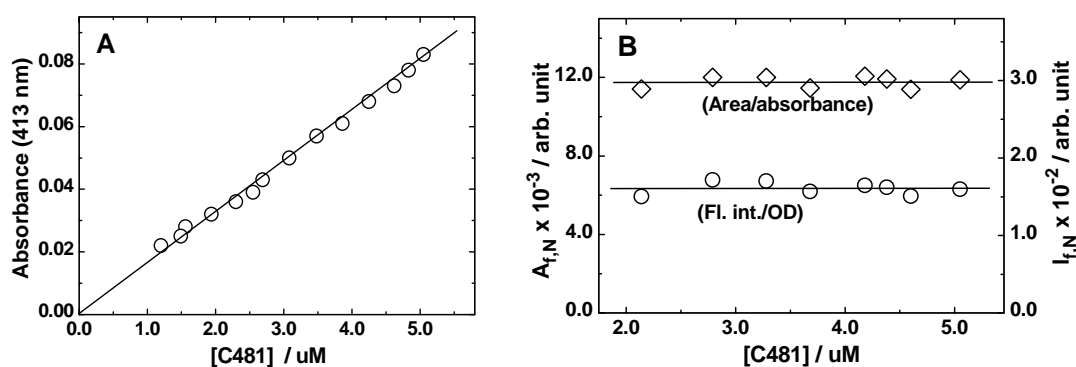


Figure 5.11: Dye concentration dependent changes in the (A) absorbance at 413 nm and (B) normalized fluorescence intensity ($I_{f,N}$) at the emission peak and the integrated area ($A_{f,N}$) under the fluorescence spectra for C481 dye in aqueous solution.

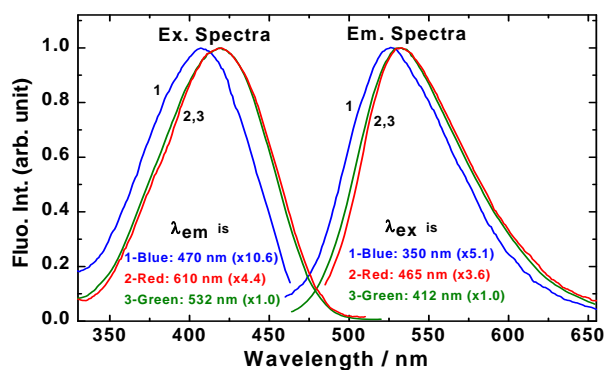


Figure 5.12: Excitation and emission spectra of C481 dye (5.05 μM) in aqueous solution recorded with measuring wavelengths at the blue edge (blue: 1), red edge (red: 2) and at the peak position (green: 3) of the emission and absorption spectra, respectively.

5.3.B.2. TR fluorescence measurements. As TR fluorescence measurements are more sensitive than the SS measurements,^{1-4,118,119} the fluorescence decays for C481 dye in aqueous solution were systematically measured as a function of both emission wavelengths and dye concentrations. In all the cases the decays are found to be non-single exponential in nature.

Moreover, at all the monitoring wavelengths the decays are seen to change appreciably with the changing dye concentration, the effect being more substantial at the shorter emission wavelengths. Typical dye concentration dependent fluorescence decays measured at 460 nm, a wavelength far into the blue edge of the emission spectrum, are shown in Figure 5.13. At least three-exponential function was required to fit the decay and the estimated decay parameters thus obtained as a function of dye concentration are listed in Table 5.2.

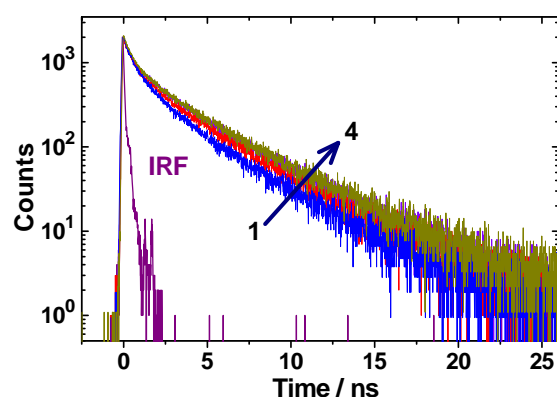


Figure 5.13: Concentration dependent fluorescence decays of C481 dye at 460 nm. [C481] = 5.05 (1: Blue), 2.53 (2: Red), 0.63 (3: Magenta) and 0.32 μM (4: Dark yellow), respectively. $\lambda_{\text{ex}} = 374$ nm.

Table 5.2: Fluorescence decay parameters for C481 dye in aqueous solution as a function of the dye concentration used. The decays were measured at 460 nm with λ_{ex} as 374 nm.

[C481] / μM .	a_1 %	τ_1 / ns [§]	a_2 %	τ_2 / ns	a_3 %	τ_3 / ns	χ^2
5.05	15.1	0.20	24.6	1.12	60.3	3.70	1.09
2.53	12.1	0.20	22.6	1.17	65.3	3.81	1.08
1.26	10.8	0.20	22.0	1.26	67.2	3.94	1.16
0.63	11.0	0.20	21.8	1.35	67.2	4.03	1.09
0.32	11.6	0.20	19.4	1.36	69.0	4.10	1.18

[§]The τ_1 component was always close to 0.2 ns. Thus, this component was fixed to obtain consistent results for all the estimated decay parameters.

As indicated from Table 5.2, there is a clear increase in the contribution of the longer lifetime component (τ_3) with concomitant decrease in the contributions of both the shortest (τ_1) and the intermediate (τ_2) lifetime components as the dye concentration is decreased in the solution. Moreover, there is also a clear increase in the τ_2 and τ_3 values with the decreasing dye concentration, though the τ_1 value apparently remains constant. Beyond a certain reduction in the dye concentration (about 0.63 μM or less), however, the observed decays

effectively show no further change and accordingly the decay parameters attend a kind of respective limiting values (*cf.* Table 5.2). To be mentioned here that the observations made at the other emission wavelengths are qualitatively very similar to those observed at 460 nm, except that on moving to longer wavelengths the contributions of the τ_2 and τ_3 components gradually decrease and beyond about 500 nm, the contribution of the τ_2 component is reduced so largely that the decays effectively become bi-exponential in nature, showing only τ_1 and τ_3 components. These TR fluorescence results clearly suggest that there are at least three emitting species present for C481 dye in the aqueous solution. We propose that in the present case the dye monomer, dimer and higher dye aggregates jointly contribute in the observed decays and their contributions change appreciably on changing the dye concentration as well as the monitoring emission wavelength. As indicated from Figure 5.13 and Table 5.2, the emitting species apparently attend a kind of quasi-equilibrium in the solution at very low dye concentration ($\sim 0.63 \mu\text{M}$ or less). At these situations, it is likely that very large aggregates would be hardly present in the solution. Since three emitting species still contribute at this extremely low dye concentration, it is proposed that these species could possibly be the dye monomers, dimers and trimers present in the solution. As the fluorescence intensity becomes extremely weak at a dye concentration much lower than $\sim 0.32 \mu\text{M}$, no meaningful TR measurements could be made with such extremely low dye concentrations.

As discussed in Section 5.3.A.2, the monomeric C481 undergoes an unusually fast ICT to TICT conversion in high polarity solvent causing its Φ_f and τ_f values to be reduced drastically.^{82,210} Thus, in EtOH and ACN solvents the τ_f values of monomeric C481 dye are as short as about 0.64 ns and 0.67 ns, respectively, while in lower polarity organic solvents, where ICT to TICT conversion is absent, the τ_f values are reported to be quite long, in the range of 4.0-4.5 ns.^{82,210} As the ICT to TICT conversion is expected to be much more pronounced in highly polar water solvent than in EtOH and ACN, the shortest τ_1 component of ~ 0.2 ns is justifiably assigned to C481 monomer in aqueous solution. Considering that the TICT formation will be sterically restricted in the dye aggregates and also the nonradiative relaxation of the aggregates will increase with an increase in the aggregate size (*cf.* Section 5.3.A.2),^{1-4,91,92,242,243} we propose that at extremely low dye concentration in aqueous solution the longest τ_3 component of ~ 4.1 ns is mainly due to dye dimers and the intermediate τ_2 component of ~ 1.4 ns is mainly due to dye trimers present in the solution. That the τ_2 and τ_3 values are always somewhat shorter than ~ 1.4 ns and ~ 4.1 ns, respectively, at higher dye concentrations (*cf.* Table 5.2) suggest that in these cases there are also contributions from

other higher dye aggregates than only dimer and trimer. Though in these cases, a four-exponential analysis was also attempted, the estimated parameters did not show any meaningful correlation. Thus, in the present study, we eventually relied upon the tri-exponential analysis of the decays to correlate the observed results.

As already mentioned, the fluorescence decays measured at shorter wavelengths show much higher contributions for the dye aggregates (τ_2 and τ_3 components) than at the longer wavelengths. This observation suggests that like in EtOH and ACN solutions, as discussed in part 5.3.A, the dye C481 also forms H-type of emissive aggregates in aqueous medium. The fact that the decays measured above 500 nm are effectively bi-exponential in nature with major contribution arising from the dye monomer ($\tau_1 \sim 0.2$ ns) and only minor contribution arising from the dye dimer ($\tau_3 \sim 4.1$) is also in accordance with the H-type of aggregation of the dye, because the emission from higher dye aggregates hardly contributes beyond 500 nm. Important point to be noted here is that the emission contributions of the dye aggregates appearing as the extended tails in the fluorescence decays gradually increase with a decrease in the dye concentration. This observation apparently seems unusual, because aggregation is expected to be less favored on decreasing the dye concentration in the solution. The reason behind the present observation is that a decrease in the dye concentration actually leads to an increase in the proportion of the dye dimers relative to higher dye aggregates, which eventually causes an apparent increase in the decay tail. This happens because the lifetime of the aggregates expectedly reduces on increasing the aggregate size due to the increased density of the excitonic states which facilitate the non-radiative deexcitation channels for the excited dye aggregates as discussed in Section 5.3.A.2.^{1-4,91,92,242,243}

5.3.B.3. Construction and analysis of TRES and TRANES for C481 dye. To understand the spectral features of different emitting species, TRES and TRANES were constructed for C481 dye in aqueous solution following the procedure given in Section 1.5. Typical wavelength-dependent decays measured in the present study are shown in Figure 5.14. The dye concentration of 0.51 μM was used where quasi-equilibrium among different emitting species is apparently attended (*cf.* Table 5.2).

Figures 5.15A and B show the TRES and TRANES for C481 dye in aqueous solution. As the TRES indicate, fluorescence intensity decreases (*cf.* Figure 5.15A, inset) very sharply (by $\sim 90\%$) in the initial ~ 1 ns time span but the decrease is quite slow at longer times, beyond ~ 1 ns. This observation clearly suggests that monomer emission of the dye ($\tau_1 \sim 0.2$ ns)

actually dominate in the system and accordingly justifies why SS results could not show the signature of the weakly emitting dye aggregates in the solution (*cf.* Section 5.3.B.1).

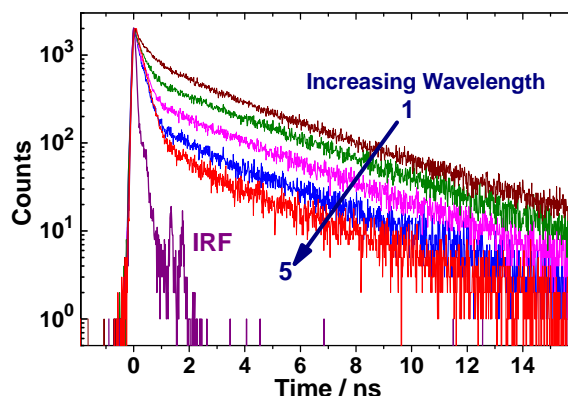


Figure 5.14: Wavelengths dependent decays of C481 dye (0.51 μM) in aqueous solution. Decays 1-5 correspond to 460, 480, 500, 530 and 660 nm, respectively. $\lambda_{\text{ex}} = 374$ nm.

In the TRES, there is also a large time-dependent blue shift, which becomes very obvious from the TRANES and the plot of the $\bar{\nu}_{\text{max}}$ with time (*cf.* Figure 5.15B and its inset). As it is indicated, the blue shift is just nominal during the initial ~ 0.5 ns, becomes very large during the intermediate time span of ~ 0.5 to 2 ns and again becomes quite less at longer times. These results are rationalized considering dominance of emission from monomer ($\tau_1 \sim 0.2$ ns) in the initial time span, from trimer/higher aggregates ($\tau_2 \sim 1.4$ ns) in the intermediate time span and from the dimer ($\tau_3 \sim 4.1$ ns) at the longer time span.

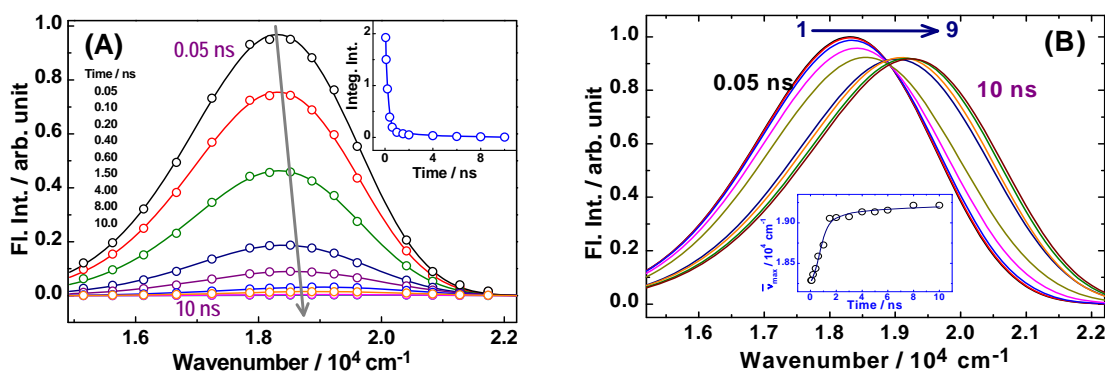


Figure 5.15: (A) TRES and (B) TRANES for C481 dye in aqueous solution (0.51 μM). Circles are experimental data and continuous curves are the log-normal fits. Inset of Panel A shows the time dependent changes in the integrated intensity and inset of Panel B shows time dependent changes of emission maxima in the TRES/TRANES.

For TRES/TRANES the spectral shift is often attributed to solvent relaxation dynamics.^{52,157,158} In the present case, however, spectral shift in TRES/TRANES cannot be

due to solvent relaxation because in that case the shift should have been towards red than blue. Further, solvent relaxation in water occurs within sub-picosecond time scale,^{52,157,158} which is orders of magnitude faster than the time scale observed in the present study. Therefore, the blue shift in the TRES/TRANES for C481 dye in aqueous solution is attributed to the H-type of aggregation of the dye in this solvent.

As indicated from TRANES in Figure 5.15B, there is a clear isoemissive point in for the initial time span upto ~ 0.5 ns, suggesting the simultaneous presence of at least two emitting species in the solution.^{253,254} For the present three component system as $\tau_1 \ll \tau_3$, at the initial times, the contribution of τ_3 will be quite negligible and hence the system will behave effectively as a two component system, τ_1 and τ_2 .^{253,254} During intermediate times, as all the τ_1 , τ_2 and τ_3 components give reasonable contributions, the isoemissive point becomes obscured. At longer times, since τ_1 contribution will be negligible, a new isoemissive point considering τ_2 and τ_3 was expected.^{253,254} However, this second isoemissive point is not observed in the TRANES possibly due to the overlapping contributions from number of aggregates than only dimers and trimers. It is, however, necessary to mention in the present context that even though appearance of an isoemissive point in the TRANES assures the presence of two emitting species, the absence of such isoemissive point can neither nulify nor support the presence of multiple emitting species in the system.^{253,254}

5.3.B.4. Temperature dependent TR fluorescence study. To understand the behavior of C481 dye in aqueous solution further, temperature-dependent fluorescence decays were measured at 460 nm. Figure 5.16 shows these decays and Table 5.3 lists their tri-exponential analysis results. As indicated, with increasing temperature the monomer contribution (τ_1) gradually increases, suggesting the expected dissociation of dye aggregates at elevated temperatures. The τ_1 component also becomes faster at higher temperatures due to enhanced ICT to TICT conversion.^{82,210} Small reduction in the τ_2 and τ_3 values with temperature suggests that the dimer/trimer emissions are also moderately temperature dependent. Present results are qualitatively in support of the dye aggregation in the solution. To understand if the monomers and aggregates maintain any equilibrium in the solution, fluorescence decays were measured at 25 °C before and after the heating and cooling cycle. Interestingly, the decays thus measured match quite well (*cf.* Figure 5.16 Inset) suggesting that the monomers and aggregates apparently maintain a kind of quasi-equilibrium in the solution.

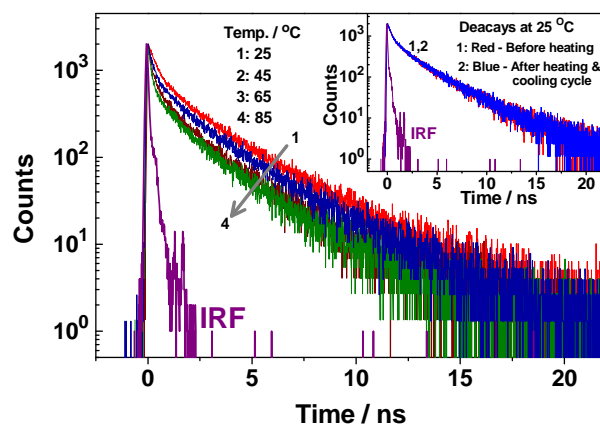


Figure 5.16: Temperature-dependent decays of C481 dye in aqueous solution. **Inset:** Decays at 25 °C; before (red) and after (blue) the heating and cooling cycle. $\lambda_{\text{ex}} = 374$ nm and $\lambda_{\text{em}} = 460$ nm.

Table 5.3: List of the fluorescence decay parameters for C481 dye in saturated aqueous solution as a function temperature monitored at 460 nm.

Temp / °C	a ₁ %	τ_1 / ns ^S	a ₂ %	τ_2 / ns	a ₃ %	τ_3 / ns	χ^2
25	15.8	0.21	25.6	1.38	58.6	3.86	1.01
45	20.1	0.17	26.1	1.32	53.8	3.53	1.18
65	24.9	0.13	25.8	1.23	49.3	3.24	1.19
75	26.2	0.11	25.7	1.24	48.1	3.12	1.20

5.3.B.5. Fluorescence up-conversion measurements. The fluorescence kinetic traces for C481 dye in saturated aqueous solution were recorded using femtosecond fluorescence up-conversion measurements, to get some insight of the system at the ultrafast time scales. In this study, since the dye concentration was significantly low even in the saturated solution (~5.05 μM), the up-converted signal intensities were exceptionally low and hence extensive measurements were not possible. Hence, in the present study, we carried out only selective measurements, collecting the kinetic traces at two chosen wavelengths, one at the emission peak (532 nm) and the other at a reasonably blue shifted wavelength (512 nm, about 20 nm blue shifted from the peak), as are shown in Figures 5.17.

As indicated from Figure 5.17, there is a much faster ultrafast decay component at the blue shifted wavelength than at the emission peak. These are expected due to ultrafast (sub-picosecond) solvent relaxation dynamics in water.^{52,157,158} To understand if the observed kinetic traces in the up-conversion measurements also carry some information regarding the aggregation of the dye, we also carried out similar measurements for the dye in 50:50 (v/v) water-ACN solvent mixture, one at emission peak (520 nm) and the other at similarly blue

shifted wavelength (500 nm), as used in aqueous solution. The kinetic traces thus measured in water-ACN solvent mixture are also shown in Figure 5.17, for a direct comparison.

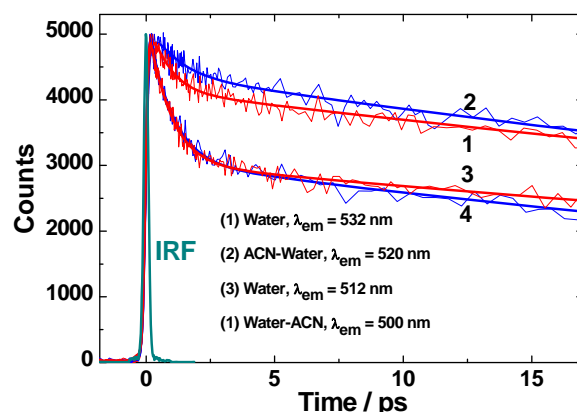


Figure 5.17: Kinetic traces for C481 dye (5.05 μM) in water and in 50:50 (v/v) water-ACN solvent mixture, recorded using fluorescence up-conversion measurements. The traces 1 and 3 are in water at 532 nm (peak) and 512 nm (blue edge), respectively. Similarly, the traces 2 and 4 are in water-ACN mixture at 520 nm (peak) and 500 nm (blue edge), respectively.

In both water and water-ACN solvent mixture the kinetic traces could be fitted with a tri-exponential function and the decay and/or growth parameters thus estimated are listed in Table 5.4. The role of solvent relaxation dynamics in the observed kinetic traces in both the solvent systems is clearly indicated by the presence of the first initial decay at the blue wavelength and fast growth component (negative amplitude for τ_1) in the traces at the emission maxima. Interesting to note from Figure 5.17 and Table 5.4 that the initial parts of the kinetic traces (τ_1 and τ_2 components) at both the emission wavelengths studied are comparatively slower in water-ACN mixture than in water solution. This is certainly due to relatively slower solvent relaxation dynamics in water-ACN mixture than in water.^{52,157,158,260} Most interestingly, however, it is indicated from Figure 5.17 and Table 5.4 that the slower τ_3 component is distinctly longer in water than in water-ACN solvent mixture, which seems to be an apparently unusual finding considering the faster solvent relaxation dynamics^{52,157,158,260} lower fluorescence yield and shorter lifetime^{82,210} of the monomeric dye in water than in ACN. Observed behavior can, however, be expected if there are some dye aggregates present in solution in addition to the dye monomers. It is expected that dye aggregation will be very pronounced in aqueous solution (due to low dye solubility) but not in water-ACN solvent mixture. Accordingly, the ultrafast fluorescence kinetic traces measured in water are expected to be modulated more by the dye aggregates than in water-ACN mixture. We thus feel that the relatively longer τ_3 components in aqueous solution are related to the higher dye

aggregation in this solution. It is also possible that in water there are some larger dye aggregates than dimers and trimers which actually contribute to make the τ_3 component relatively longer in water than in water-ACN solvent mixture. Another possible cause for this longer τ_3 component in water could be that the emission spectra of the different aggregated species are not similarly blue shifted both in water and in water-ACN solvent mixture, and accordingly equivalent kinetic traces might not be obtained by selecting blue wavelengths shifted similarly from the peak positions in the two solvent systems. Since in the present study the up-conversion measurements could not be carried out very extensively recording decays at large number of monitoring wavelengths, no further details of the aggregation behavior could be extracted from the present study. Observed up-conversion results, however, qualitatively indicate that for C481 dye in water (as well as in water-ACN solvent mixture) the ultrafast fluorescence kinetics are not simply due to solvent relaxation dynamics but are also modulated significantly by the presence of the dye aggregates in the solution.

Table 5.4: Ultrafast fluorescence decay components for C481 dye in water and water-acetonitrile solvent mixtures as obtained from fluorescence up-conversion measurements.

Solvent	λ_{em} / nm	B_1	τ_1 / ps	B_2	τ_2 / ps	B_3	τ_3 / ns
Water	512	4.02	0.135	30.99	0.847	38.36	80.6
Water	532	-21.63	0.093	18.01	0.735	53.49	87.5
Water-ACN	500	4.56	0.181	30.30	0.91	39.30	59.3
Water-ACN	520	-15.28	0.120	11.47	1.05	55.89	76.1

5.3.B.6. Dynamic light scattering measurements. To characterize if the dye aggregates in the present cases are formed with appreciable sizes, dynamic light scattering (DLS) measurements were carried out with saturated dye solution in water at ambient temperature. In the present measurements, however, the scattered light intensity was found to be extremely low and quite similar to that of the reference bulk water. This is understandable because the dye concentration in the experimental solution is exceedingly low (5.05 μM) and accordingly there is only a small extent of dye aggregation, which is not sufficient to give enough light scattering to distinguish it from reference bulk water. As expected, no reasonable time autocorrelation function could also be constructed for the present system that can be analyzed for particle size estimation. Considering the dimers and trimers are the major aggregates in the solution (*cf.* Section 5.3.B.2) and that the dimension of C481 molecule is about 10 Å,⁸²

the aggregate sizes in the present cases are expected to be about 10-20 nm and thus were not detectable in the DLS measurements. For larger aggregates, greater than dimers/trimers, as the number of the species would be too less, they cannot contribute significantly in the DLS signals. In any case, from DLS measurements it is suggested that the aggregation of C481 dye in aqueous solution certainly lead to the formation of smaller aggregates, mostly dimers and trimers, as also inferred earlier from the TR fluorescence studies.

5.3.B.7. Measurements with supersaturated aqueous solution of C481 dye. Since in the normal procedure given in Section 5.2, it was not possible to dissolve more than $\sim 5.05 \mu\text{M}$ C481 in aqueous solution, in the present context a kind of supersaturated solution of the dye in water was made following an indirect procedure. Thus, a highly concentrated solution of C481 in ACN was first prepared and this solution was then added drop by drop to 10 ml water kept under sonication. With this procedure a supersaturated transparent solution of C481 could be made in water where the dye concentration ($\sim 31.5 \mu\text{M}$) is much higher than that in the saturated solution prepared through normal procedure (*cf.* Section 5.2). To be mentioned here that an excessive addition of the concentrated ACN solution of the dye in water ultimately leads to the turbidity of the solution which we intentionally avoided in the present study. The absorption and fluorescence spectra recorded for the supersaturated transparent solution of the dye in water are shown in Figure 5.18 along with those of the saturated dye solution, after their peak normalization, for a comparison.

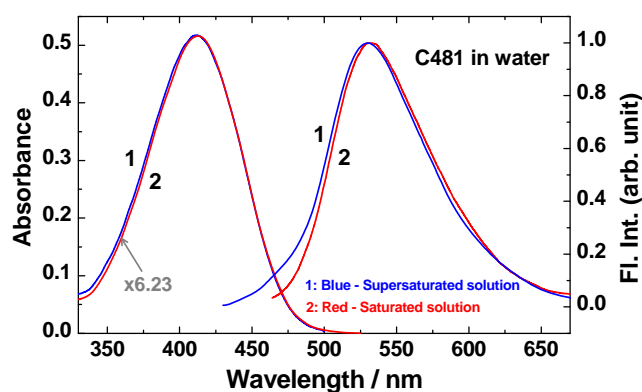


Figure 5.18: The absorption and fluorescence spectra for the supersaturated transparent solution of C481 dye in water (1: blue). The peak normalized spectra for the saturated dye solution prepared following normal procedure (2: red; *cf.* Section 5.2) are also shown for a comparison.

As indicated from Figure 5.18, the absorption and fluorescence spectra for the supersaturated solution are not only slightly blue shifted but also have relatively higher absorbance/fluorescence intensity at the blue edge of the spectra in comparison to the spectra

obtained with normal saturated dye solution. Since a higher degree of aggregation is expected in supersaturated solution than in normal saturated solution of the dye, present observations are certainly in accordance with the H-type of aggregation of the dye in aqueous solution, as discussed in the earlier sections.

Part 5.3.C

Photophysical behavior of C153 dye in polar organic solvents

In part 5.3.A and 5.3.B, it is observed that C481 dye undergoes H-type of aggregation in polar organic solvents as well as in aqueous solution. Knowing this intriguing behavior of C481 dye that has a flexible 7-N,N-diethyl group the study was logically extended for C153 dye that has rigid julolidinyl rings (*cf.* chart 1) as a part of its 7-aminogroup. To be mentioned that while weakly fluorescent H-aggregates of the C481 dye was quite easily observed in the solution due to the low Φ_f and τ_f values of the dye caused by the ICT to TICT conversion process, it was a challenge if similar very weakly fluorescent aggregates can also be detected in the presence of very high Φ_f and τ_f values of C153 dye. With this inquisitiveness, systematic measurements were carried out with C153 dye in polar aprotic (ACN) and polar protic (EtOH) solvents as discussed in this section.

5.3.C.1. Ground-state absorption and SS fluorescence measurements. For C153 dye, the absorption and emission maxima appear at 418 nm and 515 nm, respectively, in ACN and at 424 nm and 525 nm, respectively, in EtOH solution. Concentration dependent studies on the absorption and SS fluorescence spectra of C153 dye in both ACN and EtOH solution do not indicate any unusual behavior of the dye in the solutions, possibly due to less sensitive nature of these measurement techniques.

Excitation spectra were also recorded for the dye, keeping monitoring wavelengths both at blue and red edge of the emission spectra. In ACN solution, the excitation spectra with different monitoring wavelengths do not show any observable differences. In EtOH solution, however, the excitation spectra are found to be significantly blue shifted when monitoring wavelengths are at the blue edge of the emission spectrum, but there is no

appreciable change in the excitation spectra with monitoring wavelengths at the emission peak or at the red edge of the spectrum, as are shown in Figure 5.19B. These results are quite indicative of the presence of more than one emitting species in the system,^{1-4,118,119} which we attribute to small extent of dye aggregation in EtOH solution.

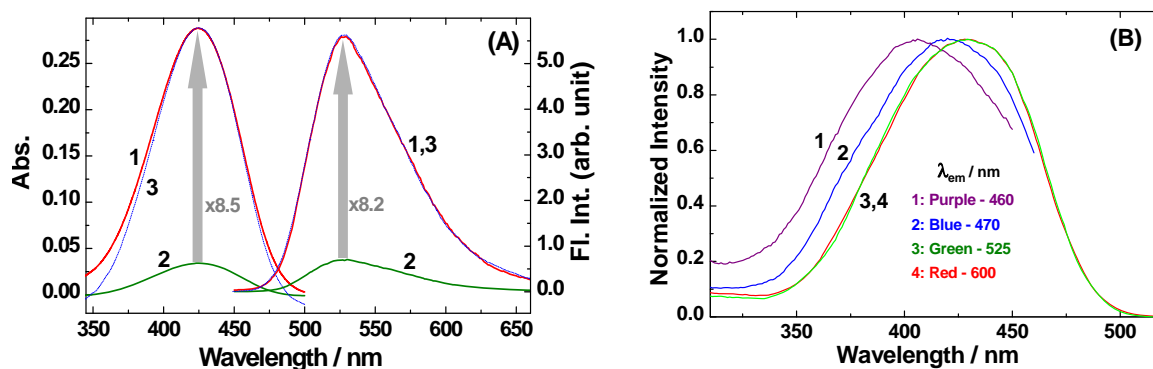


Figure 5.19: (A) SS fluorescence spectra of C153 dye in EtOH solution. Spectra in red (1) and green (2) correspond to 15.2 μM and 1.8 μM dye concentrations, respectively. Spectrum in blue (3) is the normalized spectrum for 1.8 μM dye solution to the peak height of the spectrum for 15.2 μM dye solution. (B) Peak normalized excitation spectra of C153 dye in EtOH. $[\text{C153}] = 31.8 \mu\text{M}$.

5.3.C.2. TR fluorescence measurements. Fluorescence decays of C153 dye in ACN and EtOH solutions were measured at different emission wavelengths, covering the whole SS emission spectra of the dye, as are shown in Figure 5.20A and B respectively. The fluorescence decays in ACN are always single exponential with a long lifetime of ~ 5.6 ns and is independent of monitoring wavelength. On the contrary, fluorescence decays in EtOH solution are non-single exponential at the blue edge of the spectrum, though the decays are effectively single exponential at the longer wavelengths, beyond about 500 nm. While a long lifetime component of ~ 4.8 ns always dominates in EtOH solution throughout the emission wavelengths, additional shorter lifetime components are also evident at the blue edge of the spectrum, albeit with relatively lower contributions. Present observation evidently suggests that there are more than one emitting species present for C153 dye in EtOH solution.

Fluorescence decays of the dye were also measured at different emission wavelengths as a function of the dye concentration used. In ACN solution, the decays show no obvious changes with dye concentration at any of the monitoring wavelengths. Typical of these decays at 460 nm with varying dye concentrations are shown in Figure 5.21. These results suggest that in ACN solution the dye behaves very normally almost exclusively existing as the monomeric dye and with no obvious dye aggregates. In EtOH solution, however, the decays at the blue edge of the spectrum are found to change very significantly with dye

concentration (*cf.* Figure 5.21 B), though the decays measured at the longer wavelengths (above about 500 nm) are effectively independent of the dye concentration (*cf.* inset of Figure 5.21 B) with a lifetime of ~ 4.8 ns. At the blue edge of the spectrum, there is an obvious, unusually short lifetime component whose contribution decreases in the decays on decreasing the dye concentration. These decays required tri-exponential analysis in general and the decay parameters thus estimated at 460 nm are listed in Table 5.5. These results clearly suggest that there are at least three emitting species present for C153 dye in EtOH solution.

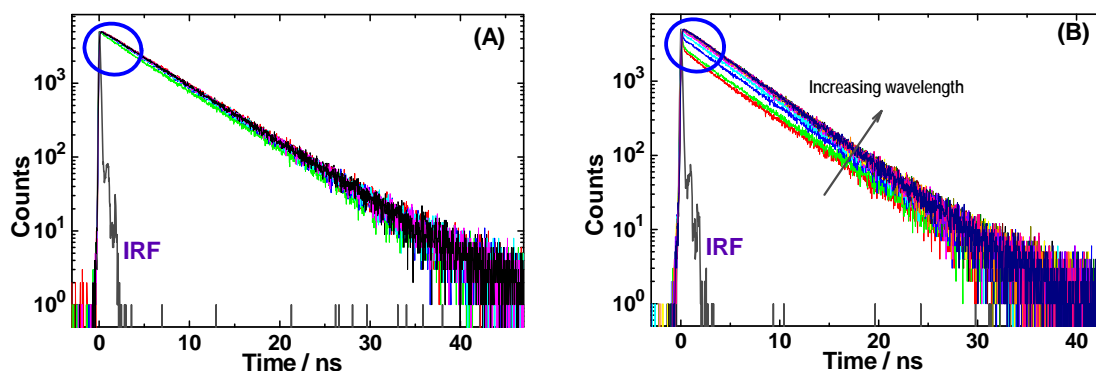


Figure 5.20: Emission wavelength dependent decays of C153 dye ($\sim 2.7 \mu\text{M}$) in (A) ACN and (B) EtOH solutions. $\lambda_{\text{ex}} = 374$ nm.

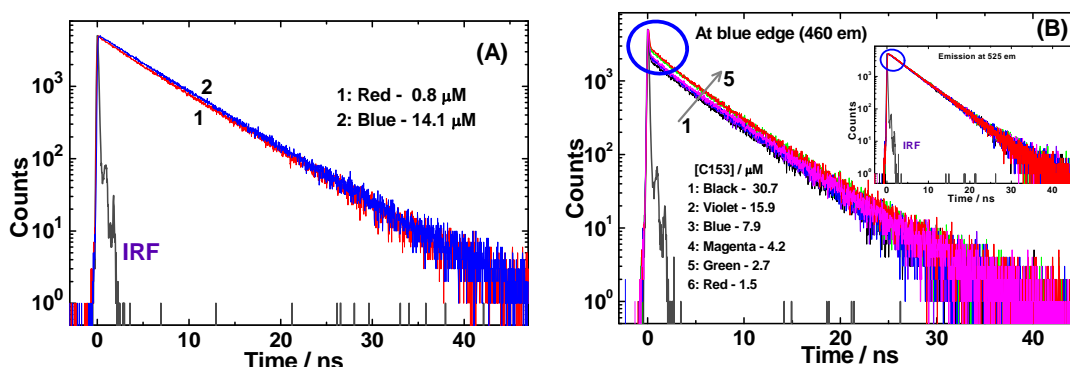


Figure 5.21: Dye concentration dependent decays measured at 460 nm (blue edge) in (A) ACN and (B) EtOH solutions. $\lambda_{\text{ex}} = 374$ nm. **Panel B Inset:** Decays measured at emission peak of the dye in EtOH solution.

As indicated from Table 5.5, with decreasing dye concentration, there is a clear decrease in the contribution of the shortest lifetime component (τ_1) with the concomitant increase in the contribution of the intermediate (τ_2) lifetime component in EtOH solution. The contribution of the longest (τ_3) lifetime component, however, remains more or less unchanged. Qualitatively, very similar results were obtained at the other wavelengths in the blue edge of the spectrum except that the contributions of both τ_1 and τ_2 gradually decrease

on increasing the monitoring wavelength, causing the decays to eventually become single-exponential beyond 500 nm.

Table 5.5: Fluorescence decay parameters for C153 dye in EtOH solution as a function of the dye concentration. The decays were measured at 460 nm with 374 nm excitation.

[C153] / μM .	a_1 %	τ_1 / ns ^s	a_2 %	τ_2 / ns	a_3 %	τ_3 / ns	χ^2
30.7	12.4	0.04	4.4	1.57	83.2	4.75	1.02
15.9	11.5	0.04	5.5	1.64	83.0	4.81	1.10
7.9	10.5	0.04	5.5	1.30	84.0	4.81	1.03
4.2	10.1	0.04	6.4	1.38	83.5	4.87	1.05
2.7	8.8	0.04	6.2	1.49	85.4	4.82	1.08
1.5	7.7	0.04	7.2	1.35	85.1	4.79	1.10

^sThe τ_1 component was always close to 0.04 ns. Thus, this component was fixed to obtain consistent results for all the estimated decay parameters.

Present results of C153 dye in EtOH solution can suitably be rationalized considering a small extent of aggregation of the dye. It is suggested that dye monomers along with dye aggregates jointly contribute in the observed decays in EtOH solution and the contributions of different component change quite significantly on changing the dye concentration as well as the monitoring emission wavelength. That the absorption and SS fluorescence results presented in the previous section could not reveal this aggregation is certainly due to the less sensitive nature of these SS measurements.^{118,119,233-235} The degree of aggregation being small and the fluorescence yields being low and lifetimes being shorter for the dye aggregates than the dye monomers (*cf.* Table 5.6) it is understood that the detection of these aggregates by the less sensitive absorption and SS fluorescence measurements were not possible.

In the literature, photophysical properties of different coumarin dyes, are reported mainly based on measurements at their emission and absorption maxima.^{194-208,231} Based on these reports, the longest lifetime component ($\tau_3 = 4.8$ ns) should correspond to the monomeric dye in EtOH solution.^{208,231} The two shorter lifetime components (τ_1 and τ_2) observed in EtOH solution are accordingly ascribed to dye aggregates. That the contributions of τ_1 and τ_2 components are progressively higher at the shorter wavelengths, suggest that the C153 dye also form H-type of aggregates in the solution (*cf.* Kasha's theory; Section 1.8).^{1-4,91,92} Considering that the non-radiative de-excitation in larger aggregates will be faster than the smaller aggregates,^{1-4,91,92,242,243} the shortest component ($\tau_1 \sim 0.04$ ns) is assigned to

relatively larger H-aggregates and the intermediate component ($\tau_2 \sim 1.4$ ns) to relatively smaller H-aggregates. Interestingly, contributions of both of these aggregates remain quite appreciable even when the dye concentration is exceedingly low, only about 1.5 μM (*cf.* Table 5.5), suggesting that in polar protic EtOH solution one cannot get a purely monomeric dye solution even at a very low C153 concentration, though in polar aprotic solvent ACN the dye aggregation is apparently absent (*cf.* Figure 5.20 and 5.21). An important point to be mentioned here is that the dye C153 apparently shows quite high solubility both in ACN (~ 76 mM) and EtOH (~ 30 mM) solvents. Considering such high solubility, its aggregation in EtOH seems quite unusual. It is thus inferred that over and above the solvent polarity, an additional effect, possibly arises due to dye-solvent hydrogen bonding interaction in EtOH solvent, that provides an extra stability and hence facilitates H-type of aggregation of the highly dipolar C153 dye (dipole moment, $\mu \sim 6.4$ D),¹⁹⁶ similar to that of C481 dye as shown in Scheme 5.1 and discussed in Section 5.3.A.2.

5.3.C.3. TRES and TRANES analysis for C153 dye. TRES and TRANES for C153 dye in EtOH solution were constructed following the procedure discussed in Section 1.5 and are shown in Figure 5.22A and B, respectively.^{52,157,158} As indicated from the TRES, fluorescence intensity decreases very sharply at the initial times but the decrease is quite slow at the longer times (*cf.* inset of Figure 5.22A). The initial sharp decrease corroborates well with the very short τ_1 value of ~ 0.04 ns for larger dye aggregates. The significantly slow decrease at longer times also agrees well with the long τ_3 value of ~ 4.8 ns for dye monomers. In the intermediate times, the rate of decrease is intermediary, as expected, considering the intermediate τ_2 value of ~ 1.4 ns for smaller dye aggregates. In fact, the data in the inset of Figure 5.22A could be fitted well with a tri-exponential function giving decay parameters as 0.04 ns (0.44 %), 1.40 ns (3.80 %) and 4.80 ns (95.76 %) with R^2 value of 0.999, which are quite consistent with the τ_1 , τ_2 and τ_3 values estimated from the fluorescence decay analysis (*cf.* Table 5.5). Therefore, the results from TRES analysis strongly support the co-existence of dye monomers along with small extent of aggregates for C153 dye in EtOH solution.

An interesting observation from the TRANES in Figure 5.22B is that there is a clear iso-emissive point during the initial time span of 0.005 to 0.1 ns (*cf.* left inset of Figure 5.22B), indicating the simultaneous presence of at least two emitting species in the solution.^{253,254} As discussed earlier in Section 5.3.B.3, for C153 dye in EtOH solution also the condition $\tau_1 \ll \tau_3$ prevails and hence observation of iso-emissive point is quite expected at

the initial time span. For the intermediate to longer times, since monomer emission effectively dominates, no iso-emissive point is evident during these times.

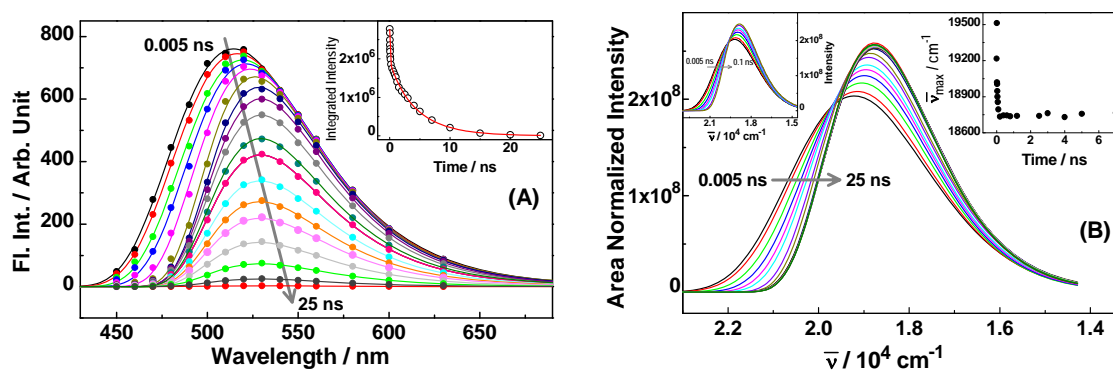


Figure 5.22: (A) TRES and (B) TRANES for C153 dye (2.7 μM) in EtOH solution. Inset of Panel A shows the decrease in the integrated intensity with time. Left inset of Panel (B) shows isoemissive point in the time span of 0.005 to 0.1 ns and right inset shows $\bar{\nu}_{\text{max}}$ versus time plot.

From the TRES and TRANES, one more interesting point to note that there is a large time-dependent red shift for $\bar{\nu}_{\text{max}}$. As clearly indicated from the right inset of Figure 5.22B, the shift in $\bar{\nu}_{\text{max}}$ is very large at the initial times (upto about 0.2 ns) and quite nominal at longer times. The large shift in $\bar{\nu}_{\text{max}}$ at the initial times is due to large decrease in the contributions of the larger H-aggregates ($\tau_1 \sim 0.04$ ns). During the intermediate times, though further red shift was expected due to decay of smaller H-aggregates ($\tau_2 \sim 1.4$ ns), this could not be realized distinctively because the lifetime of the smaller aggregates ($\tau_2 \sim 1.4$ ns) is not that drastically different from that of the dye monomers ($\tau_3 \sim 4.8$ ns) and also the contribution of these smaller aggregates is relatively very less compared to the very strong emission of the dye monomers. Therefore, beyond about 0.2 ns, TRES/TRANES do not undergo any appreciable shift as the monomer emission largely dominates throughout intermediate to longer times.

5.3.C.4. Temperature effect on TR fluorescence of C153 in EtOH solution. To understand the behavior of C153 dye in EtOH solution further, temperature dependent fluorescence decays were measured at the emission maximum (525 nm) and at a blue shifted emission wavelength (460 nm) as are shown in Figure 5.23A and B, respectively. There is no observable temperature dependent change in the decays at the emission peak (*cf.* Figure 5.23A), at least for the studied temperature range of 25 - 65 $^{\circ}\text{C}$. However, substantial temperature dependent changes are observed for the decays at the blue shifted wavelength

(*cf.* Figure 5.23B). These decays fit with a tri-exponential function and decay parameters are listed in Table 5.6. As expected, with increasing temperature, the monomer contribution (τ_3) increases with a concomitant decrease in the aggregate contributions (τ_1 and τ_2), suggesting disintegration of the dye aggregates at elevated temperatures. Further, on increasing temperature, the contribution of the larger aggregates (τ_1) decreases more than that of the smaller aggregates (τ_2), as expected. Therefore, present results are qualitatively in support of the aggregation of C153 dye in EtOH solution. To understand if the dye monomers and aggregates maintain any equilibrium in the solution, the decays at 460 nm were measured at 25 °C before and after the heating and cooling cycle and interestingly, these decays match each other quite nicely (*cf.* Figure 5.27B Inset) suggesting that the dye monomers and aggregates apparently maintain a kind of quasi-equilibrium in the solution.

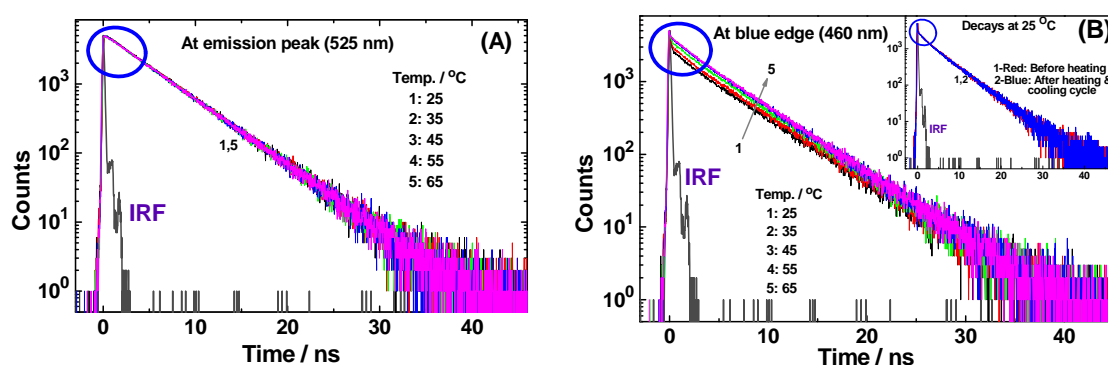


Figure 5.23: Temperature-dependent fluorescence decays of C153 dye (15.3 μM) in EtOH solution at (A) emission peak and (B) blue shifted wavelength. Panel B inset shows fluorescence decays at 25 °C, recorded before (1:red) and after (2:blue) the heating and cooling cycle. $\lambda_{\text{ex}} = 374 \text{ nm}$.

Table 5.6: Fluorescence decay parameters for C153 dye (15.3 μM) in EtOH solution as a function of temperature. The decays were measured at 460 nm with 374 nm excitation light.

Temperature / °C	a_1 %	τ_1 / ns ^s	a_2 %	τ_2 / ns	a_3 %	τ_3 / ns	χ^2
25	8.27	0.04	6.57	1.31	85.16	4.94	1.07
35	6.89	0.04	6.79	1.36	86.32	4.92	1.12
45	5.26	0.04	6.59	1.40	88.16	4.88	1.17
55	4.39	0.04	5.43	1.26	90.18	4.80	1.32
65	3.83	0.04	5.63	1.33	90.54	4.79	1.37

5.3.C.5. TR fluorescence anisotropy studies. To obtain additional evidence for aggregation of C153 dye in EtOH solution, TR fluorescence anisotropy was measured both in ACN and EtOH solutions. These measurements were carried both at the emission maxima (515 nm for

ACN and 525 nm for EtOH) and at the blue edge of the emission spectra (460 nm) of the dye. Observed anisotropy decays in the two solvents are shown in Figure 5.24A and B, respectively. The anisotropy decays in ACN solution are very similar at both the monitoring wavelengths and fit with a single-exponential function giving rotational correlation time (τ_r) as ~ 0.1 ns. Accordingly, it is indicated that C153 dye in ACN solution is almost exclusively present in the monomeric form. In EtOH solution, the anisotropy decay at the blue wavelength is evidently much slower than that at the emission peak (*cf.* Figure 5.24B). Both the decays fit well with a single-exponential function, giving τ_r values as ~ 0.13 ns at the emission peak and ~ 0.21 ns at blue shifted wavelength. Though based on the multi-exponential fluorescence decays at 460 nm (*cf.* Table 5.5) the corresponding anisotropy decay was expected to be multi-exponential in EtOH solution, an attempt for multi-exponential analysis, did not give us any meaningful anisotropy parameters. Thus, we eventually relied upon single-exponential analysis for the anisotropy decay, even at 460 nm in EtOH solution.

The τ_r value of 0.13 ns estimated at the emission peak in EtOH solution, which is also quite similar to that observed in ACN solution, undoubtedly due to dye monomers in the solution. Distinctly higher τ_r value (~ 0.21 ns) at 460 nm in EtOH solution clearly suggests that at this wavelength there is a significant contribution arising from the dye aggregates in the observed anisotropy decay. In brief, observed fluorescence anisotropy results are in accordance with the H-type of aggregation for C153 dye in polar protic EtOH solvent.

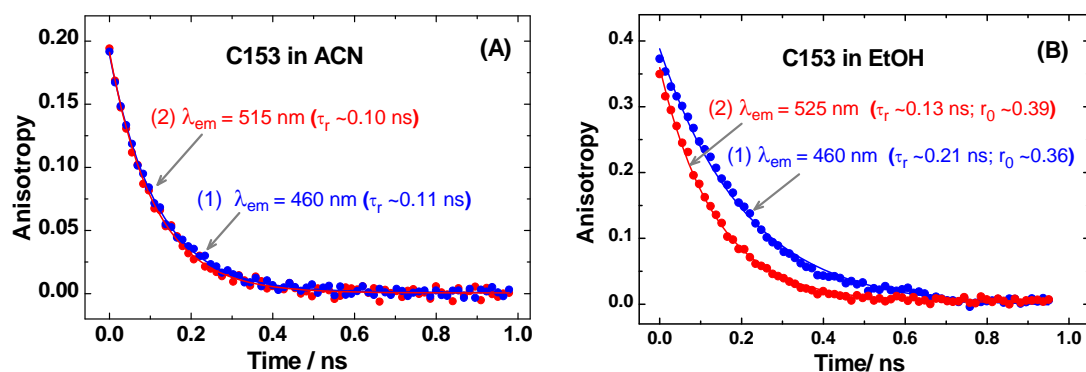


Figure 5.24: Fluorescence anisotropy decays of C153 dye ($\sim 28 \mu\text{M}$) in (A) ACN and (B) EtOH solutions, measured at blue edge (1) and at the emission maximum (2) in the respective solvents.

5.3.C.6. Femtosecond fluorescence up-conversion measurements. To understand the ultrafast fluorescence characteristics of C153 dye in ACN and EtOH solutions, fluorescence up-conversion measurements were carried out, recording kinetic traces at the blue edge of the emission spectra (470 nm), employing largely different dye concentrations in the solutions.

Figure 5.25A shows the kinetics traces measured in ACN solution at 470 nm employing 760 μM and 190 μM dye concentrations. There is no difference in the kinetics traces with largely different dye concentrations, confirming no unusual behavior for the dye in ACN solution. In this case, the initial unusually fast decay is understandably due to ultrafast solvent relaxation ($\langle\tau_s\rangle \sim 0.26$ ps in ACN).²⁶¹ The flat fluorescence signal with no apparent decay during the latter time span of the up-conversion trace corroborates well with the very long single-exponential fluorescence decay ($\tau_f \sim 5$ ns) of the dye in ACN solution (*cf.* Section 5.3.C.2).

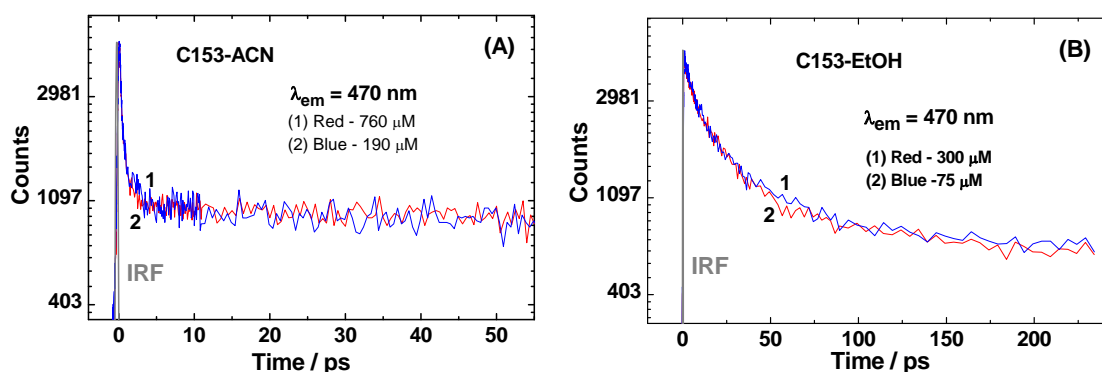


Figure 5.25: Fluorescence up-conversion traces for C153 dye at blue edge of the spectra in (A) ACN with (1) 760 μM and (2) 190 μM dyes and (B) EtOH solutions with (1) 300 μM and (2) 75 μM dyes.

Figure 5.25B shows the kinetics traces measured for C153 dye in EtOH solution at 470 nm, keeping the dye concentrations as 300 μM and 75 μM , respectively. In the present case also, there is no obvious change in the traces for the two largely different dye concentrations used. The initial significantly fast decay in the kinetic traces in EtOH solution is necessarily due to solvation dynamics ($\langle\tau_s\rangle \sim 16$ ps).²⁶¹ Interestingly, in EtOH solution, the kinetic traces show a slow continuously decaying feature even for the longer time span (till about 230 ps as recorded in the present measurements), which is distinctly different than the flat fluorescence signal observed in ACN solution at the longer time span. Thus, observed kinetic traces in EtOH solution apparently indicate the presence of the emitting species having much shorter decay times than the fluorescence lifetime of the monomeric dye in this solvent ($\tau \sim 4.8$ ns; *cf.* Table 5.5). These ultrafast fluorescence kinetic traces, however, could not be analyzed convincingly to extract any meaningful decay parameters for the dye aggregates in the solution, due to strong interference from the solvent relaxation. In any case, observed up-conversion traces in EtOH are qualitatively in accordance with the inferences drawn from TR fluorescence results obtained earlier using TCSPC measurements, supporting the aggregation of the dye in polar protic EtOH solvent.

5.3.C.7. DLS and SEM measurements. DLS measurements were carried out to understand the presence of any scattering particles in the EtOH solution of C153 dye. The scattering signal from the dye solution was not only very weak but also quite similar to that of the blank EtOH solvent. Moreover, no reasonable correlation function could be constructed from the scattering signals, either for the dye solution or the bulk solvent. These results suggest that the dye aggregates in the solution are too small in size and concentration, possibly dominated by dye dimers, trimers, etc., difficult to be detected by DLS measurements.

To explore the present system further, SEM measurements were also carried out for the dye solutions both in ACN and EtOH solvents. The SEM pictures thus obtained for the microfilms obtained on using the dye solutions in ACN and EtOH are shown in Figure 5.26A and B, respectively. As indicated from Figure 5.26A, there are large islands of dye aggregates in the microfilms formed by using ACN solution of the dye. This is likely because during evaporation from the dye solution on the copper stub there must be some micro bubble formation at the latter stages of the drying where the dye molecules are eventually deposited forming islands of varying sizes. Interestingly, SEM image formed from the EtOH solution of the dye shows unique thread like structures of the deposited dyes on the microfilm, which are distinctively very different than the SEM image obtained from ACN solution.

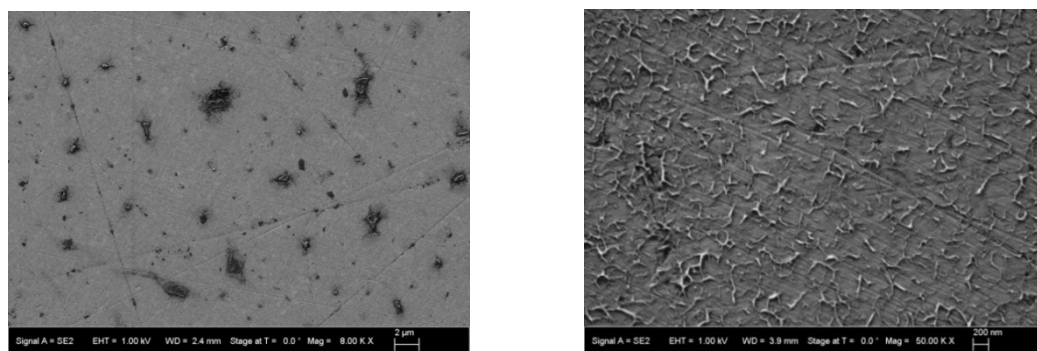


Figure 5.26: SEM images of the microfilms formed by using the C153 solutions in (A) polar aprotic ACN and (B) polar protic EtOH solvents.

Though from this study we cannot understand exactly how the thread like structures are formed during evaporation of EtOH solution, yet the observation clearly suggests that during the evaporation process the protic EtOH actively participates in associating the dyes in a specific manner that eventually causes the dyes deposited on the copper stub forming thread like structures. From the present observation one can thus infer that, the dye-solvent hydrogen bonding interaction helps in the formation of small dye aggregates in EtOH solution, possibly in the forms of dye dimers, trimers, etc.

5.3.C.8. TR fluorescence studies in strongly protic trifluoroethanol solvent. As it is indicated that the protic nature of the solvent apparently favors the aggregation of C153 dye in the solution, selective TR fluorescence measurements were carried out in a strongly protic solvent, namely, 2,2,2-trifluoroethanol (TFE). Figure 5.27A shows the comparison of the fluorescence decays of C153 dye in TFE and EtOH solutions, measured at 470 nm. As indicated from this figure, the decay in TFE shows larger contribution for the faster decay component than in EtOH, suggesting a better dye aggregation in the former solvent due to its stronger protic character. Figure 5.31B shows the wavelength dependent fluorescence decays in TFE solution, covering the whole SS fluorescence spectrum of C153 dye. The changes in the decays with changing wavelength are qualitatively very similar to those in EtOH solution (*cf.* Figure 5.22B). Present observations in TFE solvent are thus in support to our inference that aggregation of C153 dye is largely supported by the protic nature of the solvent used.

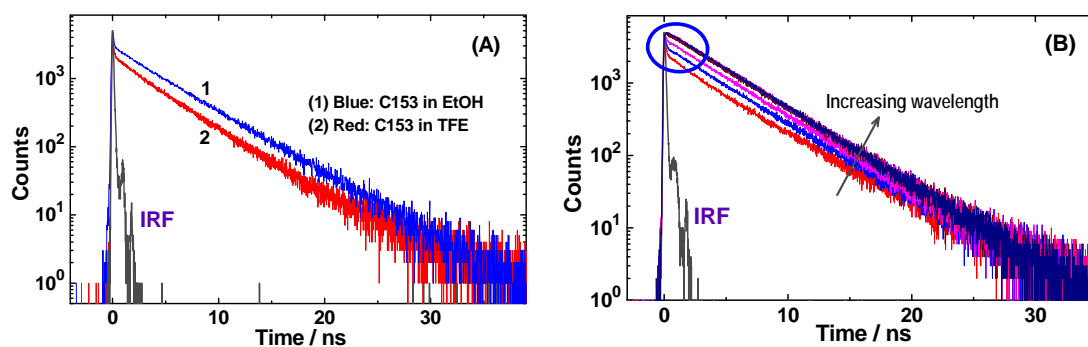


Figure 5.27: (A) Comparison of the fluorescence decays of C153 dye ($\sim 8 \mu\text{M}$) in TFE and EtOH solutions, measured at 470 nm. (B) Wavelength dependent fluorescence decays for C153 dye ($\sim 13 \mu\text{M}$) in TFE solution, covering the whole SS fluorescence spectrum of the dye.

Part 5.3.D

Photophysical behavior of C153 dye in aqueous solution

5.3.D.1. Ground-state absorption and SS fluorescence measurements. The ground state absorption and SS fluorescence spectra of C153 dye in aqueous solution with varying dye concentrations are shown in Figure 5.28A and B, respectively, displaying $\lambda_{\text{abs}}^{\text{max}}$ at 430 nm and $\lambda_{\text{fl}}^{\text{max}}$ at 546 nm. It is observed that the shape of both absorption and fluorescence spectra

remained effectively unchanged even on sufficient dilution of the saturated dye solution. These observations are apparently not in support of dye aggregation in the aqueous solution.

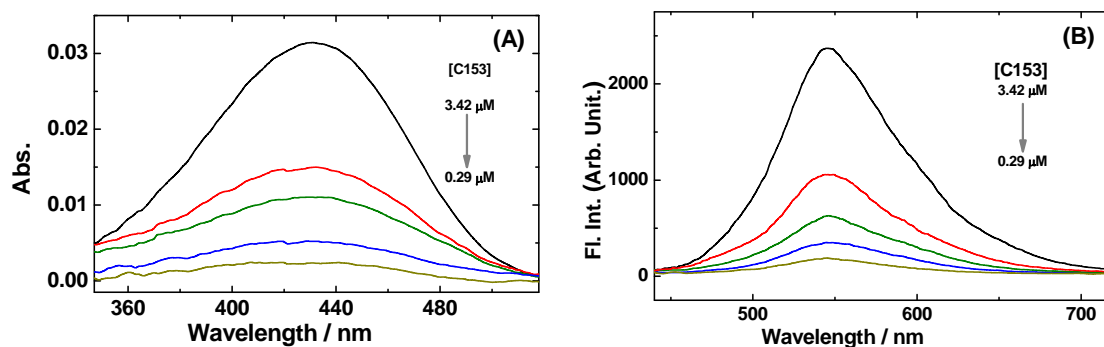


Figure 5.28: (A) Absorption and (B) SS fluorescence spectra of C153 dye in aqueous solution. Dye concentrations of the spectra are 3.42, 1.71, 1.14, 0.57 and 0.29 μM respectively.

The excitation spectra of the saturated dye solution (3.42 μM) in water were recorded for different emission wavelengths and the results indicate that though there is no appreciable difference in the spectra for emission wavelengths at the red edge and at the peak, the spectra for emission wavelength at the blue edge is distinctly blue shifted (*cf.* Figure 5.29A). The emission spectra were also recorded for the above solution with different excitation wavelengths and the results indicate that though there is no appreciable difference in the spectra for excitation at red edge and absorption peak, the spectrum recorded with blue edge excitation is distinctly blue shifted (*cf.* Figure 5.33B). These results are suggestive of the small extent of aggregation of C153 dye in aqueous solution.

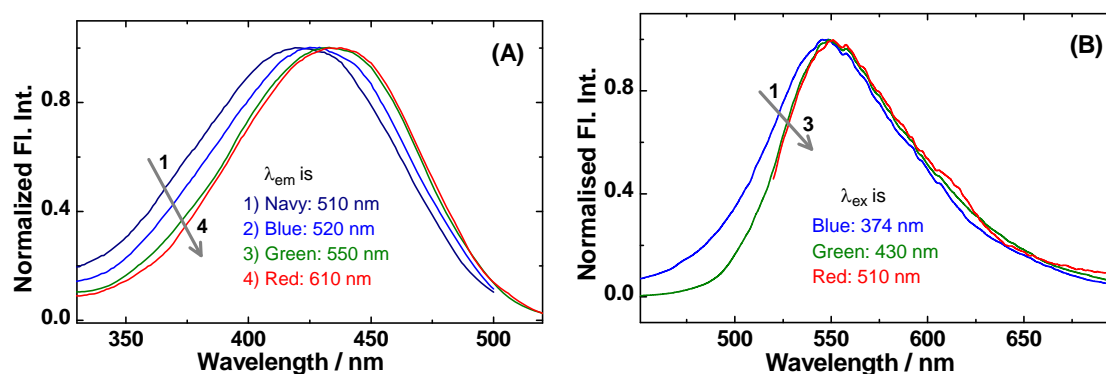


Figure 5.29: (A) Excitation and (B) Emission spectra of C153 dye (3.42 μM) in aqueous solution, recorded with respective emission and excitation wavelengths covering blue to red edge of the corresponding emission and absorption spectra.

5.3.D.2. TR fluorescence measurements. As TR fluorescence measurements are more sensitive than the SS measurements,^{1-4,118,119} the fluorescence decays of C153 dye in aqueous solution were also systematically measured, both with changing dye concentration and with

changing monitoring wavelengths, to get more insight of the present systems. Observed results are qualitatively very similar to the cases of C481 dye in aqueous solutions as discussed earlier at part B of this chapter. Typical wavelength dependent changes in the fluorescence decays in the present cases are shown in the inset of Figure 5.30A and the TRES and TRANES thus constructed are shown in Figure 5.30A and B, respectively. Comparing these results with those present and discussed in the earlier part of the chapter, it is evident that C153 dye undergoes a small extent of aggregation in aqueous solution as well.

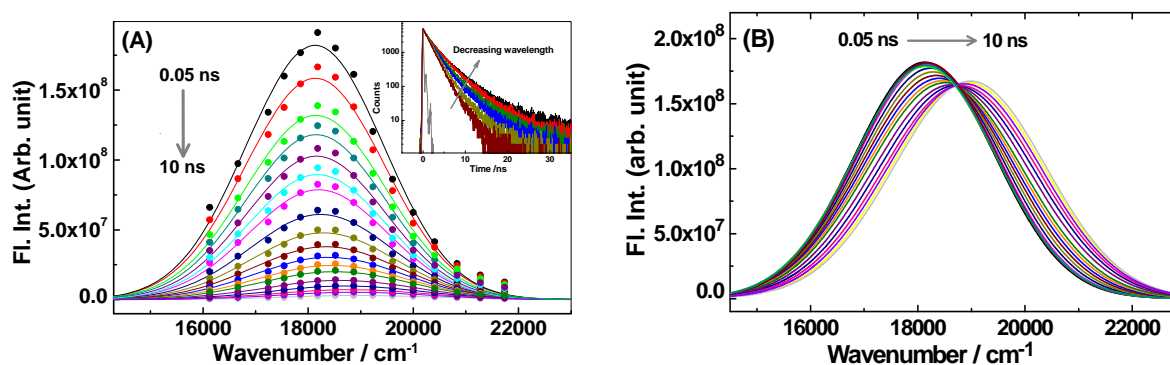


Figure 5.30: (A) TRES and (B) TRANES of C153 dye (3.42 μM) in aqueous solution as constructed from the wavelength dependent fluorescence decays shown in the inset of Panel A.

5.4. Conclusions

Aggregation behavior of two 7-aminocoumarin dyes, namely C481 and C153, has been investigated both in polar organic solvents and in aqueous solution. For C481 dye, the concentration, temperature and wavelength dependent fluorescence decays and the analysis of the constructed TRES and TRANES clearly suggest the coexistence of dye aggregates along with dye monomers in the studied solutions. Due to efficient ICT to TICT conversion, monomers of C481 dye show significantly short fluorescence lifetimes (0.2 ns in water, 0.64 ns in EtOH and 0.68 ns in ACN) while dye aggregates show relatively longer lifetimes due to steric hindrance towards ICT to TICT conversion. There is a systematic increase in the lifetime of the aggregated species on reducing dye concentration in the solution, indicating disintegration of higher aggregates to smaller aggregates and dye monomers. The TRES and TRANES analysis show that the emission spectra of the aggregates are substantially blue shifted, suggesting H-type of aggregation of C481 dye in the studied solvents.

For C153 dye, no aggregation behavior is observed in polar aprotic solvent ACN but quite reasonable aggregation is observed in polar protic solvent EtOH and also in aqueous solution. The concentration, temperature and wavelength dependent fluorescence decays and

the analysis of the TRES and TRANES clearly suggest a small extent of H-type of dye aggregation in EtOH and aqueous solution. For the present dye, lifetimes of the aggregates ($\tau_1 \sim 0.04$ ns for larger aggregates and $\tau_2 \sim 1.4$ ns for smaller aggregates) are much smaller than its monomeric lifetime ($\tau_3 \sim 4.8$ ns). This observation is clearly in accordance with the fact that unlike C481 dye the C153 dye is devoid of ICT to TICT conversion process.

It is understood from the present study that the highly dipolar character of the coumarin dyes (dipole moment ~ 6 D) drives the aggregation process through strong dipole-dipole interaction among the stacked dyes arranged face to face one above other with their permanent dipoles arranged in anti-parallel orientations. Due to this electrostatic interaction the aggregation of the studied dyes are favored in polar solvents. Very important aspect of the present work is that unlike the most other chromophoric dyes, the H-aggregates of the present coumarin dyes are fluorescent in nature, which is quite an unusual phenomena following Kasha's exciton theory (*cf.* Section 1.8). It is suggested that the emissive nature of the H-aggregates for the studied dyes is also due to the dipole-dipole interaction that helps in overcoming the restriction on the electronic transitions in H-aggregates arising from Kasha's exciton theory. Protic nature of the solvents, e.g. EtOH and water, evidently assists the aggregation process, certainly through dye-solvent hydrogen bonding interaction, which is evidently indicated from scanning electron microscopy results.

As clearly indicated from the observed results, there is a modulation in the photophysical characteristics of the coumarin dyes in the studied polar solvents due to aggregation process. Importantly, these modulations are related mainly at the blue edge of the emission spectra due to the H-type of aggregation of the dyes. Accordingly, the emission characteristics of the dyes effectively show no appreciable modulation at longer wavelengths including emission maxima and the red edge of the emission spectra, where the observations correspond mainly to the monomeric dyes in the solution. In the present context it is thus important to be mentioned that in our PET studies as discussed in Chapter 3 and 4, since all the measurements involving coumarin dyes were carried out at their emission maxima, assured that the observed PET results are not influenced by the aggregation of the dyes in the studied solutions.

Chapter 6

Photoinduced Electron Transfer and Charge Transfer Interactions of Lanthanide and Uranyl Ion with Fluorogenic Diphenyl Amine Donor

Abstract

Photoinduced electron transfer (PET) and charge transfer (CT) interactions of trivalent lanthanide (Ln^{3+}) and uranyl (UO_2^{2+}) ions with fluorogenic diphenylamine (DPA) donor have been investigated in aqueous and acetonitrile medium. Present study has a relevance to the leaching out and mitigation of $\text{Ln}^{3+}/\text{UO}_2^{2+}$ ions in geoenvironment where DPA finds its presence as industrial and agricultural waste. Formation of weak ground state CT complexes in the present systems is confirmed from absorption studies. There is no emissive exciplex formation as evidenced from SS fluorescence spectra. The SS fluorescence quenching results, however, indicate substantial static quenching contribution, attributed to ground state CT complex formation. The TR fluorescence quenching results show quite efficient dynamic quenching. It is established that the TR fluorescence quenching of DPA by $\text{Ln}^{3+}/\text{UO}_2^{2+}$ ions is not due to energy transfer but due to PET from excited DPA to $\text{Ln}^{3+}/\text{UO}_2^{2+}$ ions. Direct evidence for PET mechanism is obtained from laser flash photolysis measurements where transient absorption band with peak around 670 nm for DPA cation is clearly evident. Time constant for the DPA cation growth confirms that PET occurs from the excited S_1 state of DPA to Ln^{3+} ions. No correlation is, however, observed for the estimated quenching constants with the free energy changes of the PET reactions, due to the participation of multiple vacant electronic states of lanthanide ions in the PET process. As realized, lanthanide and uranyl ions are complex electron acceptors in the PET reactions and many extensive follow up studies are expected to understand the details of these multichannel PET processes in these geologically important systems.

6.1. Introduction

In continuation to our studies on PET and Charge Transfer (CT) processes, this last chapter of the thesis describes the studies on PET and CT interactions of trivalent lanthanide ions (Ln^{3+}) and uranyl ion (UO_2^{2+}) as electron acceptors with diphenylamine (DPA) dye as the electron donor under diffusive conditions in aqueous and acetonitrile (ACN) medium, unlike the PET studies reported in Chapters 3 and 4 where investigations have been carried out in microheterogeneous media under non-diffusive conditions. Present investigations have been carried out with an aim to study the photophysical and photochemical aspects of the prospective organic ligands in the presence of lanthanide and uranyl ions, which can directly or indirectly be useful in understanding the migration behavior of the concerned heavy ions in the geoenvironment.²⁶²⁻²⁶⁴ Redox properties of $\text{Ln}^{3+}/\text{UO}_2^{2+}$ ions and their consequent interactions with various potential electron donating agents have a strong bearing towards their migration behavior in the geological environments when leached out from spent nuclear fuels. Photochemical studies are envisaged as a useful tool to understand the interaction of $\text{Ln}^{3+}/\text{UO}_2^{2+}$ ions with various ET and CT agents present in the geological environments.

Excited uranyl ion, $^*\text{UO}_2^{2+}$, is a strongly oxidizing species ($E^\circ = + 2.6 \pm 0.1 \text{ V}$),^{265,266} unlike the ground state UO_2^{2+} ($E^\circ = + 0.05 \text{ V}$), and is capable to react with a variety of substrates through PET mechanism. The electronic structure²⁶⁷ and photochemistry^{268,269} of uranyl ion have recently been reviewed. The favorable redox properties of uranyl ion had made impact in various fields of science and technology.²⁷⁰⁻²⁷² The photochemical reduction of uranyl ion by different agents has been extensively studied.²⁷³⁻²⁷⁷ Substantial studies on PET reactions involving uranyl ion as the acceptor and excited states of different organic and inorganic compounds as the donors have also been reported in the literature.²⁷⁸⁻²⁸²

The Lanthanide series (4f series) in the periodic table effectively consists of 15 elements with atomic numbers from 57 (Lanthanum) to 71 (Lutetium). In this series, the 4f orbital is gradually filled with increasing the atomic number. At lanthanum, the 5d subshell is lower in energy than 4f, so lanthanum has the electron configuration $[\text{Xe}] 6s^2 5d^1 4f^0$ (cf. Table 6.1). As more protons are added to the nucleus, the 4f orbitals contract rapidly and become gradually more stable than the 5d (as the 4f orbitals penetrate the 'xenon core' more), so that Ce has the electron configuration $[\text{Xe}] 6s^2 5d^1 4f^1$ and the elements Pr to Eu have general electronic configuration of $[\text{Xe}] 6s^2 4f^n$ ($n = 3-7$). After europium, due to unusual stability of the half-filled f subshell the next electron is added to the 5d orbital than 4f so that Gd has a configuration of $[\text{Xe}] 6s^2 5d^1 4f^7$. At terbium, however, the earlier pattern reverts

and it continues till Yb with general configuration as $[\text{Xe}] 6s^2 4f^n$ ($n = 9-14$). For the last element lutetium, as the 4f subshell is already completely filled, its electronic configuration is predictably $[\text{Xe}] 6s^2 5d^1 4f^{14}$.

Table 6.1: Electronic Configurations of lanthanides and their trivalent ions along with one-electron reduction potentials of trivalent lanthanide ions.

Element	Symbol	Atomic No.	Electronic configuration		$E_{\text{Ln(III)/Ln(II)}}(\text{versus NHE}), \text{V}$
			Atom	Ln^{3+}	
Lanthanum	La	57	$[\text{Xe}] 4f^0 5d^1 6s^2$	$[\text{Xe}]$	-3.1
Cerium	Ce	58	$[\text{Xe}]4f^1 5d^1 6s^2$	$[\text{Xe}]4f^1$	-3.2
Praseodymium	Pr	59	$[\text{Xe}]4f^3 6s^2$	$[\text{Xe}]4f^2$	-2.7
Neodymium	Nd	60	$[\text{Xe}]4f^4 6s^2$	$[\text{Xe}]4f^3$	-2.6
Promethium	Pm	61	$[\text{Xe}]4f^5 6s^2$	$[\text{Xe}]4f^4$	----
Samarium	Sm	62	$[\text{Xe}]4f^6 6s^2$	$[\text{Xe}]4f^5$	-1.55
Europium	Eu	63	$[\text{Xe}]4f^7 6s^2$	$[\text{Xe}]4f^6$	-0.35
Gadolinium	Gd	64	$[\text{Xe}]4f^7 5d^1 6s^2$	$[\text{Xe}]4f^7$	-3.9
Terbium	Tb	65	$[\text{Xe}]4f^9 6s^2$	$[\text{Xe}]4f^8$	-3.7
Dysprosium	Dy	66	$[\text{Xe}]4f^{10} 6s^2$	$[\text{Xe}]4f^9$	-2.6
Holmium	Ho	67	$[\text{Xe}]4f^{11} 6s^2$	$[\text{Xe}]4f^{10}$	-2.9
Erbium	Er	68	$[\text{Xe}]4f^{12} 6s^2$	$[\text{Xe}]4f^{11}$	-3.1
Thulium	Tm	69	$[\text{Xe}]4f^{13} 6s^2$	$[\text{Xe}]4f^{12}$	-2.3
Ytterbium	Yb	70	$[\text{Xe}]4f^{14} 6s^2$	$[\text{Xe}]4f^{13}$	-1.15
Lutetium	Lu	71	$[\text{Xe}]4f^{14} 5d^1 6s^2$	$[\text{Xe}]4f^{14}$	----

Lanthanides are most commonly used as luminescence probes and have found applications in various visible and near-IR radiation sources, light emitting diodes, lasers, optical sensors and devices, biological systems, etc., as have been widely reviewed.²⁸³⁻²⁸⁸ In lanthanides, the most common oxidation state is +3. Redox behaviour of trivalent lanthanide

ions (Ln^{3+}) is expected to be quite interesting, especially that of Sm, Eu and Yb and having electronic configuration attending or approaching half filled or full filled 4f orbitals. One-electron reduction potentials of trivalent lanthanide ions $E_{\text{Ln(III)/Ln(II)}}$ are listed in Table 1.²⁸⁹⁻²⁹¹ The reduction potential of Eu(III) is most favourable in the series due to the stabilization of Eu(II) with half-filled f-subshell. Similarly one electron reduction potential of Yb(III) is also quite favourable due to the formation of completely filled f-subshell in Yb(II). In case of reduction of Sm(III), approaching half-filled f-subshell of its divalent ion is reported to stabilize the latter quite significantly. For other trivalent lanthanide ions, their reduction potentials are not quite favourable (*cf.* Table 1) for their participation in ET reactions involving reactants in the ground state. Thus, even though studies on the formation of divalent lanthanide ions have been reported in the literature, they are not quite extensive.²⁹²⁻²⁹⁷ Similarly, limited studies have also been carried out on the ET processes involving divalent lanthanide ions as the electron donors.²⁹⁴⁻²⁹⁷ For trivalent lanthanide ions, even though their reduction potentials are not very favorable in most cases, yet they can participate in PET reactions, as the excitation energy provided to any of the reactant (donor or acceptor) favourably adds to the energetics of the ET process.⁵⁻¹¹ Understanding the PET processes involving lanthanides have mostly been driven by the development of ‘responsive’ lanthanide complexes that are used as sensor probes.²⁹⁸⁻³⁰¹

Considering the large range of the reduction potentials of the Ln^{3+} ions (*cf.* Table 1), it is interesting to know if these ions participate in diverging manner in the photoinduced redox processes involving electron rich reacting species i.e. electron donors, having significant occurrences in the geoenvironments. In the literature, substantial research interest has been shown on ET and CT interactions of lanthanides ions with variety of organic and inorganic ligands/reactants.³⁰²⁻³⁰⁸ In this work, we have investigated the PET and CT interactions of Ln^{3+} ions with a geologically important compound, that is, diphenylamine (DPA). Studies have also been extended involving UO_2^{2+} ion, an important reagent in the actinide series having quite reasonable oxidizing capability, using the same DPA as the electron donor. Important to note here that DPA finds its significant presence in the geoenvironment as an industrial and agricultural waste, as it is extensively used as a stabilizer in many rubber products, plastics, pesticides, pharmaceuticals, dyes, explosives and propellants and is thus exposed to geoenvironment quite abundantly.³⁰⁹⁻³¹⁵ In addition to its strong electron donating ability, DPA is also reasonably fluorescent in nature. Therefore, ET and CT interactions of DPA with $\text{Ln}^{3+}/\text{UO}_2^{2+}$ ions were expected to be explored efficiently using photochemical studies, as investigated in the present work.

6.2. Experimental Methods and Materials

DPA was obtained from Qualigens Fine Chemicals, India and was purified by recrystallization from cyclohexane. Perchlorate salts of Ln³⁺ ions were procured from Alfa Aesar and used as received. Perchlorate salt of UO₂²⁺ ion was prepared in house by dissolving UO₂ in nitric acid, drying the solution and then adding perchloric acid to it. The perchloric acid was finally evaporated till dryness. The residue was dissolved in nanopure water, the solution was neutralized with NaOH and its volume was made up with water. Saturated aqueous solution of DPA was prepared by adding solid DPA sample in nanopure water and stirring the solution overnight and collecting the supernatant solution after centrifugation. Experimental solutions for photochemical studies were prepared using this saturated DPA solution after appropriate dilution. Concentration of DPA in the experimental solution was estimated from the observed absorbance at the peak position (~278 nm), using molar absorption coefficient as $\epsilon_{\max} = 18,800 \text{ dm}^3 \text{ cm}^{-1}$, estimated in aqueous solution based on its reported ϵ_{\max} value in ethanol solution ($\epsilon_{278} = 19,500 \text{ dm}^3 \text{ mol}^{-1} \text{ cm}^{-1}$).³¹⁶ For the studies in acetonitrile (ACN) solution, DPA was directly dissolved in the solvent and its concentration was adjusted appropriately following its peak absorbance at 350 nm ($\epsilon_{\max} = 20100 \text{ dm}^3 \text{ mol}^{-1} \text{ cm}^{-1}$). Perchlorate salts of lanthanides/uranyl ions were gradually added to the DPA solutions to investigate the PET and CT interaction in DPA-Ln³⁺/UO₂²⁺ systems. All the measurements in the present study were carried out at ambient temperature (~25 °C).

Instruments used for ground-state absorption, SS fluorescence, TR fluorescence and LFP studies are discussed in Chapter 2. In TR fluorescence measurements, 292 nm LED was used as the excitation source for which IRF was ~800 ps at FWHM. Some TR measurements for monitoring lanthanide emissions were carried out using a TR fluorescence spectrometer from Edinburgh Instruments, UK, (model FLSP 920) where 60 W microsecond Xe flash lamp was used as the excitation source and a red sensitive PMT as the photodetector.

6.3. Results and Discussion

6.3.1. Investigations in aqueous solution

Interaction of DPA with Ln³⁺/UO₂²⁺ ions was investigated in aqueous solution under diffusive condition following the changes in the ground state absorption spectra, SS fluorescence spectra and fluorescence decay kinetics of DPA with the gradually increasing concentrations of Ln³⁺/UO₂²⁺ ions. In these measurements, the DPA concentration was in

general kept quite low, only in the range of $\sim 10 \mu\text{M}$. The concentration of $\text{Ln}^{3+}/\text{UO}_2^{2+}$ ions were gradually increased till up to a maximum concentration of about 100 mM. For LFP studies, however, the DPA concentration was kept $\sim 53 \mu\text{M}$ and the lanthanide ion concentration was kept in the range of 100-200 mM. The results obtained from different photochemical studies on the $\text{DPA-Ln}^{3+}/\text{UO}_2^{2+}$ systems in aqueous solution are systematically presented and discussed below.

6.3.1.1. Ground state interaction of DPA with lanthanide ions: Formation of charge transfer complexes. Absorption spectrum of DPA ($\sim 10 \mu\text{M}$) in aqueous solution shows a broad absorption band in the 240-320 nm regions, with peak at $\sim 278 \text{ nm}$. On addition of trivalent lanthanide ions, there is an obvious reduction in the absorbance of DPA, suggesting a small extent of ground state complex formation in the studied systems.¹⁻⁴ Figure 6.1A shows the representative changes in the absorption spectra of DPA with addition of Eu^{3+} ion .

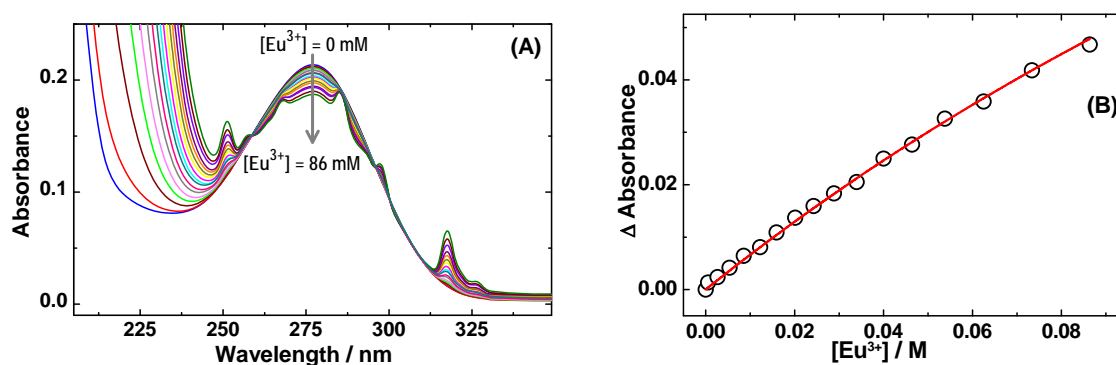


Figure 6.1: (A) Changes in the absorption spectra of DPA ($10 \mu\text{M}$) with Eu^{3+} concentration in aqueous solution. (B) Changes in the absorbance of DPA with the changing concentration of Eu^{3+} .

The absorbance changes of DPA with the increasing concentration of lanthanide ions were correlated to estimate the formation constants for the ground state complexes in different DPA-lanthanide systems. In the studied systems, since DPA concentration ($\sim 10 \mu\text{M}$) is much lower than the lanthanide ion concentrations (up to 100 mM) used, the ground state complexes are expected exclusively to have 1:1 stoichiometry, where one DPA ligand (L) would be binding to an interacting lanthanide ion (M). Therefore, formation of the ML complexes in the present systems can be represented as,



For this equilibrium, under the present experimental condition of $[\text{M}] \gg [\text{L}]$, the formation constant for the ML complex can be expressed as,

$$K_f = \frac{[ML]}{[L][M]} = \frac{[ML]}{([L]_0 - [ML])[M]_0} \quad (6.2)$$

where $[L]_0$ and $[M]_0 \approx [M]$ are the total DPA and lanthanide concentrations in the solution. With the situation prevailed for the present systems, the observed absorbance at a suitable wavelength should be given as,

$$\text{Abs.} = \varepsilon_L[L] + \varepsilon_{ML}[ML] = \varepsilon_L\{[L]_0 - [ML]\} + \varepsilon_{ML}[ML] \quad (6.3)$$

where ε_L and ε_{ML} are the molar extinction coefficients for free L and ML complex, respectively. Thus, using Eqs. 6.2 and 6.3 and following some rearrangements, we can express the changes in the DPA absorbance with added lanthanide ions as,

$$\Delta\text{Abs.} = \frac{\Delta\varepsilon[L]_0[M]_0K_f}{1 + [M]_0K_f} \quad (6.4)$$

where $[M]_0$ is the concentration of the lanthanide ion used and $\Delta\varepsilon$ is the difference between the molar extinction coefficients of the complex (ε_{ML}) and the free DPA (ε_L).

Correlating $\Delta\text{Abs.}$ with $[M]_0$, following Eq. 6.4, we could estimate the K_f values for the studied DPA-lanthanide ion systems. Representative $\Delta\text{Abs.}$ vs $[M]_0$ plot for DPA/Eu³⁺ system along with the fit of the experimental data following Eq. 6.4 is shown in Figure 6.1B. To be mentioned here that with the concentration range of the Ln³⁺ ions used, the $\Delta\text{Abs.}$ vs $[M]_0$ plots are largely away from reaching the saturation range for all the studied systems. Accordingly, the estimated K_f values have significantly large errors (~20%). Nevertheless, these K_f values give an idea of the extent of ground state interaction of DPA with the lanthanide ions. Table 6.2 lists the K_f values obtained for different DPA-Ln³⁺ systems investigated in the present study.

As indicated from Table 6.2, for most of the DPA/Ln³⁺ systems the K_f values are reasonably low, only in the range of 0.8 to 4 M⁻¹. Present results suggest that the ground state complex formation in these systems is in general quite weak, though not negligible. From the estimated K_f values it is evident that under the present experimental conditions only a small fraction of DPA is used up in the ground state complex formation and accordingly the major part of DPA still remains free for other interactions following photoexcitation. In the present context, as DPA is a strong electron donor^{162,317-319} and Ln³⁺ ions have reasonable electron accepting abilities (*cf.* Table 6.1 for $E_{Ln(III)/Ln(II)}$ values), the ground state complex formation in the present systems is attributed to the weak CT interaction between DPA donor and lanthanide ion acceptors. Considering the very low K_f values, we did not attempt any further detailed studies on the ground state complexes in the present systems.

Table 6.2: Formation constants (K_f) for the DPA-Ln³⁺ CT complexes in aqueous medium. Parameters relevant to the lanthanide ions and their ET interaction with DPA are also listed.

Ln ³⁺	K_f (M ⁻¹)	Diffusion Coefficient (Dx10 ⁶ , cm ² s ⁻¹)	Hydrated Radius (pm)	λ_s (eV)
La	4	6.29	389.6	1.43
Pr	1.2	6.12	400.4	1.41
Nd	1.8	6.18	396.5	1.42
Sm	2.2	6.09	402.4	1.41
Eu	2.7	5.85	418.9	1.39
Gd	2.8	5.76	425.4	1.38
Tb	2.4	5.64	434.4	1.37
Dy	0.5	5.57	439.9	1.36
Er	0.8	5.61	436.8	1.36
Yb	1.1	5.39	454.5	1.34

6.3.1.2. SS and TR fluorescence studies following DPA excitation and monitoring DPA emission. For the dilute aqueous solution of DPA (~10 μ M), the SS fluorescence spectral measurement show the emission peak of DPA at ~390 nm and the TR fluorescence measurement give the fluorescence lifetime of DPA as ~3.8 ns (*cf.* Figure 6.2). Both the SS and TR measurements show significant fluorescence quenching for DPA by the lanthanide ions. Typical results obtained from SS and TR fluorescence quenching of DPA by Eu³⁺ ion are shown in Figure 6.2A and B, respectively. As indicated from Figure 6.2A, consequent to the SS fluorescence quenching of DPA by Eu³⁺, there is no observable change in the fluorescence spectral features of DPA, suggesting that there is no excited state complex (exciplex) formation in the present systems. Similarly, in the TR fluorescence quenching, the decay of DPA gradually becomes faster, suggesting an efficient dynamic fluorescence quenching in the studied system. Similar observations are in general made for both SS and TR fluorescence quenching of DPA by most other lanthanide ions (including UO₂²⁺ ion) except in few cases, e.g. Pr³⁺ and Gd³⁺ ions, where an observable change in the fluorescence spectral shape and appearance of substantial decay tails at the higher quencher concentrations were observed which were unambiguously assigned to some inherent emissive impurities in the respective salt samples. In these cases, thus, SS and TR fluorescence quenching data were analyzed for the possible lower salt concentration ranges to avoid any untoward effect in the estimations. Accordingly, ignoring these effects, we could interpret the interactions of excited

DPA with $\text{Ln}^{3+}/\text{UO}_2^{2+}$ ions mainly due to dynamic quenching process without involving any excited state complex formation.

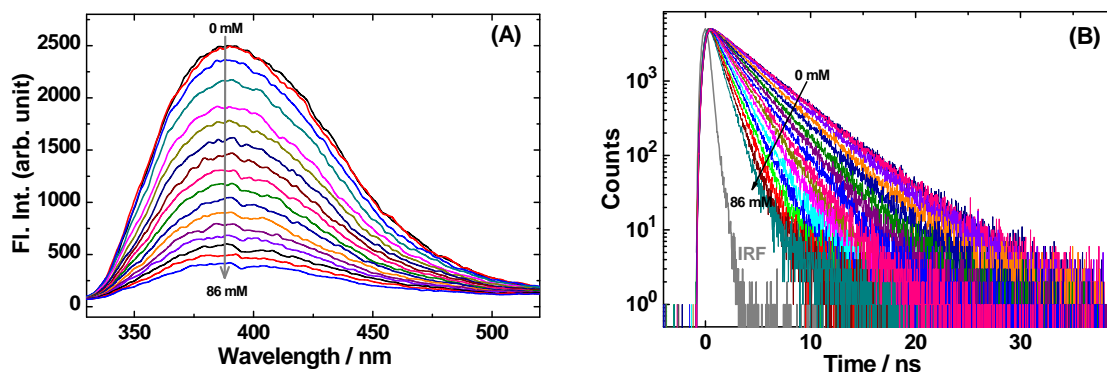


Figure 6.2: (A) SS and (B) TR fluorescence quenching of DPA with Eu^{3+} ion in aqueous solution. Excitation and emission wavelengths were 292 and 390 nm, respectively.

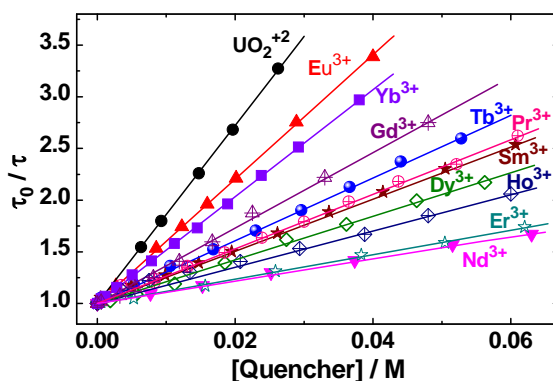


Figure 6.3: Stern-Volmer plots for TR fluorescence quenching of DPA by $\text{Ln}_3^+/\text{UO}_2^{2+}$ ions.

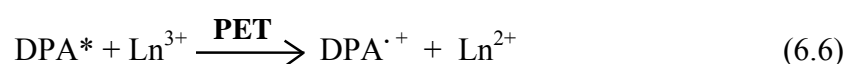
For the present systems, SS fluorescence quenching results were analyzed following Stern-Volmer relation (*cf.* Eq. 1.37; Section 1.6). The Stern-Volmer plots thus obtained mostly showed a positive deviation with increasing $\text{Ln}^{3+}/\text{UO}_2^{2+}$ ion concentration. This was in fact expected because significant static-quenching contribution arises for the present systems due to ground state complex formation,^{1-4,307} as discussed in Section 6.2.1.1. Due to this positive deviation, accurate estimations of K_{SV} and hence k_{q} values were not possible from the SS fluorescence quenching results for the present systems. Thus, quenching constants were estimated from the analysis of TR fluorescence quenching following the relevant Stern-Volmer equation (*cf.* Eq. 1.38; Section 1.6). For all the DPA- $\text{Ln}^{3+}/\text{UO}_2^{2+}$ systems, the τ_0/τ vs $[\text{Q}]$ plots are found to be linear for a reasonable range of the quencher concentrations used (*cf.* Figure 6.3). The K_{SV} values were thus obtained from the slopes of these plots and the k_{q} values ($K_{\text{SV}} = k_{\text{q}}\tau_0$) were subsequently estimated from these K_{SV} values for different DPA- $\text{Ln}^{3+}/\text{UO}_2^{2+}$ systems, as are listed in Table 6.3. Observed TR fluorescence

quenching results suggest that the excited singlet state of DPA undergoes a reasonably strong dynamic quenching by the Ln³⁺/UO₂²⁺ ions studied.

Table 6.3: Bimolecular quenching constants of DPA by Ln³⁺/UO₂²⁺ ions in aqueous medium.

Ion ^s	ΔG° (eV)	k _q x 10 ⁻⁹ (M ⁻¹ s ⁻¹)
Eu ³⁺	-2.63	15.9
Yb ³⁺	-1.83	13.9
Sm ³⁺	-1.43	6.5
Nd ³⁺	-0.38	2.9
Dy ³⁺	-0.38	5.7
Pr ³⁺	-0.28	8.7
Ho ³⁺	-0.08	4.4
Er ³⁺	0.12	3.0
Tb ³⁺	0.71	7.8
Gd ³⁺	0.91	10.6
UO ₂ ²⁺	-3.00	18.4

In the literature there are number of PET studies following fluorescence quenching of organic dyes by Ln³⁺/UO₂²⁺ ions.^{278-282,302-308} Drawing an analogy to these studies and since DPA is a good electron donor,^{162,317-318} observed fluorescence quenching in the present study is proposed as due to PET from DPA donor to Ln³⁺/UO₂²⁺ acceptor ions (*cf.* Eq. 6.5 and 6.6). A direct evidence for the PET process in the present systems has in fact been obtained from LFP studies, as will be discussed in the later Section 6.2.1.4. In the present context, however, we feel it to be interesting to understand if lanthanide ions on excitation can also participate in the ET interaction with the ground state DPA donor. Accordingly, we carried out independent studies following lanthanide excitation as are discussed in the following section.



6.3.1.3. Studies following lanthanide excitation and monitoring lanthanide emission. As discussed in the previous section, DPA fluorescence is strongly quenched by the lanthanide ions. Assuming that PET from excited DPA to lanthanide ions is the mechanism for the observed fluorescence quenching, we were curious to know if a similar PET process can also

occur between excited lanthanide ions and ground state DPA. Thus, studies were carried out selectively exciting the lanthanide ions at suitable wavelengths where DPA does not absorb. Subsequently, any changes in the emission of Ln^{3+} were monitored with gradually increasing the concentration of DPA in the experimental solution.

Considering the required criteria of the present set of experiments, i.e., (i) the lanthanide ion should have reasonable emission yield, (ii) the absorption of the lanthanide ion should be at wavelengths above about 350 nm such that there is no overlapping of DPA absorption and (iii) there should not be any long wavelength absorption band for the lanthanide ion, possibly not beyond about 400 nm, such that the excitation energy provided to the lanthanide ions does not cascade down easily leading to negligible emission yield. Sm^{3+} , Eu^{3+} and Tb^{3+} were thus identified as the suitable lanthanide ions for the present experiments.

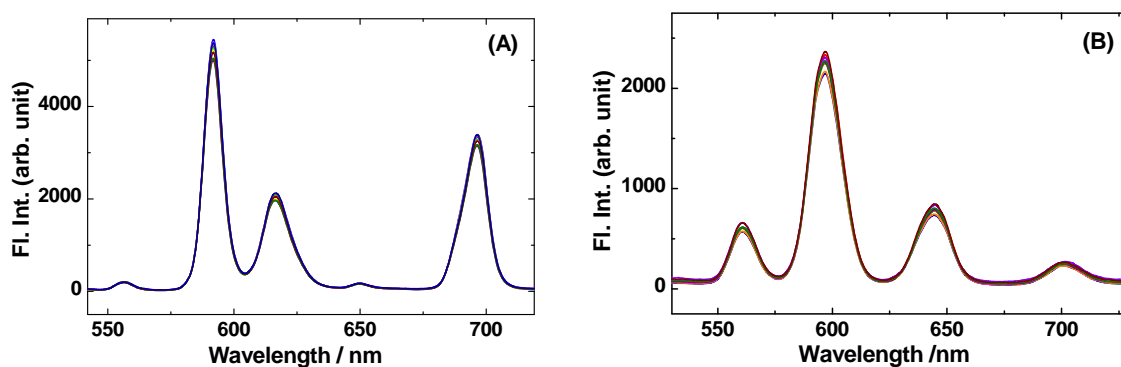


Figure 6.4: SS emission spectra of (A) DPA- Eu^{3+} and (B) DPA- Sm^{3+} systems with gradual addition of DPA. Excitation wavelengths were 395 and 401 nm for Eu^{3+} and Sm^{3+} , respectively.

Typical results for DPA- Eu^{3+} and DPA- Sm^{3+} systems following the excitation of lanthanide ions are shown in Figure 6.4A and B, respectively. As indicated from these results, there is no observable quenching for the lanthanide emissions, confirming that no ET takes place from ground state DPA to the excited lanthanide ions. PET in the DPA-lanthanide systems following excitation of lanthanide ions is not occurring possibly due to (i) the process is not energetically feasible because the excitation energy supplied to the system is significantly less compared to that supplied in the case of DPA excitation, and (ii) as lanthanides have rich electronic spectra with large number of lower energy electronic levels (energy landscapes), the excitation energy on the lanthanide ions can easily cascade down making the PET process kinetically unfavorable. From the present results it is thus inferred that for DPA- Ln^{3+} system, PET is not feasible following excitation of the lanthanide ions, through an efficient PET process occurs in these system on exciting the DPA donor.

6.3.1.4. Laser flash photolysis studies: Direct evidence for PET reaction. As discussed earlier, the observed SS and TR fluorescence quenching of DPA by $\text{Ln}^{3+}/\text{UO}_2^{2+}$ ions are assigned to PET from excited DPA to ground state $\text{Ln}^{3+}/\text{UO}_2^{2+}$ ions. To support this mechanism, LFP studies were carried out on some selective DPA- Ln^{3+} systems looking for transient absorption spectra of the DPA radical cation formed by the PET reaction. Transient absorption spectra obtained from the LFP studies of DPA- Eu^{3+} system in aqueous solution following 266 nm laser excitation are shown in Figure 6.5. Similar results were also obtained for DPA- Sm^{3+} and DPA- Dy^{3+} systems following LFP studies.

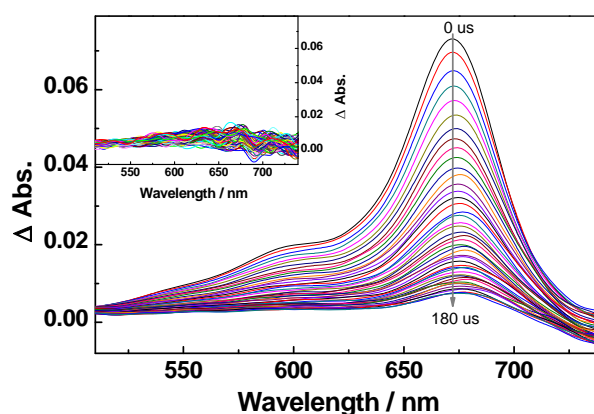


Figure 6.5: Transient absorption spectra for DPA/ Eu^{3+} system. The DPA and Eu^{3+} concentrations were 53 μM and 179 mM, respectively. **Inset:** Transient absorption spectra for DPA alone.

Observed results from the present study show the initial development of broad transient absorption band following the laser excitation with absorption peak at around 670 nm, which matches well with the reported absorption spectra of DPA cation.^{162,317-320} The LFP results thus unambiguously establish the involvement of PET process from the excited DPA to the $\text{Ln}^{3+}/\text{UO}_2^{2+}$ ions (*cf.* Eq. 8). To be mentioned here that no DPA cation formation was observed following LFP of DPA alone (*cf.* Figure 6.5 inset). Signature of divalent lanthanide ions formed from the PET reaction in the present systems could not be observed in the transient absorption spectra, possibly either due to very weak/negligible absorption of the Ln^{2+} ions in the present spectral window or due to very fast quenching (oxidation) of Ln^{2+} ions in the studied solution.^{291,297} The other point to be mentioned here is that there is no signal for DPA triplet absorption observed in the present systems, probably due to very low quantum yield of the DPA triplet formation,^{320,321} which could also be further reduced in the present systems because the major part of the excited DPA would undergo the PET reaction in the presence of the high concentration of the lanthanide ions used in this study.

The decay of DPA cation in the present systems is significantly slow (*cf.* Figure 6.6A), occurs effectively with a first order kinetics having time constants in the range of 50-100 μs , depending on the systems studied. Though, the reason behind the first order decay kinetics and the observed differences in the kinetics for different DPA/Ln³⁺ systems is not very clear, one of the possible decay channel could be the deprotonation of the DPA radical cation to the solvent bath as the radical is quite protic in nature.³¹⁷. Nevertheless, the observed results suggest that the recombination reaction in the studied systems is unusually slow under the present experimental conditions. In any case, from the observed LFP results it can be unambiguously concluded that PET mechanism is the main reason for the observed fluorescence quenching of DPA by lanthanide ions in the studied systems. Time constants for the growth of DPA cation in the studied DPA/lanthanide systems are found to be close to about 6 ns (*cf.* Figure 6.6B), quite similar to the IRF of the present LFP setup, and hence considered to be comparable to the fluorescence lifetime of DPA (~ 4 ns). Such a fast growth of DPA cation clearly suggests that PET occurs from the excited singlet state (S₁) of DPA to Ln³⁺/UO₂²⁺ ions, which is thus responsible for the observed fluorescence quenching of DPA.

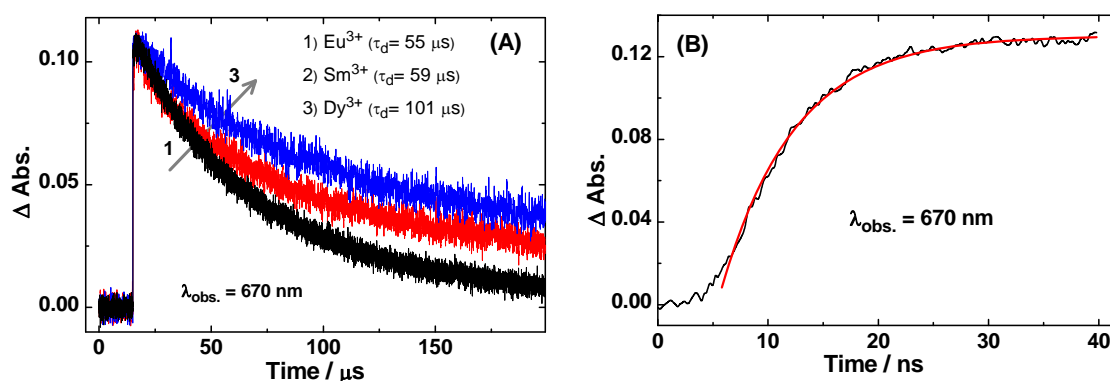


Figure 6.6: (A) Decay and (B) growth of DPA cation in DPA/Ln³⁺ system. DPA concentration was 53 μM and Eu³⁺, Sm³⁺ and Dy³⁺ concentrations were 179, 203 and 76 mM, respectively.

6.3.1.5. Correlation of k_q values with free energy changes of ET reaction. Since k_q value is a measure of ET rate under diffusive condition,^{1-11,49} it is interesting to see how k_q values correlate with the free energy changes (ΔG^0) of the ET reactions. The ΔG^0 values for the present PET systems were calculated following Rehm-Weller relation (*cf.* Eq. 1.22; Section 1.3). In this estimation, the excitation energy of DPA (3.81 eV) was calculated from the intersecting wavelength of the normalized emission and excitation spectra. The E_{D/D^+} value for DPA was considered as 0.85 V.^{162,317-319} The radius of DPA was estimated as 3.39 Å by using Edwards volume addition method.¹⁶⁴ Radii of hydrated Ln³⁺ ions (*cf.* Table 6.2) were

obtained from the reported diffusion coefficient values in the aqueous solution³²² using Stokes-Einstein relation.¹⁻⁴ The radius of hydrated uranyl ion was considered as 0.46 nm.³²³ The donor-acceptor separation was considered as the sum of their radii. The ΔG^0 values thus calculated for different ET systems are listed in Table 6.3.

It is observed from the estimated k_q and the corresponding ΔG^0 values in Table 3 that there exists no systematic correlation between two parameters in the present systems. The absence of such a correlation possibly indicates that instead of a simple PET mechanism involving just one reactant and one product energy states, as normally encountered in most PET reactions (*cf.* Figure 6.7A), there might be the participation of multiple PET channels in the present systems (*cf.* Figure 6.7B), arising due to the involvement of number of electronic energy states of the lanthanide ions, resulting a stronger fluorescence quenching in the present systems than otherwise expected. Moreover, there could also be some energy transfer from DPA* to lanthanide ions to give additional quenching channel than just the PET mechanism. Though exploring the participation of the multiple PET channels was beyond the scope of our present study, we could explore the possibility of the energy transfer mechanism in the studied systems, as discussed in the following section.

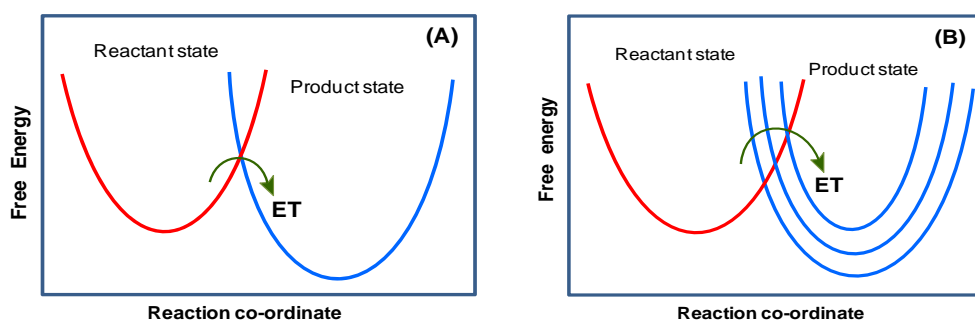


Figure 6.7: Qualitative free energy diagram for the ET process: (A) Considering single ET channel (B) Considering multiple ET channel.

6.3.1.6. Studies on the possibility of energy transfer from excited DPA to lanthanide ions.

Assuming that there could be energy transfer from excited DPA to lanthanide ions causing an additional quenching of DPA fluorescence, we carried out studies to explore the possibility of this mechanism. In this part of the study, DPA was preferentially excited and the sensitized emissions expected from the lanthanide ions were looked for with systematically increasing the DPA concentration, keeping the lanthanide concentration constant (in the range of 100-200 mM). Figure 6.8 A and B shows the SS emission spectra for Dy^{3+} -DPA and Tb^{3+} -DPA systems, respectively, investigated as the representative systems in the present study. In Dy^{3+} -DPA system, initially the system was excited with the 325 nm light, where Dy^{3+} is directly

excited to find the location of Dy^{3+} emission peaks. Two emission peaks are thus located at 480 and 574 nm. After identification of Dy^{3+} emission peaks, excitation was then done at 269 nm where DPA is mainly excited and direct excitation of Dy^{3+} is very nominal. Absorption spectra with different composition of DPA and Dy^{3+} are shown in the inset of the Figure 6.8A. It is observed that there is no observable emergence of Dy^{3+} emission peaks even with a large addition of DPA in the solution, as shown in Figure 6.8A, suggesting that there is no energy transfer from excited DPA to Dy^{3+} ion.

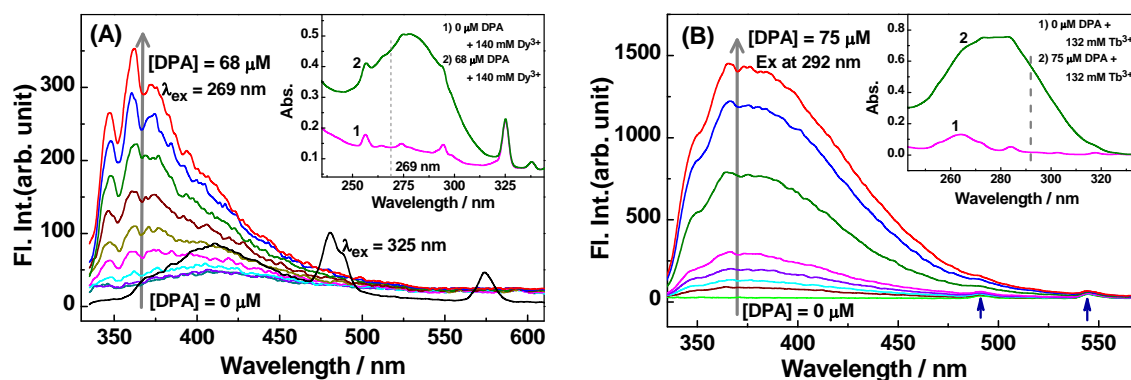


Figure 6.8: (A) SS emission spectra of (A) DPA- Dy^{3+} and (B) DPA- Tb^{3+} systems with increasing DPA concentration, to observe sensitized Ln^{3+} emissions. Spectrum due to direct Dy^{3+} excitation (325 nm) is also shown in panel A. Insets of panels A and B show the corresponding absorption spectra.

For DPA- Tb^{3+} system (*cf.* Figure 6.8B), excitation was done at 292 nm to avoid direct excitation of Tb^{3+} as far as possible. Absorption spectra with different compositions of DPA and Tb^{3+} are shown in the inset of Figure 6.8B. For this case, emission spectra were recorded with increasing DPA concentration but keeping Tb^{3+} concentration constant (132 mM). As indicated from Figure 6.8B, there is an increase in the background fluorescence at the emission wavelengths of Tb^{3+} ions (indicated by arrows in Figure 6.8B), arising due to the increasing emissions of DPA as more DPA is added in the experimental solution. For the present system thus, Tb^{3+} emission peaks are significantly distorted, causing the interpretation difficult on the possibility of energy transfer from excited DPA to Tb^{3+} ions.

To circumvent the above interference, we subsequently carried out TR emission measurements where the DPA fluorescence was avoided by time gating, taking the advantage of the fact that the fluorescence lifetime of DPA is very short, only about 4 ns, whereas the lanthanide emission is in the microsecond timescale. These TR measurements were carried out using a spectrometer from Edinburgh Instrument, UK, where excitation was done at 278 nm, i.e. the peak of the DPA absorbance. TR emission spectra (TRES) were constructed

through measurements of the emission kinetic traces at 2 nm intervals, covering the concerned spectral bands of the lanthanide emissions. TRES were thus obtained exclusively for the lanthanide ions, completely avoiding the DPA emissions by using a suitable initial time delay. Experiments were repeated with increasing concentration of DPA, keeping the lanthanide concentration constant. There was no observable enhancement in the TRES for lanthanide emission with an increase in the DPA concentration. Representative results for DPA-Eu³⁺ and DPA-Tb³⁺ systems are shown in Figures 6.9A and B, respectively. Observed results convincingly exclude the possibility of energy transfer from excited DPA to lanthanide ions. Present inference is also supported by the fact that in the TR emission studies there is no growth component observed in the kinetic traces monitored for the lanthanide emissions while sample was excited at the DPA absorption band. To be mentioned here that the weak lanthanide emissions observed in these studies are due to small extent of direct excitation of lanthanide ions that could not be avoided completely. Since the extent of this excitation gradually decreases on increasing the DPA concentration, there is a systematic decrease in the lanthanide emission band as the DPA concentration is increased in the solution (*cf.* Figure 6.9A and B).

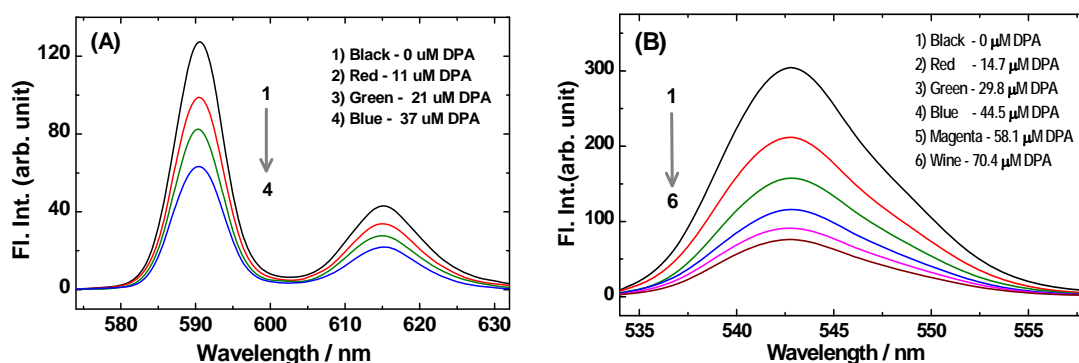


Figure 6.9: (A) TRES of DPA-Eu³⁺ system. [Eu³⁺]=225 mM and DPA is added till 37 μM (B) TRES of DPA-Tb³⁺ system. [Tb³⁺] = 64 mM and DPA is added till 70.4 μM. Excitation was at 292 nm.

6.3.1.7. Visualization of multiple PET channels for DPA-Ln³⁺ systems. From the results discussed so far, it is evident that the dynamic fluorescence quenching of DPA by Ln³⁺ ions is exclusively due to ET from photoexcited DPA to lanthanide ions, with no obvious contribution from energy transfer mechanism. However, since the estimated bimolecular quenching constants do not correlate with the free energy of the ET reaction, it is indicative that there must be more than one ET channel operating in the reaction mechanism for the studied DPA-Ln³⁺ systems. Considering the relative energies of different electronic states of lanthanide ions (*cf.* Figure 6.10),³²⁴ it can be seen that there are many electronic energy levels

of the lanthanide ions that fall within the available free energy changes and thus can take part in the ET interaction with the excited DPA donor. Thus the excited DPA can easily transfer an electron to the Ln^{3+} ions involving a number of high energy electronic states of the latter, and the excess energy can then easily be cascaded down to the lower energy states of the divalent lanthanide ions through fast non-radiative deexcitation processes.

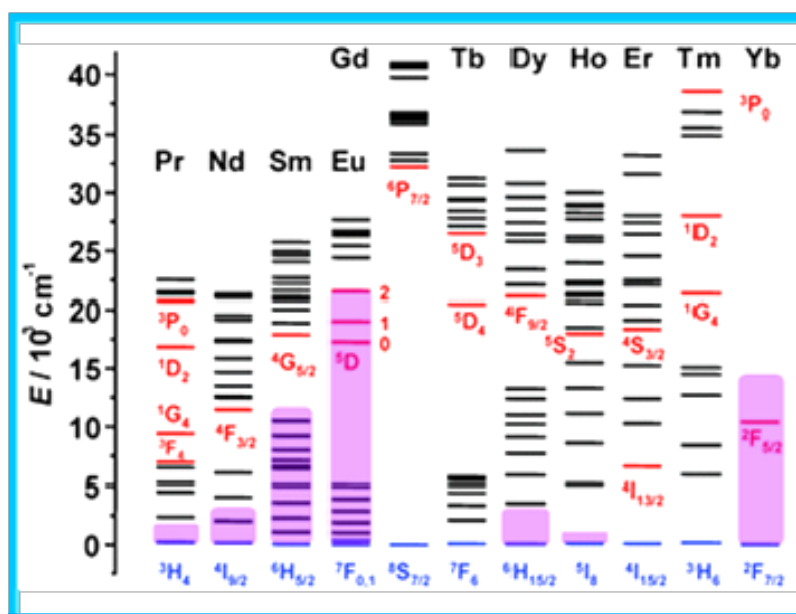


Figure 6.10: Potential Energy Diagram of Ln^{3+} ions (reproduced from Ref. 324, with permission from The Royal Society of Chemistry).. The bars show the available energies in different cases to involve the higher energy states of the lanthanide ions in the PET reaction.

Considering the discussion above, for the DPA- Ln^{3+} systems, it is apparent that not only the lowest possible vacant electronic state but also a number of higher energy vacant states of the Ln^{3+} ions can participate in the PET mechanism, resulting the fluorescence quenching of DPA to be stronger than otherwise expected. Evidently, the number of vacant states participate in the PET process would vary with the Ln^{3+} ion concerned (*cf.* Figure 6.10). Accordingly, it becomes difficult to draw any correlation between the observed quenching constants with the free energy changes for the ET reactions estimated for different Ln^{3+} ions based on their redox potential values. Understandably, thus the PET process involving Ln^{3+} ions is a complex process and cannot lead to any straightforward Marcus⁵⁻¹¹ or Rehm-Weller^{5-11,49} kind of correlations of the quenching rates with free energy changes of the ET reactions, as indicated from the observed results (*cf.* Table 3). Nevertheless, present results undoubtedly establish that the PET process acts as the main interaction mechanism for the studied DPA- Ln^{3+} systems over the alternative energy transfer mechanism.

6.3.2. Investigations in acetonitrile solution.

It is well known that the extent of solvation plays an important role in the PET reactions.^{5-11,291} For the DPA-Ln³⁺/UO₂²⁺ systems, to understand the role of solvent polarity on the PET reactions, studies were also carried out following the changes in the the ground state absorption spectra, SS fluorescence spectra and TR fluorescence traces of DPA (~10 μM) with the gradual addition of lanthanide/uranyl ions (upto 100 mM) in acetonitrile (ACN) medium under diffusive condition.

Absorbance maximum of DPA in ACN solution appears at 280 nm (*cf.* Figure 6.11), while SS fluorescence spectra show the emission peak at about 350 nm (*cf.* Figure 6.12A). The lifetime of DPA is estimated to be about 3.8 ns following TR fluorescence measurements of DPA in ACN solution (*cf.* Figure 6.12B). In this study, excitation wavelength was kept at 292 nm for both SS and TR fluorescence measurements, as it is the emission wavelength of the pulsed LED available with the TCSPC setup. Both the SS and TR measurements show significant fluorescence quenching for DPA by the lanthanide ions (up to about 100 mM) in the ACN solution. Results obtained from SS and TR fluorescence quenching studies using Eu³⁺ as the quencher are shown in Figure 6.12A and B, respectively. In SS fluorescence quenching, there is no observable change in the fluorescence spectral features of DPA by the presence of Ln³⁺ ions, indicating that there is no excited state complex (exciplex) formation in the present systems. The strong fluorescence quenching observed from both SS and TR studies in ACN solution are qualitatively very similar to those observed in aqueous solution for the studied systems. Thus, drawing an analogy, we infer that in acetonitrile solution also the PET from excited DPA to Ln³⁺/UO₂²⁺ ions is the main reason for the strong fluorescence quenching observed in the present systems.

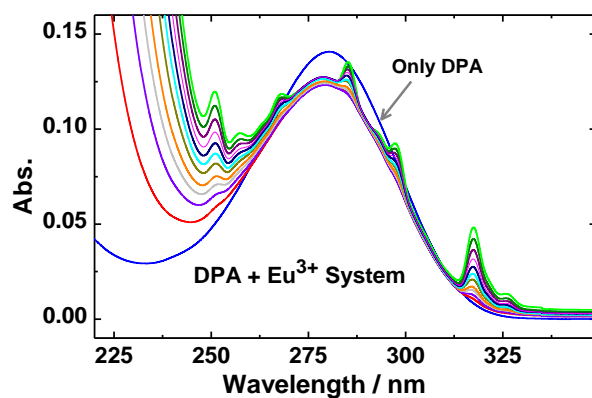


Figure 6.11: Absorption spectra of DPA (10 μM) on each addition of Eu³⁺ in acetonitrile medium.

Bimolecular quenching constants for the studied donor-acceptor systems in ACN solution were calculated following Stern-Volmer relation for the fluorescence lifetime quenching as discussed in Section 6.2.1.2 and the k_q values thus estimated are listed in Table 6.4. On comparing the quenching constant values in ACN medium with that in the aqueous medium, it is observed that the k_q values are somewhat lower in the present solvent than in aqueous solution. The decrease in the PET rates in ACN as compared to aqueous solution is probably due to lesser stabilization of the ion-pairs in the former solvent which is relatively less polar in character than water. Observed k_q values in water and ACN solvents are thus in accordance with the suggested PET mechanism for the observed fluorescence quenching of DPA by lanthanide/uranyl ions.

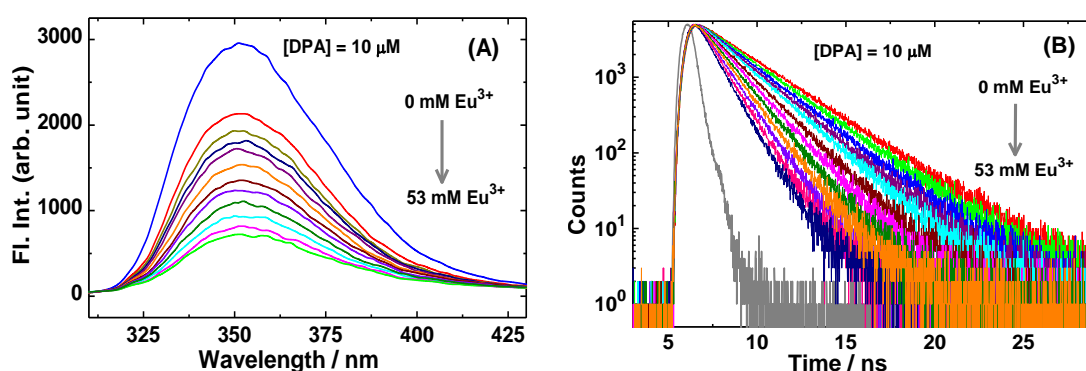


Figure 6.12: (A) SS and (B) TR fluorescence quenching of DPA by Eu^{3+} ion in acetonitrile medium.

Table 6.4: Bimolecular quenching constants for the DPA- Ln^{3+} systems in acetonitrile solution.

Ln^{3+} Ions	Eu^{3+}	Yb^{3+}	Sm^{3+}	Nd^{3+}	Dy^{3+}	Er^{3+}	Tb^{3+}
$k_q, 10^{-9} \text{ M}^{-1} \text{ s}^{-1}$	11.5	10.1	7.2	2.1	3.1	3.0	4.5

6.4. Conclusion

Ground state absorption, SS fluorescence, TR fluorescence and LFP measurements were carried out to investigate the interactions of $\text{Ln}^{3+}/\text{UO}_2^{2+}$ ions with DPA fluorophore. Formation of ground state CT complexes in the present systems is very evident from the ground state absorption studies, though the formation constants for these complexes are in general found to be substantially low. Fluorescence quenching measurements showed that both SS and TR fluorescence of DPA undergo strong quenching by $\text{Ln}^{3+}/\text{UO}_2^{2+}$ ions. Stronger SS fluorescence quenching was attributed to the combined effect of dynamic

quenching and ground state CT complex formation while the TR fluorescence quenching was due to an efficient dynamic quenching process only. Bimolecular quenching constants, (k_q) were estimated from TR fluorescence quenching studies for the present systems following Stern-Volmer analysis. Logically, two interaction mechanisms were anticipated for the observed fluorescence quenching, namely, the energy transfer from excited DPA to lanthanide ions and the PET from DPA to lanthanide ions. Systematic SS and TR fluorescence measurements in relation to the possible energy transfer from excited DPA to lanthanides negate this possibility of interaction. Excluding energy transfer, the other probable quenching mechanism anticipated was the PET from DPA to $\text{Ln}^{3+}/\text{UO}_2^{2+}$ ions. The direct evidence for the PET mechanism in the present systems was obtained from LFP measurements. Thus, the transient absorption band observed around 670 nm for the DPA- Ln^{3+} systems clearly establishes the DPA cation formation, ascertaining the PET mechanism in the studied systems. Time constant for the growth of DPA cation also confirms that the PET occurs from the excited singlet state (S_1) of DPA to lanthanide ions, which is thus responsible for the efficient fluorescence quenching of DPA observed in the studied systems. It is however observed that there is no correlation for the estimated k_q values with the ΔG^0 values for the ET reactions in the studied DPA- Ln^{3+} systems. It is realized that for the present systems apart from the simple PET mechanism involving just one reactant and one product energy surfaces, there is the possible participation of multiple PET channels, arising from the involvement of the multiple vacant electronic states of the lanthanide ions, resulting a stronger fluorescence quenching of DPA by these ions than otherwise expected. In brief, $\text{Ln}^{3+}/\text{UO}_2^{2+}$ ions appear to be extremely complex but very efficient electron acceptors for PET reactions with chromophoric dyes, rendering the prospects of more elaborate studies to understand these PET systems unambiguously.

Chapter 7

Concluding Summary and Future Scope

The major objective of the present thesis was (i) to understand the energetics and kinetics of the photoinduced electron transfer (PET) reactions that lead towards the modulation and designing of the ET reactions as per our requirement and (ii) to investigate the photoinduced interactions of lanthanides and uranyl ions with geologically relevant organic molecules to understand their photochemical behavior in the geoenvironment. The conclusions and the major achievements of the present work are summarized in this chapter along with its future prospects.

7.1. Concluding Summary of the Present Study

7.1.1. Tuning of PET reactions in organic donor-acceptor pairs involving pluronic micelles and pluronic-surfactant mixed micellar media

The PET reactions depend on various parameters like polarity, viscosity, orientational flexibility of solvent, etc. around the donor-acceptor pair in reaction media.^{1-10,25-29,136-145,179}

Role of these parameters in the kinetics and energetics of PET reactions should be understood explicitly to be able to modulate the PET reactions. Since it is difficult to play with the kinetics and energetics of PET reactions in homogeneous medium due to fast solvation process (maximum contribution of solvent reorganization energy) and reactant diffusion (rate determining step at higher exergonicities limiting the maximum PET reaction rate to be observed),^{1-10,25-29} the restricted micellar media have been used to fulfill the objective by restricting/retarding the reactant diffusion as well as the solvent relaxation (rate decreases and consequently reduces the contribution of solvent reorganization energy towards ET reaction).^{136-145,179} With this perspectives, the PET reactions involving coumarin donors and N,N-dimethylaniline (DMAN) donor have been investigated in the present study in pluronic micelles and pluronic-surfactant mixed micellar media and the results are summarized as the following:

As discussed in chapter 3, Marcus inversion for the bimolecular PET reactions (inversion of the ET rates at the lower and higher exergonicity ($-\Delta G^0$) regions giving bell-shaped correlation for rate vs ΔG^0 plot) was realized in coumarin-amine acceptor-donor pairs taking advantage of the conducive reaction environment of the heterogeneous media of pluronic F88 (EO₁₀₃-PO₃₉-EO₁₀₃; EO: ethylene oxide and PO: propylene oxide) micelle. Knowing the exergonicity for the onset of the Marcus inversion helps in designing the PET reactions whereby forward ET reactions is desired to occur in region close to this onset (as it corresponds to the 'barrierless' condition for ET) such that the associated back ET (BET) reaction is forced to occur at the inverted regime to suppress the rate of energy wasting back ET process. With F88 micellar medium, Marcus Inversion was achieved at an exergonicity ($-\Delta G^0$) of about 0.77 eV, which is significantly lower than what is otherwise expected in a conventional solvent of comparable polarity (much greater than 1 eV).^{5-11,25-29,136-141} Onset of Marcus inversion at lower exergonicity thus helps in overcoming the difficulty of using donor-acceptor pairs with extremely high reaction exergonicity to realize Marcus inversion behavior as is the limitation for ET reactions in conventional solvents. Studied micellar media also help to overcome the constraining factors of reactant diffusions that limit the observed

ET rates in conventional solvents, causing the reaction to occur under non-diffusive condition and thus making it easy to realize Marcus inversion in microheterogeneous solvent media.

Important point to note from the present study is that the onset of Marcus inversion in F88 (EO₁₀₃-PO₃₉-EO₁₀₃) micelle appeared at an exergonicity of about 0.77 eV while that in P123 (EO₂₀-PO₇₀-EO₂₀) micelle is observed at an exergonicity of about 0.68 eV.^{140,141} Appearance of Marcus inversion in F88 micelle at a higher exergonicity than that in P123 micelle is understood to be due to higher contribution of solvent reorganization energy in the former micelle than in the latter because of the higher number of the labile water molecules in the corona region of F88 micelle due to its higher EO to PO ratio than that in P123 micelle.¹⁴⁰ Additionally, the ET rates in F88 micelle are also comparatively higher because the ion pair formed after ET reaction is better stabilized in this micelle due to the higher polarity of its corona region as a consequence of its higher EO to PO ratio than that of the P123 micelle.¹⁴⁰ From the observed results it is therefore evident that the energetics and kinetics of the PET reaction can be suitably tuned by the appropriate selection of EO to PO ratios of the tri-block copolymers used for the pluronic micellar media.

In continuation with the previous work and with the objective of the modulation of the PET kinetics, a convenient and better strategy has been devised in a study using mixed micellar systems composed of pluronic polymers (F88 or P123) and cationic surfactant (CTAC: cetyltrimethylammonium chloride). Incorporation of cationic surfactant into these mixed micelles induces the formation of positively charged layer deep inside these mixed micelles.^{75-77,90,176-184} PET reactions between an anionic acceptor, C343 and a neutral donor DMAN demonstrated a large modulation in the PET kinetics with the increasing CTAC to pluronic ratio in the mixed micelles because the anionic C343 dye, initially dissolved at the micelle-water interface, experienced a gradually increasing electrostatic attraction and thereby systematically dragged deeper inside the micellar corona closer to DMAN. Therefore, a large modulation in the ET rates is achieved by changing the surfactant to pluronic molar ratios in the mixed micellar systems, a strategy very convenient to implement for a desired outcome from an ET reaction.¹⁷⁹

As PET studies was carried out using coumarin dyes as the fluorescence probes and electron acceptors, it was important to understand if these dyes show any unusual solution behaviour which might affect the PET results. Thus, detailed photophysical characterization was carried out for two selected coumarin dyes (C481-with TICT character and C153-without TICT character) in polar organic solvents and in aqueous solution with special emphasis on their possible aggregation behaviour in the solution. Both the dyes demonstrated the

coexistence of smaller and larger H-type of dye aggregates (having blue shifted emissions as compared to that of monomers) along with the dye monomers, especially in polar protic solvents, as the dye-solvent hydrogen bonding interaction provides extra stability of the dye aggregates. The dipolar character of the coumarin dyes (dipole moment ~ 6 D) drives the aggregation process through strong electrostatic dipole-dipole interaction among the stacked dyes and thus accordingly favored in polar solvents. The important finding of the present work is that unlike the most other chromophoric dyes, the H-aggregates of the present coumarin dyes are fluorescent in nature.²³³⁻²³⁵ It is realized that the dye aggregation do not affect the of PET results as the observed fluorescence changes due to H-type dye aggregation mainly occur at the extreme blue edge of the emission spectra while the PET process is investigated following the changes in the fluorescence and absorption of the dye at their respective peak positions.^{140,179}

7.1.2. Photochemical interactions of lanthanides and uranyl ions with geologically relevant organic molecules

Photophysical and photochemical investigations have been carried out to understand the interaction of $\text{Ln}^{3+}/\text{UO}_2^{2+}$ ions with organic fluorophore, diphenylamine (DPA) present in geological environment,³⁰⁹⁻³¹⁵ considering the reasonable electron accepting quality of the former and the strong electron donating ability of the latter. Ground state charge transfer complexes of DPA and Ln^{3+} ions are observed to be formed in these systems, as evidenced from the absorbance changes of DPA with the increasing concentration of Ln^{3+} ions. These complexes formed are in general quite weak as revealed from the estimated formation constant values. Occurrence of PET from the excited singlet state of DPA to $\text{Ln}^{3+}/\text{UO}_2^{2+}$ ions is revealed by dynamic fluorescence quenching of DPA by $\text{Ln}^{3+}/\text{UO}_2^{2+}$ ions and confirmed from laser flash photolysis studies by observing the transient absorption spectrum of DPA cation. There is no PET from excited Ln^{3+} ions to ground state DPA. There is also no obvious energy transfer from excited DPA to Ln^{3+} ions. However, no correlation was observed for the estimated quenching constants with the free energy changes of the PET reactions, possibly, due to the participation of multiple vacant electronic states of lanthanide ions in the PET process. As realized, lanthanide and uranyl ions are complex electron acceptors in the PET reactions. Nevertheless, multichannel PET mechanism acts as the main interaction process in the present DPA- Ln^{3+} systems.

7.2. Future scope of work

Electron transfer reactions in mixed micellar systems involving suitably selected ionic surfactant in combination with a triblock copolymer and charged electron donor and/or acceptor can lead to large modulation in the ET rates, as revealed in the present study. Such systems are the prospective candidates to investigate their usefulness as templates in the synthesis of nanomaterials for different applications. In this context other copolymers like branched copolymers, star copolymers, graft copolymers, dendrimers, etc. can be explored for the better modulations in the ET rates with enhanced application potentials.

As discussed in the later part of the thesis, photochemical interactions of lanthanides and uranyl ions with organic molecules were investigated. This work has a huge potential with the scope to investigate the charge transfer complex formation as well as to investigate the photoinduced electron transfer and energy transfer processes of lanthanides/actinides with various geologically relevant organic/inorganic donors. Such investigations would enhance knowledge about the mitigation behaviour of the lanthanides/actinides in the geoenvironment.

REFERENCES

1. J. B. Birks, *Photo Physics of Aromatic Molecules*; Wiley-Interscience: New York, 1970.
2. A. Gilbert, J. Baggott and P. J. Wagner, *Essential of Molecular Photochemistry*; Blackwell science Inc.: Cambridge, USA, 1991.
3. J. R. Lackowicz, *Principles of fluorescence spectroscopy*, 3rd ed.; Springer: New York, 2006.
4. K. K. Rohatgi-Mukherjee, *Fundamentals of Photochemistry*; Wiley Eastern Ltd: India, 1986
5. V. Balzani (Ed.), *Electron Transfer in Chemistry*, Wiley-VCH Publishers Inc., New York, **2001**, Vol I to V.
6. J. Jortner and M. Bixon (Eds.), *Electron Transfer from Isolated Molecules to Biomolecules, Advances in Chem. Phys.* Wiley, New York, **1999**, Parts 1 & 2, Vols. 106 and 107.
7. G. J. Kavarnos, *Fundamentals of Photoinduced Electron Transfer*, VCH Publishers, New York, **1993**.
8. J. R. Bolton, N. Mataga and G. L. McLendon (Eds.), *Electron Transfer in Inorganic, Organic and Biological Systems*, American Chemical Society, Washington, DC, **1991**.
9. A. M. Fox, Special Issue on Electron Transfer, *Chem. Rev.*, **1992**, 92, 365.
10. M. A. Fox and M. Chanon (Eds.), *Photoinduced Electron Transfer*, Elsevier, Amsterdam, **1988**.
11. M. Gratzel, *Heterogeneous Photochemical Electron Transfer*, CRC Press, Boca Raton, FL, **1989**.
12. H. Petek and J. Zhao, *Chem. Rev.*, **2010**, 110, 7082.
13. S. J. Formosinho, L. G. Arnaut, and R. Fausto, *Prog. React. Kin.*, **1998**, 23, 1.
14. R. D. J. Miller, G. L. McLendon, A. J. Nozik, W. Schmickler and F. Willig, *Surface Electron Transfer Processes*, VCH Publishers, Inc., New York, **1995**.
15. M. Hambourger, G. F. Moore, D. M. Kramer, D. Gust, A. L. Moore and T. A. Moore, *Chem. Soc. Rev.*, **2009**, 38, 25-35.
16. D. Gust, T. A. Moore and A. L. Moore, *Acc. Chem. Res.*, **2009**, 42, 1890.
17. N. Serpone, E. Pelizzetti, *Photocatalysis: Fundamentals and Applications*, Wiley, New York, **1989**.

18. P. V. Kamat and D. Meisel, *Semiconductor Nanoclusters: Physical, Chemical and Catalytic Aspects*, Elsevier, Amsterdam, **1997**.
19. H. Weller and A. Eychmuller, *Semiconductor Nanoclusters-Studies in Surface Science and Catalysis*, P. V. Kamat, D. Meisel (Eds.), Elsevier Science, **1996**, 103, 5.
20. D. F. Ollis, E. Pelizzetti and N. Serpone, *Environ. Sci. Technol.*, **1991**, 25, 1523.
21. R. A. Marcus and N. Sutin, *Biochim. Biophys. Acta*, **1985**, 811, 265.
22. R. A. Marcus, *J. Chem. Phys.*, **1956**, 24, 966.
23. R. A. Marcus, *J. Chem. Phys.*, **1956**, 24, 979.
24. R. A. Marcus, *Annu. Rev. Phys. Chem.*, **1964**, 15, 155.
25. H. Sumi and R. A. Marcus, *J. Chem. Phys.*, **1986**, 84, 4894.
26. W. Nadler and R. A. Marcus, *J. Chem. Phys.*, **1987**, 86, 3906.
27. H. Heitele, *Angew. Chem. Int. Ed. Engl.*, **1993**, 32, 359.
28. G. C. Walker, E. Akesson, A. E. Johnson, N. E. Levinger and P. F. Barbara, *J. Phys. Chem.*, **1992**, 96, 3728.
29. M. D. Newton and N. Sutin, *Annu. Rev. Phys. Chem.*, **1984**, 35, 437.
30. P. F. Barbara and W. Jarzeba, *Adv. Photochem.*, **1990**, 15, 1.
31. G. J. Kavarnos, *Topics in Current Chemistry*, J. Mattay (Ed.), Springer-Verlag, Berlin, **1990**, Vol. 156, p 21.
32. J. R. Miller, L. T. Calcaterra and G. L. Closs, *J. Am. Chem. Soc.*, **1984**, 106, 3047.
33. G. L. Closs and J. R. Miller, *Science*, **1988**, 240, 440.
34. J. R. Miller, J. V. Beitz and R. K. Huddleston, *J. Am. Chem. Soc.*, **1984**, 106, 5057.
35. G. L. Closs, L. T. Calcaterra, N. J. Green, K. W. Penfield and J. R. Miller, *J. Phys. Chem.*, **1986**, 90, 3673.
36. I. Rips and J. Jortner, *J. Chem. Phys.*, **1987**, 87, 2090.
37. D. F. Calef and P. G. Wolynes, *J. Phys. Chem.*, **1983**, 87, 3387.
38. L. D. Zusman, *Chem. Phys.*, **1980**, 49, 295.
39. I. Rips and J. Jortner, *J. Chem. Phys.*, **1987**, 87, 6513.
40. I. Rips and J. Jortner, *J. Chem. Phys.*, **1988**, 88, 818.
41. M. Bixon and J. Jortner, *Chem. Phys.*, **1993**, 176, 467.
42. M. Bixon, J. Jortner, J. Cortes, H. Heitele and M. E. Michel-Beyerle, *J. Phys. Chem.*, **1994**, 98, 7289.
43. J. Jortner and M. Bixon, *J. Chem. Phys.*, **1988**, 88, 167.

44. M. Newton, *Chem Rev.*, **1991**, *91*, 767.
45. J. T. Hynes, *J. Phys. Chem.*, **1986**, *90*, 3701.
46. N. Sutin, *Prog. Inorg. Chem.*, **1983**, *30*, 441.
47. M. Bixon and J. Jortner, *Adv Chem. Phys.*, **1999**, *106*, 35.
48. M. Bixon and J. Jortner, *J. Phys. Chem.*, **1988**, *92*, 7148.
49. D. Rehm and A. Weller, *Isr. J. Chem.* 1970, **8**, 259-271.
50. M. Maroncelli, *J. Mol. Liq.*, **1993**, *57*, 1.
51. M. Maroncelli, J. MacInnis and G. R. Fleming, *Science*, **1989**, *243*, 1674.
52. M. Maroncelli and G. R. Fleming, *J. Chem. Phys.*, **1987**, *86*, 6221.
53. E. W. Castner, Jr., G. R. Fleming, B. Bagchi and M. Maroncelli, *J. Chem. Phys.*, **1988**, *89*, 3519.
54. N. Sarkar, A. Datta, S. Das and K. Bhattacharyya, *J. Phys. Chem.*, **1996**, *100*, 15483.
55. N. Nandi, K. Bhattacharyya and B. Bagchi, *Chem. Rev.*, **2000**, *100*, 2013.
56. P. Sen, S. Mukherjee, A. Halder and K. Bhattacharyya, *K. Chem. Phys. Lett.*, **2004**, *385*, 357.
57. A. Datta, S. K. Pal, D. Mandal and K. Bhattacharyya, *J. Phys. Chem. B*, **1998**, *102*, 6114.
58. D. M. Willard, R. E. Riter and N. E. Levinger, *J. Am. Chem. Soc.*, **1998**, *120*, 4151.
59. H. Shirota and K. Horie, *J. Phys. Chem. B*, **1999**, *103*, 1437.
60. P. Alexandridis and T. A. Hatton, *Colloids Surf. A*, **1995**, *96*, 1.
61. P. Alexandridis, J. F. Holzwarth and T. A. Hatton, *Macromolecules*, **1994**, *27*, 2414.
62. E. D. Goddard, *J. Colloid Interface Sci.*, **2002**, *256*, 228.
63. K. Mortensen, W. Brown and B. Norden, *Phys. Rev. Letts.*, **1992**, *68*, 2340.
64. K. Mortensen and J. S. Pederson, *Macromolecules*, **1993**, *26*, 805.
65. P. Bahadur and G. Riess, *Tenside, Surfactants, Deterg.*, **1991**, *28*, 173.
66. V. Y. Alakhov and A. V. Kabanov, *Expert Opin. Invest. Drugs*, **1998**, *7*, 1453.
67. E. V. Batrakova, H. Y. Han, , D. W. Miller and A. V. Kabanov, *Pharm. Res.*, **1998**, *15*, 1525.
68. M. Guzman, F. F. Garcia, J. Molpeceres and M. R. Aberturas, *Int. J. Pharm.*, **1992**, *80*, 119.
69. A. Kabanov, J. Zhu and V. Alakhov, *Adv. Genet.*, **2005**, *53*, 231.
70. M. Yokoyama, *Crit. Rev. Therapeutic Drug Carrier Syst.*, **1992**, *9*, 213.

71. H. Wang, W. Lin, K. Fritz, G. Scholes, M. Winnik and I. Manners, *J. Am. Chem. Soc.*, **2007**, *129*, 12924.
72. H. Wang, A. J. Patil, K. Liu, S. Petrov, S. Mann, M. A. Winnik and I. Manners *Adv. Mater.*, **2009**, *21*, 1805.
73. B. Chu and Z. Zhou, Physical chemistry of polyoxyalkylene block copolymer surfactants. In *Nonionic surfactants*; Nace, V. M., Ed.; Marcel Dekker: New York, 1996; Vol. 60; pp 67.
74. G. Wanka, H. Hoffmann and W. Ulbricht, *Macromolecules*, **1994**, *27*, 4145.
75. R. Ganguly, V. K. Aswal, P. A. Hassan, I. K. Gopalakrishnan and S. K. Kulshreshth, *J. Phys. Chem. B*, **2006**, *110*, 9843.
76. J. Jansson, K. Schillen, M. Nilsson, O. Soderman, G. Fritz, A. Bergmann and O. Glatter, *J. Phys. Chem. B*, **2005**, *109*, 7073.
77. J. Jansson, K. Schillen, G. Olofsson, R. C. d. Silva and W. Loh, *J. Phys. Chem. B*, **2004**, *108*, 82-92.
78. J. R. Lopes and W. Loh, *Langmuir*, **1998**, *14*, 750.
79. P. Alexandridis, T. Nivaggioli and T. A. Hatton, *Langmuir*, **1995**, *11*, 1468.
80. K. S. Mali and G. B. Dutt, *J. Chem. Sci.*, **2007**, *119*, 147.
81. K. S. Mali, G. B. Dutt, R. Ganguly and T. Mukherjee, *J. Chem. Phys.*, **2005**, *123*, 144913.
82. S. Nad, M. Kumbhakar and H. Pal, *J. Phys. Chem. A*, **2003**, *107*, 4808.
83. C. D. Grant, K. E. Steege, M. R. Bunagan and E. W. Castner, *J. Phys. Chem. B*, **2005**, *109*, 22273.
84. S. Ghosh, A. Adhikari, U. Mandal, S. Dey and K. Bhattacharyya, *J. Phys. Chem. C*, **2007**, *111*, 8775.
85. M. Kumbhakar and R. Ganguly, *J. Phys. Chem. B*, **2007**, *111*, 3935.
86. M. Kumbhakar, T. Geol, S. Nath, T. Mukherjee and H. Pal, *J. Phys. Chem. B*, **2006**, *110*, 25646.
87. E. J. Pancheri and M. H. K. Mao, Comprising anionic surfactant polymeric nonionic surfactant and betaine surfactant US Patent, 1992.
88. R. Schafer, Use of pluronic surfactant to enhance the cleaning effect of pancreatin on contact lenses US Patent, 1997.
89. K. C. Tama E. Wyn-Jonesb, *Chem. Soc. Rev.*, **2006**, *35*, 693.
90. Y. Li, R. Xu, S. Couderc, D. M. Bloor, J. F. Holzwarth and E. Wyn-Jones, *Langmuir*, **2001**, *17*, 5742.
91. M. Kasha, H. R. Rawls and M. A. El-Bayoumi, *Pure Appl. Chem.*, **1965**, *11*, 371.

92. M. Kasha, *Radiation Research* **1963**, 20, 55.
93. S. K. Pal, D. Mandal, D. Sukul and K. Bhattacharyya, *Chem. Phys.*, **1999**, 249, 63.
94. E. J. C. Olson, D. Hu, A. Hormann, A. M. Jonkman, M. R. Arkin, E. D. A. Stemp, J. K. Barton and P. F. Barbara, *J. Am. Chem. Soc.*, **1997**, 119, 11458.
95. D. Grand and S. Hauteclouque, *J. Phys. Chem.*, **1990**, 94, 837.
96. M. Gratzel, J. J. Kozak and J. K. Thomas, *J. Chem. Phys.*, **1975**, 62, 1632.
97. L. K. Patterson and M. Gratzel, *J. Am. Chem. Soc.*, **1975**, 79, 956.
98. N. E. Katz, S. L. Mecklenburg, D. K. Graff, P. Chen and T. J. Mayer, *J. Phys. Chem.*, **1994**, 98, 8959.
99. N. E. Katz, S. L. Mecklenburg and T. J. Mayer, *Inorg. Chem.*, **1995**, 34, 1282.
100. E. H. Yonemoto, G. B. Saupe, R. H. Schmehl, S. M. Hubig, R. L. Reley, B. L. Iverson and T. E. Mallouk, *J. Am. Chem. Soc.*, **1994**, 116, 4786.
101. S. L. Larson, L. F. Cooley, C. M. Elliott and D. F. Kelley, *J. Am. Chem. Soc.*, **1992**, 114, 9504.
102. I. R. Gould and S. Farid, *Acc. Chem. Res.*, **1996**, 29, 522.
103. H. Segawa, C. Takehara, K. Honda, T. Shimidzu, T. Asahi and N. Mataga, *J. Phys. Chem.*, **1992**, 96, 503.
104. J. S. Zhou and M. A. J. Rodgers, *J. Am. Chem. Soc.*, **1991**, 113, 7728.
105. C. Turro, J. M. Zaleski, Y. M. Karabatsos and D. G. Nocera, *J. Am. Chem. Soc.*, **1996**, 118, 6060.
106. C. Li and M. Z. Hoffman, *J. Phys. Chem. A*, **1998**, 102, 6052.
107. S. Fukuzumi, Y. Yoshida, T. Umano, T. Suenobu and H. Imahori, *J. Am. Chem. Soc.*, **2001**, 123, 11331.
108. S. Fukuzumi, M. Nishimine, K. Ohkubo, N. V. Tkachenko and H. Lemmetyinen, *J. Phys. Chem. B*, **2003**, 107, 12511-12518.
109. D. M. Guldi and K. D. Asmus, *J. Am. Chem. Soc.*, **1997**, 119, 5744.
110. M. Tachiya and S. Murata, *J. Phys. Chem.*, **1992**, 96, 8441.
111. E. L. Quitevis, A. H. Marcus and M. D. Fayer, *J. Phys. Chem.*, **1993**, 97, 5762.
112. N. C. Maiti, M. M. G. Krishna, P. J. Britto and N. Periasamy, *J. Phys. Chem. B*, **1997**, 101, 11051.
113. G. B. Dutt, *J. Phys. Chem. B*, **2003**, 107, 10546.
114. I. D. Charlton and A. P. Doherty, *J. Phys. Chem. B*, **2000**, 104, 8327.
115. J. A. Molina-Bolivar, J. Aguiar and C. C. Ruiz, *J. Phys. Chem. B*, **2002**, 106, 870.

116. J. E. Yambert and J. D. Philies, *Langmuir*, **1996**, *12*, 3431.
117. R. A. Velapoldi and K. D. Mielenz, *Standard Reference Materials: A fluorescence standard reference material: Quinine sulfate dihydrate* **1980**, Nat. Bur. Stand. (US) Spec. Publ. 260.
118. D. V. O'Connor and D. Phillips, *Time Correlatated Single Photon Counting*; Academic: New York, 1984
119. W. Becker, *Advanced time correlated single photon counting technique*; Springer: New York, 2005.
120. J. N. Demas, *Excited state lifetime measurement*; Academic press: New York, 1983.
121. P. R. Bevington, *Data Reduction and Error Analysis for the Physical Sciences*; McGraw-Hill: New York, 1969.
122. M. A. Kahlow, W. Jarzeba, T. P. DuBruil and P. F. Barbara, *Rev. Sci. Instrum.* **1988**, *59*, 1098.
123. H. Mahr and M. D. Hirsch, *Opt. Commun.* **1975**, *13*, 96.
124. J. Shah, *IEEE J. Quant. Elect.* **1988**, *24*, 276.
125. T. C. Kippeny, M. J. Bowers II, A. D. Dukes III, J. R. McBride, R. L. Orndorff, M. D. Garrett and S. J. Rosenthal, *J. Chem. Phys.* **2008**, *128*, 084713/1.
126. D. F. Underwood, T. Kippeny and S. J. Rosenthal, *J. Phys. Chem. B* **2001**, *105*, 436.
127. R. G. W. Norrish and G. Porter, *Nature* **1949**, *164*, 658.
128. G. Porter, *Proc. Roy. Soc.* **1950**, *A200*, 284
129. A. J. Bard and L. R. Faulkner, *Electrochemical Methods-Fundamental & Applications*, 2nd Edn., Wiley & Sons, NY, **2001**.
130. B. J. Berne and R. Pecora, *Dynamic Light Scattering: With Applications to Chemistry, Biology, and Physics*, Dover publications: New York, **2000**.
131. J. R. Durrant, S. A. Haque and E. Palomares, *Coord. Chem. Rev* **2004**, *248*, 1247.
132. J. M. Mayer, *Ann. Rev. Phys. Chem.*, **2004**, *55*, 363.
133. K. R. Rodgers and G. S. Lukat-Rodgers, *Comprehen. Coord. Chem. II* **2004**, *8*, 17.
134. M. Tachiya, *Kinetics of Non-homogeneous Processes*; Wley, NY, **1987**.
135. M. Tachiya, *J. Phys. Chem.* **1993**, *97*, 5911.
136. M. Kumbhakar and H. Pal, *ScienceJet* 2015, *4*:139, 1.
137. M. Kumbhakar, S. Nath, T. Mukherjee and H. Pal, *J. Indian Chem. Soc.* **2010**, *87*, 173.
138. M. Kumbhakar, P. K. Singh, A. K. Satpati, S. Nath and H. Pal, *J. Phys. Chem. B* **2010**, *114*, 10057.

139. M. Kumbhakar, P. K. Singh, S. Nath, A. C. Bhasikuttan and H. Pal, *J. Phys. Chem. B*, **2008**, *112*, 6646.
140. P. Verma, S. Nath, P. K. Singh, M. Kumbhakar and H. Pal, *J. Phys. Chem. B*, **2008**, *112*, 6363.
141. A. K. Satpati, M. Kumbhakar, S. Nath and H. Pal, *J. Phys. Chem. B*, **2007**, *111*, 7550.
142. M. Lopez-Lopez, F. Sanchez and M. Marchena, *Prog. Reac. Kin. Mech.* **2012**, *37*, 203.
143. C. Ghatak, V. G. Rao, S. Mandal and N. Sarkar, *Phys. Chem. Chem. Phys.* **2012**, *14*, 8925.
144. A. Chakraborty, D. Seth, P. Setua and N. Sarkar, *J. Chem. Phys.* **2008**, *128*, 204510.
145. U. Mandal, S. Ghosh, S. Dey, A. Adhikari and K. Bhattacharyya, *J. Chem. Phys.* **2008**, *128*, 164505.
146. S. Nad and H. Pal, *J. Phys. Chem. A*. **2000**, *104*, 673.
147. N. J. Jain, V. K. Aswal, P. S. Goyal and P. Bahadur, *J. Phys. Chem. B*, **1998**, *102*, 8452.
148. K. Nakashima and P. Bahadur, *J. Controlled Release* **2002**, *82*, 189.
149. J. Yang and G. Wegner, *Macromolecules* **1992**, *25*, 1786.
150. Grant, C. D.; DeRitter, M. R.; Steege, K. E.; Fadeeva, T. A.; Jr., E. W. C. *Langmuir* **2005**, *21*, 1745.
151. Zhou, Z.; Chu, B. *J. Colloid Interface Sci.* **1988**, *126*, 171.
152. K. Kalyanasundaram, Photochemistry in Microheterogeneous systems; Academic Press Inc.: Orlando, 1987.
153. S. Nad, and H. Pal , *J. Phys. Chem. A*. **2001**, *105*, 1097.
154. H. Pal, S. Nad, and M. Kumbhakar , *J. Chem. Phys.* **2003**, *119*, 443.
155. A. Barik, S. Nath and H. Pal, *J. Chem. Phys.* **2003**, *119*, 10202-10208
156. J. A. Dean, (editor) *Lange's Handbook of Chemistry*. 13th ed. McGraw-Hill, New York, **1987**.
157. C. J. Fecko, J. D. Eaves, J. J. Loparo, A. Tokmakoff and P. L. Geissler, *Science* **2003**, *301*, 1698.
158. R. Jimenez, G. R. Fleming, P. V. Kumar and M. Maroncelli, *Nature* **1994**, *369*, 471.
159. M. Kumbhakar, S. Nath, T. Mukherjee and H. Pal, *J. Chem. Phys.* **2004**, *121*, 6026.
160. J. S. Lettow, T. M. Lancaster, C. J. Glinka and J. Y. Ying, *Langmuir* **2005**, *21*, 5738.
161. S. Nad and H. Pal, *J. Chem. Phys.* **2002**, *116*, 1658.
162. S. Nad and H. Pal, *J. Photochem. Photobiol. A: Chem.* **2000**, *134*, 9.

163. S. Ghosh, S. K. Mondal, K. Sahu and K. Bhattacharyya, *J. Chem. Phys.*, **2007**, *126*, 204708.
164. J. T. Edwards, *J. Chem. Edu.*, **1970**, *47*, 261.
165. S. F. Swallen, K. Weidemaier, H. L. Tavernier, and M. D. Fayer, *J. Phys. Chem.*, **1996**, *100*, 8106.
166. M. Kumbhakar, S. Dey, P. K. Singh, S. Nath, A. K. Satpati, R. Ganguly, V. K. Aswal and H. Pal, *J. Phys. Chem. B*, **2011**, *115*, 1638.
167. T. K. Mukherjee, P. P. Mishra and A. Datta, *Chem. Phys. Lett.*, **2005**, *407*, 119.
168. C. Tablet, I. Matei and M. Hillebrand, *J. Mol. Liq.*, **2011**, *160*, 57.
169. K. Glusac, A. Goun and M. D. Fayer, *J. Chem. Phys.*, **2006**, *125*, 054712.
170. R. Ganguly and V. K. Aswal, *J. Phys. Chem. B*, **2008**, *112*, 7726.
171. T. Goel, M. Kumbhakar, T. Mukherjee and H. Pal, *J. Photochem. Photobiol. A: Chem.*, **2010**, *209*, 41.
172. M. Kumbhakar, T. Goel, T. Mukherjee and H. Pal, *J. Phys. Chem. B*, **2004**, *108*, 19246.
173. R. Ganguly, M. Kumbhakar and V. K. Aswal, *J. Phys. Chem. B*, **2009**, *113*, 9441.
174. K. Hara, N. Baden and O. Kajimoto, *J. Phys.: Condens. Matter*, **2004**, *16*, S1207.
175. T. Molotsky, N. Koifman and D. Huppert, *J. Phys. Chem. A*, **2002**, *106*, 12185.
176. P. K. Singh, M. Kumbhakar, H. Pal and S. Nath, *J. Phys. Chem. B*, 2009, **113**, 1353.
177. P. K. Singh, M. Kumbhakar, R. Ganguly, V. K. Aswal, H. Pal and S. Nath, *J. Phys. Chem. B*, 2010, **114**, 3818.
178. P. K. Singh, A. K. Satpati, M. Kumbhakar, H. Pal and S. Nath, *J. Phys. Chem. B*, 2008, **112**, 11447.
179. P. Verma and H. Pal, *Phys. Chem. Chem. Phys.*, **2015**, *17*, 15400.
180. R. C. daSilva, G. Olofsson, K. Schille'n and W. Loh, *J. Phys. Chem. B*, **2002**, *106*, 1239.
181. Y. Li, R. Xu, D. M. Bloor and J. F. Holzwarth, *Langmuir*, **2000**, *16*, 10515.
182. T. Thurn, S. Couderc, J. Sidhu, D. M. Bloor, J. Penfold, J. F. Holzwarth and E. Wyn-Jones, *Langmuir*, **2002**, *18*, 9267.
183. D. Lof, M. Tomsic, O. Glatter, G. Fritz-Popovski and K. Schillen, *J. Phys. Chem. B*, **2009**, *113*, 5478.
184. P. K. Singh, M. Kumbhakar, H. Pal and S. Nath, *J. Phys. Chem. B*, 2008, **112**, 7771.
185. M. Murakami, K. Ohkubo, T. Nanjo, K. Souma, N. Suzuki and S. Fukuzumi, *Chem. Phys. Chem.*, **2010**, *11*, 2594.
186. H. N. Ghosh, *J. Phys. Chem. B*, **1999**, *103*, 10382-

187. R. E. Riter, E. P. Undiks and N. E. Levinger, *J. Am. Chem. Soc.*, **1998**, *120*, 6062.
188. K. Tominaga and G. C. Walker, *J. Photochem. Photobiol. A: Chem.* **1995**, *87*, 127.
189. C. Ghatak, V. G. Rao, S. Mandal and N. Sarkar, *Phys. Chem. Chem. Phys.*, **2012**, *14*, 8925.
190. S. Sarkar, S. Mandal, R. Pramanik, C. Ghatak, V. G. Rao and N. Sarkar, *J. Phys. Chem. B*, **2011**, *115*, 6100.
191. S. S. Anufrik and V. V. Tarkovsky, *J. Appl. Spec.* 2010, *77*, 640.
192. Y. Yang, J. Zou, H. Rong, G. D. Qian, Z. Y. Wang and M. Q. Wang, *Appl. Phys. B*, **2007**, *86*, 309.
193. J. Donovalova, M. Cigan, H. Stankovicova, J. Gaspar, M. Danko, A. Gaplovsky and P. Hrdlovic, *Molecules*, **2012**, *17*, 3259.
194. A.K. Satpati, M. Kumbhakar, S.Nath and H.Pal, *Photochem. Photobiol.*, **2009**, *85*, 119.
195. A. K. Satpati, M. Kumbhakar, S. Nath and H. Pal, *Chem. Phys. Chem.*, **2009**, *10*, 2966.
196. K. Rechthaler and G. Köhler, *Chem. Phys.*, **1994**, *189*, 99.
197. T. N. Burai and A. Datta, *J. Phys. Chem. B*, **2009**, *113*, 15901.
198. B. D. Wagner, *Molecules*, **2009**, *14*, 210.
199. S. George, M. Kumbhakar, P. K. Singh, R. Ganguly, S. Nath and H. Pal, *J. Phys. Chem. B*, **2009**, *113*, 5117.
200. M. Grazula and E. Budzisz, *Coord. Chem. Rev.*, **2009**, *253*, 2588.
201. E. Oliveira, C. Nunez, B. Rodriguez-Gonzalez, J. L. Capelo and C. Lodeiro, *Inorg. Chem.*, **2011**, *50*, 8797.
202. M. Y. Berezin and S. Achilefu, *Chem. Rev.*, **2010**, *110*, 2641.
203. M. V. Kulkarni, G. M. Kulkarni, C. -H. Lin and C. -M. Sun, *Curr. Med. Chem.*, **2006**, *13*, 2795.
204. Madhavan, G. R.; Balraju, V.; Mallesham, B.; Chakrabarti, R.; Lohray, V. B. *Bioorg. Med. Chem. Lett.*, **2003**, *13*, 2547.
205. E. Krystkowiak, K. Dobek, G. Burdzinski and A. Maciejewski, *Photochem. Photobiol. Sci.*, **2012**, *11*, 1322.
206. N. Barooah, J. Mohanty, H. Pal and A.C. Bhasikuttan, *Org. Biomol. Chem.*, **2012**, *10*, 5055.
207. T. Sakata, Y. Kawashima and H. Nakano, *J. Phys. Chem. A*, **2010**, *114*, 12363.
208. T. M. Arbeloa, F. M. Arbeloa, M. J. Tapia and I. M. Arbeloa, *J. Phys. Chem.*, **1993**, *97*, 4704.
209. Barik, A.; Kumbhakar, M.; Nath, S.; Pal, H. *Chem. Phys.*, **2005**, *315*, 277.

210. Dahiya, P.; Kumbhakar, M.; Mukherjee, T.; Pal, H. *Chem. Phys. Lett.*, **2005**, *414*, 148.
211. Senthilkumar, S.; Nath, S.; Pal, H. *Photochem. Photobiol.*, **2004**, *80*, 104.
212. P. K. Singh, S. Nath, M. Kumbhakar, A. C. Bhasikuttan and H. Pal, *J. Phys. Chem. A*, **2008**, *112*, 5598.
213. E. E. Jelley, *Nature*, **1936**, *138*, 1009.
214. J. R. Norris and M. Schiffer, *Chem. Eng. News Archive*, **1990**, *68*, 22.
215. A. Mishra and P. Bäuerle, *Angew. Chem. Int. Ed.*, **2012**, *51*, 2020.
216. T. M. Clarke and J. R. Durrant, *Chem. Rev.*, **2010**, *110*, 6736.
217. A. D. Schwab, D. E. Smith, B. Bond-Watts, D. E. Johnston, J. Hone, A. T. Johnson, J. C. de Paula and W. F. Smith, *Nano Lett.*, **2004**, *4*, 1261.
218. C. Wang, H. Dong, W. Hu, Y. Liu and D. Zhu, *Chem. Rev.*, **2012**, *112*, 2208.
219. F. C. Spano and S. Siddiqui, *Chem. Phys. Lett.*, **1999**, *314*, 481.
220. Y. Wang, *Chem. Phys. Lett.*, **1986**, *126*, 209.
221. X. Liu, J. M. Cole and K. S. Low, *J. Phys. Chem. C*, **2013**, *117*, 14723.
222. D. Lee, L. Greenman, M. Sarovar and K. B. Whaley, *J. Phys. Chem. A*, **2013**, *117*, 11072.
223. D. Roy, S. Pionteka and R. A. Walker, *Phys. Chem. Chem. Phys.*, **2011**, *13*, 14758.
224. D. Li, J. Zhang, M. Anpo, M. Xue and Y. Liu, *Materials Letters*, **2005**, *59*, 2120.
225. M. Cigan, J. Donovalova, V. Szocs, J. Gaspar, K. Jakusova and A. Gaplovsky, *J. Phys. Chem. A*, **2013**, *117*, 4870.
226. M. Mille, J. -F. Lamere, F. Rodrigues and S. Fery-Forgues, *Langmuir*, **2008**, *24*, 2671.
227. S. Chakraborty, D. Bhattacharjee and S. A. Hussain, *Appl. Phys. A*, **2013**, *111*, 1037.
228. Z. R. Grabowski, K. Rotkiewicz and W. Rettig, *Chem. Rev.*, **2003**, *103*, 3899.
229. G. Jones II, W. R. Jackson, C. Y. Choi and W. R. Bergmark, *J. Phys. Chem.*, **1985**, *89*, 294.
230. G. Jones II, W. R. Jackson and A. M. Halpern, *Chem. Phys. Lett.*, **1980**, *72*, 391.
231. Jones, II, G.; Rahman, M. A. *J. Phys. Chem.*, **1994**, *98*, 13028.
232. Robert, K.; Jarzeba, W. *J. Phys. Chem. A*, **2002**, *106*, 1708.
233. P. Verma and H. Pal, *J. Phys. Chem. A*, **2014**, *118*, 6950.
234. P. Verma and H. Pal, *J. Phys. Chem. A*, **2012**, *116*, 4473.
235. P. Verma and H. Pal, *J. Phys. Chem. A*, **2013**, *117*, 12409.
236. V. Kumar, G. A. Baker and S. Pandey, *Chem. Commun.*, **2011**, *47*, 4730.

237. M. Cigan, M. Danko, J. Donovalova, J. Gaspar, H. Stankovicova, A. Gaplovsky and P. Hrdlovic, *Spectrochim. Acta, Part A*, **2014**, *126*, 36.
238. W. I. Gruszecki, G. Gagos´ and M. Herec´, *J. Photochem. Photobiol. B: Biol.*, **2003**, *69*, 49.
239. J. Chang, Y. Lu, S. He, C. Liu and L. Zhao, Zeng, X. *Chem. Commun.*, **2013**, *49*, 6259.
240. A. Satake and Y. Kobuke, *Org. Biomol. Chem.*, **2007**, *5*, 1679.
241. F. Zhu, C. Galli and R. M. Hochstrasser, *J. Chem. Phys.*, **1993**, *98*, 1042.
242. P. Changenet-Barret, T. Gustavsson, D. Markovitsi, I. Manet and S. Monti, *Phys. Chem. Chem. Phys.*, **2013**, *15*, 2937.
243. D. Liu and P. V. Kamat, *J. Chem. Phys.*, **1996**, *105*, 965.
244. H. Yao and K. Ashiba, *RSC Adv.*, **2011**, *1*, 834.
245. C. Peyratout and L. Daehne, *Phys. Chem. Chem. Phys.*, **2002**, *4*, 3032.
246. U. Rosch, S. Yao, R. Wortmann and F. Wurthner, *Angew. Chem. Int. Ed.*, **2006**, *45*, 7026.
247. V. Karunakaran, D. D. Prabhu and S. Das, *J. Phys. Chem. C*, **2013**, *117*, 9404.
248. M. Itoh, *Chem. Phys. Lett.*, **1968**, *2*, 371.
249. Wurthner, F.; Yao, S. *Angew. Chem., Int. Ed.*, **2000**, *39*, 1978.
250. G. J. Smith, A. P. Middleton, D. J. Clarke, A. Teshome, A. J. Kay, M. D. H. Bhuiyan, I. Asselberghs and K. Clays, *Opt. Mater.*, **2010**, *32*, 1237.
251. Z. Chen, A. Lohr, C. R. Saha-Moller and F. Wurthner, *Chem. Soc. Rev.*, **2009**, *38*, 564.
252. S. De, S. Das, A. Girigoswami, *Spectrochim. Acta Part A*, **2005**, *61*, 1821.
253. A. S. R. Koti and N. Periasamy, *J. Chem. Phys.*, **2001**, *115*, 7094.
254. A. S. R. Koti, M. M. G. Krishna and N. Periasamy, *J. Phys. Chem. A.*, **2001**, *105*, 1767.
255. Y. Xu, Z. Li, A. Malkovskiy, S. Sun and Y. Pang, *J. Phys. Chem. B.*, **2010**, *114*, 8574.
256. B. Boruah, P. M. Saikia and R. K. Dutta, *Dyes and Pigments*, **2010**, *85*, 16.
257. H. Tajalli, A. G. Gilani, M. S. Zakerhamidi and M. Moghadam, *Spectrochim. Acta Part A.*, **2009**, *72*, 697.
258. S. Gadde, E. K. Batchelor, J. P. Weiss, Y. Ling and A. E. Kaifer, *J. Am. Chem. Soc.*, **2008**, *130*, 17114.
259. A. Furstenberg, T. G. Deligeorgiev, N. I. Gadjev, A. A. Vasilev, E. Vauthey, *Chem. Eur. J.*, **2007**, *13*, 8600.
260. M. A. Kahlow, T. J. Kang and P. F. Barbara, *J. Chem. Phys.*, **1988**, *88*, 2372.

261. M. L. Horng, J. A. Gardecki, A. Papazyan and M. Maroncelli, *J. Phys. Chem.*, **1995**, 99, 17311.
262. J.F. McCarthy, W. E. Sanford and P. L. Stafford, *Environ. Sci. Technol.*, 1998, **32** 3901.
263. C. Poinssot and H. Geckeis (Eds.) *Radionuclide Behaviour in the Natural Environment: Science, Implications and Lessons for the Nuclear Industry*. Woodhead Publishing, Cambridge, U.K., 2012.
264. D. A. Atwood (Ed.), *Radionuclides in the Environment*. John Wiley & Sons Inc., 2010.
265. M. D. Marcantonatos, *J. Chem. Soc., Faraday Trans. 1 : Physical Chemistry in Condensed Phases*, 1979, 75, 2252.
266. S. J. Formosinho, H. D. Burrows, M. da G. Miguel, M. E. D. G. Azenha, I. M. Saraiva, A. C. D. N Ribeiro, I. V. Khudyakov, R. G. Gasanov, M. Bolte and M. Sarakha, *Photochem. Photobiol. Sci.*, **2003**, 2, 569.
267. R. G. Denning, Electronic structure and bonding in actinyl ions, *Struct. Bonding (Berlin)*, **1992**, 79, 215.
268. C. P. Baird and T. J. Kemp, *Prog. React. Kinet.*, **1997**, 22, 87.
269. H. D. Burrows, *Chem. Soc. Rev.*, **1974**, 3, 139.
270. T. M. McCleskey, T. M. Foreman, E. E. Hallman, C. J. Burns and N. N. Sauer, *Environ. Sci. Technol.*, **2001**, 35, 547.
271. B. Gu, H. Yan, P. Zhou and D. B. Watson, *Environ. Sci. Technol.*, **2005**, 39, 5268.
272. M. R. Duff, Jr. and C. V. Kumar, *Angew. Chem. Int. Ed.*, **2006**, 45, 137.
273. S. S. Sandhu, K. B. Kohli, and A. S. Brar, *Inorg. Chem.*, **1984**, 23, 3609.
274. M.S. Sidhu and K. Vandana, *J. Radioanal. Nucl. Chem.*, **1995**, 198, 429.
275. R. Nagaishi, Y. Katsumura, K. Ishigure, H. Aoyagi, Z. Yoshida, T. Kimura, Y. Kato, *J. Photochem. Photobiol. A*, **2002**, 146, 157.
276. S. D. Taylor, M. C. Marcano, K. M. Rosso, U. Becker, *Geochim. Cosmochim. Acta*, **2015**, 156, 154.
277. X. Rui, M. J. Kwon, E. J. O'Loughlin, S. Dunham-Cheatham, J. B. Fein, B. Bunker, K.M. Kemner and M. I. Boyanov, *Environ. Sci. Technol.*, **2013**, 47, 5668.
278. W. A. Massad and G. A. Argüello, *J. Radioanal. Nucl. Chem.*, **2000**, 245, 407.
279. M. Sarakha, M. Bolte and H. D. Burrows, *J. Phys. Chem. A*, **2000**, 104, 3142.
280. M.S.Sidhu, Anju and P.V.K. Bhatia, *J. Radioanal. Nucl. Chem. Letters*, **1994**, 188, 243.
281. S. Tsushima, C. Gçtz, and K. Fahmy, *Chem. Eur. J.*, **2010**, 16, 8029.
282. V. P. Kazakov, S. S. Ostakhov, I. O. Osina, A. S. Alyab'ev, S. G. Gainetdinova, and G. Kh. Akhmadeeva, *Radiochemistry*, **2006**, 48, 452.

283. K. Binnemans, *Chem. Rev.*, **2009**, *109*, 4283.
284. L. Armellao, S. Quici, F. Barigelletti, G. Accorsi, G. Bottoro, M. Cavazzini and E. Tondello, *Coord. Chem. Rev.*, **2010**, *254*, 487.
285. C. S. Bonnet, F. Buron, F. Caillé, C. M. Shade, B. Drahoš, L. Pellegatti, J. Zhang, S. Villette, L. Helm, C. Pichon, F. Suzenet, S. Petoud and E. Tóth, *Chem. Eur. J.*, **2012**, *18*, 1419.
286. J. L. Ferrari, M. A. Schiavon, R. R. Gonçalves, A. M. Pires and M. R. Davolos, *Thin Solid Films*, **2012**, *524*, 299.
287. M. L. Cable, J. P. Kirby, H. B. Gray and A. Ponce, *Acc. Chem. Res.*, **2013**, *46*, 2576.
288. A.P. De Silva, D. B. Fox, T. S. Moody and S. M. Weir, *Acc. Chem. Res.*, **2001**, *73*, 503.
289. L. R. Morss, *Chem. Rev.*, **1976**, *76*, 827.
290. W. J. Evans, *Coord. Chem. Rev.*, **2000**, *206–207*, 263.
291. S. Maity and E. Prasad, *J. Photochem. Photobiol. A: Chem.*, **2014**, *274*, 64–72.
292. J. Jiang, N. Higashiyama, K.-I. Machida and G.-Y. Adachi, *Chem. Soc. Rev.*, **1998**, *170*, 1.
293. N. -D. H. Gamage, Y. Mei, J. Garcia and M. J. Allen, *Angew. Chem. Int. Ed.*, **2010**, *49*, 8923.
294. L. Yan, H. Liu, J. Wang, Y. Zhang and Q. Shen, *Inorg. Chim. Acta*, **2012**, *51*, 4151.
295. M. Szostak, M. Spain, and D. J. Procter, *Chem. Soc. Rev.*, **2013**, *42*, 9155.
296. M. Szostak and D. J. Procter, *Angew. Chem. Int. Ed.*, **2012**, *51*, 9238.
297. E. Prasad, B. W. Kettle and R. A. Flowers II, *Chem. Eur. J.*, **2005**, *11*, 3105.
298. T. Terai, K. Kikuchi, S. -Y. Iwasawa, T. Kawabe, Y. Hirata, Y. Urano and T. Nagano, *J. Am. Chem. Soc.*, **2006**, *128*, 6938.
299. R. M. Supkowski and W. D. Horrocks Jr., *Met. Ions Biol. Syst.*, **2003**, *40*, 281.
300. T. Gunnlaugsson, M. Glynn, G. M. Tocci, P. E. Kruger, and F. M. Pfeffer, *Coord. Chem. Rev.*, **2006**, *250*, 3094.
301. H. Tan, B. Liu and Y. Chen, *ACS Nano*, **2012**, *6*, 10505.
302. T. Lazarides, M. A. H. Alamiry, H. Adams, S. J. A. Pope, S. Faulkner, J. A. Weinstein and M. D. Ward, *Dalton Trans.*, **2007**, 1484.
303. T. Inada, Y. Funasaka, K. Kikuchi, Y. Takahashi and H. Ikeda, *J. Phys. Chem. A*, **2006**, *110*, 2595.
304. F. Kielar, C. P. Montgomery, E. J. New, D. Parker, R. A. Poole, S. L. Richardson and P. A. Stenson, *Org. Biomol. Chem.*, **2007**, *5*, 2975.

305. D. Sykes, A. J. Cankut, N. M. Ali, A. Stephenson, S. J. P. Spall, S. C. Parker, J. A. Weinstein and M. D. Ward, *Dalton Trans.*, **2014**, 43, 6414.
306. J. R. Choi, T. Tachikawa, M. Fujitsuka and T. Majima, *Langmuir*, **2010**, 26, 10437.
307. P. Dorenbos, *J. Phys.: Condens. Matter*, **2003**, 15, 8417.
308. Y. Nosaka, A. Kira and M. Imamura, *J. Phys. Chem.*, **1981**, 85, 1353.
309. T. Kahl, K. -W. Schröder, F. R. Lawrence, W. J. Marshall, H. Höke and R. Jäckh, "Aniline" in *Ullmann's Encyclopedia of Industrial Chemistry*, Wiley-VCH, Weinheim, 2005.
310. O. Drzyzga, A review, *Chemosphere*, **2003**, 53, 809.
311. S. Avirah and R. Joseph, *Polym. Degrad. Stab*, **1994**, 46, 251.
312. D. E. A. Rahman, *Chem. Pharm. Bull.*, **2013**, 61, 151.
313. M. López-López, J. C. Bravo, C. Garcíá-Ruiz and M. Torre, *Talanta*, **2013**, 103, 214.
314. C.-L. Liu, C.-J. Zheng, X.-K. Liu, Z. Chen, J.-P. Yang, F. Li, X.-M. Ou and X.-H. Zhang, *J. Mater. Chem. C*, **2015**, 3, 1068.
315. A. P. DeDiego Martínez, M. L. Tascón, M. D. Vázquez and P. S. Batanero, *Talanta*, **2004**, 62, 165.
316. NIST Chemistry WebBook, NIST Standard Reference Database Number 69, Eds. P.J. Linstrom and W.G. Mallard, National Institute of Standards and Technology, Gaithersburg MD, 20899, (2011). <http://webbook.nist.gov>. ($\epsilon = 19500$ in EtOH).
317. H. N. Ghosh, H. Pal, A. V. Sapre, and J. P. Mittal, *J. Am. Chem. Soc.*, **1993**, 115, 11722.
318. A.J. Bard, H. Lund, *Encyclopedia of Electrochemistry of the Elements*, Vol. XV, Marcel Dekker, New York, 1984.
319. Reported $E_{D/D}^+$ value of DPA is 0.64 vs SCE in ACN solution.³¹⁸ This value was shifted by +0.24 V to consider NHE as the reference electrode and added by -0.03 V based on Born correction for changing solvent from ACN to water.
320. T. Shida, *Electronic Absorption Spectra of Radical Ions*, Elsevier, Amsterdam, 1988 (in physical science data)
321. L. J. Johnston and R. W. Redmond, *J. Phys. Chem. A*, **1997**, 101, 4660
322. F. Martelli, S. Abadie, J. -P. Simonin, R. Vuilleumier and R. Spezia, *Pure Appl. Chem.*, **2013**, 85, 237.
323. P. Nichols, E. J. Bylaska, G. K. Schenter and W. de Jong, *J. Chem. Phys.*, **2008**, 128, 24507.
324. J. -C. G. Bunzli and C. Piguet, *Chem. Soc. Rev.*, 2005, **34**, 1048.